Crystalline-Core Micelles
Based on Triblock Terpolymers
with Polyethylene Middle Blocks

Dissertation

zur Erlangung des akademischen Grades eines Doktors der
Naturwissenschaften (Dr. rer. nat.) im Fach Chemie der Fakultät für
Biologie, Chemie und Geowissenschaften der Universität Bayreuth

vorgelegt von

Joachim Schmelz

Geboren in Lauterbach/Hessen

Bayreuth, 2012

Die vorliegende Arbeit wurde in der Zeit von Juli 2008 bis Mai 2012 in Bayreuth am Lehrstuhl Makromolekulare Chemie II unter der Betreuung von Herrn Prof. Dr. Axel H. E. Müller angefertigt.

Vollständiger Abdruck der von der Fakultät für Biologie, Chemie und Geowissenschaften der Universität Bayreuth zur Erlangung des akademischen Grades eines Doktors der Naturwissenschaften genehmigten Dissertation.

Promotionsgesuch eingereicht am: 07.05.2012

Zulassung durch die Promotionskommission: 16.05.2012

Wissenschaftliches Kolloquium: 13.07.2012

Amtierender Dekan: Prof. Dr. Beate Lohnert

Prüfungsausschuss:

Prof. Dr. Axel H. E. Müller (Erstgutachter)

Prof. Dr. Stephan Förster (Zweitgutachter)

Prof. Dr. Karlheinz Seifert

Prof. Dr. Josef Breu (Vorsitz)

dedicated to Theresia and Annika,

my parents and grandparents

Table of Contents

Summary

This thesis is focused on the crystallization-induced structure formation of polyethylene containing triblock terpolymers in organic solvents to surface-compartmentalized worm-like crystalline-core micelles (wCCMs). Obtaining profound knowledge of the parameters controlling the self-assembly process allowed the production of a variety of complex one-dimensional micellar architectures with many potential applications, such as adaptive surfactants.

At first, the basic parameters that control the crystallization-induced self-assembly were explored using symmetric polystyrene-*block*-polyethylene-*block*-poly(methyl methacrylate) (PS-*b*-PE-*b*-PMMA) triblock terpolymers and a PS-*b*-PE-*b*-PS triblock copolymer. In good solvents for the PE block, *e.g.* THF and toluene, the selective formation of wCCMs was observed over a wide range of concentration, applied crystallization temperature and polymer composition. Whereas wCCMs produced by PS-*b*-PE-*b*-PS showed a homogeneous PS corona, a patch-like compartmentalization of the corona was observed if the micelles were formed by PS-*b*-PE-*b*-PMMA. As THF shows equal solvent quality for both corona blocks, wCCMs with almost alternating PS and PMMA compartments of about 15 nm were observed in this solvent. However, if structure formation was conducted in bad solvents for PE, such as dioxane or dimethylacetamide, spherical micelles with amorphous PE cores were formed already before crystallization. Hence, the subsequent crystallization of PE resulted in spherical CCMs with a patchy or a homogeneous corona depending on the used triblock. These findings allow the highly selective production of stable spherical or worm-like CCMs from the same polymer.

As the corona structure of the patchy micelles self-assembled from triblock terpolymers was mainly deduced from transmission electron microscopy (TEM) performed on dried samples, a small-angle neutron scattering (SANS) study was performed in order to elucidate the morphology in solution. Therefore a partly deuterated triblock terpolymer was synthesized and measured at different contrasts to allow the selective detection of the different corona compartments. The resulting SANS curves could be interpreted using a form factor model for

core-shell cylinders with alternating PS and PMMA hemishells including interparticle interactions, thus validating the TEM observations. Notably, Janus-type and patchy cylinders can be clearly distinguished using the applied form factor model.

Moreover, the controlled formation of wCCMs with tunable corona composition and structure was achieved using the cocrystallization of different triblock copolymers. *Via* random cocrystallization of PS-*b*-PE-*b*-PMMA and PS-*b*-PE-*b*-PS the corona morphology could be tuned continuously from a mixed corona at low PMMA content over spherical PMMA patches of increasing number and size to alternating PS and PMMA patches. This approach allows to manufacture wCCMs with predefined corona structure omitting the need to synthesize a new tailor-made triblock terpolymer for every desired morphology.

By establishing the controlled crystallization-driven self-assembly of triblock terpolymers with PE middle blocks, it was further possible to prepare wCCMs with predefined average lengths up to 500 nm and length polydispersities as low as $L_w/L_n = 1.1$. Here, self-assembled spherical CCMs of PS-*b*-PE-*b*-PS were used as seeds for the controlled growth of PS-*b*-PE-*b*-PS unimers. Upon further addition of PS-*b*-PE-*b*-PMMA unimers these grew epitaxially onto the preexisting wCCMs, resulting in triblock *co*-micelles that consisted of middle blocks with a homogeneous PS corona and outer blocks with alternating PS/PMMA compartments. These structures represent not only the first block *co*-micelles including blocks with a patchy corona, but also the first ones produced from purely organic block copolymers.

In view of application, the ability of patchy wCCMs formed by PS-*b*-PE-*b*-PMMA to stabilize interfaces was investigated using pendant-drop tensiometry. The observed reduction of the interfacial tension at the toluene/water interface was significantly higher than that of comparable triblock terpolymer single chains and that of wCCMs with a homogeneous PS corona. Interestingly, the obtained equilibrium interfacial tension equaled that of Janus cylinders with similar dimensions. To explain this unexpected finding the corona chains were proposed to adapt to the interface *via* selective collapse and shielding of the incompatible part of the corona chains. Studying wCCMs formed by several triblock terpolymers with different compositions, the interfacial activity was found to increase with increasing overall length of the corona chains, and to a certain extent with the molar fraction of PS units in the corona.

Zusammenfassung

Die vorliegende Doktorarbeit befasst sich mit dem Themenkomplex der kristallisations-induzierten Selbstoganisation von Triblockterpolymeren zu wurmartigen Mizellen mit kristallinem Kern (wCCMs) und kompartimentierter Oberfäche. Nachdem zu Beginn grundlegende Erkenntnisse über den Strukturbildungssprozess gewonnen wurden, konnten diese im weiteren Verlauf dazu genutzt werden, eine Reihe komplexer eindimensionaler Mizellarchitekturen zu realisieren. Als Beispiel für mögliche Anwendungsgebiete wurde die Grenzflächenaktivität dieser Strukturen untersucht.

Zunächst wurden die der kristallisationsinduzierten Selbstorganisation zugrundeliegenden Parameter am Beispiel von symmetrischen Polystyrol-*block*-polyethylen-*block*-polymethyl-methacrylat (PS-*b*-PE-*b*-PMMA) Triblockterpolymeren und einem PS-*b*-PE-*b*-PS Triblock-copolymer inspiziert. In guten Lösungsmitteln für PE, wie THF oder Toluol, wurden selektiv wCCMs gebildet. Diese Selbstorganisation zu eindimensionalen Strukturen konnte dabei über große Bereiche von Polymerzusammensetzung, gewählter Kristallisationstemperatur und Konzentration beobachtet werden. Aus PS-*b*-PE-*b*-PS entstehen so wCCMs mit homogener PS-Korona, aus PS-*b*-PE-*b*-PMMA solche mit patch-artiger PS/PMMA-Korona. Strukturen, die in THF gebildet wurden, zeigten eine nahezu alternierende Abfolge von etwa 15 nm großen PS- und PMMA-Kompartimenten aufgrund der gleich guten Lösungseigenschaften beider Blöcke. Wird hingegen die Strukturbildung in schlechten Lösungsmitteln für PE, wie Dioxan oder Dimethylacetamid, durchgeführt, so liegen bereits vor der Kristallisation sphärische Mizellen mit amorphem PE-Kern vor, deren sphärische Struktur bei der Kristallisation des PE-Kerns erhalten bleibt. Auf diese Weise entstehen sphärische Mizellen mit kristallinem Kern (sCCMs) und homogener (aus PS-*b*-PE-*b*-PS) sowie patch-artiger (aus PS-*b*-PE-*b*-PMMA) Korona. Aus ein und demselben Polymer können daher über die Wahl eines geeigneten Lösemittels selektiv sphärische oder wurmartige Mizellen gebildet werden.

Da die patch-artige Koronamorphologie der aus Triblockterpolymeren gebildeten wCCMs lediglich durch Transmissionselektronenmikroskopie (TEM) an getrockneten Proben nach-

gewiesen werden konnte, folgte eine Untersuchung mittels Neutronenkleinwinkelstreuung (SANS), um die Morphologie direkt in Lösung zu untersuchen. Das Einbringen eines deuterierten PS-Blocks erlaubte hier die selektive Detektion der unterschiedlichen Korona-kompartimente mittels Kontrastvariation. Die erhaltenen SANS-Daten konnten mit einem Modell für Kern-Schale-Zylinder mit alternierenden Halbschalen unter Einbeziehung von Partikel-Wechselwirkungen zwischen einzelnen Mizellen beschrieben werden, was die patch-artige Struktur bestätigt, wie sie durch TEM gefunden wurde. Außerdem wurde gezeigt, dass sich mit dem benutzten Modell patch-artige klar von Janus-Mizellen unterscheiden lassen.

Des Weiteren konnte über statistische Cokristallisation von PS-*b*-PE-*b*-PS mit PS-*b*-PE-*b*-PMMA die Koronastruktur der wCCMs auf einfache Weise eingestellt werden. Während bei sehr kleinem PMMA-Anteil eine gemischte Korona vorlag, wurden bei steigendem Anteil zunächst sphärische PMMA-Kompartimente mit zunehmender Anzahl und Größe in einer PS-Matrix und schließlich wieder eine mehr und mehr alternierende Struktur beobachtet. Durch die Möglichkeit, die Koronazusammensetzung durch das Mischungsverhältnis der zwei Polymere kontinuierlich zu variieren, kann die zeitaufwändige Synthese von neuen Triblockterpolymeren mit maßgeschneiderten PS/PMMA-Verhältnissen umgangen werden.

Die Übertragung des Konzepts der kontrollierten, kristallisationsinduzierten Selbstorganisa-tion auf PE-haltige Triblockcopolymere ermöglichte weiterhin, wCCMs mit einer Länge bis zu 500 nm sowie einer niedrigen Längenpolydispersität um $L_w/L_n = 1{,}1$ gezielt herzustellen. Hierzu wurden vorher gebildete sCCMs aus PS-*b*-PE-*b*-PS als Keime für das kontrollierte Wachstum von PS-*b*-PE-*b*-PS Unimeren verwendet. Durch Zugabe von PS-*b*-PE-*b*-PMMA Unimeren zu den so erhaltenen wCCMs konnten Triblockcomizellen über epitaktische Kristallisation hergestellt werden. Die entstandenen Mizellen besitzen Mittelblöcke mit einer homogenen PS-Korona und Außenblöcke mit wiederum alternierenden PS- und PMMA-Kompartimenten. Zum ersten Mal konnten so Blockcomizellen aus rein organischen Blockcopolymeren sowie solche mit patch-artigen Blöcken hergestellt werden.

Im Hinblick auf mögliche Anwendungsgebiete wurde die Grenzflächenaktivität von aus PS-*b*-PE-*b*-PMMA gebildeten, patch-artigen wCCMs mittels „Pendant-Drop"-Tensiometrie unter-sucht. Die durch diese Partikel erreichte Herabsetzung der Grenzflächenspannung an einer

Toluol/Wasser-Grenzfläche war wesentlich höher als für vergleichbare Triblockterpolymer-Einzelketten und wCCMs mit homogener PS Korona. Interessanterweise war der Effekt vergleichbar zu dem verursacht durch PS/PMMA Januszylinder. Dies wurde durch das selektive Kollabieren und Abschirmen des jeweils inkompatiblen Teils der Korona erklärt. Untersuchungen an wCCMs mit unterschiedlichen Koronazusammensetzungen zeigten weiterhin einen positiven Effekt der Gesamtlänge beider Koronablöcke sowie in gewissem Maße einen Einfluss des PS-Anteils in der Korona auf die Grenzflächenaktivität.

1. Introduction

1.1. Block Copolymer Self-Assembly

Over the past decades a myriad of different nanostructures has been produced by harnessing the ability of block copolymers to self-organize into supramolecular aggregates (Figure 1.1).[1-7] The key to these unique properties is the interplay between short-range attraction on one hand, *i.e.* the covalent bond between the polymer blocks, and long-range repulsion due to the different properties of the blocks on the other hand.[1] For diblock copolymers in bulk, the block incompatibility leads to the formation of distinct morphologies, such as spheres with cubic packing, hexagonal cylinders and lamellae, depending on the volume ratios and incompatibility of the polymer blocks.[8-10]
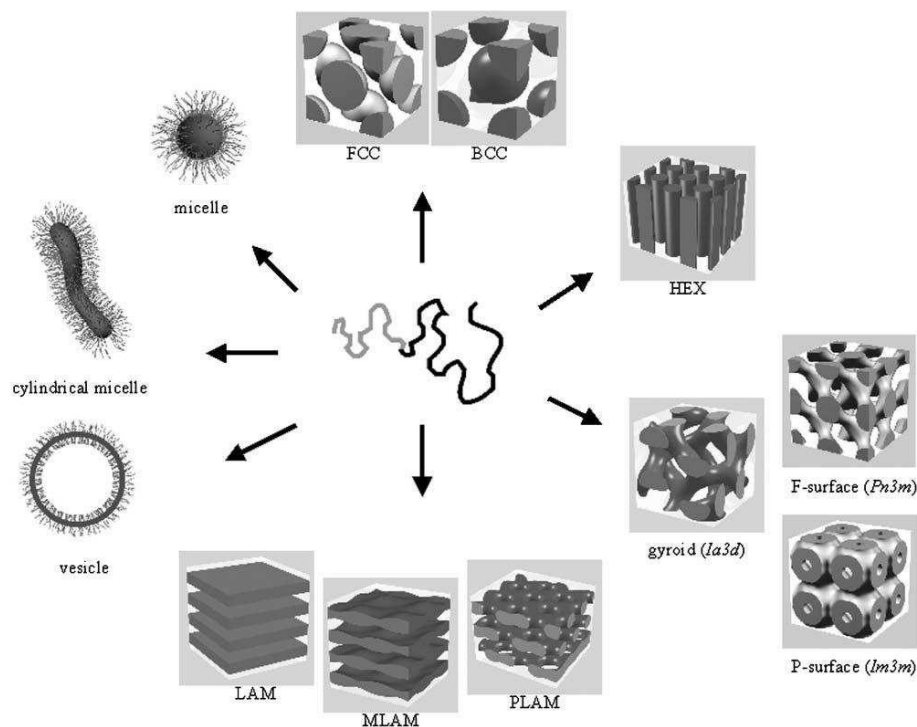
Figure 1.1. Self-assembled structures of block copolymers and surfactants: spherical micelles, cylindrical micelles, vesicles, fcc- and bcc-packed spheres (FCC, BCC), hexagonally packed cylinders (HEX), various minimal surfaces (gyroid, F-surface, P-surface), simple lamellae (LAM), as well as modulated and perforated lamellae (MLAM, PLAM).[11]

For suitable conditions, more complex structures like bicontinuous gyroids or perforated lamellae are accessible, too. Typically, the feature sizes of these ordered arrays are in the

range of 1 to 100 nm, dimensions where *e.g.* lithography as the common method for the production of small structures, reaches its limits. In solution, block copolymer self-assembly is usually achieved by rendering one of the blocks insoluble triggered by parameters like solvent polarity, temperature or pH.[3,5,12] In most cases, spherical micelles are formed consisting of a collapsed core block and a corona of the still soluble block preventing precipitation. Other architectures, such as cylinders or vesicles are mainly observed in "crew-cut" systems, *i.e.* the soluble block is significantly shorter than the insoluble block, and usually require dialysis into a selective solvent or solvent mixture.[13-17] In some cases, cylindrical micelles have also been produced by direct dissolution in a selective solvent.[18-21] The extension of this concept to triblock terpolymers and the resulting higher structural diversity will be discussed in section 1.3. The majority of research on block copolymer self-assembly, especially in solution, however, focused on block copolymers only consisting of amorphous blocks.

1.2. Block Copolymers with Crystallizable Blocks
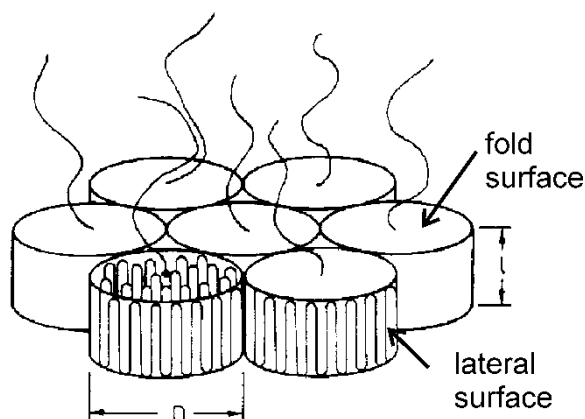
Figure 1.2. Schematic representation of a coil-crystalline lamella indicating the different crystal surfaces.[22]

In contrast to block copolymers that purely consist of amorphous blocks, those bearing a crystallizable block have been less well examined. In 1991, Vilgis and Halperin established a theoretical background for micelles with crystalline cores using a chain folding model.[22] Here, spheres, cylinders and lamellae (platelets) were considered. Due to the chain folding, the cores of these aggregates exhibit two different surfaces with different surface tensions: the fold surface or basal surface, where the polymer chains fold back into the crystal and

where the soluble corona blocks are attached, and the lateral surface (Figure 1.2). This gives rise to significant core anisotropy even for aggregates with a spherical overall shape so that a more accurate term would be "hockey-puck" micelles rather than spherical micelles. The resulting morphology, *i.e.* the morphology showing the lowest total free energy, is mainly determined by three competing factors.[22,23] A low amount of chain folds is advantageous in view of the crystallization enthalpy. However, at the same time this leads to a higher grafting density of the soluble corona chains on the fold surface forcing these chains to stretch, which is entropically unfavorable. Additionally, a minimization of the high energy crystal surface results in a lower free energy.

Whereas in early experimental works on block copolymers bearing polyethylene (PE) and poly(ethylene oxide) (PEO) blocks mostly platelet-like aggregates have been observed,[23-27] during the past decade several block copolymers containing different crystallizable blocks were shown to enable the selective production of one-dimensional structures.[28] More recently, the discovery of crystallization-induced "living" self-assembly by Winnik and Manners *et al.* for block copolymers with crystallizable poly(ferrocenyl dimethylsilane) (PFDMS) blocks allowed to manufacture cylindrical micelles with controlled lengths,[29-31] block *co*-micelles[29,32] and even more sophisticated architectures, such as scarf-like micelles or micellar brush-layers grafted on homopolymer surfaces.[33]

In the course of this introduction significant achievements regarding semicrystalline micellar structures are ordered according to the crystallizable polymer block that induces micellization with special emphasis on the crystallization-induced formation of cylindrical or worm-like structures. In section 1.2.8, general parameters determining the formed morphologies are discussed.

1.2.1. Poly(ethylene oxide)

In 1982, Dröscher and Smith studied the crystallization kinetics of a symmetric PEO-*b*-PPO-*b*-PEO (PPO: poly(propylene oxide)) triblock copolymer forming platelets in ethylbenzene using the field-free decay of the electrical birefringence.[26] An increase in the temperature of isothermal crystallization of 6.5 °C was shown to increase the half-time of crystallization by a factor of 30 in this case highlighting the importance of this parameter. Gast et al. studied the self-assembly of PEO-*b*-PS (PS: polystyrene) in cyclopentane with trace amounts of water.[27]

For low water contents large aggregates are formed, whereas higher amounts of water led to spherical micelles. Large aggregates formed by such diblock copolymers after heating above the melting temperature of PEO and cooling back to room temperature turned out to be platelet-like micelles with cylinders protruding from the lateral surfaces.[24] The same group also found good agreement between small angle X-ray (SAXS) and neutron (SANS) scattering measurements on PEO-b-PS platelets in cyclopentane and self-consistent mean field (SCF) calculations regarding the crystallite thickness of the cores.[23] Ryan, Xu and coworkers observed an interesting phenomenon in PEO-b-PBO (PBO: poly(butylene oxide)) diblock copolymers with equal block ratios but variations in the overall molecular weight.[34] While the precipitation of platelets from solution occurred for low molecular weights, a long diblock copolymer only formed hockey-puck micelles. This is explained by the shielding of the lateral core surfaces by the longer corona chains, an effect called "over-spilling", which prevents further aggregation of the hockey-puck micelles. Using the same block copolymers the formation of platelets from initially formed spheres was observed in blends with PBO homopolymer, too.[35] Cheng's group used PEO-b-PS platelets as seeds for the further nucleation of PEO homopolymer from the lateral crystal surfaces.[36] Interestingly, an increased length of the PS corona blocks resulted in selective PEO growth only from the four edges of the platelets (Figure 1.3B). Furthermore, by alternating addition of PEO-b-PS with short PS blocks and PEO homopolymer channel-wire arrays with spacings down to 50 nm could be achieved (Figure 1.3A). By controlling the lamellar thickness and hence the reduced tethering density of the corona blocks in PEO-PS platelets the onsets of chain overcrowding and the transition to a highly stretched brush regime were determined.[37] Platelet formation was also observed for PEO-b-P2VP-b-PS (P2VP: poly(2-vinyl pyridine)) triblock terpolymers consequently possessing a corona of tethered diblock copolymer chains.[38] More recently, Ballauff, Schmalz et al. produced spherical,[39-41] meander-,[39,41,42] rod-[40,41] and needle-like[40,41] structures as well as twisted lamellae[42] and platelets[41] from PEO-b-PB (PB: polybutadiene) diblock copolymers.
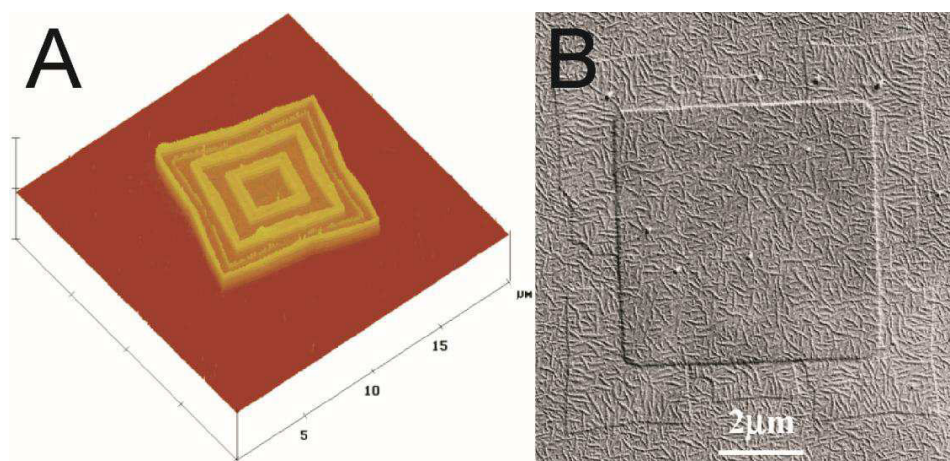
Figure 1.3. (A) AFM height image of a single crystal constructed by alternating PEO-*b*-PS and homo-PEO growth. (B) TEM image of homo-PEO crystal growth from the edges of PEO-*b*-PS diblock copolymer platelets.[36]

1.2.2. Poly(ε-caprolactone)

In 2007, Chang, Kuo and coworkers studied the self-assembly of poly(ε-caprolactone)-*block*-poly(4-vinylpyridine) (PCL-*b*-P4VP) diblock copolymers by dissolution in DCM as a common solvent followed by the addition of the selective solvents toluene (selective for PCL) and methanol (for P4VP).[43] If the amorphous P4VP forms the core, spheres, vesicles and large compound micelles were formed, while spheres, worm-like rods, vesicles and platelets are observed when the core consists of the semicrystalline PCL. Xu's group conducted self-assembly of PCL-*b*-PEO diblock copolymers by PCL crystallization in water.[44] For a low degree of polymerization of the PEO block (DP = 44) a variation in PCL block length resulted in spherical and worm-like micelles as well as lamellae. If the soluble PEO block is considerably longer (DP = 113), mainly spherical aggregates with increasing sizes were observed. Only for the longest PCL block a few coexisting lamellar structures could be found showing that for these long corona blocks no worm-like micelles occur. The structure formation of these polymers can be influenced further by varying the temperature of isothermal crystallization[45] as well as the salt concentration in solution.[46]

1.2.3. Polyacrylonitrile

Cylindrical morphologies obtained from polyacrylonitrile (PAN) based block copolymers have been investigated by Lazzari and coworkers. By crystallization of PAN-*b*-PS or PAN-*b*-PMMA (PMMA: poly(methyl methacrylate)) together with different amounts of PAN homopolymer

one-dimensional micelles with tunable core diameters were obtained and used for the production of carbon nanofibers *via* pyrolysis.[47,48]

1.2.4. Poly(ferrocenyl dimethylsilane)

PFDMS is, by far, the most extensively investigated crystallizable polymer block, at least with respect to the formation of cylindrical micelles. In 1998, Winnik and Manners *et al.* for the first time reported their formation from PFDMS-*b*-PDMS (PDMS: polydimethylsiloxane) diblock copolymers with a block ratio of 1:6 after the dissolution of a hexagonally packed cylindrical bulk structure in *n*-hexane.[49] It was further demonstrated that ultrasound treatment of such a micellar solution results in their partial scission and consequently a reduction in average length. Further studies revealed that the formation of cylinders occurred in various *n*-alkanes and not only by direct dissolution of the bulk structure but also by dialysis from the common solvent THF.[50] If PFDMS is replaced by non-crystalline poly(ferrocenyl methylphenylsilane) (PFMPS) or poly(ferrocenyl methylethylsilane) (PFMES) or self-assembly is carried out above the melting point of PFDMS, spherical micelles are formed, revealing the crystallinity of the core as the driving force for cylinder formation. PFDMS-*b*-PDMS-*b*-PFDMS triblock copolymers were self-assembled resulting in flower-like spherical and cylindrical structures.[51,52] Using a block ratio of about 1:12 nanotubes could be prepared from PFDMS-*b*-PDMS diblock copolymers in decane.[53,54] These structures were shown to undergo a reversible tube-to-rod transition upon increasing the temperature.[55] However, later light scattering studies suggested that the tubular micelles probably formed upon TEM sample preparation from one-dimensional micelles with ribbon-like cores.[56] The self-assembly of PFP-*b*-PFDMS-*b*-PDMS (PFP: poly(ferrocenyl phenylphosphine)) triblock terpolymers with very short PFP blocks yields cylindrical micelles for DP(PFP) ≤ 6 and spherical micelles for DP(PFP) = 11 due to increasing disruption of PFDMS crystallization.[57] Cylindrical micelles were also obtained when PDMS is substituted by different corona blocks like polyisoprene (PI)[58] and PMMA.[59] For PFDMS-*b*-PI, cylinders were formed for block ratios from 1:6 to 1:12 (Figure 1.4A), whereas for equal PI block lengths and longer PFDMS blocks the tendency to form rectangular platelets increased (Figure 1.4B).[58] In case of cylinders produced from PFDMS-*b*-PMMA in acetone Vancso *et al.* found that the core is not in a crystalline state as PFDMS signals could be traced in ^{1}H-NMR spectra.[59] One-dimensional micelles can also be formed in more polar solvents like alcohols. Here, the tendency of

cylinder formation decreases for increased Hildebrandt solubility parameters of these solvents, *i.e.* reduced solubility of PFDMS, as shown for PFDMS-*b*-P2VP.[60] Using poly(N,N-dimethylaminoethyl methacrylate) (PDMAEMA) corona blocks water-soluble cylindrical micelles are feasible, too.[61]
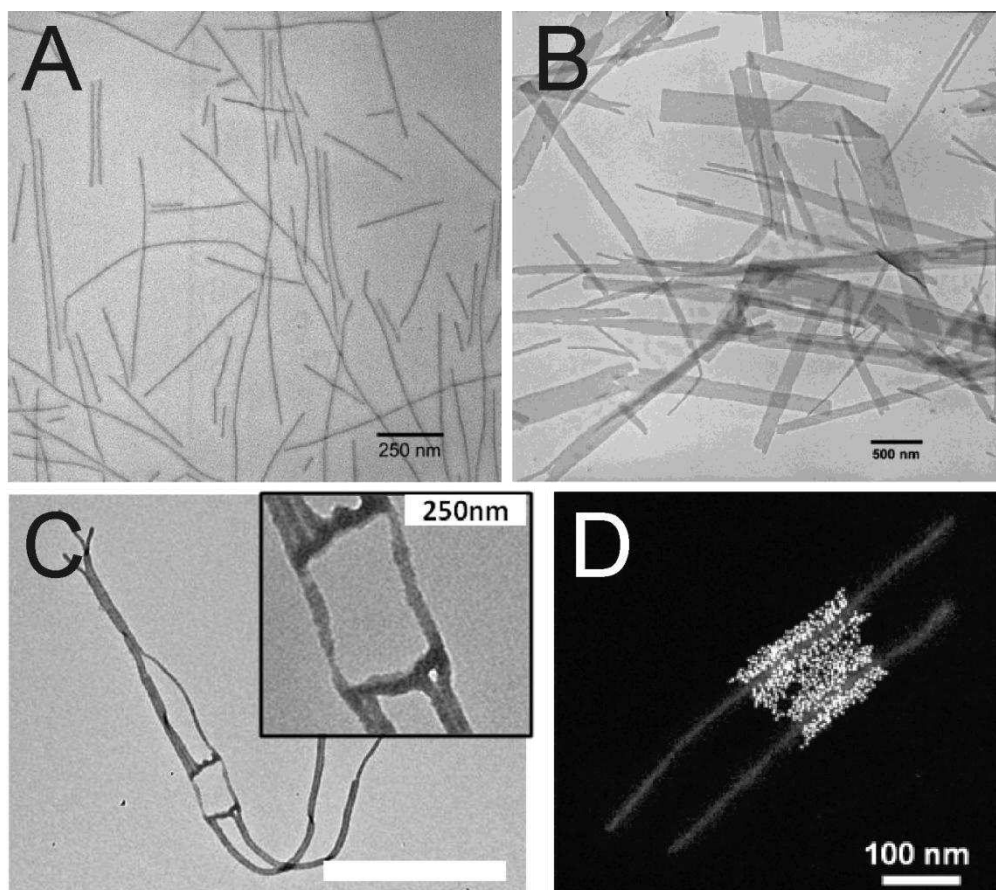
Figure 1.4. TEM micrographs of cylinders (A) and elongated platelets (B) formed by PFDMS-*b*-PI with block ratios of 1:6 and 2:1, respectively.[58] (C) TEM of a scarf-like micelle after redissolution of the middle part.[62] Large scale bar: 2 µm. (D) Dark-field TEM of triblock *co*-micelles, selectively functionalized with PbS quantum dots in the corona of the middle block.[32]

The discovery of "living" self-assembly, that is, micelles with PFDMS cores grow epitaxially upon the addition of further unimers, in 2007 allowed to control the cylinder length and to produce block *co*-micelles and, thus, paved the way to complex micellar architectures.[29] Length control in PFDMS containing micelles is performed by the addition of unimers in a small amount of common solvent, usually THF, to seeds preformed by the sonication of cylindrical micelles at low temperatures (-78 °C)[30] or by self-seeding, *i.e.* the partial dissolution of the cylinder-forming block copolymer so that only small crystalline fragments remain as seeds for crystallization.[31] By this means, length polydispersity indices (*PDI*) down

to 1.01 could be achieved. The ability to produce block *co*-micelles was further exploited by the block-selective corona functionalization with Au and PbS nanoparticles (Figure 1.4D),[32] titania layers[63] and fluorescent labels.[64] For the latter, even 9-block *co*-micelles were synthesized. If the crystalline structure does not differ significantly heteroepitaxial growth, *i.e.* the growth of a block copolymer containing a different crystallizable block, is possible, too, as demonstrated for poly(ferrocenyl dimethylgermane) (PFDMG) blocks.[33] Using rectangular platelets or homopolymer surfaces as seeds for unimer addition results in scarf-like micelles and micellar brush layers, respectively.[33] Furthermore, the possibility to cross-link PI corona chains allows the production of new architectures, *e.g.* scarf-like micelles, in which the PFDMS-*b*-PDMS center of the rectangular precursor platelet is selectively dissolved in THF whereas the surrounding crosslinked PFDMS-*b*-PI part remains intact (Figure 1.4C).[62] Recently, monodisperse short cylindrical micelles were reported to undergo end-to-end coupling when provided with block copolymer "glue", *i.e.* PFDMS homopolymer or block copolymers with comparably high PFDMS block ratios.[65] Besides the block-type architectures, the crystallization of mixtures of PFDMS-*b*-PDMS and PFDMS-*b*-PI resulted in *co*-micelles in which both block copolymers contributed equally to the formed micelles.[66]

1.2.5. Poly(3-hexylthiophene)

Only lately, Winnik, Manners and coworkers succeeded in the preparation of cylindrical micelles from P3HT-*b*-PDMS diblock copolymers.[67] In the same way as for PFS-containing diblock copolymers, the preparation of small seed micelles and subsequent addition of unimers resulted in controlled cylindrical lengths up to 300 nm with PDIs down to 1.02. However, the production of even longer micelles was unsuccessful showing that self-assembly in this case does not work exactly as well as for crystallizable PFS blocks.

1.2.6. Enantiopure Polylactides

For the sake of clarity, it has to be mentioned that the enantiopure polymers poly(L-lactide) (PLLA) and poly(D-lactide) (PDLA) are capable of crystallization, in either pure form or by stereocomplexation of equimolar mixtures. Inherently racemic polylactide blocks on the other hand are completely amorphous.

In 2001, Kimura *et al.* observed the aggregation of nanostructured bands from PLLA-*b*-PEO and PLLA-*b*-PEO-*b*-PLLA di- and triblock copolymers upon heat treatment of previously

formed discoid structures on mica substrates.[68] Later, the formation of rod-like structures in solution was reported for stereocomplexes of PLLA-*b*-PEO and PDLA-*b*-PEO in water.[69] Cylindrical micelles were also produced from triblock copolymers of PEO, PCL and polylactide in water, when crystallizable PLLA was used, while the use of racemic polylactide resulted in spherical micelles.[70] Bouteiller, Reiter and coworkers further showed that in the formation of elongated worm-like objects from mixtures of PDLA-*b*-PCL and PLLA-*b*-PCL, only stereo complexation occurs and no unspecific aggregation of the homochiral block copolymers.[71] Recent work by O'Reilly's group on PLLA-*b*-PAA (PAA: poly(acrylic acid)) diblock copolymers resulted in cylindrical micelles by dissolution in water at temperatures above the glass transition temperature of PLLA.[72] By heating to 65 °C for different time spans the length of these cylinders could be controlled.

1.2.7. Polyethylene

As the thesis at hand deals with the structure formation induced by PE crystallization, this section gives a detailed overview of micellar morphologies assembled from PE-containing block copolymers, even though one-dimensional structures up to now represented the rare exception.

Together with PEO-*b*-PS diblock copolymers also PE-*b*-PEP (PEP: poly(ethylene-*alt*-propylene)) was investigated by Lin and Gast in 1996, who studied their aggregation behavior to platelets in decane solution finding the equilibrium platelet thickness and the tethered chain density profile in compliance with SCF calculations. Richter *et al.* varied composition and molecular weight of these block copolymers and again observed platelet formation in all cases.[25] Although these platelets underwent macroaggregation to needle-like structures, this phenomenon is not comparable to the formation of one-dimensional structures *via* crystallization as the van der Waals attraction between the PEP brush layers on the platelet surface is responsible for this supramicellar aggregation. Platelets like these were proposed as additives in diesel fuel as they take up longer alkanes, *e.g.* decane, that otherwise can clog the filters of engines at low temperatures.[73] For the same purpose, a study on the self-assembly of different poly(*co*-olefins) in decane was performed.[74] Here, PE-PEP diblock copolymer stars formed one-dimensional structures when the PE blocks were situated in the center, whereas platelets were observed if the PE blocks formed the outer

rim of the stars. Furthermore, a tapered PE-PEP copolymer and a random poly(ethylene-*stat*-butylene) copolymer showed signs of one-dimensional structure formation. In an investigation of miktoarm star polymers with PE and PEP arms Prager and coworkers again exclusively observed platelet formation.[75] A mixture of platelets and small disk-like micelles were observed for slow cooling of PE-*b*-PDMS-*b*-PE in toluene (Figure 1.5A).[76] Recently, interesting semiconductor-insulator-semiconductor lozenge-shaped platelets were formed by Yang *et al.* assembling poly(3-butylthiophene)-*b*-PE in *o*-dichlorobenzene solution.
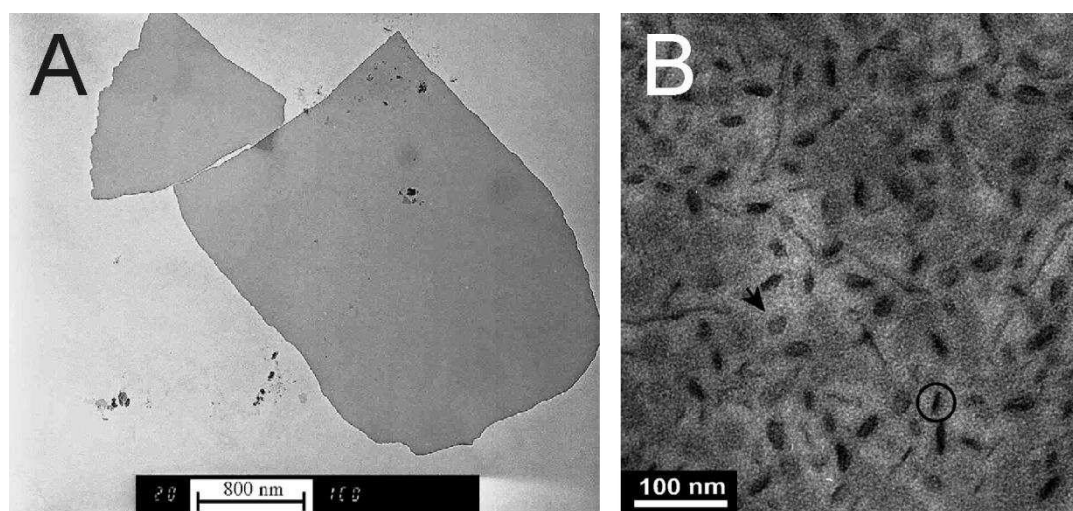

Figure 1.5. (A) TEM micrograph of platelets formed by PE-*b*-PDMS-*b*-PE.[76] (B) *Cryo*-TEM of disk-like micelles coexisting with few one-dimensional structures formed by PE-*b*-PDMA. Highlighted examples show micelles viewed edge-on (circle) or face-on (arrow).[77]

In contrast to structure formation in solvents that are able to dissolve PE at elevated temperatures, the self-assembly of PE-containing block copolymers with hydrophilic second blocks like PEO,[78] poly(*N*,*N*-dimethyl acrylamide) (PDMA)[77] and poly(oligo(ethylene glycol) methacrylate) (POEGMA)[79] in water usually results in spherical or small disk-like aggregates with anisotropic PE cores. Notably, after the self-assembly of PE-*b*-PDMA in water at 120 °C a few one-dimensional objects were found coexisting with the vast majority of disk-shaped aggregates (Figure 1.5B).[77]

1.2.8. General Considerations on Crystallization-Induced Self-Assembly

In compliance with the predictions made by Vilgis and Halperin,[22] the morphologies formed by the self-assembly of block copolymers with crystallizable blocks can be tuned by the block ratios. Increasing the fraction of the corona forming block hereby leads to structures with higher curvature (cylindrical, spherical micelles) in order to accommodate the space

requirements of the corona chains, as shown for block copolymers containing PFDMS[58], PCL[44] and PEO[41] as the crystallizing blocks. For comparably long corona blocks, however, the so-called "over-spilling" effect can prevent the formation of morphologies with low curvature (platelets) even though the block ratios would suggest their stability.[34,44] Here, the core of the initially formed spherical micelles is shielded by the bulky corona chains and, thus, further growth of these structures is prohibited.
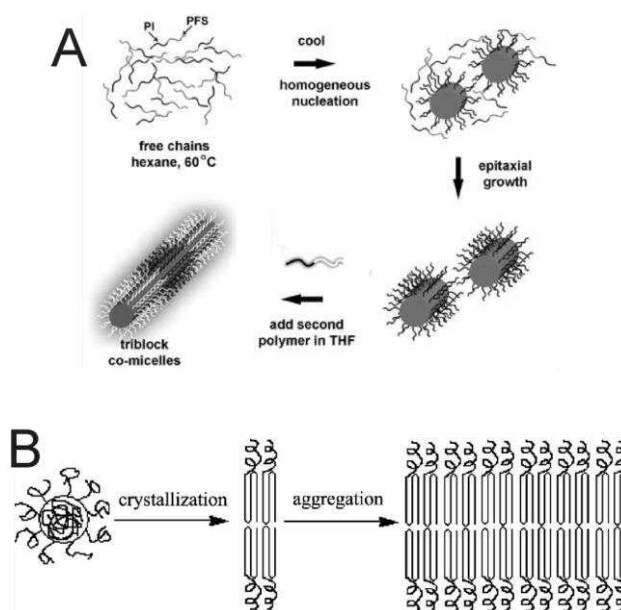
Figure 1.6. Proposed mechanisms for crystallization-induced self-assembly of 1D and 2D structures: (A) nucleation and growth process[29] and (B) the aggregation of initially formed small micelles with crystalline cores.[35]

Another important parameter influencing the structure formation is the crystallization temperature. Studies on PEO-*b*-PB diblock copolymers in *n*-heptane showed that smaller structures (spheres or cylinders) are favored if the solution is quenched in liquid nitrogen whereas structure formation at the crystallization temperature also leads to larger aggregates, *e.g.* lamellar and platelet-like structures for PEO blocks of sufficient lengths.[41,42] A similar observation was made for PCL-*b*-PEO diblock copolymers with comparably short corona chains, in which PCL is crystallized in water at 20 °C forming lamellar micelles.[45] When isothermal crystallization was conducted at 0 °C, spheres and cylinders were formed. Unexpectedly, the behavior was reversed if the PEO corona chains were significantly longer. For crystallization at 20 °C these diblock copolymers showed the tendency to form smaller micelles, whereas larger micelles were formed at 0 °C. In this case, the tethering density of

the corona chains was assumed to control the morphology rather than the perfection of the PCL crystals.

For the formation of one- (1D) and two-dimensional (2D) structures by crystallization-induced self-assembly, different mechanisms are discussed (Figure 1.6). The aggregation of initially formed small crystalline micelles was proposed in the formation of 1D structures from PE-*b*-PEP diblock copolymer stars with PE in the star's center[74] as well as for 2D platelets formed from PEO-*b*-PBO.[34,35] On the other hand, 1D structures formed by PFDMS containing block copolymers supposedly grow *via* the addition of unimers to a small number of initially formed crystalline nuclei (nucleation and growth process).[29] However, these processes are far from being fully understood and further research is needed to expand the theoretical background and to gain a better control of this unique type of self-assembly.

1.3. Compartmentalized Nanostructures
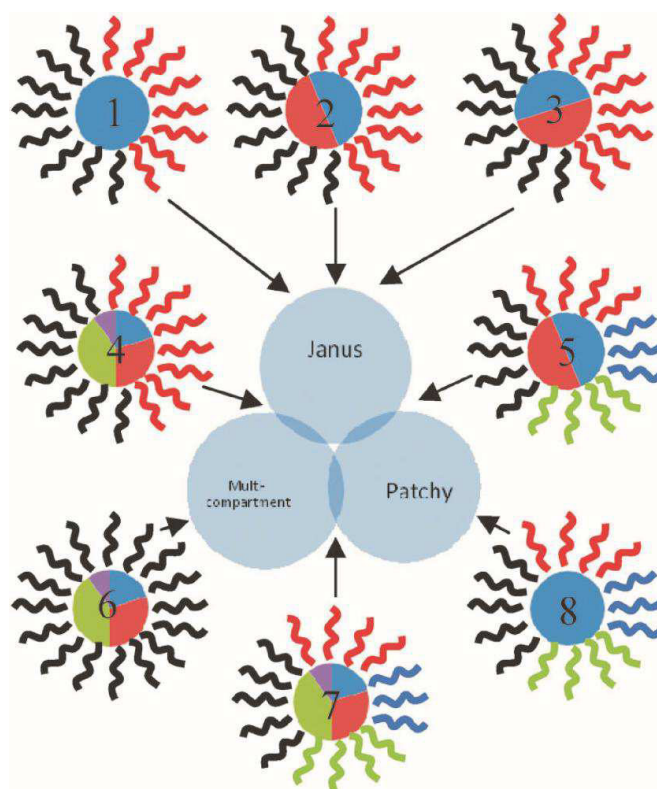
**Figure 1.7.** Illustration of micellar structures with a compartmentalization in the core and/or corona.[80]

By the use of triblock terpolymers instead of diblock copolymers the variety of accessible architectures can be increased even further (Figure 1.7).[81,82] While the solution self-assembly

of a diblock copolymer by rendering one block insoluble commonly can only result in ordinary core-corona micelles, triblock terpolymers are able to form structures with an additional compartmentalization in the core (two insoluble and one soluble block) or the corona (one insoluble and two soluble blocks).[80] These nanoparticles exhibit different chemical environments in close proximity and defined spatial confinement, which renders them potential candidates for the delivery of multiple incompatible payloads, *e.g.* drugs, or applications in photonics, sensors and nanocatalysis.[83,84] Over the past few years, the formation of multicompartment (core) micelles (MCMs) was investigated in more detail[83] and first steps towards their controlled preparation were undertaken.[85] The produced structures can be subdivided into spherical MCMs consisting of a continuous core decorated with multiple surface compartments[85-88] and linear MCMs with alternating core compartments.[85,89,90] Core-shell-corona micelles with the second insoluble block completely surrounding the inner part of the core exhibit different compartments in the cores, too.[91-95] However, as the inner compartment cannot be directly accessed from the solvent, there is ongoing discussion whether or not these structures should be regarded multicompartment micelles in view of application as carriers of multiple payloads.[83,96] The following sections now will concentrate on surface-compartmentalized particles. In corona- or surface-compartmentalized nanostructures (SCNs) one can mainly distinguish between two different kinds of particles: Janus particles and patchy particles.

1.3.1. Janus Particles

Janus particles, named after the two-faced Roman god, contain exactly two opposite hemishells of different chemistry and/or polarity. Over the last two decades several synthetic approaches for their production were established.[97,98] In 1988, Janus "pearls", *i.e.* glass beads with a hydrophilic and a hydrophobic side were produced by immobilization of the particles on a substrate followed by anchoring alkyl chains to the free side.[99,100] Similar two-dimensional approaches were also used by other groups producing PS latex particles with a gold or platinum layer on one side.[101,102] Granick's group transferred this technique to the surface of wax droplets in a Pickering emulsion with water to enhance production output.[103] In addition, microfluidic devices[104,105] and electrified co-jetting[106] were used for the fabrication of dense, solid Janus particles. Most of the particles produced with these techniques exhibit spherical shapes. Cohen Stuart *et al.* produced self-assembled Janus disks

using a mixture of an AB and a CD diblock copolymer with oppositely charged B and C blocks.[107,108] In this case, B and C form a complex coacervate core with microphase-separated A and D corona blocks on opposite sides. The Müller group was able to synthesize spherical,[109] cylindrical[110] and disk-like[111] Janus micelles by cross-linking the polybutadiene (PB) phase in the corresponding lamella-sphere, lamella-cylinder and lamella-lamella bulk structures of PS-*b*-PB-*b*-PMMA and PS-*b*-PB-*b*-P*t*BMA (P*t*BMA: poly(*tert*-butyl methacrylate)) triblock terpolymer films (Figure 1.8). More recently, three different morphologies, cylindrical, ribbon-like and disk-like, of Janus particles could be produced from a single P*t*BS-*b*-PB-*b*-P*t*BMA (P*t*BS: poly(*tert*-butoxystyrene)) triblock terpolymer by altering the swelling and cross-linking conditions.[112]
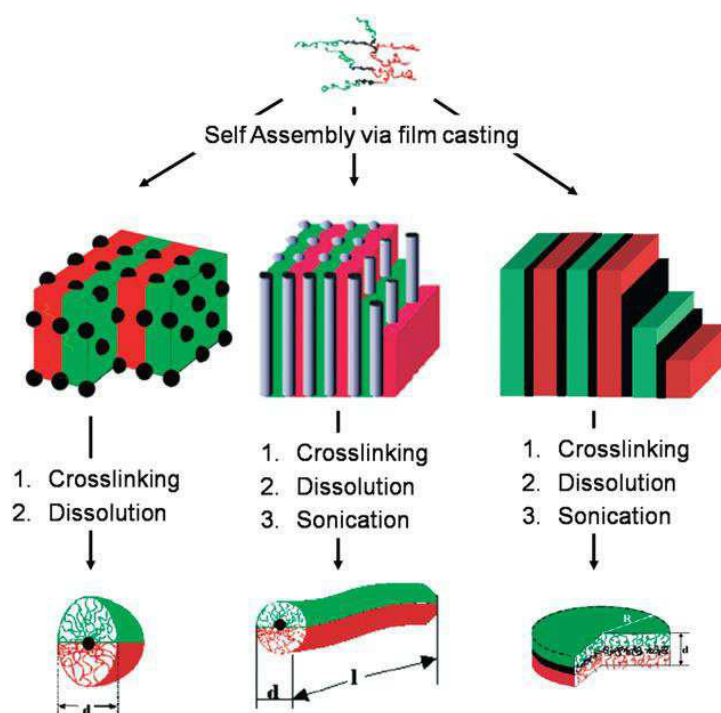
Figure 1.8. Illustration of the production of spherical, cylindrical and disk-like Janus particles by crosslinking the butadiene segments of suitable triblock terpolymer bulk films.[97]

1.3.2. Patchy Particles

In contrast to Janus particles, patchy particles consisting of multiple surface compartments are less intensively investigated.[84,113] One example are patchy "Janus" particles from McConnell *et al.* produced by electrostatic assembly of gold nanoparticles on immobilized silica particles.[114] Granick's group recently self-assembled a kagome lattice from spherical particles with two hydrophobic surface patches (Figure 1.9).[115] This work is a promising

example of the unique properties arising from defined surface compartments that may act as "binding sites" comparable to those in atoms. Kuo and coworkers reported spherical block copolymer micelles from the self-assembly of AB and CD block copolymers by hydrogen bonding between B and C blocks that bear a microphase-separated corona of A and D.[116] Liu's group was very active in the fabrication of patchy micelles with spherical, cylindrical, tubular and vesicular structures using triblock terpolymers in mid-block-selective solvents or solvent mixtures.[117,118] In a specific solvent mixture, even double and triple helices consisting of patchy cylinders were obtained, showing that these particles exhibit the potential of further self-assembly into fascinating superstructures.[119,120] However, these one-dimensional patchy micelles represent a rare exception, as the vast majority of the produced patchy particles is spherical in nature.
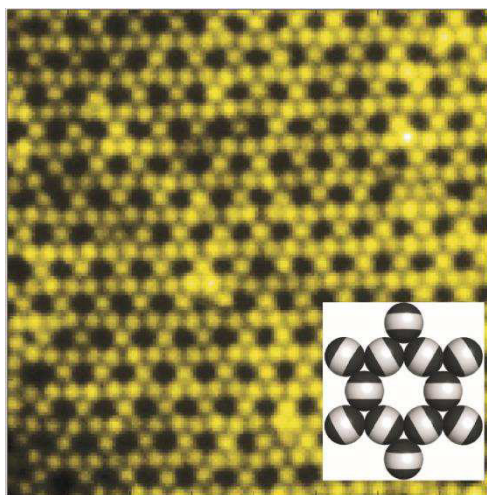
Figure 1.9. Kagome lattice assembled from spherical particles with two hydropobized surface patches.[115]

1.3.3. Surface-Compartmentalized Nanostructures as Surfactants

Besides the ability to form hierarchical assemblies, a multitude of applications for SCNs are under investigation, such as switchable devices in displays,[121] nanosensors[122] or self-motile particles[101]. Certainly one of the most intriguing features of SCNs is the combination of the Pickering effect[123,124] of small particular matter with the amphiphilicity of ordinary surfactants. Binks and Fletcher predicted an up to 3-fold increase in surface activity for Janus particles with respect to those with a homogeneous surface.[125] Inspired by this work, Krausch *et al.* studied the interfacial tension of Janus-type gold/iron oxide nanoparticles at the hexane-water interface using pendant-drop tensiometry.[126] The ability of the Janus

particles to reduce the interfacial tension was found to be significantly higher than for homogeneous nanoparticles of either gold or iron oxide. In 2007, the Müller group investigated the behavior of block terpolymer based Janus discs at the cyclohexane-water interface and experienced a much higher reduction of the interfacial tension with respect to the corresponding single triblock terpolymer chains.[111] Recently, the interfacial activity of Janus cylinders at the dioxane/perfluorooctane interface was confirmed to be higher than that of corresponding terpolymer unimers as well as that of comparable cylinders with a homogeneous corona.[127]

1.4. Objective of the Thesis

In earlier work, the self-assembly of PS-*b*-PE-*b*-PMMA triblock terpolymers in organic media was investigated. Unexpected at this time, these polymers formed worm-like micelles, which was rarely observed before in the crystallization-induced self-assembly of PE-containing block copolymers.[128] Consisting of incompatible PS and PMMA chains, the corona of these micelles showed the tendency to microphase separate. Even though, this discovery opened up a new route towards one-dimensional surface-compartmentalized nanostructures, the mechanisms behind this self-assembly and the key parameters controlling it, were only marginally understood. Thus, the main objective of this doctoral thesis was to elucidate the mechanism of structure formation in order to gain control over this process.

In 2007, highly recognized work of Winnik and Manners *et al.* highlighted the unprecedented structural control that can be achieved by the solution self-assembly of block copolymers bearing crystallizable PFDMS blocks, *e.g.* length control and the formation of block *co-*micelles *via* a mechanism of "living" self-assembly.[29] However, due to the sophisticated metal-containing polymer block, the production of these block copolymers is expensive in labor and not easy to upscale. Hence, the applicability of these processes to block copolymers comprising "everyday" crystallizable polymer blocks, such as PE, would mean a major breakthrough.

Furthermore, manufacturing surface-compartmentalized structures with feature sizes in the nanometer range is tedious and, as discussed in section 1.3.2., convenient pathways towards stable, elongated structures hardly exist. Therefore, the production and characterization of

one-dimensional micelles with defined corona patchiness using crystallization-driven self-assembly was another aim of this thesis. Even though patchy micelles like these should benefit from their inhomogeneous coronas in terms of interfacial activity, no such study was conducted up to now. Other envisaged applications are templates for the directed incorporation of metal nanoparticles, dyes and/or drugs in defined spatial confinement or the controlled formation of hierarchically ordered mesoscopic superstructures. Thus, the availability of simple methods to produce patchy particles in a time- and cost-effective way might boost the development in various research disciplines.

1.5. References

(1)   Förster, S.; Konrad, M. *J. Mater. Chem.* **2003**, *13*, 2671.

(2)   Haberkorn, N.; Lechmann, M. C.; Sohn, B. H.; Char, K.; Gutmann, J. S.; Theato, P. *Macromol. Rapid Commun.* **2009**, *30*, 1146.

(3)   Motornov, M.; Roiter, Y.; Tokarev, I.; Minko, S. *Prog. Polym. Sci.* **2010**, *35*, 174.

(4)   Ruzette, A. V.; Leibler, L. *Nat. Mater.* **2005**, *4*, 19.

(5)   Rodríguez-Hernández, J.; Chécot, F.; Gnanou, Y.; Lecommandoux, S. *Prog. Polym. Sci.* **2005**, *30*, 691.

(6)   Whitesides, G. M.; Grzybowski, B. *Science* **2002**, *295*, 2418.

(7)   Stupp, S. I.; LeBonheur, V.; Walker, K.; Li, L. S.; Huggins, K. E.; Keser, M.; Amstutz, A. *Science* **1997**, *276*, 384.

(8)   Matsen, M. W.; Bates, F. S. *Macromolecules* **1996**, *29*, 1091.

(9)   Förster, S.; Khandpur, A. K.; Zhao, J.; Bates, F. S.; Hamley, I. W.; Ryan, A. J.; Bras, W. *Macromolecules* **1994**, *27*, 6922.

(10)   Khandpur, A. K.; Förster, S.; Bates, F. S.; Hamley, I. W.; Ryan, A. J.; Bras, W.; Almdal, K.; Mortensen, K. *Macromolecules* **1995**, *28*, 8796.

(11)   Förster, S.; Plantenberg, T. *Angew. Chem. Int. Ed.* **2002**, *41*, 688.

(12)   Riess, G. *Prog. Polym. Sci.* **2003**, *28*, 1107.

(13)   Bhargava, P.; Tu, Y.; Zheng, J. X.; Xiong, H.; Quirk, R. P.; Cheng, S. Z. D. *J. Am. Chem. Soc.* **2007**, *129*, 1113.

(14)   Zhang, L.; Eisenberg, A. *Science* **1995**, *268*, 1728.

(15)   Zhang, L.; Yu, K.; Eisenberg, A. *Science* **1996**, *272*, 1777.

(16)   Antonietti, M.; Förster, S. *Adv. Mater.* **2003**, *15*, 1323.

(17)   Discher, D. E.; Eisenberg, A. *Science* **2002**, *297*, 967.

(18)   Won, Y.-Y.; Davis, H. T.; Bates, F. S. *Science* **1999**, *283*, 960.

(19)   Jain, S.; Bates, F. S. *Science* **2003**, *300*, 460.

(20)   Borsali, R.; Minatti, E.; Putaux, J.-L.; Schappacher, M.; Deffieux, A.; Viville, P.; Lazzaroni, R.; Narayanan, T. *Langmuir* **2003**, *19*, 6.

(21)   Yan, X.; Liu, G.; Li, H. *Langmuir* **2004**, *20*, 4677.

(22)   Vilgis, T.; Halperin, A. *Macromolecules* **1991**, *24*, 2090.

(23)   Lin, E. K.; Gast, A. P. *Macromolecules* **1996**, *29*, 4432.

(24)   Gast, A. P.; Vinson, P. K.; Cogan-Farinas, K. A. *Macromolecules* **1993**, *26*, 1774.

(25)   Richter, D.; Schneiders, D.; Monkenbusch, M.; Willner, L.; Fetters, L. J.; Huang, J. S.; Lin, M.; Mortensen, K.; Farago, B. *Macromolecules* **1997**, *30*, 1053.

(26)   Dröscher, M.; Smith, T. L. *Macromolecules* **1982**, *15*, 442.

(27)   Cogan, K. A.; Gast, A. P. *Macromolecules* **1990**, *23*, 745.

(28)   Lazzari, M.; Lopez-Quintela, M. A. *Macromol. Rapid Commun.* **2009**, *30*, 1785.

(29)   Wang, X.; Guerin, G.; Wang, H.; Wang, Y.; Manners, I.; Winnik, M. A. *Science* **2007**, *317*, 644.

(30)   Gilroy, J. B.; Gädt, T.; Whittell, G. R.; Chabanne, L.; Mitchels, J. M.; Richardson, R. M.; Winnik, M. A.; Manners, I. *Nat. Chem.* **2010**, *2*, 566.

(31)   Qian, J.; Guerin, G.; Lu, Y.; Cambridge, G.; Manners, I.; Winnik, M. A. *Angew. Chem. Int. Ed.* **2011**, *50*, 1622.

(32)   Wang, H.; Lin, W.; Fritz, K. P.; Scholes, G. D.; Winnik, M. A.; Manners, I. *J. Am. Chem. Soc.* **2007**, *129*, 12924.

(33)   Gädt, T.; Ieong, N. S.; Cambridge, G.; Winnik, M. A.; Manners, I. *Nat. Mater.* **2009**, *8*, 144.

(34)   Xu, J.-T.; Fairclough, J. P. A.; Mai, S.-M.; Ryan, A. J. *J. Mater. Chem.* **2003**, *13*, 2740.

(35)   Xu, J.-T.; Jin, W.; Liang, G.-D.; Fan, Z.-Q. *Polymer* **2005**, *46*, 1709.

(36)   Chen, W. Y.; Li, C. Y.; Zheng, J. X.; Huang, P.; Zhu, L.; Ge, Q.; Quirk, R. P.; Lotz, B.; Deng, L.; Wu, C.; Thomas, E. L.; Cheng, S. Z. D. *Macromolecules* **2004**, *37*, 5292.

(37)   Zheng, J. X.; Xiong, H.; Chen, W. Y.; Lee, K.; Van Horn, R. M.; Quirk, R. P.; Lotz, B.; Thomas, E. L.; Shi, A.-C.; Cheng, S. Z. D. *Macromolecules* **2006**, *39*, 641.

(38)   Huang, W.; Luo, C.; Zhang, J.; Yu, K.; Han, Y. *Macromolecules* **2007**, *40*, 8022.

(39)   Mihut, A. M.; Chiche, A.; Drechsler, M.; Schmalz, H.; Di Cola, E.; Krausch, G.; Ballauff, M. *Soft Matter* **2009**, *5*, 208.

(40)   Mihut, A. M.; Drechsler, M.; Möller, M.; Ballauff, M. *Macromol. Rapid Commun.* **2010**, *31*, 449.

(41)   Mihut, A. M.; Crassous, J. J.; Schmalz, H.; Drechsler, M.; Ballauff, M. *Soft Matter* **2012**, *8*, 3163.

(42)   Mihut, A. M.; Crassous, J. J.; Schmalz, H.; Ballauff, M. *Colloid Polym. Sci.* **2010**, *288*, 573.

(43)   Chan, S.-C.; Kuo, S.-W.; Lu, C.-H.; Lee, H.-F.; Chang, F.-C. *Polymer* **2007**, *48*, 5059.

(44)   Du, Z.-X.; Xu, J.-T.; Fan, Z.-Q. *Macromolecules* **2007**, *40*, 7633.

(45)   Du, Z.-X.; Xu, J.-T.; Fan, Z.-Q. *Macromol. Rapid Commun.* **2008**, *29*, 467.

(46)   He, W. N.; Xu, J. T.; Du, B. Y.; Fan, Z. Q.; Wang, X. S. *Macromol. Chem. Phys.* **2010**, *211*, 1909.

(47)   Lazzari, M.; Scalarone, D.; Hoppe, C. E.; Vazquez-Vazquez, C.; Lopez-Quintela, M. A. *Chem. Mater.* **2007**, *19*, 5818.

(48)   Lazzari, M.; Scalarone, D.; Vazquez-Vazquez, C.; Lopez-Quintela, M. A. *Macromol. Rapid Commun.* **2008**, *29*, 352.

(49)   Massey, J.; Power, K. N.; Manners, I.; Winnik, M. A. *J. Am. Chem. Soc.* **1998**, *120*, 9533.

(50)   Massey, J. A.; Temple, K.; Cao, L.; Rharbi, Y.; Raez, J.; Winnik, M. A.; Manners, I. *J. Am. Chem. Soc.* **2000**, *122*, 11577.

(51)   Resendes, R.; Massey, J. A.; Dorn, H.; Power, K. N.; Winnik, M. A.; Manners, I. *Angew. Chem. Int. Ed.* **1999**, *38*, 2570.

(52)   Resendes, R.; Massey, J. A.; Temple, K.; Cao, L.; Power-Billard, K. N.; Winnik, M. A.; Manners, I. *Chem. Eur. J.* **2001**, *7*, 2414.

(53)   Raez, J.; Barjovanu, R.; Massey, J. A.; Winnik, M. A.; Manners, I. *Angew. Chem. Int. Ed.* **2000**, *39*, 3862.

(54) Raez, J.; Manners, I.; Winnik, M. A. *J. Am. Chem. Soc.* **2002**, *124*, 10381.

(55) Raez, J.; Tomba, J. P.; Manners, I.; Winnik, M. A. *J. Am. Chem. Soc.* **2003**, *125*, 9546.

(56) Guérin, G.; Raez, J.; Manners, I.; Winnik, M. A. *Macromolecules* **2005**, *38*, 7819.

(57) Wang, X. S.; Winnik, M. A.; Manners, I. *Macromolecules* **2002**, *35*, 9146.

(58) Cao, L.; Manners, I.; Winnik, M. A. *Macromolecules* **2002**, *35*, 8258.

(59) Korczagin, I.; Hempenius, M. A.; Fokkink, R. G.; Cohen Stuart, M. A.; Al-Hussein, M.; Bomans, P. H. H.; Frederik, P. M.; Vancso, G. J. *Macromolecules* **2006**, *39*, 2306.

(60) Wang, H.; Winnik, M. A.; Manners, I. *Macromolecules* **2007**, *40*, 3784.

(61) Wang, X.; Winnik, M. A.; Manners, I. *Macromolecules* **2005**, *38*, 1928.

(62) Rupar, P. A.; Cambridge, G.; Winnik, M. A.; Manners, I. *J. Am. Chem. Soc.* **2011**, *133*, 16947.

(63) Wang, H.; Patil, A. J.; Liu, K.; Petrov, S.; Mann, S.; Winnik, M. A.; Manners, I. *Adv. Mater.* **2009**, *21*, 1805.

(64) He, F.; Gädt, T.; Manners, I.; Winnik, M. A. *J. Am. Chem. Soc.* **2011**, *133*, 9095.

(65) Mohd Yusoff, S. F.; Gilroy, J. B.; Cambridge, G.; Winnik, M. A.; Manners, I. *J. Am. Chem. Soc.* **2012**, *133*, 11220.

(66) Cambridge, G.; Guerin, G.; Manners, I.; Winnik, M. A. *Macromol. Rapid Commun.* **2010**, *31*, 934.

(67) Patra, S. K.; Ahmed, R.; Whittell, G. R.; Lunn, D. J.; Dunphy, E. L.; Winnik, M. A.; Manners, I. *J. Am. Chem. Soc.* **2011**, *133*, 8842.

(68) Fujiwara, T.; Miyamoto, M.; Kimura, Y.; Iwata, T.; Doi, Y. *Macromolecules* **2001**, *34*, 4043.

(69) Slager, J.; Brizzolara, D.; Cantow, H. J.; Domb, A. J. *Polym. Adv. Technol.* **2005**, *16*, 667.

(70) Zhang, J.; Wang, L.-Q.; Wang, H.; Tu, K. *Biomacromolecules* **2006**, *7*, 2492.

(71) Portinha, D.; Boué, F.; Bouteiller, L.; Carrot, G.; Chassenieux, C.; Pensec, S.; Reiter, G. *Macromolecules* **2007**, *40*, 4037.

(72) Petzetakis, N.; Dove, A. P.; O'Reilly, R. K. *Chem. Sci.* **2011**, *2*, 955.

(73) Monkenbusch, M.; Schneiders, D.; Richter, D.; Willner, L.; Leube, W.; Fetters, L. J.; Huang, J. S.; Lin, M. *Physica B* **2000**, *276-278*, 941.

(74) Schwahn, D.; Richter, D.; Wright, P. J.; Symon, C.; Fetters, L. J.; Lin, M. *Macromolecules* **2002**, *35*, 861.

(75) Ramzi, A.; Prager, M.; Richter, D.; Efstratiadis, V.; Hadjichristidis, N.; Young, R. N.; Allgaier, J. B. *Macromolecules* **1997**, *30*, 7171.

(76) Wang, J.; Horton, J. H.; Liu, G.; Lee, S.-Y.; Shea, K. J. *Polymer* **2007**, *48*, 4123.

(77) Yin, L. G.; Hillmyer, M. A. *Macromolecules* **2011**, *44*, 3021.

(78) Li, T.; Wang, W. J.; Liu, R.; Liang, W. H.; Zhao, G. F.; Li, Z.; Wu, Q.; Zhu, F. M. *Macromolecules* **2009**, *42*, 3804.

(79) Wang, W.; Liu, R.; Li, Z.; Meng, C.; Wu, Q.; Zhu, F. *Macromol. Chem. Phys.* **2010**, *211*, 1452.

(80) Du, J.; O'Reilly, R. K. *Chem. Soc. Rev.* **2011**, *40*, 2402.

(81) Fustin, C. A.; Abetz, V.; Gohy, J. F. *Eur. Phys. J. E* **2005**, *16*, 291.

(82) Hadjichristidis, N.; Iatrou, H.; Pitsikalis, M.; Pispas, S.; Avgeropoulos, A. *Prog. Polym. Sci.* **2005**, *30*, 725.

(83) Moughton, A. O.; Hillmyer, M. A.; Lodge, T. P. *Macromolecules* **2012**, *45*, 2.

(84) Pawar, A. B.; Kretzschmar, I. *Macromol. Rapid Commun.* **2010**, *31*, 150.

(85) Gröschel, A. H.; Schacher, F. H.; Schmalz, H.; Borisov, O. V.; Zhulina, E. B.; Walther, A.; Müller, A. H. E. *Nat. Commun.* **2012**, *3*, 710.

(86) Von Berlepsch, H.; Böttcher, C.; Skrabania, K.; Laschewsky, A. *Chem. Commun.* **2009**, 2290.

(87) Marsat, J.-N.; Heydenreich, M.; Kleinpeter, E.; Berlepsch, H. V.; Böttcher, C.; Laschewsky, A. *Macromolecules* **2011**, *44*, 2092.

(88) Walther, A.; Barner-Kowollik, C.; Müller, A. H. E. *Langmuir* **2010**, *26*, 12237.

(89) Fang, B.; Walther, A.; Wolf, A.; Xu, Y.; Yuan, J.; Müller, A. H. E. *Angew. Chem. Int. Ed.* **2009**, *48*, 2877.

(90) Dupont, J.; Liu, G. J. *Soft Matter* **2010**, *6*, 3654.

(91) Yu, G. E.; Eisenberg, A. *Macromolecules* **1998**, *31*, 5546.

(92) Gohy, J. F.; Willet, N.; Varshney, S.; Zhang, J. X.; Jerome, R. *Angew. Chem. Int. Ed.* **2001**, *40*, 3214.

(93) Kempe, K.; Hoogenboom, R.; Hoeppener, S.; Fustin, C.-A.; Gohy, J.-F.; Schubert, U. S. *Chem. Commun.* **2010**, *46*, 6455.

(94) Hu, J.; Njikang, G.; Liu, G. *Macromolecules* **2008**, *41*, 7993.

(95) Schacher, F.; Walther, A.; Müller, A. H. E. *Langmuir* **2009**, *25*, 10962.

(96) Lutz, J. F.; Laschewsky, A. *Macromol. Chem. Phys.* **2005**, *206*, 813.

(97) Walther, A.; Müller, A. H. E. *Soft Matter* **2008**, *4*, 663.

(98) Wurm, F.; Kilbinger, A. F. M. *Angew. Chem. Int. Ed.* **2009**, *48*, 8412.

(99) Casagrande, C.; Veyssie, M. *C. R. Acad. Sci. Ser. 2* **1988**, *306*, 1423.

(100) Casagrande, C.; Fabre, P.; Raphael, E.; Veyssie, M. *Europhys. Lett.* **1989**, *9*, 251.

(101) Howse, J. R.; Jones, R. A. L.; Ryan, A. J.; Gough, T.; Vafabakhsh, R.; Golestanian, R. *Phys. Rev. Lett.* **2007**, *99*, 4.

(102) Paunov, V. N.; Cayre, O. J. *Adv. Mater.* **2004**, *16*, 788.

(103) Hong, L.; Jiang, S.; Granick, S. *Langmuir* **2006**, *22*, 9495.

(104) Dendukuri, D.; Pregibon, D. C.; Collins, J.; Hatton, T. A.; Doyle, P. S. *Nat. Mater.* **2006**, *5*, 365.

(105) Nie, Z.; Li, W.; Seo, M.; Xu, S.; Kumacheva, E. *J. Am. Chem. Soc.* **2006**, *128*, 9408.

(106) Roh, K.-H.; Martin, D. C.; Lahann, J. *Nat. Mater.* **2005**, *4*, 759.

(107) Voets, I. K.; de Keizer, A.; de Waard, P.; Frederik, P. M.; Bomans, P. H. H.; Schmalz, H.; Walther, A.; King, S. M.; Leermakers, F. A. M.; Cohen Stuart, M. A. *Angew. Chem. Int. Ed.* **2006**, *45*, 6673.

(108) Voets, I. K.; Fokkink, R.; Hellweg, T.; King, S. M.; de Waard, P.; de Keizer, A.; Cohen Stuart, M. A. *Soft Matter* **2009**, *5*, 999.

(109) Erhardt, R.; Böker, A.; Zettl, H.; Kaya, H.; Pyckhout-Hintzen, W.; Krausch, G.; Abetz, V.; Müller, A. H. E. *Macromolecules* **2001**, *34*, 1069.

(110) Liu, Y.; Abetz, V.; Müller, A. H. E. *Macromolecules* **2003**, *36*, 7894.

(111) Walther, A.; André, X.; Drechsler, M.; Abetz, V.; Müller, A. H. E. *J. Am. Chem. Soc.* **2007**, *129*, 6187.

(112) Wolf, A.; Walther, A.; Müller, A. H. E. *Macromolecules* **2011**, *44*, 9221.

(113) Glotzer, S. C.; Solomon, M. J. *Nat. Mater.* **2007**, *6*, 557.

(114) McConnell, M. D.; Kraeutler, M. J.; Yang, S.; Composto, R. J. *Nano Lett.* **2010**, *10*, 603.

(115) Chen, Q.; Bae, S. C.; Granick, S. *Nature* **2011**, *469*, 381.

(116)   Kuo, S.-W.; Tung, P.-H.; Lai, C.-L.; Jeong, K.-U.; Chang, F.-C. *Macromol. Rapid Commun.* **2008**, *29*, 229.

(117)   Hoppenbrouwers, E.; Li, Z.; Liu, G. *Macromolecules* **2003**, *36*, 876.

(118)   Njikang, G.; Han, D. H.; Wang, J.; Liu, G. J. *Macromolecules* **2008**, *41*, 9727.

(119)   Dupont, J.; Liu, G. J.; Niihara, K.; Kimoto, R.; Jinnai, H. *Angew. Chem. Int. Ed.* **2009**, *48*, 6144.

(120)   Dou, H.; Liu, G.; Dupont, J.; Hong, L. *Soft Matter* **2010**, *6*, 4214.

(121)   Nisisako, T.; Torii, T.; Takahashi, T.; Takizawa, Y. *Adv. Mater.* **2006**, *18*, 1152.

(122)   Behrend, C. J.; Anker, J. N.; Kopelman, R. *Appl. Phys. Lett.* **2004**, *84*, 154.

(123)   Pickering, S. U. *J. Chem. Soc.* **1907**, *91*, 2001.

(124)   Ramsden, W. *Proc. R. Soc. London* **1903**, *72*, 156.

(125)   Binks, B. P.; Fletcher, P. D. I. *Langmuir* **2001**, *17*, 4708.

(126)   Glaser, N.; Adams, D. J.; Böker, A.; Krausch, G. *Langmuir* **2006**, *22*, 5227.

(127)   Ruhland, T. M.; Gröschel, A. H.; Walther, A.; Müller, A. H. E. *Langmuir* **2011**, *27*, 9807.

(128)   Schmalz, H.; Schmelz, J.; Drechsler, M.; Yuan, J.; Walther, A.; Schweimer, K.; Mihut, A. M. *Macromolecules* **2008**, *41*, 3235.

2. Overview of the Thesis

This thesis consists of five individual publications. The central theme connecting all the presented work is the production and application of worm-like crystalline-core micelles, for which the abbreviation wCCMs was established. These were self-assembled mainly from polystyrene-*block*-polyethylene-*b*-poly(methyl methacrylate) (SEM) triblock terpolymers and exhibited a PE core surrounded by a patchy corona of PS and PMMA.

In the beginning, research concentrated on the understanding of the mechanisms that trigger the formation of one-dimensional micelles in the case of the applied PE-containing triblock co- and terpolymers. **Chapter 3** gives insight on the basic parameters directing the self-assembly to patchy wCCMs, like choice of solvents, temperature protocols and polymer composition. Careful exertion of these guidelines allowed the selective formation of spherical or worm-like CCMs from the same triblock copolymer. Moreover, a one-dimensional array of alternating corona compartments of PS and PMMA was achieved by the use of symmetric triblock terpolymers in a non-selective solvent for these blocks.

The evidence for this unprecedented 1D array structure in the micellar corona was mainly based on transmission electron microscopy (TEM) investigations on samples in the dried state. Thus, a small-angle neutron scattering (SANS) study including contrast variation was performed on wCCMs formed by a partly deuterated triblock terpolymer in order to elucidate the corona structure for an ensemble of micelles in solution. The results presented in **Chapter 4** reveal that it is possible to discriminate *in-situ* between micelles with patchy and Janus-type coronas using this technique. Contrast variation allowed focusing on different compartments, and fitting of the resulting SANS curves validated the patchy structure with feature sizes similar to those obtained from TEM.

In **Chapter 5** the concept of crystallization-driven self-assembly is extended to wCCMs with asymmetric corona compositions, *i.e.* the content of PS and PMMA differs significantly. This could not only be achieved by the use of tailor-made triblock terpolymers, but also by random cocrystallization of a PS-*b*-PE-*b*-PS (SES) triblock copolymer with a symmetric SEM triblock terpolymer. Using this approach, the corona structure could be tuned continuously

from a mixed corona over spherical PMMA patches of increasing number and size in a PS matrix to the alternating corona structure known from the initially investigated symmetrical triblock terpolymer.

Strategies toward the controlled growth of wCCMs and more complex architectures are depicted in **Chapter 6**. By the use of spherical CCMs produced by SES as nuclei for the growth of single chains from the same triblock copolymer, micelles with predefined lengths up to 500 nm and low length polydispersities down to L_w/L_n = 1.1 could be produced. Moreover, upon addition of SEM triblock terpolymer single chains to the grown wCCMs these unimers grew onto the micelles epitaxially resulting in ABA triblock *co*-micelles with middle blocks bearing a homogeneous PS corona and patchy outer blocks with alternating PS and PMMA compartments.

In view of application, **Chapter 7** deals with the interfacial activity of wCCMs with patchy PS/PMMA coronas at the toluene/water interface. The obtained reduction of the interfacial tension was considerably larger compared to that of single chains of the precursor triblock terpolymer (PS-*b*-PB-*b*-PMMA, PB = polybutadiene) and to that of wCCMs with a homogeneous PS corona. Unexpectedly, it equaled that of PS/PMMA Janus cylinders with comparable length and corona composition. To explain this peculiar finding an adaptation of the corona chains to the interface was proposed. Furthermore, the interfacial tension decreased when the total degree of polymerization of both corona chains was increased.

In the following a brief summary of the results is given.

## 2.1. General Pathway toward Crystalline-Core Micelles with Tunable Morphology and Corona Segregation

In the first part of this publication the basic parameters influencing the crystallization-driven self-assembly of the PS-*b*-PE-*b*-PMMA triblock terpolymer $S_{340}E_{700}M_{360}$ (subscripts denote the number-average degree of polymerization of the respective polymer block) to wCCMs in good solvents for the PE middle block are investigated. As the first step, the polymer was dissolved at temperatures above the melting temperature of the PE block, in order to eliminate influences by its thermal history. Subsequent isothermal crystallization of toluene solutions at different temperatures resulted in wCCMs with a patchy PS/PMMA corona and a semicrystalline PE core (Figure 2.1). TEM images in all publications were obtained after staining of the samples with RuO_4, which selectively stains PS (dark). From static light scattering, we could deduce that the time needed for structure formation increases for increasing crystallization temperatures. Additionally, the final scattering intensity increased, leading to the assumption that larger structures are formed at higher temperatures, which could be verified by length statistics on the wCCMs obtained from TEM images showing a clear trend towards longer micelles for elevated temperatures of isothermal crystallization.
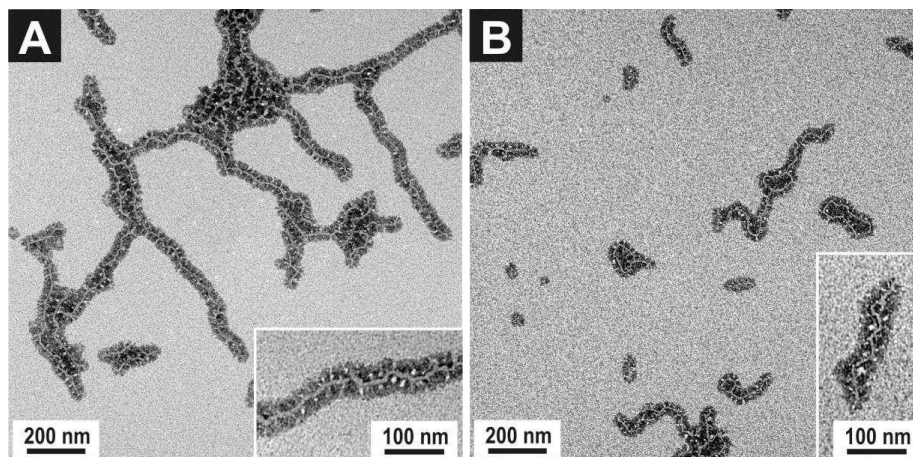
Figure 2.1. WCCMs obtained from 2 g/L toluene solutions of $S_{340}E_{700}M_{360}$ by isothermal crystallization at 20 °C (A) and 5 °C (B).

Furthermore the peak crystallization temperature of these polymers as determined by micro-differential scanning calorimetry (µDSC) on toluene solutions increased continuously from 8.5 to 21.7 °C upon an increase in concentration from 1 to 20 g/L, while the peak

melting temperatures only increased slightly. To gain information about the initial state of structure formation at high temperatures, SANS was performed on a 10 g/L toluene solution at 70 °C. The resulting scattering curve could be fitted using a form factor model for Gaussian polymer coils with a radius of gyration of 8 ± 2 nm. Combination of the obtained results pointed to a nucleation and growth mechanism originating from a unimer solution. As a method to achieve more regular structures, annealing at 45 °C, a temperature slightly below the peak melting temperature of the PE middle block, was performed after isothermal crystallization at 20 °C. µDSC measurements after annealing revealed a narrower main melting peak which was shifted to higher temperatures indicating a more defined crystallite thickness distribution as well as a slight increase of the crystallite thickness in the PE core (Figure 2.2A). Moreover, in TEM images of annealed wCCMs the corona microphase separation appeared more pronounced, but still the PMMA patches were significantly smaller than the PS parts of the corona despite equal lengths of both corona blocks. The overall morphology and the core structure were more regular, as well (Figure 2.2B).
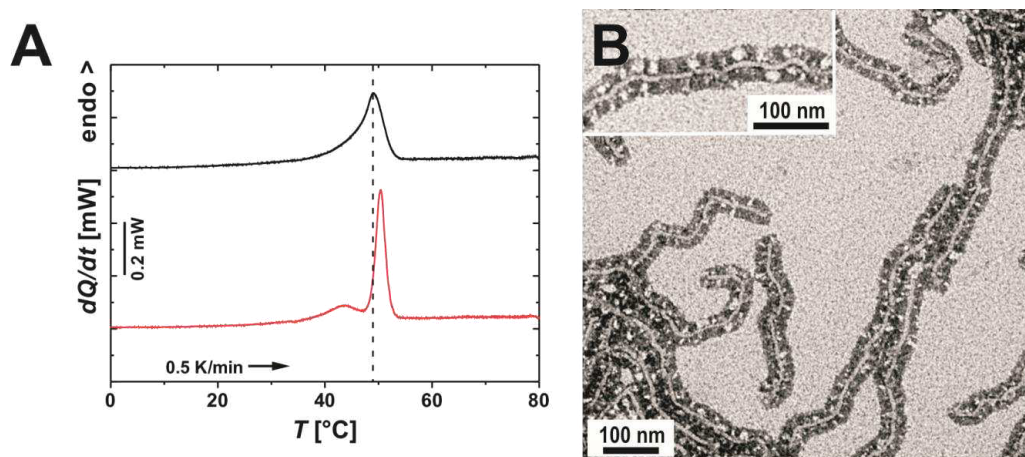
Figure 2.2. (A) µDSC heating traces of toluene solutions of $S_{340}E_{700}M_{360}$ wCCMs without an additional annealing step (black) and after annealing at 45 °C for 3 hours (red). (B) TEM micrograph of $S_{340}E_{700}M_{360}$ wCCMs formed in toluene after additional annealing.

Structure formation in THF applying the same temperature protocol of isothermal crystallization at 20 °C followed by annealing at 45 °C yielded wCCMs with a comparable overall morphology (Figure 2.3A). However, instead of comparably small PMMA patches and large PS regions, the corona now consisted of almost alternating PS and PMMA compartments with sizes of about 15 nm. This different behavior in THF with respect to toluene is explained by the variations in solvent quality for the corona blocks. While THF is

known to be an equally good solvent for both polymer blocks, toluene dissolves PS slightly better than PMMA. Therefore, the PMMA chains are less extended and form smaller, but more dense patches. By this method of structure formation worm-like micelles with patchy coronas could also be synthesized from $S_{280}E_{1190}M_{300}$ and $S_{140}E_{690}M_{160}$ (Figure 2.3B and 2.3C), even though an increased content of the crystallizable PE block ($S_{280}E_{1190}M_{300}$) as well as a lower overall molecular weight ($S_{140}E_{690}M_{160}$) are known to promote the formation of morphologies with lower curvature, *i.e.* platelet-like structures. Furthermore, $S_{380}E_{880}S_{390}$ was found to self-assemble into wCCMs with a homogeneous corona (Figure 2.3D), excluding the possibility that the repulsion between the incompatible corona blocks is responsible for one-dimensional growth. We therefore assumed that the middle position of the PE block triggers the selective formation of worm-like micelles over a broad composition range.
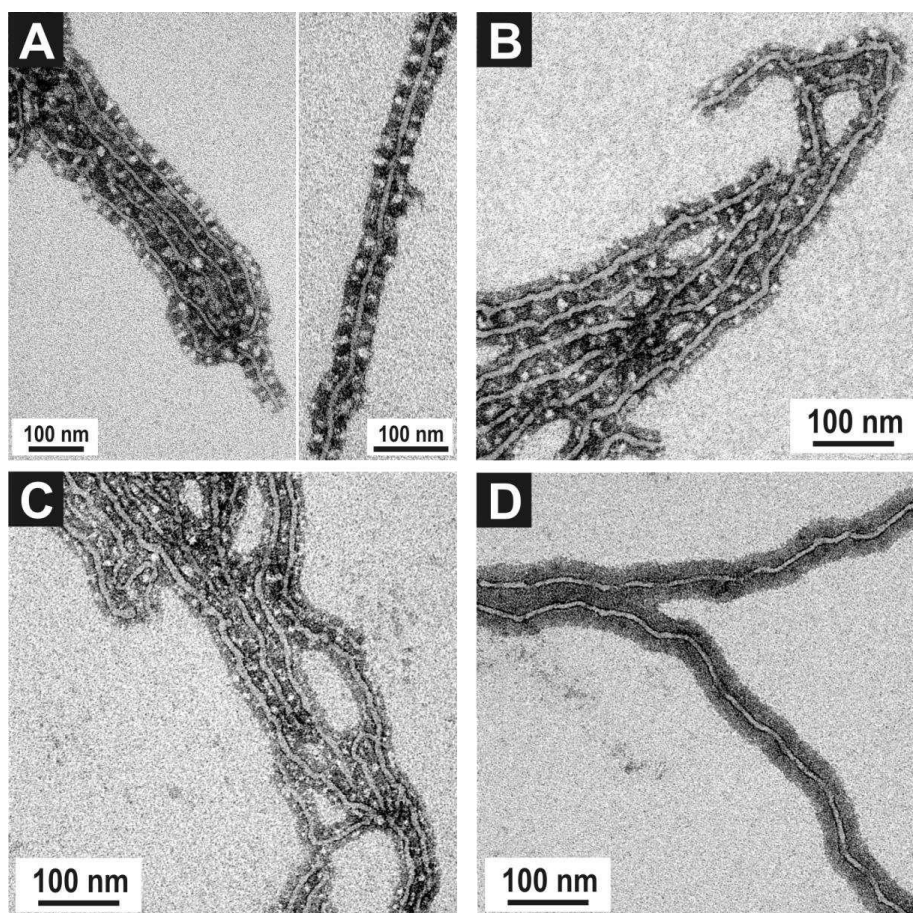
Figure 2.3. TEM micrographs of wCCMs formed by $S_{340}E_{700}M_{360}$ (A), $S_{280}E_{1190}M_{300}$ (B), $S_{140}E_{690}M_{160}$ (C) and $S_{380}E_{880}S_{390}$ (D) in 1g/L THF solutions after additional annealing.

After conducting self-assembly in good solvents for PE, *i.e.* PE is soluble above its melting temperature, we performed structure formation in dioxane, too. This process was followed by a combination of µDSC (Figure 2.4A) and dynamic light scattering (DLS, Figure 2.4B). The polymer was again dissolved above its melting temperature, which in this case was significantly higher as revealed by µDSC. From CONTIN analysis of the DLS autocorrelation function, at 85 °C, we obtained a peak with an apparent hydrodynamic radius ($R_{h,app}$) of 9 nm representing unimers. Already after cooling to 70 °C well-defined spherical micelles with $R_{h,app}$ = 24 nm are observed. As crystallization could not be traced until further cooling to 44 °C by µDSC, these collapsed PE chains are amorphous in the first place and crystallize later upon cooling to room temperature in the spatial confinement of the spherical micellar core. This could be confirmed by TEM showing spherical crystalline-core micelles (sCCMs) produced from $S_{340}E_{700}M_{360}$ (Figure 2.4C) and $S_{380}E_{880}S_{390}$ (Figure 2.4D) in dioxane solution.
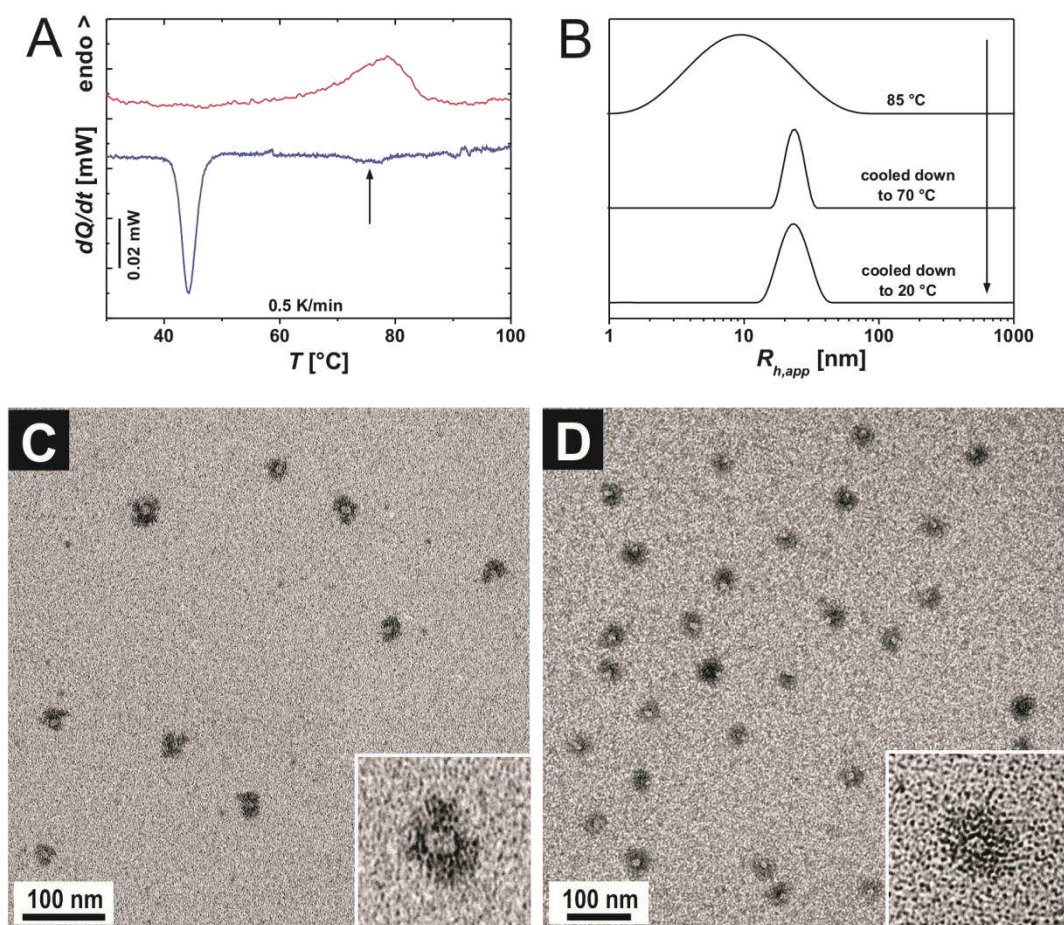
Figure 2.4. µDSC heating and cooling traces (A) and DLS CONTIN plots for different temperatures (B) of a 1 g/L $S_{340}E_{700}M_{360}$ solution in dioxane. TEM micrographs of sCCMs formed in dioxane solutions of $S_{340}E_{700}M_{360}$ (C) and $S_{380}E_{880}S_{390}$ (D). The insets are magnified 3-fold.

From the presented findings a general mechanism of self-assembly for triblock copolymers with crystallizable PE middle blocks was deduced (Figure 2.5). Here, we pointed out that the formed morphology depends on the solvent quality for PE. If PE becomes insoluble already before crystallization occurs, the spherical overall shape of the formed micelles is retained during PE crystallization at lower temperatures yielding sCCMs. Complete solubility of PE down to the temperature where crystallization occurs, on the other hand, leads to the initial formation of a few nuclei onto which the remaining unimers can deposit resulting in wCCMs.
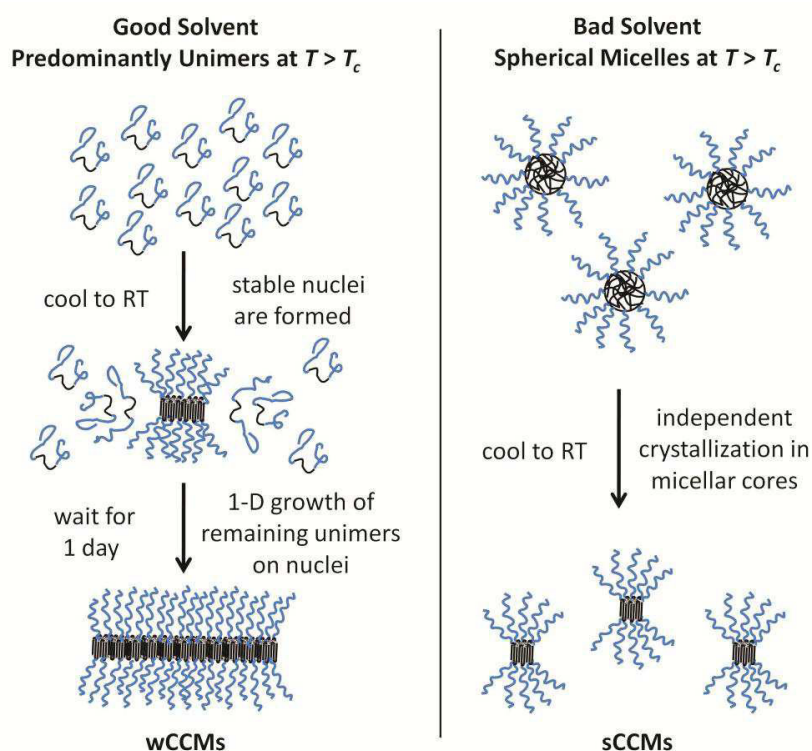
Figure 2.5. Proposed mechanism of the structure formation of triblock copolymers with a crystallizable PE middle block (black) and amorphous corona blocks (blue) in solvents of different quality.

2.2. Patchy Worm-Like Micelles: Solution Structure Studied by Small-Angle Neutron Scattering

Structure determination employing imaging techniques, such as TEM, can only provide information on a very small part of a sample. In addition, especially if it is performed on dried samples, the observed morphologies might be influenced by sample preparation procedures and, thus, might not represent the solution structure initially formed by self-assembly. Therefore, a $S_{360d}E_{750}M_{250}$ triblock terpolymer with a fully deuterated PS block was synthesized to allow the *in-situ* investigation of the corona structure *via* SANS including contrast variation. TEM investigations on wCCMs formed by $S_{360d}E_{750}M_{250}$ in common THF-h_8 and fully deuterated THF-d_8 (Figure 2.6) showed that the morphology of the formed assemblies was comparable to that observed in our earlier study and did not change significantly in dependency on the degree of deuteration of the solvent.
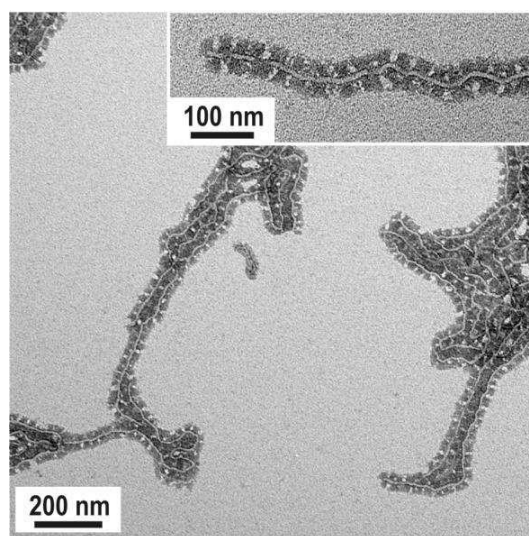
Figure 2.6. TEM micrograph of wCCMs formed by $S_{360d}E_{750}M_{250}$ in THF-d_8.

The calculated scattering intensities based on models for Janus-type and patchy cylinders revealed significant differences (Figure 2.7A). In contrast to the scattering curve for Janus cylinders, a pronounced minimum of the scattering vector was obtained at $q = 0.14$ nm^{-1}, if cylinders with alternating corona compartments are considered. The experimental scattering intensity for $S_{360d}E_{750}M_{250}$ wCCMs in THF-h_8 (almost exclusively deuterated PS is visible) is in good agreement with these calculations up to $q \approx 0.3$ nm^{-1} (Figure 2.7B). For further increased values of q the intensity scales with q^{-2} due to an increasing contribution of

polymer concentration fluctuations. Notably, moderate polydispersities in compartment sizes that have to be expected in the self-assembled structures did not markedly alter the calculated scattering intensity.
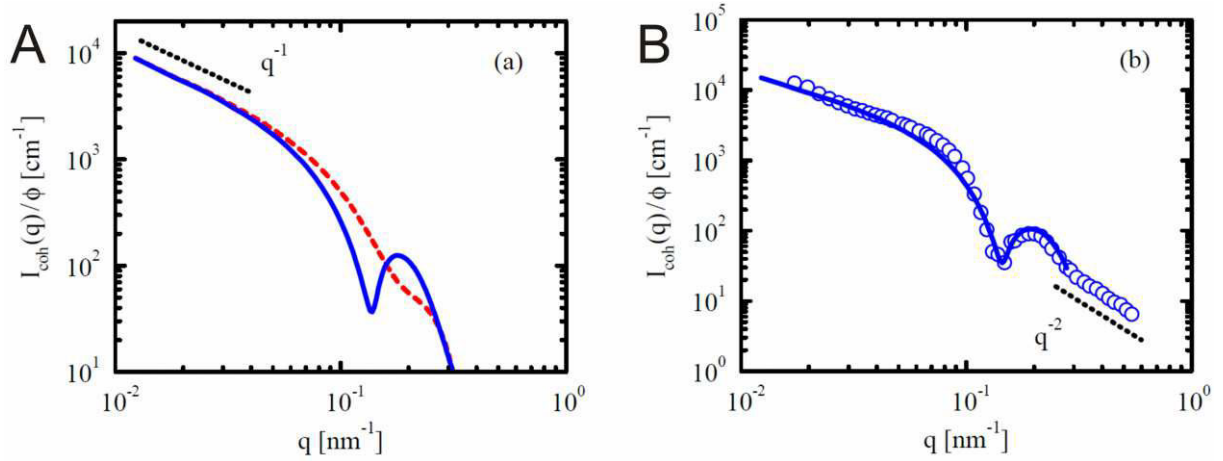
Figure 2.7. (A) Comparison of the calculated scattering intensity of Janus-type (dashed red line) and patchy (solid blue line) cylinders. (B) Measured scattering intensity of the triblock terpolymer micelles in THF-h_8 (symbols) together with the calculated results for noninteracting patchy cylinders (solid line).

In the contrast variation series 5 different contrasts were investigated realized by structure formation of $S_{360d}E_{750}M_{250}$ in THF-h_8/THF-d_8 solvent mixtures (Figure 2.8). In contrast to the scattering intensity obtained in pure THF-h_8, for a better description of the resulting curves at higher scattering length densities, interparticle interactions described by a total correlation function were taken into account.
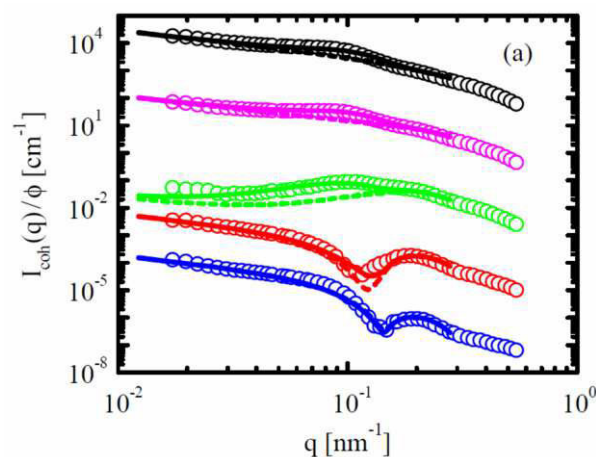
**Figure 2.8.** Measured scattering intensity of $S_{360d}E_{750}M_{250}$ wCCMs in THF-h_8/THF-d_8 solvent mixtures. The scattering length density of the solvent decreases from top (pure THF-d_8) to bottom (THF-h_8). The dashed lines represent calculated results for noninteracting cylinders, for the solid lines the total correlation function is included reflecting pair correlations between the micelles.

With this SANS study the patch-like surface-compartmentalized structure of the wCCM coronas as observed in TEM of dried samples could be confirmed using an *in-situ* method probing an ensemble of particles.

2.3. Corona Structure on Demand: Tailor-Made Surface Compartmentalization in Worm-Like Micelles via Random Cocrystallization

This work aimed at the facile production of wCCMs with significantly asymmetric corona compositions, in which the contents of PS and PMMA are significantly different. One route applied for this purpose is the self-assembly of specifically designed triblock terpolymers. Therefore, $S_{660}E_{1350}M_{350}$ and $S_{330}E_{1360}M_{760}$ were synthesized, exhibiting PS/PMMA molar ratios of about 2/1 and 1/2, respectively. Applying the established preparation protocol of dissolution at high temperatures in THF followed by isothermal crystallization and annealing slightly below the melting temperature of PE, wCCMs could be prepared from these polymers, too (Figure 2.9).
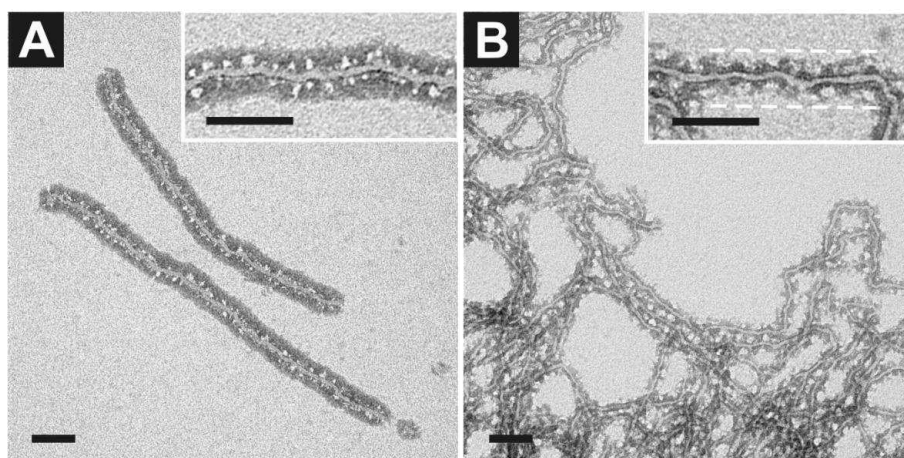
Figure 2.9. TEM micrographs of wCCMs formed by $S_{660}E_{1350}M_{350}$ (A) and $S_{330}E_{1360}M_{760}$ (B) in THF solution, respectively. The white dotted line in (B) indicates the extension of the PMMA corona as estimated from scanning force microscopy. Scale bars: 100 nm.

The unequal corona composition of PS and PMMA resulted in nearly spherical PMMA patches in a continuous corona of PS for $S_{660}E_{1350}M_{350}$ (Figure 2.9A) and the reverse situation – PS patches in a PMMA matrix – for $S_{330}E_{1360}M_{760}$ (Figure 2.9B). The total extension of the PMMA corona in case of $S_{330}E_{1360}M_{760}$ had to be determined by scanning force microscopy as

it is not stained by RuO_4 and, hence, appears as bright as the background in TEM micrographs.

The fact that the synthesis of new triblock terpolymers for each desired corona composition is arduous and time-consuming led to the idea to cocrystallize different triblock copolymers in order to obtain defined corona compositions. As a blank test, we mixed preformed wCCM solutions of $S_{380}E_{880}S_{390}$ and $S_{340}E_{700}M_{360}$ that after one week of stirring at room temperature still showed the two separate species. Thus, no unimer exchange can take place once the structures are formed. In the following, mixtures of both polymers were subjected to the standard procedure used for wCCM formation. For all samples, TEM micrographs showed a similar corona structure throughout all micelles without any signs of the formation of pure $S_{380}E_{880}S_{390}$ and $S_{340}E_{700}M_{360}$ wCCMs. Upon increasing the PMMA content x_M of the corona, *i.e.* the fraction of $S_{340}E_{700}M_{360}$ in the mixture, the morphology could be tuned from a homogeneously mixed corona over spherical PMMA patches of increasing number and size to almost rectangular PMMA patches as known from pure $S_{340}E_{700}M_{360}$ wCCMs (Figure 2.10, left). Strikingly, the PMMA patch sizes of a mixed sample with x_M = 35 % closely matched those of $S_{660}E_{1350}M_{350}$ (x_M = 34 %).
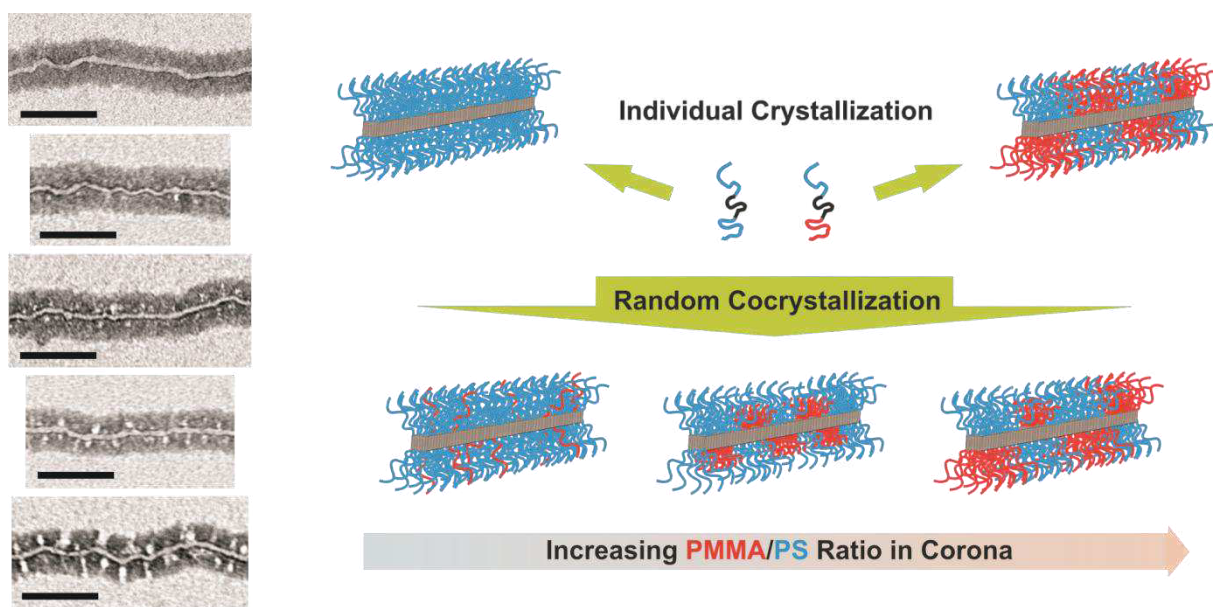
Figure 2.10. Left: TEM micrographs of wCCMs formed by random cocrystallization of mixtures of $S_{380}E_{880}S_{390}$ and $S_{340}E_{700}M_{360}$ in THF solution. The fraction of $S_{340}E_{700}M_{360}$ in the mixtures increases from top to bottom. Scale bars: 100 nm. Right: Sketch of structures that can be self-assembled from $S_{380}E_{880}S_{390}$ and $S_{340}E_{700}M_{360}$ in THF (PS: blue, PMMA: red, PE: black/grey).

The trend of increasing size and number of PMMA patches could also be followed by analyzing brightness distributions of the corona pixels from TEM micrographs of the different samples. Here, PMMA is represented by increased brightness values as it is not affected by RuO_4 and, thus, exhibits low contrast. Using a small ensemble of micelles, the obtained brightness distribution exhibited an increasingly pronounced shoulder towards higher values for cocrystallized mixtures with increasing x_M. As an overview, the scheme in Figure 2.10 illustrates the structural variety accessible by simple random cocrystallization of two triblock copolymers.

2.4. Length Control and Block-Type Architectures in Worm-Like Micelles with Polyethylene Cores

While the wCCMs produced so far exhibited defined diameters of the core and the corona, the micellar lengths remained broadly distributed. In the following, the controlled growth of wCCMs using uniform sCCMs as seeds for the growth of single polymer chains (unimers) is demonstrated.
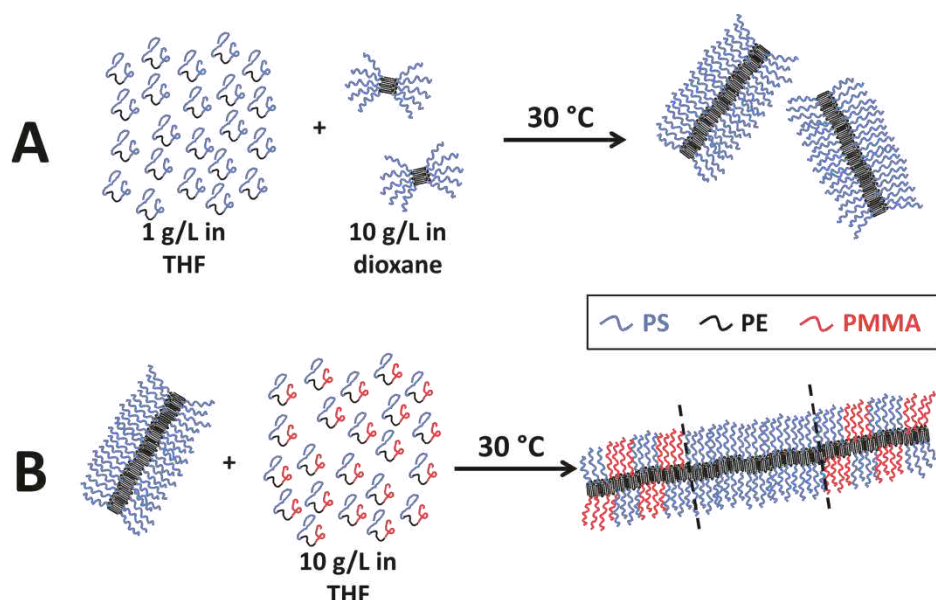
Figure 2.11. Principle of wCCM preparation with controlled lengths (A) and subsequent epitaxial growth to triblock *co*-micelles (B).

Therefore, $S_{380}E_{880}S_{390}$ (SES) seeds were produced by self-assembly in a 10 g/L dioxane solution and added in different amounts to 1 g/L unimer solutions of the same triblock copolymer in THF (Figure 2.11A). These unimer solutions were produced by dissolution above the melting temperature of PE and subsequent quenching to 30 °C, a temperature between the melting and the crystallization temperature, in order to allow the unimers to grow to the seeds in the absence of significant homogeneous nucleation.
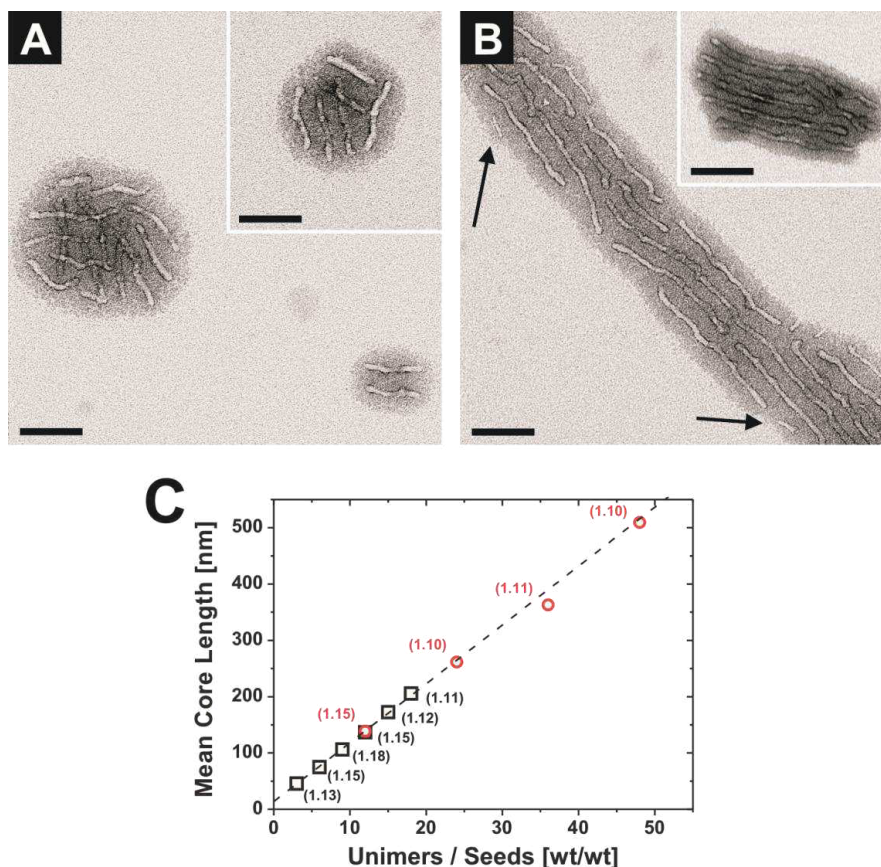
Figure 2.12. TEM micrographs of wCCMs formed from SES by seeded growth at U/S = 9 (A) and 18 (B). Scale bars: 100 nm. (C) Mean core length L_n *vs.* applied U/S ratio for wCCMs prepared in a one-step growth process (black squares) and *via* repetitive unimer addition (red circles). The values given in brackets correspond to the length polydispersities (L_w/L_n) and the dashed line represents a linear fit to the length *vs.* U/S ratio data.

TEM investigation revealed the production of wCCMs with length polydispersities down to $L_w/L_n = 1.1$ (Figure 2.12). Their number-average length, L_n, increased linearly with increasing unimer to seed (U/S) ratio indicating that the controlled growth of unimers to the sCCM seeds was successful. For high U/S ratios, however, a few small micelles with thinner PE cores were observed, too (arrows in Figure 2.12B). These must have formed after structure formation at 30 °C during the subsequent sample preparation indicating that not all unimers

were able to grow onto the wCCMs in the given time span (2 weeks), which was ascribed to the low seed concentration at high U/S ratios. As this observation would limit the controlled one-dimensional growth to rather short micelles, growth *via* repetitive unimer addition was performed to overcome this drawback. Therefore, to wCCMs produced as described above at U/S = 6 the same amounts of unimers were added as 10 g/L THF solutions every 2-4 days to avoid significant dilution of the growing wCCMs. Using this approach micellar lengths up to 500 nm could be achieved with $L_w/L_n \approx 1.1$ (Figure 2.12C).

Moreover, the propensity of SES wCCMs (formed again at U/S = 6) to add unimers of a SEM triblock terpolymer ($S_{340}E_{700}M_{360}$) in order to form triblock *co*-micelles was tested (Figure 2.11B). Here, the double amount of SEM unimers was added as a 10 g/L THF solution aiming at two outer micellar SEM blocks that have the same length as the precursor SES wCCM. In TEM, 97% of the observed structures were the desired SEM-*b*-SES-*b*-SEM triblock *co*-micelles (Figure 2.13A), representing the first block *co*-micelles produced from purely organic block copolymers and at the same time the first ones including blocks with a patchy corona.
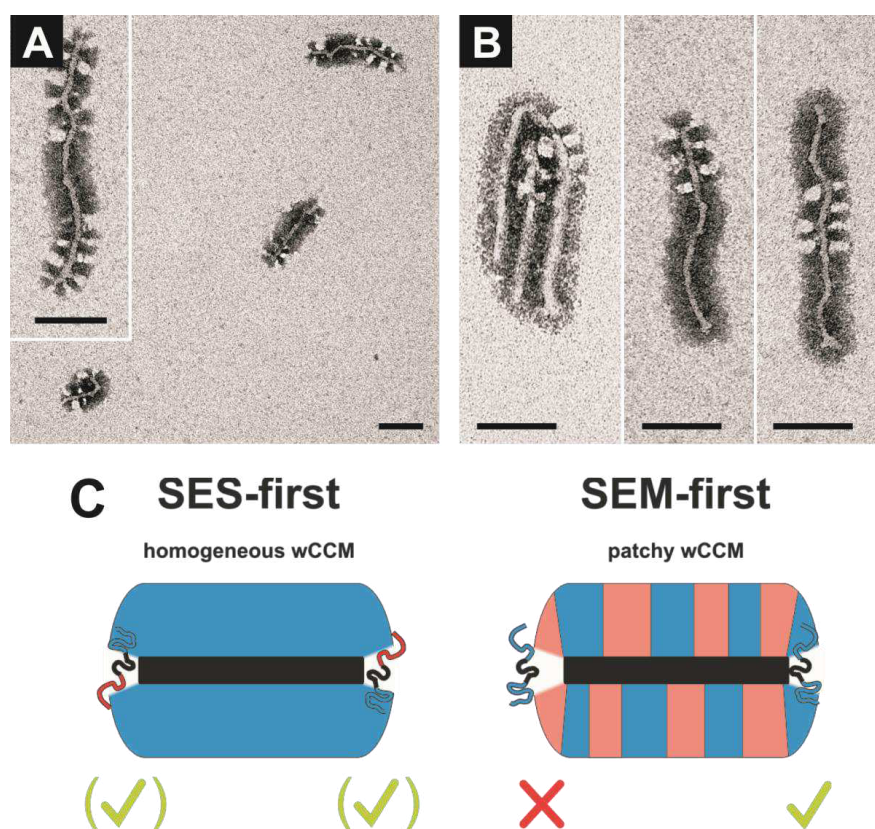
Figure 2.13. SEM-*b*-SES-*b*-SEM triblock *co*-micelles (A) and examples of SES-*b*-SEM-*b*-SES triblock *co*-micelles and SES-*b*-SEM diblock *co*-micelles (B) prepared in 1g/L THF solutions. Scale bars: 100 nm. (C) Illustration of the processes leading to the different types of block *co*-micelles.

Applying the same procedure, the production of SES-*b*-SEM-*b*-SES triblock *co*-micelles was attempted, too. Hence, after seed self-assembly of SEM in dioxane these seeds were added to a SEM unimer solution (U/S = 6) to grow wCCMs and furthermore the double amount of SES unimers was added to form the outer blocks. Yet, a completely different behavior was encountered in this case as the formed structures consisted of a mixture of SES-*b*-SEM-*b*-SES triblock *co*-micelles (26 %), SEM-*b*-SES diblock *co*-micelles (48%) and pure SEM wCCMs (26%) (Figure 2.13B).

As the block lengths as well as the microstructure of the PE middle block, *i.e.* the amount of short-chain branching, are similar for both triblock copolymers, the reason for this asymmetric behavior was assumed to originate from the different corona structure of the initially formed SES or SEM wCCMs (Figure 2.13C). Presumably, not all ends of the SEM wCCMs have the same capability to add SES unimers as the PE core might be surrounded by a majority of either PMMA or PS chains. If the core end is mainly encompassed by PMMA chains the growth of SES unimers might be significantly disturbed resulting in the observed phenomenon that a large fraction of the wCCM ends is hardly accessible for further unimer addition.

2.5. Interfacial Activity of Patchy Worm-Like Micelles

The scope of this work was to probe the potential of patchy wCCMs to reduce the interfacial tension at liquid-liquid interfaces. Toluene/water was chosen as a suitable solvent system to perform pendant-drop tensiometry as the two are immiscible and exhibit a rather high interfacial tension (γ = 33.1 mN/m). The surface activity of patchy wCCMs formed directly in toluene by $S_{340}E_{700}M_{360}$ was compared to those of single chains of the corresponding $S_{340}B_{350}M_{360}$ precursor polymer and wCCMs formed by $S_{380}E_{880}S_{390}$ bearing a homogeneous corona (Figure 2.14). The reduction in interfacial tension achieved by the patchy wCCMs was significantly higher than for the two reference systems confirming the beneficial synergy of the Pickering effect known for particles with the amphiphilicity of classical surfactants. The interfacial tension further decreased with increasing concentration of patchy wCCMs. Additionally, a comparison to PS/PMMA Janus micelles of comparable dimensions showed

similar surface activities (Figure 2.14), even though one would assume that the Janus structure, i.e. two opposing half-shells of different polarity, is more suitable for arrangement at the interface than a corona of alternating compartments on both sides.
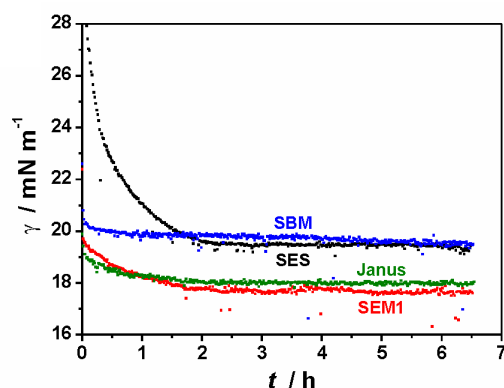
Figure 2.14. Interfacial tension isotherms for unimolecularly dissolved SBM, wCCMs formed by SES and $S_{340}E_{700}M_{360}$ (SEM1), and Janus cylinders at the toluene/water interface.

Moreover, two series of wCCMs formed by SEM triblock terpolymers of various compositions, *i.e.* three symmetric triblocks with similar molar fraction of styrene repeating units in the corona and three triblocks with similar overall length of the two corona blocks, but different PS/PMMA ratios, were investigated. Here, the values of the interfacial tension increased for longer corona blocks, but did not show a distinct dependency on the PS/PMMA ratio in the corona. The similarity in behavior to Janus cylinders led to the assumption that the corona of the patchy wCCMs is able to adapt to the toluene/water interface with the slightly more polar PMMA chains providing a shielding layer for the nonpolar PS (Figure 2.15).
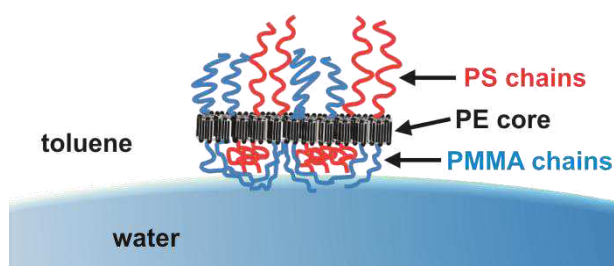
Figure 2.15. Proposed orientation of patchy wCCMs at the toluene/water interface.

2.6.Individual Contributions to Joint Publications

The research presented in the manuscripts of this thesis was done in collaboration with others and has been published or will be submitted as described below. In this section the contribution of all co-authors to the different manuscripts are denoted. The corresponding author(s) is/are marked with an asterisk.

Chapter 3

This work is published in *ACS Nano*, **2011**, *5*, 9523-9534 under the title:

"General Pathway toward Crystalline-Core Micelles with Tunable Morphology and Corona Segregation"

By Joachim Schmelz, Matthias Karg, Thomas Hellweg, and Holger Schmalz*

I conducted all the experiments and wrote the publication, exceptions stated below.

Matthias Karg assisted in the SANS experiment, performed the fit of the SANS data and co-wrote the corresponding part in the publication. Thomas Hellweg and Holger Schmalz were involved in the discussion and correction of the manuscript.

Chapter 4

This work is published in *Physical Chemistry Chemical Physics*, **2012**, *14*, 12750-12756 under the title:

"Patchy Worm-Like Micelles: Solution Structure Studied by Small-Angle Neutron Scattering"

By Sabine Rosenfeldt, Frank Lüdel, Christoph Schulreich, Thomas Hellweg*, Aurel Radulescu, Joachim Schmelz, Holger Schmalz, and Ludger Harnau*

I synthesized and characterized the deuterated triblock terpolymer, prepared the samples, performed the TEM measurements and co-wrote the manuscript.

S.R. and L.H. developed the model equations, performed the data fitting and wrote the manuscript. F.L. designed the scheme of the microphase-separated cylinders and co-wrote the manuscript. C.S. performed the SANS experiments. T.H. co-wrote and corrected the manuscript and was involved in the discussion. A.R. was the local contact at the Jülich Center of Neutron Scattering in München during the SANS experiments. H.S. was involved in the discussion and correction of the manuscript.

Chapter 5

This work is published in *Polymer*, **2012**, *53*, 4333-4337 under the title:

"Corona Structure on Demand: Tailor-Made Surface Compartmentalization in Worm-Like Micelles via Random Cocrystallization"

By Joachim Schmelz, and Holger Schmalz*

I conducted all the experiments and wrote the publication.

H.S. was involved in the discussion and correction of the manuscript.

Chapter 6

This work is published in *Journal of the American Chemical Society*, **2012**, *134*, 14217-14225 under the title:

"Length Control and Block-Type Architectures in Worm-Like Micelles with Polyethylene Cores"

By Joachim Schmelz, Andreas E. Schedl, Christoph Steinlein, Ian Manners, and Holger Schmalz*

I conducted all the experiments and wrote the publication.

A.E.S. and C.S. performed preliminary experiments during a lab course or bachelor thesis, respectively. I.M. was involved in discussions. H.S. was involved in the discussion and correction of the manuscript.

Chapter 7

This work will be submitted to *Soft Matter* under the title:

"Interfacial Activity of Patchy Worm-Like Micelles"

By Joachim Schmelz, Daniela Pirner, Marina Krekhova, Thomas M. Ruhland, and Holger Schmalz*

I supervised the master thesis of D.P., synthesized most of the used polymers and wrote the publication.

D.P. conducted all the experiments, except that M. K. prepared some additional samples. T.M.R. provided the Janus cylinders, co-wrote the publication and was involved in the discussion. H.S. was involved in the discussion and correction of the manuscript.

3. General Pathway toward Crystalline-Core Micelles with Tunable Morphology and Corona Segregation

Joachim Schmelz[a], Matthias Karg[b], Thomas Hellweg[c], and Holger Schmalz[a],*

a) Makromolekulare Chemie II, Universität Bayreuth, 95440 Bayreuth, Germany

b) Physikalische Chemie I, Universität Bayreuth, 95440 Bayreuth, Germany

c) Physikalische und Biophysikalische Chemie, Universität Bielefeld, 33615 Bielefeld, Germany
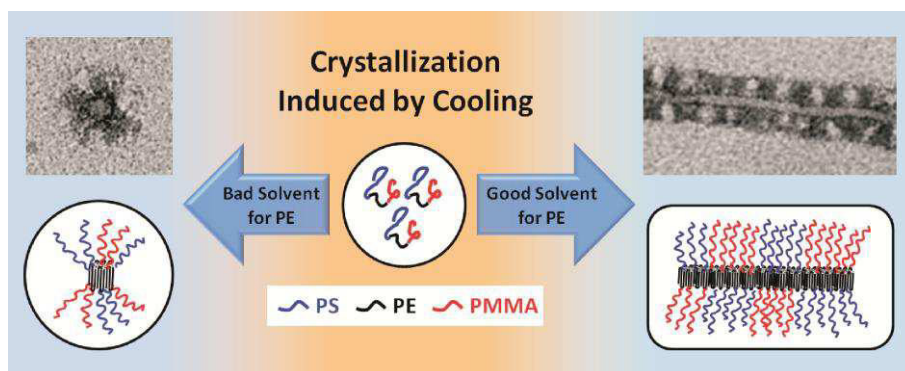
ABSTRACT:

We present a general mechanism for the solution self-assembly of crystalline-core micelles (CCMs) from triblock copolymers bearing a semicrystalline polyethylene (PE) middle block. This approach enables the production of nanoparticles with tunable dimensions and surface structures. Depending on the quality of the solvent used for PE, either spherical or worm-like CCMs can be generated in an easy and highly selective fashion from the same triblock copolymers *via* crystallization-induced self-assembly upon cooling. If the triblock copolymer stays molecularly dissolved at temperatures above the crystallization temperature of the PE block, worm-like CCMs with high aspect ratios are formed by a nucleation and growth process. Their length can be conveniently controlled by varying the applied crystallization temperature. If, on the other hand, exclusively spherical micelles with an amorphous PE core are present before crystallization, confined crystallization within the cores of the preformed micelles takes place and spherical CCMs are formed. For polystyrene-*block*-polyethylene-*block*-poly(methyl methacrylate) (PS-*b*-PE-*b*-PMMA) triblock terpolymers a patch-like microphase separation of the corona is obtained for both spherical and worm-like CCMs due to the incompatibility of the PS and PMMA blocks. The structure of the patch-like corona depends on the selectivity of the employed solvent for the PS and PMMA corona blocks, whereby non-selective solvents produce a more homogeneous patch size and distribution. Furthermore, annealing of the semicrystalline PE cores results in an increasingly uniform crystallite size distribution and thus core thickness of the worm-like CCMs as well as in a more pronounced microphase separation in the corona.

3.1. Introduction

Due to their fascinating properties, block copolymers have been investigated intensively during the past decades. In solid state as well as in solution, their self-assembly allows the production of a variety of unique structures with promising applications in *e.g.* materials science, biomedicine, and optoelectronics.[1-3] However, the majority of research in the field, especially regarding structure formation in solution, was focused on coil-coil block copolymers.[4] Even though early theoretical work predicted the formation of spherical (or "hockey-puck"), cylindrical as well as lamellar (platelet-like) structures by solution self-assembly of crystalline-coil block copolymers,[5] only recently, significant effort in exploiting their unique properties has been undertaken.[6-8] For these systems, solution self-assembly is controlled by the crystallization of one polymer block, which is triggered by the addition of a non-solvent or cooling below its crystallization temperature. Here, especially the ability to produce stable cylindrical or worm-like micelles of high aspect ratio is of rising interest in materials science and biotechnology.[6,9] Among the still rather few systems used in this field, block copolymers with a polyferrocenylsilane (PFS) block have been studied most extensively, allowing the production of cylindrical, tubular and sheet-like structures with a crystalline PFS core surrounded by various types of amorphous corona blocks.[10-12] Manners, and Winnik *et al.* showed that the cylindrical micelles are formed *via* crystallization-driven living self-assembly, which enables the precise control of the cylinder length and length distribution using seeded crystallization with small seed micelles formed by sonication or self-seeding.[7,13,14] This living self-assembly was used to produce more complex architectures, too, *e.g.* block-*co*-micelles, scarf-like micelles as well as brush layers grown from PFS homopolymer surfaces.[7,8] Other examples of one-dimensional structures formed upon crystallization include polybutadiene-*block*-poly(ethylene oxide),[15] poly(ε-caprolactone)-*block*-poly(ethylene oxide) with poly(ε-caprolactone) as the crystallizing block,[16,17] poly(3-hexylthiophene)-*b*-poly(dimethylsiloxane),[18] polyacrylonitrile-based block copolymers,[19,20] as well as enantiopure polylactide-containing diblock copolymers.[21,22]

With regard to the polyethylene (PE) containing systems studied up to now, mostly platelet- or disk-like aggregates have been observed.[23-25] To the best of our knowledge, only in our recent work about a polystyrene-*block*-polyethylene-*block*-poly(methyl methacrylate)

triblock terpolymer one-dimensional structures could be formed from a linear PE-containing block copolymer.[26] Interestingly, for PE-*b*-PEP (PEP: poly(ethylene-*alt*-propylene)) diblock copolymer stars with PE inner blocks cylindrical micelles were found, whereas platelets were formed again when the outer blocks of the stars consist of PE.[27] In this case, unimolecular hockey-puck micelles with rare events of intermolecular cocrystallization were assumed to form a pearl-necklace structure, loosely connected by amorphous segments. Similar mechanisms comprising the aggregation of initially formed spherical crystalline-core micelles to one- or two-dimensional assemblies have also been discussed for block copolymers with poly(ethylene oxide) and poly(ε-caprolactone) as crystallizable blocks.[28-30] In contrast, for PFS-containing cylindrical micelles, a partial nucleation followed by the deposition of remaining unimers to these seeds was reported.[6,7] However, understanding the processes of block copolymer crystallization in solution is still at an early stage and hence, further knowledge of the parameters, which control this promising type of self-assembly, is needed to make predictions with respect to the formed structures.

Another highly active research field, in which block copolymer self-assembly plays a decisive role, is the production of surface-compartmentalized nanostructures. Nanoparticles with defined surface anisotropies show interesting properties and offer a wide range of applications, *e.g.* outstanding surface activity, the formation of hierarchically ordered superstructures, and the potential use as scaffolds for the directed incorporation of metallic nanoparticles.[31-33] The simplest form of surface compartmentalization, two separated compartments (or faces) of different chemistry and/or polarity, can be found in Janus particles, where spherical, cylindrical and disk-like architectures have been produced.[31,34-36] Recently, the synthesis of patchy particles, consisting of more than two different compartments, came into the focus of several research groups.[32,37-41] However, mostly spherical patchy micelles have been produced so far. One-dimensional structures with distinct corona compartments have hardly been observed, even though theoretical work predicts their existence.[42] A P*t*BA-*b*-PCEMA-*b*-PGMA (Poly(*tert*-butyl acrylate)-*block*-poly(2-cinnamoyloxyethyl methacrylate)-*block*-poly(glyceryl monomethacrylate)) triblock terpolymer has been used to form a variety of structures such as cylinders, vesicles and tubes in selective solvents for the end blocks.[43] Here, the P*t*BA blocks form small circular patches in a corona mainly consisting of PGMA. From a similar P*t*BA-*b*-PCEMA-*b*-PBMA

(PBMA = poly(*n*-butyl methacrylate)) triblock terpolymer even double and triple helices could be produced *via* hierarchical self-assembly of patch-like cylindrical micelles triggered by the addition of a non-solvent for one of the corona blocks.[44] In general, the production of surface-compartmentalized nanostructures is challenging and usually requires arduous, time-consuming sample preparation including dialysis into solvent mixtures, crosslinking and/or template-assisted approaches.[31,34,35,37,38,43]

Recently, we reported the formation of worm-like micelles from a polystyrene-*block*-polyethylene-*block*-poly(methyl methacrylate) triblock terpolymer (PS-*b*-PE-*b*-PMMA) by crystallization-induced self-assembly from solution.[26] These worm-like micelles exhibit a patchy corona of PS and PMMA, thus integrating the feature of surface compartmentalization into a system with high aspect ratio. The advantage of this process over existing ones is the comparatively undemanding and time-efficient production of surface-compartmentalized one-dimensional nanostructures by simply cooling a polymer solution in order to trigger crystallization and hence self-assembly. However, the mechanism of structure formation still remains an unresolved issue. In this publication we provide a thorough investigation of the fundamental parameters influencing this self-assembly process. From the obtained results we propose a general mechanism for the self-assembly of triblock copolymers with semicrystalline middle blocks from solution. This allows not only control of the morphology of the formed crystalline-core micelles (CCMs), *i.e.*, spherical *vs.* worm-like, by a careful selection of the solvent environment, but also of the extent of surface compartmentalization, *i.e.*, patchy *vs.* homogeneous corona. Furthermore, we will show that the self-assembly of PS-*b*-PE-*b*-PMMA triblock terpolymers with identical block lengths of the PS and PMMA end blocks in THF gives access to worm-like CCMs with a unique highly regular one-dimensional array structure of equally sized alternating PS and PMMA corona patches.

3.2. Results and Discussion

In a previous work we studied the self-assembly of a polystyrene-*block*-polyethylene-*block*-poly(methyl methacrylate) triblock terpolymer in organic solvents (toluene and THF) and found exclusively worm-like crystalline-core micelles (wCCMs) with a patch-like corona.[26]

However, the mechanism of one-dimensional growth and the influence of variables like concentration, crystallization temperature, polymer composition, overall molecular weight and solvent quality were not addressed.

In this publication we now identify the key parameters for the formation of CCMs in order to tune their morphology as well as the microphase separation in the corona. First, the structure formation process of polystyrene-*block*-polyethylene-*block*-poly(methyl methacrylate) triblock terpolymers ($S_xE_yM_z$: subscripts denote the number-average degree of polymerization) in toluene and THF (good solvents for molten polyethylene; see Table 3.2) will be studied. This includes variations in crystallization temperature and polymer concentration, polyethylene (PE) content and overall molecular weight of the $S_xE_yM_z$ triblock terpolymers. In addition, a polystyrene-*block*-polyethylene-*block*-polystyrene triblock copolymer ($S_{380}E_{880}S_{390}$) is examined, in order to identify whether the incompatibility of the polystyrene (PS) and poly(methyl methacrylate) (PMMA) corona blocks influences the formed morphology. Subsequently, the solvent quality for PE is decreased using dioxane and N,N-dimethylacetamide as solvents for the self-assembly. From the obtained results we deduce a general mechanism for the selective formation of wCCMs or sCCMs (spherical crystalline-core micelles) from the same triblock copolymers.

The used $S_xE_yM_z$ triblock terpolymers and the $S_{380}E_{880}S_{390}$ were prepared *via* catalytic hydrogenation of the corresponding $S_xB_yM_z$ and $S_{380}B_{440}S_{390}$ (B = poly(1,4-butadiene)) triblock copolymer precursors, which were synthesized by sequential anionic polymerization. Details on the synthesis can be found in the *Methods* section.

Structure Formation in Good Solvents for PE. To gain a deeper insight into the mechanism of the crystallization process in solution, first the crystallization temperature was varied. Thus, isothermal crystallization was conducted at different temperatures for 2 g/L toluene solutions of $S_{340}E_{700}M_{360}$ (detailed information about the used triblock copolymers can be found in Table 3.3), which we followed in real-time by static light scattering (Figure 3.1).
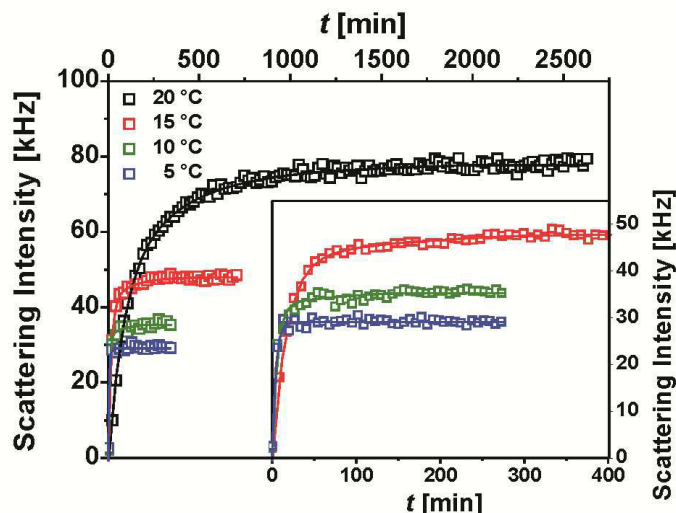
Figure 3.1. Intensity of scattered light *vs.* time for 2 g/L toluene solutions of $S_{340}E_{700}M_{360}$ cooled to different crystallization temperatures as indicated. The inset shows a zoom for the data obtained at lower crystallization temperatures.

For these crystallization experiments, all polymer solutions were preheated to 80 °C to assure complete melting of the PE blocks. After cooling to the desired crystallization temperature with a cooling rate of about 2 K/min, the scattering intensity I_S was monitored as a function of time. For all applied temperatures I_S increases with time until a plateau is reached. This increase can be attributed to the crystallization-induced structure formation process.

In addition, a clear tendency is observed for all crystallization temperatures. Faster structure formation occurs for lower crystallization temperatures, *i.e.*, a shorter time span is needed until the scattering intensity reaches its final plateau value indicating complete structure formation (Table 3.1). Furthermore, the final scattering intensity that is reached after complete structure formation decreases with decreasing crystallization temperature. This points to a decrease in the length of the formed wCCMs, since this goes along with a decrease in the radius of gyration as well as in aggregation number and thus molecular weight. However, it has to be noted that the intensity of the scattered light for worm-like objects depends on additional parameters like *e.g.* the particle form factor and, hence, only qualitative trends are extracted from the light scattering data presented in Figure 3.1.

Table 3.1. Characteristics of wCCMs formed by isothermal crystallization of 2 g/L toluene solutions of $S_{340}E_{700}M_{360}$ at different temperatures.

T_{cryst} [°C][a]	l_{wCCMs} [nm][b]	t_{SF} [min][c]	$I_{S,\infty}$ [kHz][d]
20	520 (260)	1600	78
15	330 (170)	240	48
10	280 (160)	140	36
5	240 (140)	50	29

a) applied isothermal crystallization temperature

b) average micelle length derived from TEM image analysis of at least 100 micelles (standard deviation in brackets)

c) time of structure formation, defined as the time when the scattering intensity no longer deviates more than 5% from the final scattering intensity

d) the final scattering intensity $I_{S,\infty}$ corresponds to the mean scattering intensity of the last two hours of the experiment

To verify the assumptions drawn from light scattering the formed wCCMs were investigated by transmission electron microscopy (TEM). For all TEM images shown in this publication PS was selectively stained by RuO_4 vapor prior to investigation, resulting in dark PS domains. PMMA domains and the PE core appear bright, as they are not affected by this staining procedure.[26] Figure 3.2 shows two representative TEM micrographs of wCCMs prepared by isothermal crystallization at 20 °C and 5 °C, respectively. In both images wCCMs with a PE core (bright), surrounded by a microphase-separated corona of PS (dark) and PMMA (bright) can be observed. For a crystallization temperature of 20 °C wCCMs with lengths up to about 1 µm are obtained, whereas those crystallized at 5 °C are significantly shorter on average as revealed by image analysis.
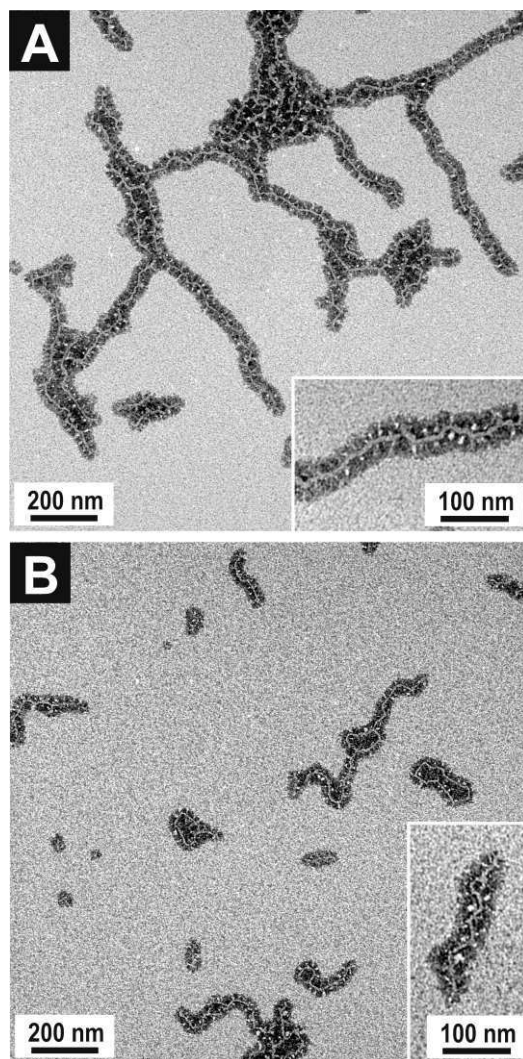
Figure 3.2. Worm-like CCMs obtained from 2 g/L toluene solutions of $S_{340}E_{700}M_{360}$ by isothermal crystallization at (A) 20 °C and (B) 5 °C. The solutions were diluted to 0.25 g/L before drop-coating onto carbon-coated copper grids.

The results summarized in Table 3.1 strongly support the previous assumption, that the observed drop in the final scattering intensity $I_{S,\infty}$ corresponds to a decrease of the average micelle length l_{wCCMs}. Moreover, the observed decrease in wCCM length upon lowering the crystallization temperature points to a nucleation and growth process. For equally concentrated solutions with respect to the crystallizable polymer the probability to form stable nuclei is expected to increase at higher supercooling, similar to the behavior for crystallization from the melt.[45] As a result, the limited amount of dissolved polymer chains has to be distributed among more nuclei, and consequently shorter wCCMs are obtained at lower temperatures. Hence, variation of the crystallization temperature provides a convenient method to tune the average micelle length.

In a nucleation and growth process the concentration of crystallizable polymer should have an influence on the crystallization, too. Accordingly, we investigated the concentration dependency of the crystallization process using micro-differential scanning calorimetry (µDSC) of differently concentrated $S_{340}E_{700}M_{360}$ solutions in toluene (Figure 3.3).
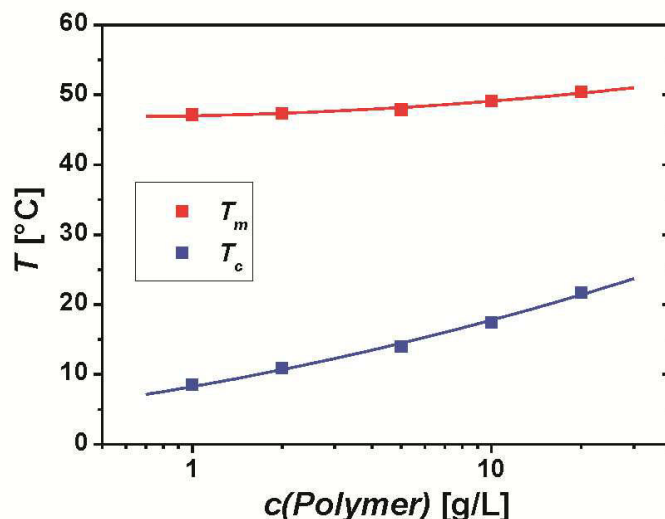

Figure 3.3. Peak melting (T_m) and crystallization (T_c) temperatures *vs.* polymer concentration as derived from µDSC measurements on $S_{340}E_{700}M_{360}$ solutions in toluene. Lines are drawn to guide the eyes.

The range of concentrations (1 - 20 g/L, for µDSC heating and cooling traces see Figure 3.11) was chosen because of practical reasons, as for concentrations ≥ 30 g/L a gel is formed upon cooling due to entanglement of the long wCCMs, which might have an impact on the crystallization process. For concentrations below 1 g/L on the other hand, the enthalpy changes of melting/crystallization are very low and, thus, reach the detection limit of the µDSC apparatus. Lowering the concentration, we observe a significant decrease in the peak crystallization temperature (T_c) from 21.7 °C for 20 g/L to 8.5 °C for 1 g/L, respectively. This again supports a nucleation and growth process. The probability of creating stable nuclei from a semicrystalline polymer in solution decreases with concentration, as is predicted by theory[46,47] and was already shown for crystallization of PE homopolymers from solution.[48] As a result, higher supercoolings are required for crystallization at low concentrations. The melting endotherms, in contrast, only show a very small shift to higher peak melting temperatures (T_m) upon increasing concentration (from 47.2 to 50.4 °C). It has to be noted that both melting and crystallization occur at significantly lower temperatures compared to

the same triblock terpolymer in bulk (T_c = 62 °C; T_m = 88 °C).[26] This can be attributed to toluene acting as a plasticizer for the semicrystalline PE block, taking into account that toluene is a good solvent for PE in the molten state (Table 3.2).[49]

In order to fully understand this nucleation and growth mechanism, knowledge about the initial state, *i.e.*, the triblock terpolymer solution at temperatures well above the melting temperature of the PE block is essential, too. Therefore, we conducted small-angle neutron scattering (SANS) on a $S_{340}E_{700}M_{360}$ solution at 70 °C in toluene-d_8 (Figure 3.4).
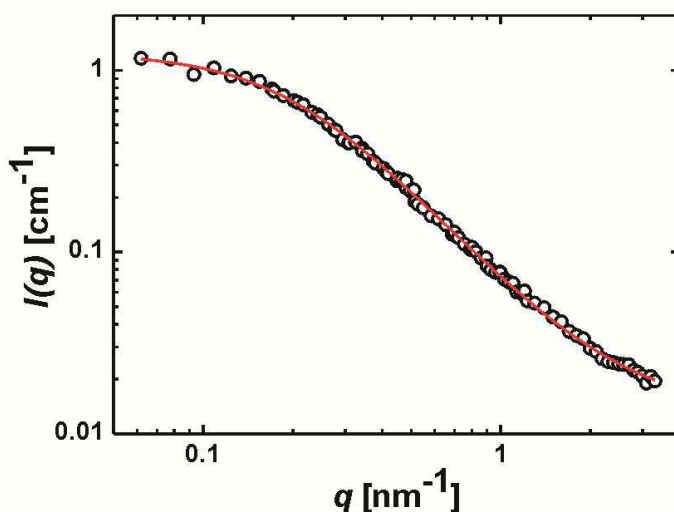
Figure 3.4: SANS profile of $S_{340}E_{700}M_{360}$ measured at 70°C in toluene-d_8 (10 g/L). The solid line is a fit with a model for Gaussian polymer coils including a Gaussian polydispersity.

The resulting scattering intensity trace could be fitted with a model for Gaussian polymer coils providing a radius of gyration of 8 ± 2 nm, showing that the majority of the triblock terpolymer is molecularly dissolved. The SANS profile does not show a significant contribution of micellar aggregates, which would give rise to an upturn of *I(q)* at low *q*-values. This is in agreement with previous results from DLS and scanning force microscopy that suggested a solution consisting of molecularly dissolved unimers and a negligible fraction of micellar aggregates.[26] It is noted, that DLS strongly overestimates the contribution of aggregates present in solution as the scattering intensity scales with R^6 in case of spherical micelles. The polymer-solvent interaction parameter $\chi_{PE\text{-}toluene}$ = 0.39 (Table 3.2) also supports a good solubility of PE above its melting temperature. Combining the

obtained information, the formation of wCCMs from $S_{340}E_{700}M_{360}$ in toluene can be described as a nucleation and growth process originating from a unimer solution.

For semicrystalline bulk polymers, annealing of existing crystallites can be used to perfect the crystallite structure, resulting in less folds and hence an increased crystallite thickness accompanied by a more uniform crystallite thickness distribution.[50] In order to see whether also in the present case an improvement of the preformed wCCMs can be achieved by subsequent solution-annealing of the PE cores or not, we performed μDSC annealing experiments on a 10 g/L toluene solution of $S_{340}E_{700}M_{360}$. A detailed description of the applied annealing procedure and the corresponding μDSC traces can be found in the *Supporting Information* (Scheme 3.2, Figure 3.12). These measurements revealed that most effective annealing takes place at 45 °C. The non-annealed wCCMs exhibit a rather broad melting peak ranging from 35 to 55 °C. In contrast, the heating trace after annealing the solution of the wCCMs at 45 °C for 3 h shows two distinct melting peaks (Figure 3.5): an intense, sharp one at a higher peak temperature compared to the initial melting endotherm (50.4 °C compared to 48.9 °C), and a very small one at lower temperatures corresponding to the fraction of unimers that were not able to participate in the annealing process and thus crystallized upon subsequent cooling. The increased melting temperature of the main peak corresponds to an increase in crystallite thickness as can be described by the Gibbs-Thomson equation.[51] In addition, the melting peak becomes significantly narrower after annealing, which indicates a more uniform crystallite thickness distribution. Annealing of samples with lower concentrations (1 g/L) shows similar effects (Figure 3.13) and is hereinafter applied as standard treatment prior to morphological studies by TEM.

The TEM image of $S_{340}E_{700}M_{360}$ wCCMs (Figure 3.6), which have been crystallized at 20 °C and subsequently annealed at 45 °C for 3 h, confirms a more uniform overall morphology and thickness of the PE cores compared to the non-annealed sample (Figure 3.2A). Moreover, the microphase separation between PS and PMMA in the micellar corona is somewhat more pronounced, which can be explained by the melting of some of the PE crystallites in the core allowing a partial rearrangement of the corona blocks during the annealing process. A similar observation of increasing microphase separation upon annealing was reported for amphiphilic block terpolymers in water.[52]
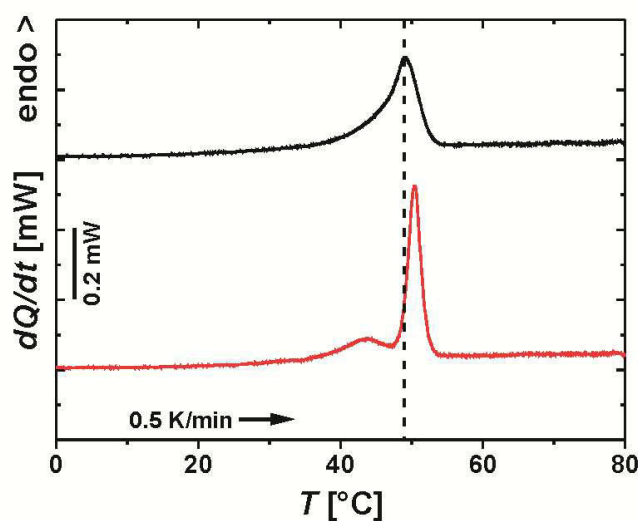
Figure 3.5. µDSC heating traces of a 10 g/L toluene solution of $S_{340}E_{700}M_{360}$ wCCMs before (——) and after (——) annealing for 3 h at 45 °C. The dashed line indicates the peak melting temperature before annealing.
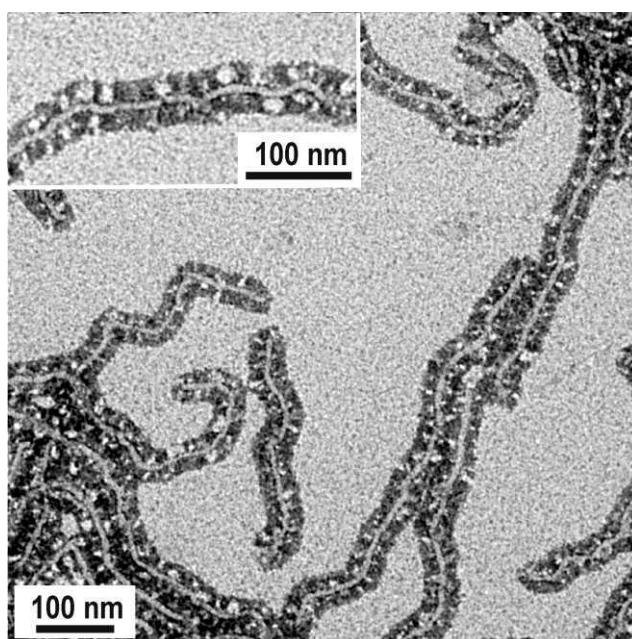
Figure 3.6. TEM micrograph of wCCMs formed in a 1 g/L solution of $S_{340}E_{700}M_{360}$ in toluene, crystallized at 20 °C and subsequently annealed for 3 hours at 45 °C.

A solvent of comparable quality to toluene is THF. The polymer-solvent interaction parameter $\chi_{PE\text{-}THF}$ = 0.41 is very similar to that for toluene ($\chi_{PE\text{-}toluene}$ = 0.39) and therefore, also THF should be able to dissolve PE in the molten state, *i.e.*, at elevated temperatures. µDSC measurements show that the transition temperatures and the annealing behavior of

$S_{340}E_{700}M_{360}$ in THF are very similar to that in toluene (Figure 3.14, Table 3.4). Due to the low boiling point of THF, $S_{340}E_{700}M_{360}$ was dissolved at 65 °C for 30 min, which is still significantly higher than the melting temperature of the PE block (T_m = 52.0 °C), followed by isothermal crystallization at 20 °C for one day and annealing at 45 °C for 3 h. As expected, TEM images again show wCCMs with a patch-like microphase separation of the corona (Figure 3.7).
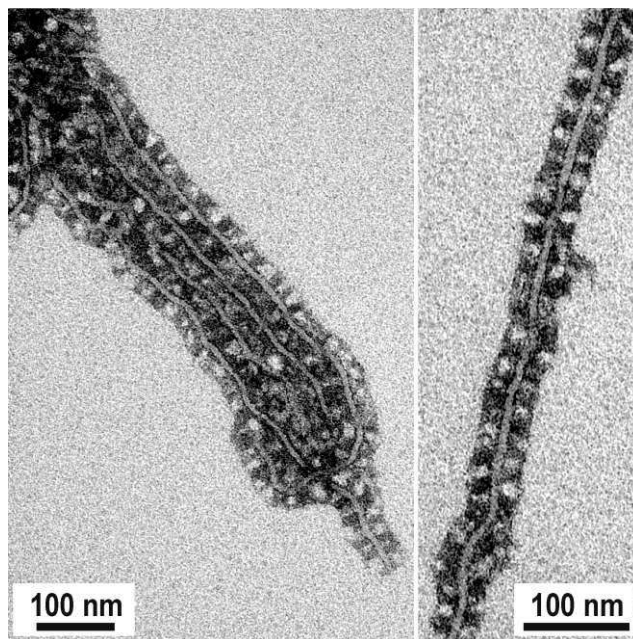
**Figure 3.7.** TEM micrographs of wCCMs formed in a 1 g/L $S_{340}E_{700}M_{360}$ solution in THF after annealing at 45 °C for 3h.

In contrast to the structures obtained from toluene, in which the diameter of the PMMA patches was rather small (D = 7 ± 4 nm), non-uniform, and they mostly were randomly distributed throughout the corona, significantly larger PMMA patches (D = 13 ± 4 nm) are observed for the wCCMs formed in THF. These PMMA patches exhibit a more defined shape spanning out from the PE core to the outer rim of the corona. In many sections, a regular one-dimensional array of alternating PS and PMMA corona patches is obtained (Figure 3.7). The observed differences should emanate from the selectivity of the used solvent for PS and PMMA. Toluene is known to be a better solvent for PS than for PMMA, whereas THF is supposed to be an equally good solvent for both corona blocks.[53] Thus, in toluene the PMMA chains are less swollen compared to PS and therefore form smaller compartments in an almost continuous PS corona despite the similar block lengths. In THF both of the corona blocks exhibit good solubility, favoring the formation of compartments of almost equal size.

Impact of the Triblock Copolymer Composition. In order to gain further understanding of the parameters favoring one-dimensional micellar growth, we synthesized two additional triblock terpolymers, $S_{280}E_{1190}M_{300}$ and $S_{140}E_{690}M_{160}$, both of them possessing a higher weight content of PE. Therefore, structures with a lower curvature, *i.e.*, lamellae (platelet-like) might be energetically favored for these copolymers, as was predicted in early theoretical works[5] and already observed several times experimentally.[24,54] Moreover, the overall molecular weight of $S_{140}E_{690}M_{160}$ is by a factor of about two lower compared to that of $S_{280}E_{1190}M_{300}$ and the previously used polymer. A decrease in overall molecular weight is expected to promote platelet formation, too, as was shown by Ryan *et al.*[30] But in our case, wCCMs with a microphase-separated corona are obtained for both, $S_{280}E_{1190}M_{300}$ and $S_{140}E_{690}M_{160}$ (Figure 3.8A,B), showing that the formation of linear structures is applicable to a wide range of block terpolymer compositions. As revealed by μDSC experiments (Figure 3.15, Table 3.4), the crystallization is shifted to higher temperatures, because of the increased PE content. Thus, crystallization was conducted at 29 °C for $S_{140}E_{690}M_{160}$ and 34 °C for $S_{280}E_{1190}M_{300}$ followed by annealing at 38 °C and 48 °C for 3h, respectively.
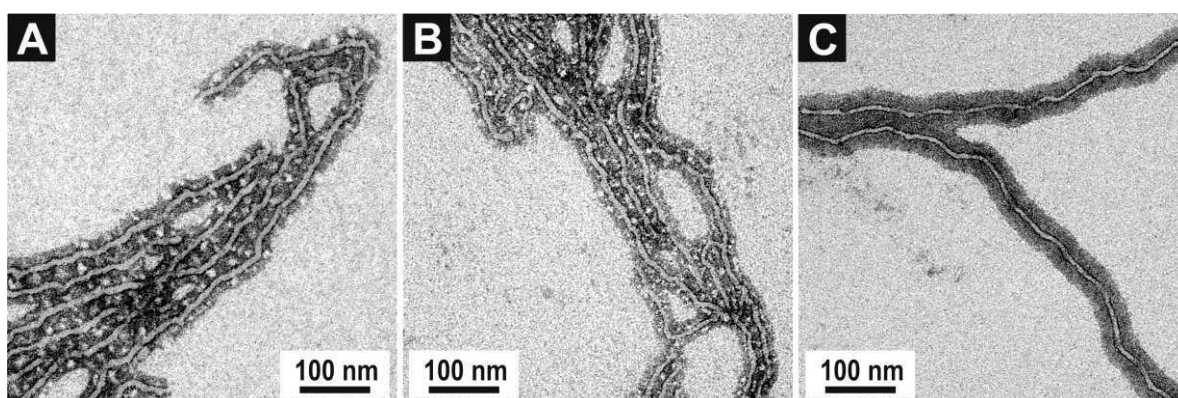
Figure 3.8. TEM images of wCCMs formed in 1 g/L THF solutions of $S_{280}E_{1190}M_{300}$ (A), $S_{140}E_{690}M_{160}$ (B), and $S_{380}E_{880}S_{390}$ (C), annealed in solution.

Another possible influence on the structure formation process might emanate from the incompatibility of the PS and PMMA corona blocks, which results in a less effective shielding of the PE core of the formed nuclei by the corona. This in turn would favor one-dimensional growth over the formation of spherical micelles, as already assumed earlier.

Consequently, a different situation might be expected for a triblock copolymer with identical end blocks. In order to address this point a $S_{380}E_{880}S_{390}$ triblock copolymer, comparable in block ratios and overall degree of polymerization to $S_{340}E_{700}M_{360}$, was synthesized. μDSC

experiments revealed similar thermal properties compared to that of $S_{340}E_{700}M_{360}$ (Table 3.4), and thus $S_{380}E_{880}S_{390}$ was crystallized at 20 °C followed by annealing at 45 °C for 3h, *i.e.*, the same protocol as applied for $S_{340}E_{700}M_{360}$. However, despite the identical PS end blocks, $S_{380}E_{880}S_{390}$ forms wCCMs in THF, too (Figure 3.8C). In this case the corona appears homogeneously dark after staining, as expected for a corona that solely consists of PS. The shown self-assembly of $S_{380}E_{880}S_{390}$ clearly shows that the formation of one-dimensional, elongated micelles does not depend on repulsive forces generated by PS/PMMA segregation in the corona, but seems to be independent of the chemical nature of the outer blocks.

The fact that wCCMs have been obtained from various $S_xE_yM_z$ triblock terpolymers as well as the $S_{380}E_{880}S_{390}$ triblock copolymer leads to the assumption that the middle position of the PE block is the key factor triggering one-dimensional growth over a broad composition range. This theory is corroborated by literature, as only one of the various studied systems with distinct PE blocks was found capable of cylinder formation upon crystallization, *i.e.*, PE-*b*-PEP diblock copolymer stars with PE in the center of the stars.[27] Here, PE is in the middle position surrounded by amorphous end blocks, in analogy to the triblock copolymers investigated in this study.

Structure Formation in Bad Solvents for PE. Up to this point, structure formation was conducted in good solvents for PE ($\chi_{PE\text{-}solvent} < 0.5$). We now focus on the self-assembly in dioxane, which is a good solvent for the corona blocks, but a bad solvent for PE ($\chi_{PE\text{-}dioxane} = 0.75$). µDSC measurements (Figure 3.9A) reveal transition temperatures of 79 °C (peak melting) and 44 °C (peak crystallization) for a 1 g/L solution of $S_{340}E_{700}M_{360}$. These temperatures are significantly higher compared to those observed in toluene (Figure 3.3, Table 3.4), which can be attributed to the lower solvent quality of dioxane for PE. Consequently, dioxane is not a good plasticizer and thus is not able to decrease melting and crystallization temperatures to a similar extent. In contrast to toluene solutions, no concentration dependency of the crystallization temperature (Figure 3.16) is observed for dioxane solutions.
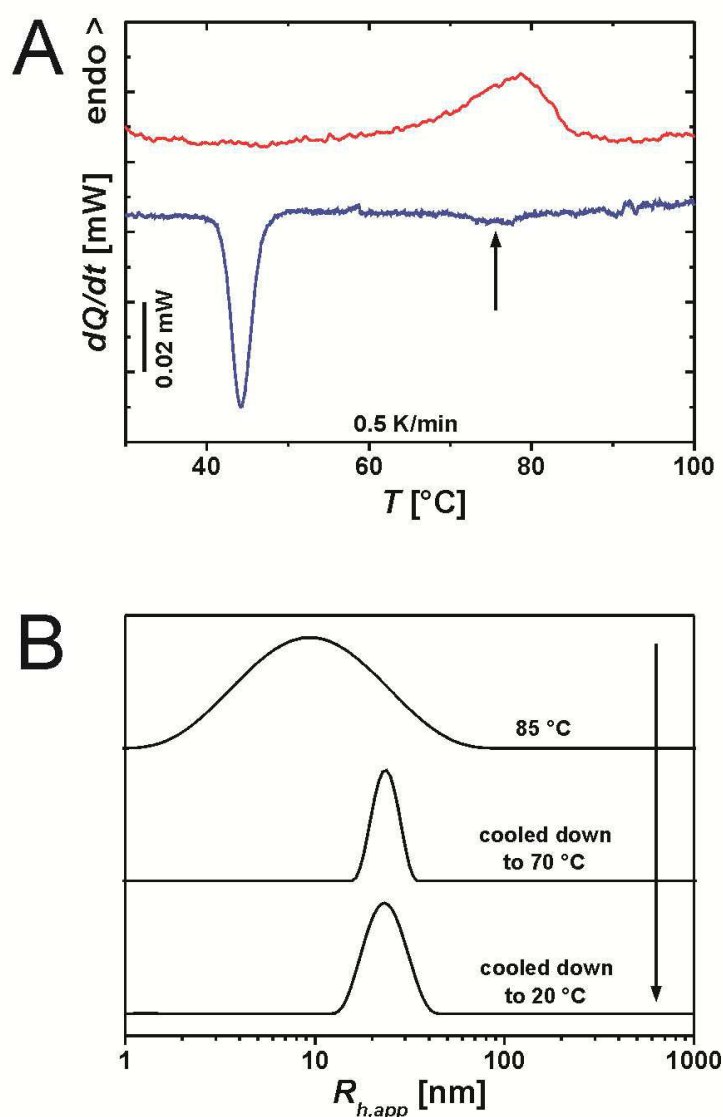
Figure 3.9. A) μDSC heating (—) and cooling traces (—) of a 1 g/L dioxane solution of $S_{340}E_{700}M_{360}$. The arrow highlights the weak micellization peak. B) Apparent hydrodynamic radii distributions obtained from DLS data measured for a 1 g/L dioxane solution of $S_{340}E_{700}M_{360}$ at temperatures as indicated.

The structure formation upon cooling was followed by dynamic light scattering (DLS) on a 1 g/L solution of $S_{340}E_{700}M_{360}$ in dioxane. First, the solution was heated to 85 °C for 2 h, *i.e.*, above the melting temperature of the PE block, and subsequently cooled down to 70 °C and then to room temperature. Figure 3.9B shows the corresponding hydrodynamic radii distributions obtained at different temperatures applying the CONTIN algorithm.[55] At 85 °C the absolute scattering intensity is very low and a broad distribution with an average apparent hydrodynamic radius of $R_{h,app} = 9$ nm can be found, which corresponds to molecularly dissolved triblock terpolymer chains. Already at 70 °C, a narrow distribution at

$R_{h,app}$ = 24 nm is observed, pointing to the formation of well-defined micelles. As mentioned above, dioxane is a rather poor solvent for PE. Thus, PE becomes insoluble upon cooling to 70 °C and spherical micelles with an amorphous PE core are formed, as the temperature is still significantly above the crystallization temperature (T_c = 44 °C). The weak peak at about 76 °C in the μDSC cooling trace (Figure 3.9A) also corresponds to this micellization process. It is exothermic in nature, as should be expected for micellization in organic solvents. The weak exotherm, attributable to the micellization process upon cooling, is present for all studied $S_{340}E_{700}M_{360}$ and $S_{380}E_{880}S_{390}$ solutions in dioxane (Figure 3.16), and has also been observed for similar block copolymers in dioxane.[56] Upon cooling down the solution to room temperature, $R_{h,app}$ does not change. Hence, the overall shape and size of the micelles is preserved and PE undergoes confined crystallization within the micellar core, resulting in spherical crystalline-core micelles (sCCMs). Similar examples of confined crystallization were reported for block copolymers in the bulk state, where the crystallizable block is confined within spherical microdomains.[57] In a PE-*b*-PS diblock copolymer, homogeneous nucleation was assumed for the crystallization of PE in spherical microdomains. Here, a supercooling $\Delta T = T_m - T_c$ of about 39 °C was necessary to induce crystallization.[58] In our case, the supercooling observed for $S_{340}E_{700}M_{360}$ in dioxane (ΔT = 35 °C) as well as the confinement in which crystallization occurs, *i.e.*, the core of spherical micelles, are comparable. Moreover, the degree of crystallinity of the PE cores in the sCCMs formed in dioxane is significantly lower compared to that of the wCCMs formed in toluene or THF (Table 3.4), which is a typical feature of confined crystallization. Consequently, a homogeneous nucleation should be the predominant nucleation mechanism for PE in the sCCMs. Structure formation of $S_{380}E_{880}S_{390}$ in dioxane proceeds in a similar way. μDSC and DLS results for $S_{380}E_{880}S_{390}$ in dioxane can be found in Figures 3.S6 and 3.S7.

TEM investigations confirm the formation of sCCMs for both types of triblock copolymers (Figure 3.10). The sCCMs formed from $S_{340}E_{700}M_{360}$ exhibit a microphase-separated corona of stained PS patches (dark) and non-stained PMMA patches (bright). Those composed of $S_{380}E_{880}S_{390}$ consequently show a uniformly dark corona of PS.
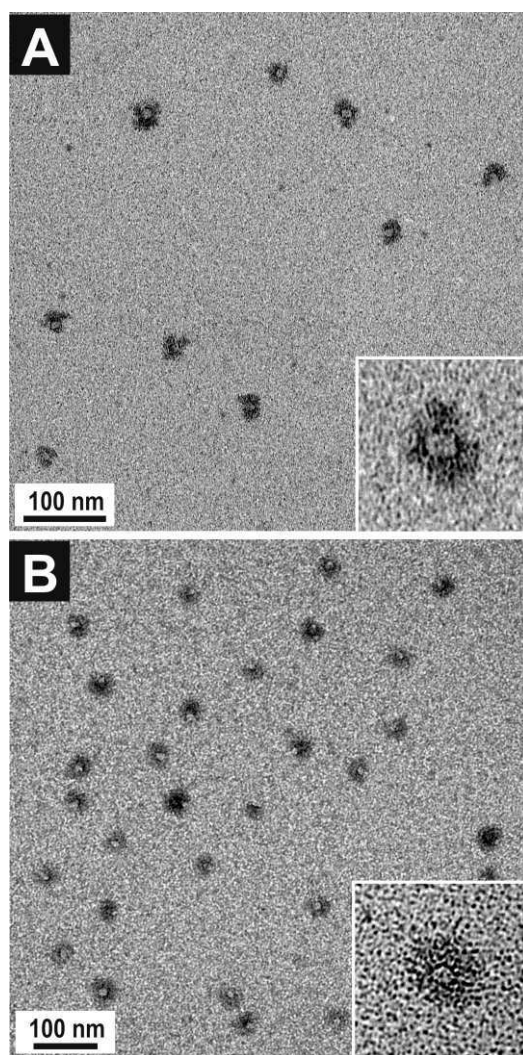
Figure 3.10. TEM micrographs of sCCMs formed in 1 g/L dioxane solutions of $S_{340}E_{700}M_{360}$ (A) and $S_{380}E_{880}S_{390}$ (B). The solutions were kept for three weeks at room temperature prior to sample preparation for TEM. (A) was diluted to 0.3 g/L before drop-coating on the TEM grid. The insets are magnified 3-fold.

Whereas the sCCMs made of $S_{380}E_{880}S_{390}$ could be nicely dispersed on the TEM grid from a 1 g/L solution, for those consisting of $S_{340}E_{700}M_{360}$ further dilution to 0.3 g/L was necessary to reduce the aggregation to superstructures during drying (Figure 3.18). The formation of such superstructures is a known feature of surface-compartmentalized polymer micelles and thus supports the patch-like structure of the corona for sCCMs based on SEM triblock terpolymers.[59] It is noted, that the TEM samples were prepared after keeping the solution at room temperature for three weeks, showing that these sCCMs are stable over time and do not form worm-like structures *via* aggregation/recrystallization processes.

In order to prove the general applicability of this concept, structure formation of $S_{340}E_{700}M_{360}$ in N,N-dimethylacetamide (DMAc) was conducted, which is an even worse solvent for PE

than dioxane ($\chi_{PE-DMAc}$ = 1.18). The solution was heated to 100 °C over night to erase any thermal history of PE and subsequently allowed to cool down to room temperature. In analogy to the structure formation in dioxane, sCCMs with a microphase-separated corona are obtained (Figure 3.19). Hence, the self-assembly in bad solvents for PE can be utilized as a general method for the production of sCCMs and is attributed to the collapse of PE upon cooling producing amorphous spherical micelles already above T_c.

Mechanism of Structure Formation. From the observed differences in the structure formation of the studied triblock copolymers with PE middle blocks a general scheme can be deduced that determines whether spherical or worm-like CCMs are formed (Scheme 3.1). The comparison of $S_xE_yM_z$ and $S_{380}E_{880}S_{390}$ revealed that the nature of the outer blocks is not important for the overall morphology, as long as they are sufficiently soluble in the chosen solvent throughout the applied temperature range. Thus, for the sake of clarity, we did not distinguish between the possibilities of different or equal outer blocks in this case.

The essential parameter determining the morphology, wCCMs *vs.* sCCMs, is the solubility of the molten PE in the applied solvent. The use of good solvents like toluene and THF where PE is completely soluble at $T > T_c$, enables the production of wCCMs with high aspect ratios. Upon lowering the temperature, at some point first nucleation events occur, producing a small number of micelles with a crystalline PE core. Over time, more and more unimers are deposited onto these crystalline micelles resulting in the observed wCCMs. In bad solvents on the other hand, *e.g.* dioxane and DMAc, sCCMs are formed. Here, PE is insoluble at $T > T_c$ and thus, spherical micelles with a molten PE core already exist prior to crystallization. The PE cores of the spherical micelles then crystallize independently upon cooling, as the sterically demanding corona chains prevent micellar fusion, an effect known as "over-spilling".[60] Thus, the availability of free unimers at the stage where crystallization occurs is identified as the key factor for the formation of highly anisotropic worm-like micelles from triblock terpolymers with a PE middle block. These findings allow the highly selective production of sCCMs and wCCMs from the same block copolymers by carefully choosing the solvent environment for the crystallization-induced structure formation.

Scheme 3.1. Proposed mechanism of the structure formation of triblock copolymers with a crystallizable PE middle block (black) and amorphous corona blocks (blue) in solvents of different quality.
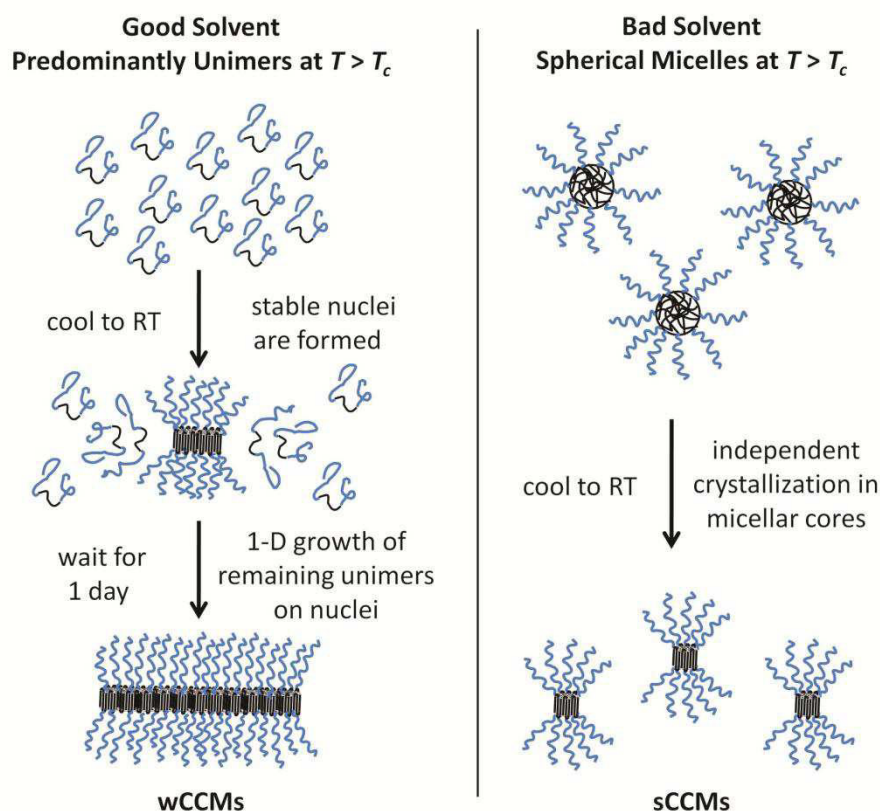
3.3. Conclusion

We introduce a general scheme predicting the crystallization-induced self-assembly of triblock copolymers with a semicrystalline PE middle block upon cooling in solution. Depending on the solubility of PE in the used solvent, the selective production of either spherical or worm-like crystalline-core micelles (CCMs) from the same block copolymers is possible. These CCMs consist of a semicrystalline PE core and a uniform (PS-*b*-PE-*b*-PS triblock copolymer) or a patchy (PS-*b*-PE-*b*-PMMA triblock terpolymer) corona. Spherical CCMs are formed in bad solvents for molten PE, *i.e.*, the PE blocks collapse upon cooling and spherical micelles with amorphous cores are formed prior to crystallization. As a result, confined crystallization of PE within the cores of the preformed spherical micelles takes place. In contrast, the triblock copolymer chains stay molecularly dissolved above the crystallization temperature for self-assembly in good solvents, and worm-like CCMs are formed *via* a nucleation and growth mechanism.

The length of the worm-like CCMs can be conveniently tuned by the applied temperature of isothermal crystallization. Further improvement of their structure is achieved by subsequent annealing in solution. This results in a more uniform thickness of the crystalline PE cores and the corona microphase separation in wCCMs based on SEM triblock terpolymers becomes more pronounced. Furthermore, the morphology of the patch-like corona depends on the selectivity of the used solvent for the PS and PMMA end blocks. In toluene, a slightly better solvent for PS, small PMMA patches in an almost continuous corona of PS are obtained. In contrast, structure formation in THF, a similarly good solvent for PS and PMMA, results in a unique one-dimensional array structure with nearly alternating PS and PMMA patches with dimensions of about 15 nm throughout the whole corona.

The presented approach enables the selective production of stable worm-like micelles with high aspect ratios and controlled surface anisotropies in an easy and reproducible manner, which is of increasing interest in materials science. Linear array structures represent promising scaffolds for waveguides in nanoscale photonic devices. Moreover, well-defined patchy nanoparticles have great potential for the tailor-made bottom-up production of hierarchical superstructures. In contrast to most of the previous approaches toward surface-compartmentalized nanostructures, the presented process of crystallization-driven solution self-assembly triggered by cooling is comparably undemanding and easy to upscale.

3.4. Methods

Synthesis of Triblock Copolymers. Detailed information about used materials, purification methods and the polymerization procedure applied for the synthesis of polystyrene-*block*-poly(1,4-butadiene)-*block*-poly(methyl methacrylate) triblock terpolymers can be found in a previous publication.[61]

The synthesis of polystyrene-*block*-poly(1,4-butadiene)-*block*-polystyrene (PS-*b*-PB-*b*-PS) was carried out in a thermostatted laboratory autoclave (Büchi Glas Uster AG) under a dry nitrogen atmosphere *via* sequential anionic polymerization of the corresponding monomers in cyclohexane. The use of a nonpolar solvent results in a PB block with a high content of 1,4-addition, which is indispensable to obtain the corresponding semicrystalline "pseudo-polyethylene" structure after hydrogenation. First, styrene was polymerized at 40 °C for 4 h

using *sec*-BuLi as the initiator. The reaction mixture was then cooled to 20 °C, and butadiene was added. Subsequently, butadiene polymerization was conducted at 50 °C for 4 h. Finally, the second portion of styrene was allowed to polymerize for 4 h at 40 °C followed by termination with methanol. The composition of the produced triblock copolymer $S_{380}B_{440}S_{390}$ (the subscripts denote the number-average degree of polymerization) was determined by ^{1}H-NMR measurements in $CDCl_3$ (Bruker AC 250 spectrometer) using the absolute molecular weight of the PS precursor, obtained from matrix-assisted laser desorption ionization-time of flight mass spectrometry (MALDI-TOF; Bruker Reflex III), for calibration of the NMR signal intensities.

Hydrogenation. Hydrogenation of the triblock copolymers in order to convert the PB block into PE was carried out *via* homogeneous catalysis in toluene at 60 °C and 60 bar H_2 pressure using Wilkinson's catalyst ($RhCl(PPh_3)_3$). A more detailed description can be found elsewhere.[26]

Sample Preparation. The triblock copolymers were dissolved at temperatures well above the melting temperature of the PE block in the used solvents to erase any thermal history. The samples prepared in toluene and THF were heated in a water bath to 70 °C and 65 °C, respectively, for at least 30 min after complete dissolution, followed by direct quenching to the desired crystallization temperature. Except for the studies on the influence of the applied crystallization temperature, all solutions of worm-like CCMs prepared for TEM measurements were subjected to subsequent annealing for 3 h at a temperature slightly below the melting temperature as indicated in the *Results and Discussion* section. The samples prepared in dioxane were heated to 90 °C, those prepared in N,N-dimethylacetamide to 100 °C over night and subsequently allowed to cool down to room temperature. In all cases moderate stirring was applied.

Micro-Differential Scanning Calorimetry (μDSC). The calorimetric measurements were performed with a Setaram μDSC III using closed "batch" cells at a scanning rate of 0.5 K/min. The pure solvent was used as a reference. The μDSC allows measurements with an extremely high sensitivity using sample masses up to 1 g and hence the detection of phase transitions of polymers in dilute solutions.

Dynamic Light Scattering (DLS), Static Light Scattering (SLS). DLS and SLS measurements were performed on an ALV DLS/SLS-SP 5022F compact goniometer system equipped with an ALV 5000/E operated in cross-correlation mode at a scattering angle of 90°. A He-Ne laser (λ_0 = 632.8 nm) was employed as light source.

Because of the large size of the aggregates formed at room temperature, the solutions were not filtered prior to the measurement to avoid any loss of material. The decalin bath of the instrument was thermostatted using a LAUDA Proline RP 845 thermostat. For the temperature steps, heating rates of about 3 K/min and cooling rates of about 2 K/min were applied. Prior to measurement, the solutions were allowed to equilibrate for at least 10 min after reaching the targeted temperature, except for the time-dependent SLS measurements of the scattering intensity, where data collection was started directly after reaching the desired crystallization temperature. The structure formation studies by SLS were conducted at a scattering angle of 90°, which represents a value of momentum transfer q = 0.014 nm^{-1}. This value of q is more than one order of magnitude lower than the expected first form factor minimum of the wCCMs q_{min}. On the basis of the diameter of $S_{340}E_{700}M_{360}$ wCCMs determined from TEM (D = 51 nm) a form factor minimum at q_{min} = 0.25 nm^{-1} can be calculated. Hence, the performed SLS measurements are in a q-range much lower than the Guinier region and form factor contributions to the scattering intensity can be neglected. However, a quantitative interpretation of the scattering intensity is difficult and not the scope of the present contribution. The results from SLS are only used to show a qualitative trend.

Data evaluation of the DLS experiments was performed using the CONTIN algorithm[55], which yields an intensity-weighted distribution of relaxation times (τ) after an inverse Laplace transformation of the intensity auto-correlation function. These relaxation times were transformed into translational diffusion coefficients and further into hydrodynamic radii using the Stokes-Einstein equation.

Transmission Electron Microscopy (TEM). Samples were prepared by placing a drop of the dilute solution (0.25–1 g/L) on a carbon-coated copper grid. After 20 s, excess solution was removed by blotting with a filter paper. Subsequently, elastic bright-field TEM was performed on a Zeiss 922 OMEGA EFTEM (Zeiss NTS GmbH, Oberkochen, Germany)

operated at 200 kV. Zero-loss filtered images ($\Delta E = 0$) were registered digitally by a bottom mounted CCD camera system (Ultrascan 1000, Gatan) and processed with a digital imaging processing system (Gatan Digital Micrograph 3.9 for GMS 1.4). Staining was performed with RuO_4 vapor for at least 20 min. RuO_4 is known to selectively stain PS, *i.e.*, PS domains appear darker compared to PMMA domains, which enables to distinguish between PS and PMMA domains in the corona of the micelles. Average values of the micelle length and PMMA patch size were determined from at least 100 measurements. Due to better visibility, the average micelle length of the wCCMs was obtained by measuring the core length.

Small-Angle Neutron Scattering (SANS). The SANS measurement was performed on the PAXY instrument of the Laboratoire Léon Brillouin (CEA de Saclay, Gif-sur-Yvette, France). The scattered neutrons were collected using a two-dimensional multi-detector. Three sample-to-detector distances of 1.05 m, 3.05 m, and 6.75 m were chosen in order to cover a sufficiently broad q-range. The sample was placed in a thermostatted holder and the temperature was controlled using a PT 100 thermoelement with stability in temperature of approximately ± 1 °C. The sample was prepared in deuterated toluene (C_7D_8) and filled in 1 mm standard quartz cells (Hellma, Germany).

All recorded scattering patterns were isotropic and hence circularly averaged. Furthermore, the resulting spectra were corrected for electronic noise, detector efficiency and the scattering of the empty cell and the solvent. The absolute intensity calibration was done using the software provided by the LLB using the approach described by Cotton.[62] Further information on the data treatment procedure of the LLB can be found elsewhere.[63] After this treatment all data from different sample-to-detector distances overlapped within the experimental precision. Finally, the normalized and merged scattering profile was analyzed applying the SASfit program by J. Kohlbrecher.[64]

3.5.References

1. Haberkorn, N.; Lechmann, M. C.; Sohn, B. H.; Char, K.; Gutmann, J. S.; Theato, P. Templated Organic and Hybrid Materials for Optoelectronic Applications. *Macromol. Rapid Commun.* **2009**, *30*, 1146-1166.

2. Motornov, M.; Roiter, Y.; Tokarev, I.; Minko, S. Stimuli-Responsive Nanoparticles, Nanogels and Capsules for Integrated Multifunctional Intelligent Systems. *Prog. Polym. Sci.* **2010**, *35*, 174-211.

3. Ruzette, A. V.; Leibler, L. Block Copolymers in Tomorrow's Plastics. *Nat. Mater.* **2005**, *4*, 19-31.

4. Rodríguez-Hernández, J.; Chécot, F.; Gnanou, Y.; Lecommandoux, S. Toward 'Smart' Nano-Objects by Self-Assembly of Block Copolymers in Solution. *Prog. Polym. Sci.* **2005**, *30*, 691-724.

5. Vilgis, T.; Halperin, A. Aggregation of Coil-Crystalline Block Copolymers: Equilibrium Crystallization. *Macromolecules* **1991**, *24*, 2090-2095.

6. Lazzari, M.; Lopez-Quintela, M. A. Micellization Phenomena in Semicrystalline Block Copolymers: Reflexive and Critical Views on the Formation of Cylindrical Micelles. *Macromol. Rapid Commun.* **2009**, *30*, 1785-1791.

7. Wang, X.; Guerin, G.; Wang, H.; Wang, Y.; Manners, I.; Winnik, M. A. Cylindrical Block Copolymer Micelles and Co-Micelles of Controlled Length and Architecture. *Science* **2007**, *317*, 644-647.

8. Gaedt, T.; Ieong, N. S.; Cambridge, G.; Winnik, M. A.; Manners, I. Complex and Hierarchical Micelle Architectures from Diblock Copolymers Using Living, Crystallization-driven Polymerizations. *Nat. Mater.* **2009**, *8*, 144-150.

9. Qian, J. S.; Zhang, M.; Manners, I.; Winnik, M. A. Nanofiber Micelles from the Self-Assembly of Block Copolymers. *Trends Biotechnol.* **2010**, *28*, 84-92.

10. Raez, J.; Barjovanu, R.; Massey, J. A.; Winnik, M. A.; Manners, I. Self-assembled Organometallic Block Copolymer Nanotubes. *Angew. Chem. Int. Ed.* **2000**, *39*, 3862-3865.

11. Raez, J.; Tomba, J. P.; Manners, I.; Winnik, M. A. A Reversible Tube-to-Rod Transition in a Block Copolymer Micelle. *J. Am. Chem. Soc.* **2003**, *125*, 9546-9547.

12. Cao, L.; Manners, I.; Winnik, M. A. Influence of the Interplay of Crystallization and Chain Stretching on Micellar Morphologies: Solution Self-Assembly of Coil-Crystalline Poly(isoprene-*block*-ferrocenylsilane). *Macromolecules* **2002**, *35*, 8258-8260.

13. Gilroy, J. B.; Gaedt, T.; Whittell, G. R.; Chabanne, L.; Mitchels, J. M.; Richardson, R. M.; Winnik, M. A.; Manners, I. Monodisperse Cylindrical Micelles by Crystallization-driven Living Self-Assembly. *Nat. Chem.* **2010**, *2*, 566-570.

14. Qian, J.; Guerin, G.; Lu, Y.; Cambridge, G.; Manners, I.; Winnik, M. A. Self-seeding in One Dimension: An Approach to Control the Length of Fiberlike Polyisoprene–Polyferrocenylsilane Block Copolymer Micelles. *Angew. Chem. Int. Ed.* **2011**, *50*, 1622-1625.

15. Mihut, A. M.; Drechsler, M.; Möller, M.; Ballauff, M. Sphere-to-Rod Transition of Micelles Formed by the Semicrystalline Polybutadiene-*block*-poly(ethylene oxide) Block Copolymer in a Selective Solvent. *Macromol. Rapid Commun.* **2010**, *31*, 449-453.

16. Du, Z.-X.; Xu, J.-T.; Fan, Z.-Q. Regulation of Micellar Morphology of PCL-*b*-PEO Copolymers by Crystallization Temperature. *Macromol. Rapid Commun.* **2008**, *29*, 467-471.

17. He, W. N.; Xu, J. T.; Du, B. Y.; Fan, Z. Q.; Wang, X. S. Inorganic-Salt-induced Morphological Transformation of Semicrystalline Micelles of PCL-*b*-PEO Block Copolymer in Aqueous Solution. *Macromol. Chem. Phys.* **2010**, *211*, 1909-1916.

18. Patra, S. K.; Ahmed, R.; Whittell, G. R.; Lunn, D. J.; Dunphy, E. L.; Winnik, M. A.; Manners, I. Cylindrical Micelles of Controlled Length with a π-Conjugated Polythiophene Core via Crystallization-driven Self-Assembly. *J. Am. Chem. Soc.* **2011**, *133*, 8842-8845.

19. Lazzari, M.; Scalarone, D.; Hoppe, C. E.; Vazquez-Vazquez, C.; Lopez-Quintela, M. A. Tunable Polyacrylonitrile-based Micellar Aggregates as a Potential Tool for the Fabrication of Carbon Nanofibers. *Chem. Mater.* **2007**, *19*, 5818-5820.

20. Lazzari, M.; Scalarone, D.; Vazquez-Vazquez, C.; Lopez-Quintela, M. A. Cylindrical Micelles from the Self-Assembly of Polyacrylonitrile-based Diblock Copolymers in Nonpolar Selective Solvents. *Macromol. Rapid Commun.* **2008**, *29*, 352-357.

21. Portinha, D.; Boué, F.; Bouteiller, L.; Carrot, G.; Chassenieux, C.; Pensec, S.; Reiter, G. Stable Dispersions of Highly Anisotropic Nanoparticles Formed by Cocrystallization of Enantiomeric Diblock Copolymers. *Macromolecules* **2007**, *40*, 4037-4042.

22.   Petzetakis, N.; Dove, A. P.; O'Reilly, R. K. Cylindrical Micelles from the Living Crystallization-driven Self-Assembly of Polylactide-containing Block Copolymers. *Chem. Sci.* **2011**, *2*, 955-960.

23.   Monkenbusch, M.; Schneiders, D.; Richter, D.; Willner, L.; Leube, W.; Fetters, L. J.; Huang, J. S.; Lin, M. Aggregation Behaviour of PE-PEP Copolymers and the Winterization of Diesel Fuel. *Physica B* **2000**, *276-278*, 941-943.

24.   Wang, J.; Horton, J. H.; Liu, G.; Lee, S.-Y.; Shea, K. J. Polymethylene-*block*-poly(dimethyl siloxane)-*block*-polymethylene Nanoaggregates in Toluene at Room Temperature. *Polymer* **2007**, *48*, 4123-4129.

25.   Yin, L. G.; Hillmyer, M. A. Disklike Micelles in Water from Polyethylene-containing Diblock Copolymers. *Macromolecules* **2011**, *44*, 3021-3028.

26.   Schmalz, H.; Schmelz, J.; Drechsler, M.; Yuan, J.; Walther, A.; Schweimer, K.; Mihut, A. M. Thermo-Reversible Formation of Wormlike Micelles with a Microphase-separated Corona from a Semicrystalline Triblock Terpolymer. *Macromolecules* **2008**, *41*, 3235-3242.

27.   Ramzi, A.; Prager, M.; Richter, D.; Efstratiadis, V.; Hadjichristidis, N.; Young, R. N.; Allgaier, J. B. Influence of Polymer Architecture on the Formation of Micelles of Miktoarm Star Copolymers Polyethylene/Poly(ethylenepropylene) in the Selective Solvent Decane. *Macromolecules* **1997**, *30*, 7171-7182.

28.   Xu, J.-T.; Jin, W.; Liang, G.-D.; Fan, Z.-Q. Crystallization and Coalescence of Block Copolymer Micelles in Semicrystalline Block Copolymer/Amorphous Homopolymer Blends. *Polymer* **2005**, *46*, 1709-1716.

29.   Chan, S.-C.; Kuo, S.-W.; Lu, C.-H.; Lee, H.-F.; Chang, F.-C. Synthesis and Characterizations of the Multiple Morphologies Formed by the Self-Assembly of the Semicrystalline P4VP-*b*-PCL Diblock Copolymers. *Polymer* **2007**, *48*, 5059-5068.

30.   Xu, J.-T.; Fairclough, J. P. A.; Mai, S.-M.; Ryan, A. J. The Effect of Architecture on the Morphology and Crystallization of Oxyethylene/Oxybutylene Block Copolymers from Micelles in *n*-Hexane. *J. Mater. Chem.* **2003**, *13*, 2740-2748.

31.   Walther, A.; Müller, A. H. E. Janus Particles. *Soft Matter* **2008**, *4*, 663-668.

32.   Kretzschmar, I.; Song, J. H. Surface-Anisotropic Spherical Colloids in Geometric and Field Confinement. *Curr. Opin. Colloid Interface Sci.* **2011**, *16*, 84-95.

33. Walther, A.; Matussek, K.; Müller, A. H. E. Engineering Nanostructured Polymer Blends with Controlled Nanoparticle Location Using Janus Particles. *ACS Nano* **2008**, *2*, 1167-1178.

34. Jiang, S.; Chen, Q.; Tripathy, M.; Luijten, E.; Schweizer, K. S.; Granick, S. Janus Particle Synthesis and Assembly. *Adv. Mater.* **2010**, *22*, 1060-1071.

35. Wurm, F.; Kilbinger, A. F. M. Polymeric Janus Particles. *Angew. Chem. Int. Ed.* **2009**, *48*, 8412-8421.

36. Voets, I. K.; Fokkink, R.; Hellweg, T.; King, S. M.; de Waard, P.; de Keizer, A.; Cohen Stuart, M. A. Spontaneous Symmetry Breaking: Formation of Janus Micelles. *Soft Matter* **2009**, *5*, 999-1005.

37. Kuo, S.-W.; Tung, P.-H.; Lai, C.-L.; Jeong, K.-U.; Chang, F.-C. Supramolecular Micellization of Diblock Copolymer Mixtures Mediated by Hydrogen Bonding for the Observation of Separated Coil and Chain Aggregation in Common Solvents. *Macromol. Rapid Commun.* **2008**, *29*, 229-233.

38. McConnell, M. D.; Kraeutler, M. J.; Yang, S.; Composto, R. J. Patchy and Multiregion Janus Particles with Tunable Optical Properties. *Nano Lett.* **2010**, *10*, 603-609.

39. Du, J.; O'Reilly, R. K. Anisotropic Particles with Patchy, Multicompartment and Janus Architectures: Preparation and Application. *Chem. Soc. Rev.* **2011**, *40*, 2402-2416.

40. Glotzer, S. C.; Solomon, M. J. Anisotropy of Building Blocks and their Assembly into Complex Structures. *Nat. Mater.* **2007**, *6*, 557-562

41. LoPresti, C.; Massignani, M.; Fernyhough, C.; Blanazs, A.; Ryan, A. J.; Madsen, J.; Warren, N. J.; Armes, S. P.; Lewis, A. L.; Chirasatitsin, S., et al. Controlling Polymersome Surface Topology at the Nanoscale by Membrane Confined Polymer/Polymer Phase Separation. *ACS Nano* **2011**, *5*, 1775-1784.

42. Theodorakis, P. E.; Paul, W.; Binder, K. Interplay between Chain Collapse and Microphase Separation in Bottle-Brush Polymers with Two Types of Side Chains. *Macromolecules* **2010**, *43*, 5137-5148.

43. Njikang, G.; Han, D. H.; Wang, J.; Liu, G. J. ABC Triblock Copolymer Micelle-Like Aggregates in Selective Solvents for A and C. *Macromolecules* **2008**, *41*, 9727-9735.

44. Dupont, J.; Liu, G. J.; Niihara, K.; Kimoto, R.; Jinnai, H. Self-assembled ABC Triblock Copolymer Double and Triple Helices. *Angew. Chem. Int. Ed.* **2009**, *48*, 6144-6147.

45. Wunderlich, B. *Macromolecular Physics*, Academic Press: New York, 1976.

46. Nielsen, A. E. Nucleation and Growth of Crystals at High Supersaturation. *Kristall und Technik* **1969**, *4*, 17-38.

47. Zhang, J. N.; Muthukumar, M. Monte Carlo Simulations of Single Crystals from Polymer Solutions. *J. Chem. Phys.* **2007**, *126*, 234904/1-234904/18.

48. Toda, A.; Kiho, H. Crystal Growth of Polyethylene from Dilute Solution: Growth Kinetics of {110} Twins and Diffusion-limited Growth of Single Crystals. *J. Polym. Sci., Part B: Polym. Phys.* **1989**, *27*, 53-70.

49. Flory, P. J. Thermodynamics of Crystallization in High Polymers. 4. A Theory of Crystalline States and Fusion in Polymers, Copolymers, and their Mixtures with Diluents. *J. Chem. Phys.* **1949**, *17*, 223-240.

50. Peterlin, A. Thickening of Polymer Single Crystals During Annealing. *J. Polym. Sci., Part B: Polym. Lett.* **1963**, *1*, 279-284.

51. Wunderlich, B.; Czornyj, G. A Study of Equilibrium Melting of Polyethylene. *Macromolecules* **1977**, *10*, 906-913.

52. Walther, A.; Barner-Kowollik, C.; Müller, A. H. E. Mixed, Multicompartment, or Janus Micelles? A Systematic Study of Thermoresponsive Bis-Hydrophilic Block Terpolymers. *Langmuir* **2010**, *26*, 12237-12246.

53. Kent, M. S.; Tirrell, M.; Lodge, T. P. Properties of Polystyrene-Poly(methyl methacrylate) Random and Diblock Copolymers in Dilute and Semidilute Solutions. *J. Polym. Sci., Part B: Polym. Phys.* **1994**, *32*, 1927-1941.

54. Richter, D.; Schneiders, D.; Monkenbusch, M.; Willner, L.; Fetters, L. J.; Huang, J. S.; Lin, M.; Mortensen, K.; Farago, B. Polymer Aggregates with Crystalline Cores: The System Polyethylene-Poly(ethylenepropylene). *Macromolecules* **1997**, *30*, 1053-1068.

55. Provencher, S. W. A Constrained Regularization Method for Inverting Data Represented by Linear Algebraic or Integral Equations. *Comput. Phys. Commun.* **1982**, *27*, 213-227.

56. Quintana, J. R.; Villacampa, M.; Katime, I. A. Micellization of a Polystyrene-*b*-poly(ethylene/propylene) Block Copolymer in *n*-Dodecane/1,4-Dioxane Mixtures. 2. Structure and Dimensions of Micelles. *Macromolecules* **1993**, *26*, 606-611.

57. Müller, A. J.; Balsamo, V.; Arnal, M. L. Nucleation and Crystallization in Diblock and Triblock Copolymers. *Adv. Polym. Sci.* **2005**, *190*, 1-63.

58. Lorenzo, A. T.; Arnal, M. L.; Müller, A. J.; de Fierro, A. B.; Abetz, V. Confinement Effects on the Crystallization and SSA Thermal Fractionation of the PE Block within PE-*b*-PS Diblock Copolymers. *Eur. Polym. J.* **2006**, *42*, 516-533.

59. Dupont, J.; Liu, G. J. ABC Triblock Copolymer Hamburger-Like Micelles, Segmented Cylinders, and Janus Particles. *Soft Matter* **2010**, *6*, 3654-3661.

60. Halperin, A. Polymeric vs. Monomeric Amphiphiles: Design Parameters. In *Supramolecular Polymers*; Ciferri, A., Ed. Marcel Dekker, Inc.: New York/Basel, 2000.

61. Ruckdäschel, H.; Sandler, J. K. W.; Altstädt, V.; Rettig, C.; Schmalz, H.; Abetz, V.; Müller, A. H. E. Compatibilisation of Immiscible Blends by Triblock Terpolymers – Correlation between Block Copolymer Composition, Morphology and Properties. *Polymer* **2006**, *47*, 2772-2790.

62. Cotton, J. P. Initial Data Treatment. In *Neutron, X-Ray and Light Scattering*; Lindner, P., Zemb, T., Eds.; Elsevier Science Publishers B. V.: Amsterdam, 1991.

63. Brulet, A.; Lairez, D.; Lapp, A.; Cotton, J.-P. Improvement of Data Treatment in Small-Angle Neutron Scattering. *J. Appl. Crystallogr.* **2007**, *40*, 165-177.

64. Kohlbrecher, J. *SASfit: A Program for Fitting Simple Structural Models to Small Angle Scattering Data*, Paul Scherrer Institute, Laboratory for Neutron Scattering: CH-5232, Villigen Switzerland, 2008.

3.6. Supporting Information

Polymer-solvent interaction parameters.[1] The polymer-solvent interaction parameter $\chi_{Polymer\text{-}Solvent}$ is used as a measure for the solubility of a polymer in the used solvent. Hereby, values of $\chi_{Polymer\text{-}Solvent} < 0.5$ point to a good solubility, whereas solvents that exhibit a $\chi_{Polymer\text{-}Solvent} > 0.5$ are considered as bad solvents for the given polymer. χ consists of an enthalpic and an entropic contribution (eq. 3.1):

$$\chi = \chi_H + \chi_S \,.$$

(eq. 3.1)

The entropic part χ_S usually is a constant between 0.3 and 0.4. For nonpolar systems as in our case $\chi_S = 0.34$ is used.[2] The enthalpic component χ_H can be calculated using the Hildebrandt solubility parameters (eq. 3.2):

$$\chi_H = \frac{V_1}{RT} \left(\delta_1 - \delta_2 \right)^2 \,.$$

(eq. 3.2)

V_1: molar volume of the solvent; R: universal gas constant; T: thermodynamic temperature; δ_1, δ_2: Hildebrandt solubility parameters of the solvent and the polymer, respectively.

The polyethylene-solvent interaction parameters $\chi_{PE\text{-}Solvent}$ used in this publication as well as the Hildebrandt solubility parameters taken for calculation[3] are summarized in Table 3.2.

Table 3.2. Hildebrandt solubility parameters δ and calculated polyethylene-solvent interaction parameters $\chi_{PE\text{-}Solvent}$ at T = 343 K.

Polymer	δ [MPa$^{1/2}$]	Solvent	δ [MPa$^{1/2}$]	$\chi_{PE\text{-}Solvent}$
PE	17.0	toluene	18.2	0.39
PE	17.0	THF	18.6	0.41
PE	17.0	dioxane	20.7	0.75
PE	17.0	DMAc	22.1	1.18

Table 3.3. Molecular characteristics of the used triblock copolymers.

Polymer[a]	Polymer[b]	PDI[c]	Ethyl branches / 100 C[d]
$S_{340}E_{700}M_{360}$	$S_{39}E_{21}M_{40}{}^{91}$	1.04	2.6
$S_{280}E_{1190}M_{300}$	$S_{32}E_{36}M_{32}{}^{93}$	1.03	2.6
$S_{140}E_{690}M_{160}$	$S_{30}E_{39}M_{31}{}^{50}$	1.04	3.4
$S_{380}E_{880}S_{390}$	$S_{38}E_{23}S_{39}{}^{105}$	1.04	2.7

a) subscripts denote the number-average degree of polymerization

b) subscripts denote the content of the respective polymer block in wt %, superscript denotes the number-average molecular weight in kg/mol

c) polydispersity index of the PB-containing precursor block copolymer (before hydrogenation) as obtained by THF-SEC using a polystyrene calibration

d) average amount of ethyl branches per 100 main chain carbon atoms resulting from 1,2-addition in the polymerization of PB, determined by ^{1}H-NMR of the precursor triblock copolymer
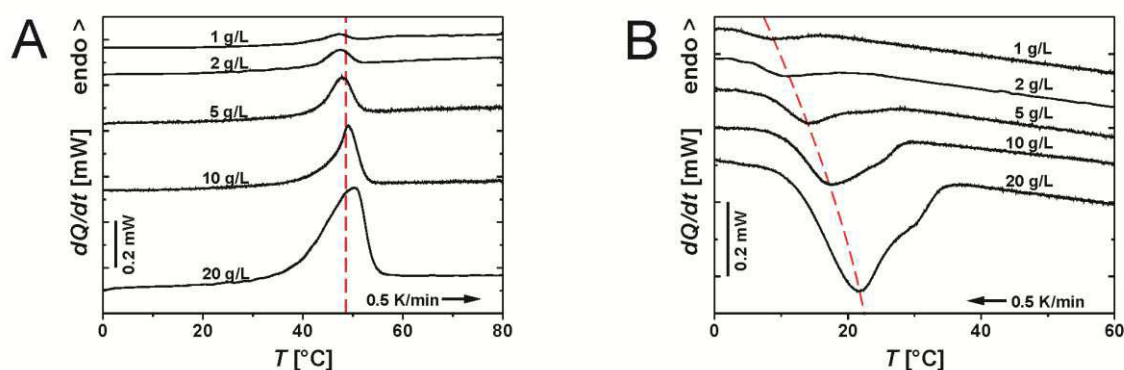
Figure 3.11. µDSC heating (A) and cooling (B) traces of $S_{340}E_{700}M_{360}$ solutions in toluene at different concentrations as indicated. Dashed red lines are drawn to guide the eye.

For the **μDSC annealing experiments on S$_{340}$E$_{700}$M$_{360}$ in toluene** (10 g/L) a procedure similar to successive self-nucleation and annealing (SSA) was applied.[4] The temperature profile of such a measurement can be found in Scheme 3.2. In the first step, the solution was always heated to 80 °C (1), which erases any thermal history, followed by cooling down to -10 °C (2) in order to guarantee complete crystallization of the PE block and thus to create a defined starting point for the annealing experiments. The sample was then heated to the desired annealing temperature T_a (3) and kept there for three hours (4) before it was again cooled down to -10 °C (5). The subsequent heating trace (6) now reveals any changes in crystallite size and/or size distribution originating from successful annealing. This is manifested by a shift of the peak melting temperature T_m to higher values and/or narrowing of the melting peak. This heating step at the same time erases the thermal history for the next measurement, which then is conducted by repeating steps (2) to (6) using a different T_a. The corresponding cooling traces of step (5) and the heating traces of step (6) are depicted in Figure 3.12.
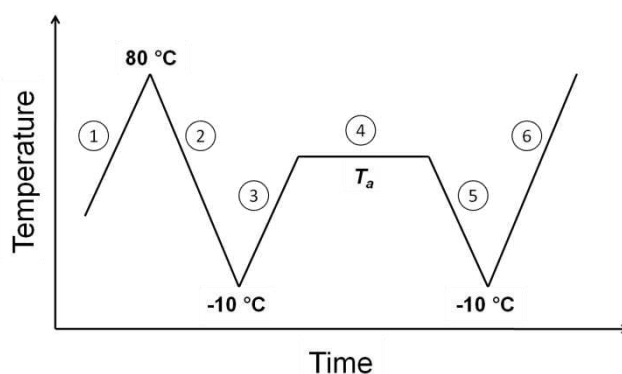

Scheme 3.2. Temperature profile of the conducted annealing experiments.

Annealing at 67 °C for 3 h is still sufficient to assure complete melting of the PE cores, as melting and crystallization temperatures are identical compared to those observed for heating to 80 °C (compare Figure 3.11). At T_a = 51 °C already a small fraction of the crystallites could be annealed (Figure 3.12B, small peak at 54 °C), whereas the majority of the polymer still crystallizes during the subsequent cooling step (Figure 3.12A). The crystallization exotherm is slightly shifted to higher temperatures, which indicates self-seeding, *i.e.*, remaining annealed crystallites serve as nuclei for the crystallization of polymer chains in solution. At T_a = 45 °C two distinct melting peaks can be observed: an intense, sharp one at a higher peak temperature compared to the initial melting endotherm (50.4 °C

compared to 48.9 °C), and a very small one at lower temperatures corresponding to a small fraction of unimers that were not able to participate in the annealing process and hence crystallized upon cooling. For an annealing temperature of 39 °C only the smaller crystallites are partially annealed resulting in a shoulder at the low-temperature side of the melting endotherm. For treatment at T_a = 30 °C the melting endotherm again resembles that after heating to at least 67 °C. Hence, up to 30 °C no annealing occurs. In conclusion, annealing at 45 °C clearly showed the best results, *i.e.*, the narrowest crystallite size distribution together with a pronounced increase in T_m.
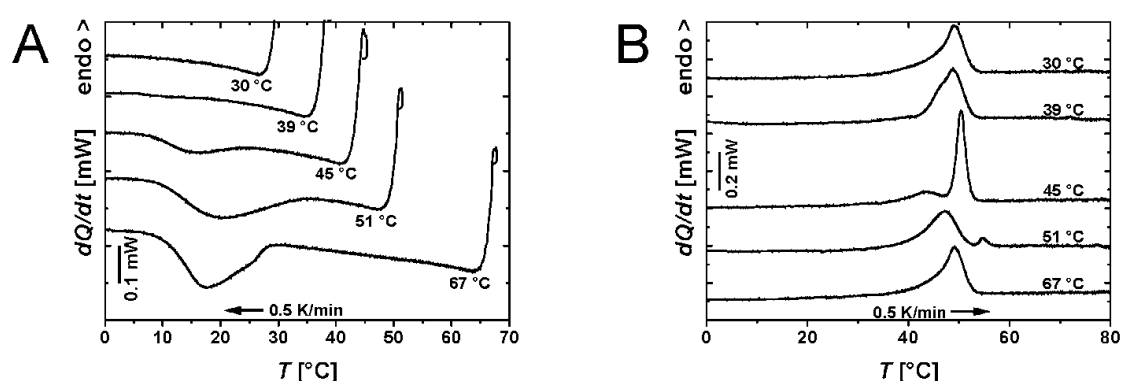

Figure 3.12. μDSC cooling (A) and heating (B) traces of a 10 g/L toluene solution of $S_{340}E_{700}M_{360}$ after annealing for 3 h at the given temperatures.

Figure 3.13 shows **μDSC heating traces of a 1g/L $S_{340}E_{700}M_{360}$ solution in toluene** (crystallized isothermally at 20 °C for 24 h) without annealing and after additional annealing at 45 °C for 3 h. The two curves clearly show that annealing of a 1 g/L solution leads to comparable results as for 10 g/L (compare Figure 3.12). Hence, this additional annealing step has been performed for all wCCMs in this publication prior to TEM imaging, except for those crystallized at different temperatures (Figure 3.2, main manuscript). Here, annealing might have influenced the length distributions caused by the different temperatures applied for isothermal crystallization.
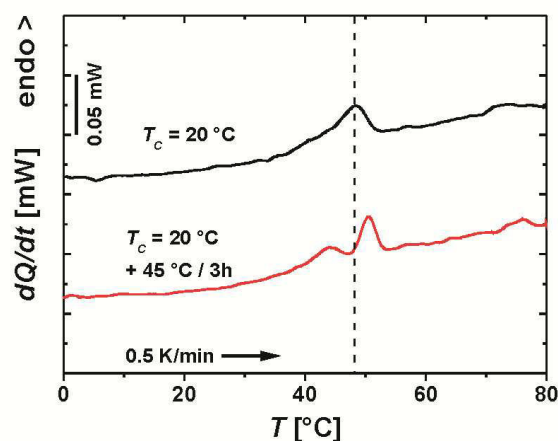
Figure 3.13. μDSC heating traces of a 1 g/L $S_{340}E_{700}M_{360}$ solution in toluene after isothermal crystallization at 20 °C for 24 h (—) and after additional annealing at 45 °C for 3 h (—).

μDSC measurements of a 10 g/L THF solution of $S_{340}E_{700}M_{360}$ reveal a similar behavior as observed in toluene (Figure 3.14). T_m, T_c and the degree of crystallinity α are comparable (Table 3.4), and effective annealing could be achieved at 45 °C, *i.e.*, at identical conditions as applied in toluene.
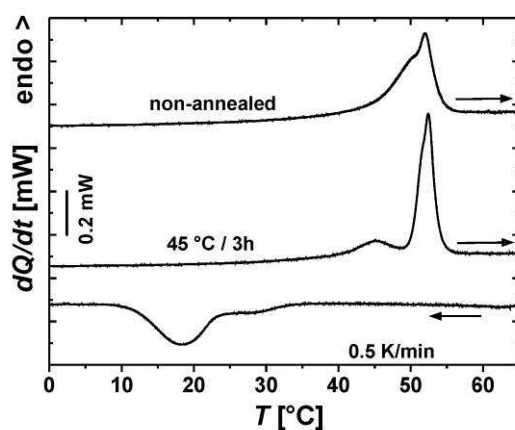
Figure 3.14. μDSC heating (before and after annealing) and cooling traces of a 10 g/L $S_{340}E_{700}M_{360}$ solution in THF.

In Figure 3.15 **µDSC measurements of $S_{280}E_{1190}M_{300}$ and $S_{140}E_{690}M_{160}$ in toluene** (10 g/L) can be found. For $S_{280}E_{1190}M_{300}$ (Figure 3.15A) the peak melting temperature is slightly increased (T_m = 53 °C) compared to $S_{340}E_{700}M_{360}$ (T_m = 49 °C). Hence, annealing at 48 °C was found to be more effective compared to annealing at 45 °C, as applied for $S_{340}E_{700}M_{360}$ and $S_{380}E_{880}S_{390}$. The observed increase in melting temperature can be attributed to the significantly higher crystallization temperature (Table 3.4), *i.e.*, T_c = 34 °C compared to about 20 °C ($S_{340}E_{700}M_{360}$, $S_{380}E_{880}S_{390}$), presumably resulting in less chain folding and hence increased crystallite thickness. Accordingly, samples for TEM investigations were prepared by isothermal crystallization at 34 °C for one day followed by annealing at 48 °C for 3 hours.

Regarding the µDSC traces of $S_{140}E_{690}M_{160}$ (Figure 3.15B) it has to be noted that the PE block of $S_{140}E_{690}M_{160}$ contains slightly more ethyl branches compared to the other three investigated SEMs (Table 3.3). This higher amount of short-chain branching has two effects. The thermal transitions are significantly broadened and shifted to lower temperatures with respect to $S_{280}E_{1190}M_{300}$, exhibiting a comparable composition (Table 3.4). Thus, crystallization was conducted at 29 °C for one day followed by annealing at 38 °C for 3 hours. Because of the similar transition temperatures and annealing behavior observed for $S_{340}E_{700}M_{360}$ in THF and toluene (Figures 3.S2, 3.S4), the annealing conditions described above for toluene solutions have been used for THF, too, without performing additional annealing studies in THF.
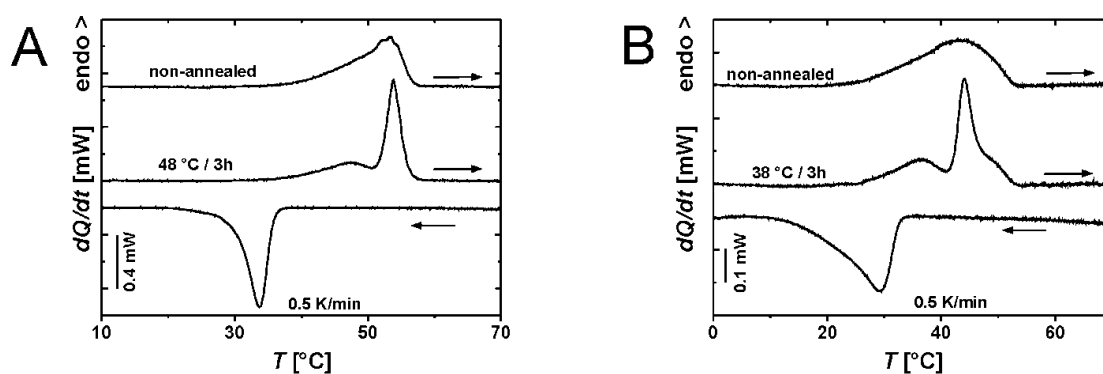
Figure 3.15. µDSC heating (before and after annealing) and cooling traces of $S_{280}E_{1190}M_{300}$ (A) and $S_{140}E_{690}M_{160}$ (B) in 10 g/L toluene solutions.

Figure 3.16 shows **μDSC traces of $S_{340}E_{700}M_{360}$ and $S_{380}E_{880}S_{390}$ in dioxane** (1 g/L and 10 g/L). In the applied concentration range, melting and crystallization temperatures do not show a concentration dependency. In contrast, measurements for $S_{340}E_{700}M_{360}$ in toluene revealed a significant shift of T_c to lower temperatures with decreasing concentration (Figure 3.11). The critical micellization (*cmt*) and demicellization (*cdt*) temperatures of $S_{380}E_{880}S_{390}$ in dioxane are about 10 °C higher compared to those of $S_{340}E_{700}M_{360}$. The increased stability of the $S_{380}E_{880}S_{390}$ micelles is attributed to the slightly longer PE middle block. As expected, *cmt* and *cdt* of the block copolymers increase with concentration. The micellization (collapse of the PE block upon cooling) and demicellization (dissolution of the PE block after melting) enthalpies are always about 10% of the corresponding heat of fusion, irrespective of the used polymer concentration.
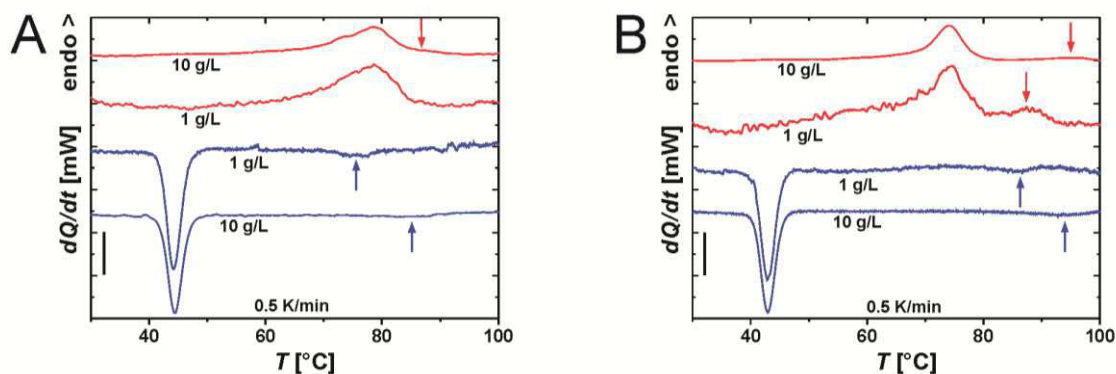
Figure 3.16. μDSC heating (——) and cooling traces (——) of 1 g/L and 10 g/L dioxane solutions of $S_{340}E_{700}M_{360}$ (A) and $S_{380}E_{880}S_{390}$ (B). The ordinate scale bar corresponds to 0.2 mW for the 10 g/L and 0.02 mW for the 1 g/L solutions, respectively; the blue arrows highlight the weak micellization peaks (*cmt*) and the red arrows the demicellization peaks (*cdt*).

In Table 3.4 the **degrees of crystallinity of the PE cores (α_{PE})** are listed for the different triblock copolymer CCMs in the investigated solvents (10 g/L). In toluene and THF, where wCCMs are formed, we find comparable α_{PE} values for $S_{340}E_{700}M_{360}$, $S_{380}E_{880}S_{390}$ and $S_{280}E_{1190}M_{300}$. Only $S_{140}E_{690}M_{160}$ exhibits a significantly lower degree of crystallinity, which can be explained by its higher content of short-chain branches (Table 3.3). However, a significantly reduced degree of crystallinity is observed for $S_{340}E_{700}M_{360}$ and $S_{380}E_{880}S_{390}$ in dioxane solutions where sCCMs are formed. This is attributed to the confined crystallization of the PE block in the micellar cores in dioxane. It has to be noted, that in THF and toluene

the triblock copolymers are molecularly dissolved as long as the PE blocks are molten and do not become insoluble before crystallization (Figure 3.4, main manuscript). As a result, dissolution/collapse of the PE blocks occurs concurrently with melting/crystallization and the corresponding enthalpies cannot be separated. In contrast, the micellization (collapse of PE upon cooling) and demicellization (dissolution of PE after melting) transitions are well separated from crystallization and fusion, respectively, in dioxane (Figure 3.16). The micellization enthalpies are about 10% of the heat of fusion in dioxane. Thus, as a rough estimate the actual α_{PE} values for the wCCMs formed in toluene and THF are presumably about 10% smaller. The measured peak melting and crystallization temperatures for all triblock copolymers in the different solvents at 10 g/L are summarized in Table 3.4, too.

Table 3.4. Degree of crystallinity (α_{PE}), peak melting (T_m) and crystallization (T_c) temperatures of the PE cores of the CCMs formed in different solvents (c = 10 g/L).

Polymer	*Solvent*	$\alpha_{PE}{}^{*}$ *[%]*	T_c [°C]	T_m [°C]
$S_{340}E_{700}M_{360}$	toluene	51	17.7	48.9
$S_{380}E_{880}S_{390}$	toluene	49	19.1	48.6
$S_{280}E_{1190}M_{300}$	toluene	49	33.7	53.4
$S_{140}E_{690}M_{160}$	toluene	38	29.3	43.2
$S_{340}E_{700}M_{360}$	THF	51	18.3	52.0
$S_{380}E_{880}S_{390}$	THF	50	21.8	51.8
$S_{340}E_{700}M_{360}$	dioxane	37	44.4	78.6
$S_{380}E_{880}S_{390}$	dioxane	35	42.9	74.0

*) determined from μDSC measurements using the heat of fusion of a 100% crystalline PE of ΔH_m^0 = 276.98 J/g.[1]

DLS measurements on S$_{380}$E$_{880}$S$_{390}$ in dioxane (1g/L) show that the formed spherical micelles are stable up to 85 °C (Figure 3.17). This is in agreement with the μDSC data, revealing a higher *cdt* for S$_{380}$E$_{880}$S$_{390}$ compared to that of S$_{340}$E$_{700}$M$_{360}$ (Figure 3.16). The hydrodynamic radius of the S$_{380}$E$_{880}$S$_{390}$ micelles does not change significantly during the crystallization of the PE core upon cooling, similar to the behavior of S$_{340}$E$_{700}$M$_{360}$ spherical micelles formed in dioxane at 70 °C (Figure 3.9B, main manuscript). Hence, the overall morphology is retained and sCCMs are formed, as confirmed by TEM (Figure 3.10B, main manuscript).
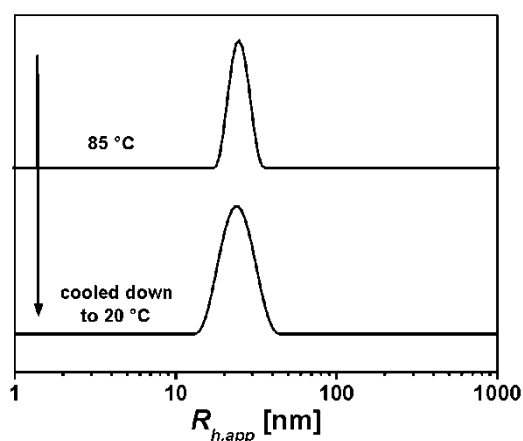
Figure 3.17. Apparent hydrodynamic radii distributions obtained from DLS data measured for a 1 g/L dioxane solution of S$_{380}$E$_{880}$S$_{390}$ at different temperatures as indicated.
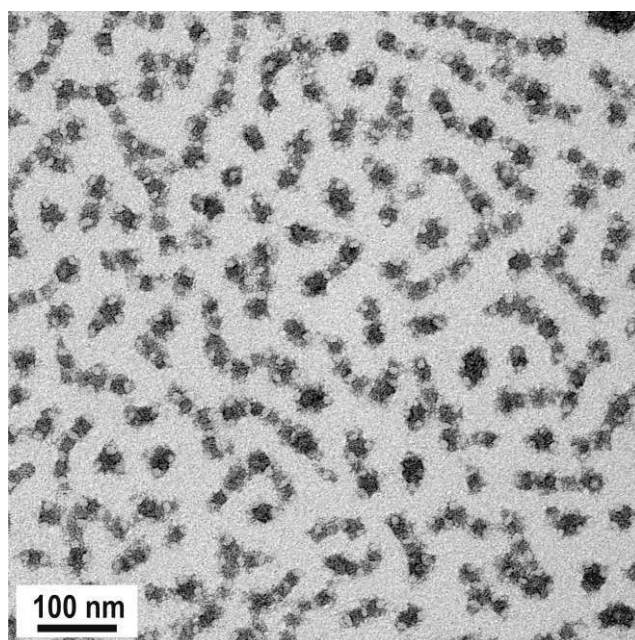
Figure 3.18. TEM micrograph of sCCMs formed by S$_{340}$E$_{700}$M$_{360}$ in dioxane (1 g/L). Because of the patch-like segregation of the corona cluster formation occurred upon drying of the solution on the carbon-coated copper grid. The sample was stained with RuO$_4$ vapor.
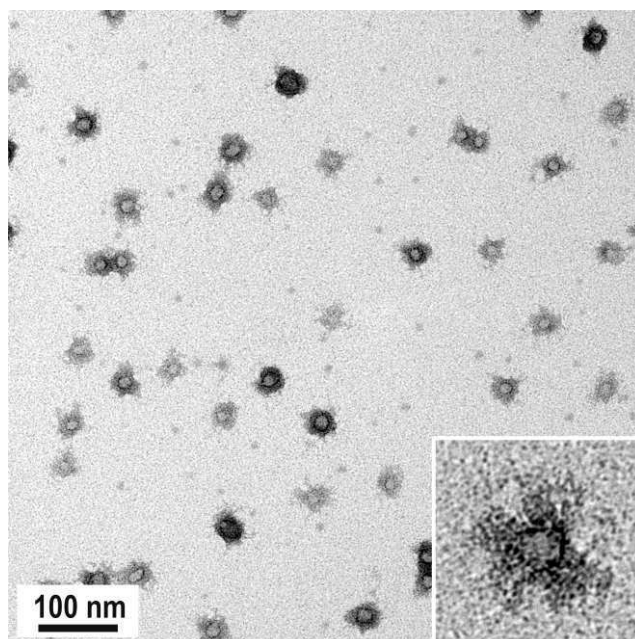
Figure 3.19. TEM micrograph of sCCMs with a patchy corona formed in a 1 g/L DMAc solution of $S_{340}E_{700}M_{360}$, dissolved at 100 °C over night and allowed to cool down to room temperature (stained with RuO_4 vapor).

References

1.   Brandrup, J.; Immergut, E. H. *Polymer Handbook*, 3rd ed.; Wiley: New York, 1989.

2.   Blanks, R. F.; Prausnitz, J. M. Thermodynamics of Polymer Solubility in Polar and Nonpolar Systems. *Ind. Eng. Chem. Fund.* **1964**, *3*, 1-8.

3.   Barton, A. F. M. *CRC Handbook of Polymer-Liquid Interaction Parameters and Solubility Parameters*, CRC Press: Boston, 1990.

4.   Müller, A. J.; Arnal, M. L. Thermal Fractionation of Polymers. *Prog. Polym. Sci.* **2005**, *30*, 559-603.

4. Patchy Worm-Like Micelles: Solution Structure Studied by Small-Angle Neutron Scattering

Sabine Rosenfeldt,[a] Frank Lüdel,[b] Christoph Schulreich,[b] Thomas Hellweg,[b,]* Aurel Radulescu,[c] Joachim Schmelz,[d] Holger Schmalz,[d] and Ludger Harnau[e,f,]*

a) Physikalische Chemie I, Universität Bayreuth, 95440 Bayreuth, Germany

b) Physikalische und Biophysikalische Chemie, Universität Bielefeld, 33615 Bielefeld, Germany

c) Jülich Centre for Neutron Science JCNS, Forschungszentrum Jülich GmbH, Außenstation am FRM II, Lichtenbergstraße 1, 85747 Garching, Germany

d) Makromolekulare Chemie II, Universität Bayreuth, 95440 Bayreuth, Germany

e) Max-Planck-Institut für Intelligente Systeme, Heisenbergstrasse 3, 70569 Stuttgart, Germany

f) Institut für Theoretische und Angewandte Physik, Universität Stuttgart, Pfaffenwaldring 57, D-70569 Stuttgart, Germany
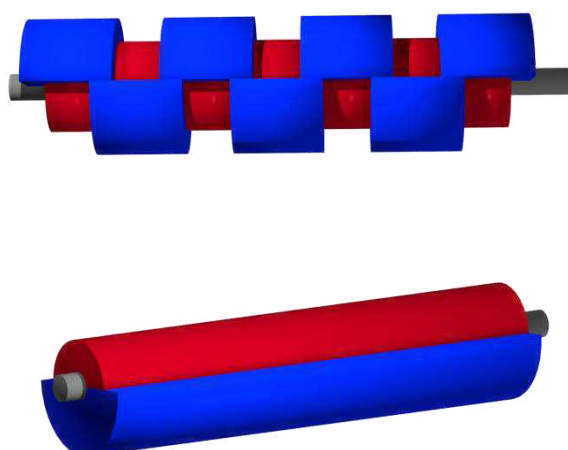
ABSTRACT:

Triblock terpolymers exhibit a rich self-organization behavior including the formation of fascinating cylindrical core-shell structures with a phase separated corona. After crystallization-induced self-assembly of polystryrene-*block*-polyethylene-*block*-poly(methyl methacrylate) triblock terpolymers (abbreviated as SEMs = Styrene-Ethylene-Methacrylates) from solution, worm-like core-shell micelles with a patchy corona of polystyrene and poly(methyl methacrylate) were observed by transmission electron microscopy. However, the solution structure is still a matter of debate. Here, we present a method to distinguish *in situ* between a Janus-type (two faced) and a patchy (multiple compartments) configuration of the corona. To discriminate between both models the scattering intensity must be determined mainly by one corona compartment. Contrast variation in small-angle neutron scattering enables us to focus on one compartment of the SEMs. The results validate the existence of the patchy structure also in solution.

4.1. Introduction

Block copolymers exhibit a rich and fascinating self-assembly behavior in bulk and in selective solvents.[1-4] A lot of the occuring structures are promising for applications in drug delivery, optoelectronics or as scaffolds for nanoparticle assembly.[5-10] Choosing the block length and the proper solvent conditions a huge variety of different structures can be generated.[11]

Many of the solution-based assemblies can be summarized under the term multicompartment micelles. Similar to proteins, multicompartment micelles combine different physical nano-environments in well-segregated compartments and exhibit a rich phase behavior including remarkably complex self-assemblies. They show a compartmentalization either of the core or the corona.[12-15] Surface-compartmentalized particles exhibit useful features for several applications, *e.g.,* the formation of hierarchically ordered superstructures, the use as potential scaffolds for the directed incorporation of metallic nanoparticles or as surfactants and emulsifiers.[16-20] Regarding corona-compartmentalized structures, Janus particles[16,21] have been formed by template-assisted approaches while solution self-assembly mostly results in patchy particles,[20,22,23] *i.e.,* structures with more than two surface compartments. Whereas there are well-known examples for one-dimensional structures with compartmentalized cores[12] or a Janus-like corona,[24,25] the majority of patchy particles are spherical in nature. Even though theoretical simulations by Binder *et al.* suggest the existence of one-dimensional nanostructures with patch-like compartmentalization of the corona,[26-28] only few examples have actually been published. For example, Liu *et al.* produced cylindrical micelles by dialysis of a triblock terpolymer against selective solvents that are able to further organize to double and triple helices.[30]

In recent years, a new way of synthesizing stable anisotropic particles exploiting block copolymers with one crystallizable block moved into the focus of several research groups.[29] Among these, polyferrocenylsilane containing block copolymers have been investigated most intensively, revealing a multitude of unprecedented structures, such as block *co-*micelles, scarf-like micelles and supramolecular brush layers.[31-33] The solution self-assembly

of these crystalline-coil block copolymers is controlled by temperature or by the addition of a non-solvent for the crystallizable block, which induces crystallization. Especially, cylindrical or worm-like micelles with high aspect ratios have raised interest in bioscience and materials science.[29,34]

Recently, we have developed the preparation of worm-like crystalline core micelles with a patchy corona from semi-crystalline polystyrene-*block*-polyethylene-*block*-poly(methyl methacrylate) (SEM) triblock terpolymers in organic solvents. Our method provides a straightforward bottom-up strategy for building up one-dimensional patchy nanostructures *via* crystallization-induced self-assembly. The structure formation is triggered simply by a decrease in temperature that induces crystallization of the polyethylene (PE) middle block.[35,36] Transmission electron microscopy revealed that the corona exhibits a patchy structure made of microphase-separated polystyrene (PS) and poly(methyl methacrylate) (PMMA) enclosing the crystalline PE core. The complexity of surface-compartmentalized nanostructures complicates the determination of the morphology and dimensions. Up to now, morphological information has been obtained by imaging techniques that usually were applied to dried samples. To get a deeper insight into dissolved worm-like crystalline core micelles, scattering methods such as small-angle neutron scattering are powerful tools as has been shown for worm-like or Janus-type structures by Fütterer *et al.*[37] and by Walther *et al.*,[38] respectively. Here, we present the first *in situ* shape sensitive investigation of patchy worm-like micelles from a SEM triblock terpolymer. To achieve this goal, a theoretical model for these complex structures is developed and experimentally verified by small-angle neutron scattering on patchy worm-like crystalline core micelles containing deuterated polystyrene blocks (dSEM) at a selected contrast.

4.2. Experimental Section

Synthesis and sample preparation. The dSEM triblock terpolymer was obtained by catalytic hydrogenation of the corresponding dSBM (B = poly(1,4-butadiene)) triblock terpolymer precursor synthesized by sequential anionic polymerization. The polystyrene block of the precursor was fully deuterated. The composition of the dSBM precursor is determined to be $S_{47d}B_{24}M_{29}^{85}$ by a combination of MALDI-TOF and ^{1}H-NMR, which results in $S_{47d}E_{24}M_{29}^{86}$ after

hydrogenation (subscripts denote the mass fraction in percent, the superscript gives the overall molecular weight in kg/mol, and d indicates that the PS block is fully deuterated). The formula of the investigated $S_{47d}E_{24}M_{29}^{86}$ can also be expressed in terms of the number of monomer units and would read $S_{359d}E_{747}M_{250}$. Full saturation of the double bonds was confirmed by ^{1}H-NMR in deuterated toluene at 65 °C. A detailed description of the synthesis of the SEM terpolymer is given in the literature.[35] Micelles of $S_{47d}E_{24}M_{29}^{86}$ are formed by crystallization induced self-assembly upon cooling.[36] As the polyethylene block in a 10 g L^{-1} solution melts at a peak melting temperature $T_m = 45$ °C and crystallizes at $T_c = 21$ °C, the solutions for the scattering experiments were prepared as follows: to eliminate any influence of thermal history, 10 g L^{-1} of the dSEM were dissolved in the corresponding solvent, *e.g.*, in tetrahydrofuran (THF) or a mixture of protonated and deuterated THF (deuteration degree 99.5%, Deutero GmbH) at 65 °C. After 1 h the solutions were quenched down to 20 °C in a water-bath and equilibrated for two days.

Small angle neutron scattering (SANS). The SANS data were obtained using the KWS 1 instrument at the FRM II in Munich, Germany. The raw data were corrected for background, solvent and empty cell scattering by the use of the software provided by the Jülich Center for Neutron Science (JCNS) at the FRM II. Absolute intensities were obtained by using a calibrated reference scatterer. For all data sets, the rate of incoherent scattering caused by the protons was determined at high scattering vector, set as a constant and subtracted from the raw data.

Transmission electron microscopy (TEM). For TEM studies the solutions were diluted to 1 g L^{-1}. Samples were prepared by placing a drop of the solution on a carbon-coated copper grid. After 20 s, excess solution was removed by blotting with a filter paper. Subsequently, elastic bright-field TEM was performed on a Zeiss 922 OMEGA EFTEM (Zeiss NTS GmbH, Oberkochen, Germany) operated at 200 kV. Staining was performed with RuO$_4$ vapor for at least 20 min. RuO$_4$ is known to selectively stain PS, which enables to distinguish between PS and PMMA domains in the corona of the micelles.

4.3. Results and Discussion

4.3.1. TEM micrographs

Recently, the formation of worm-like crystalline core micelles with a patch-like corona from a polystryrene-*block*-polyethylene-*block*-poly(methyl methacrylate) triblock terpolymer was reported.[35,36] 2D ^{1}H-NMR NOESY techniques applied to a $S_{39}E_{21}M_{40}^{91.5}$ in toluene pointed to a micro phase-separation of the corona.[35] However, this technique is not able to distinguish between a Janus-type (two-faced) or a patchy (multiple PS and PMMA compartments) configuration of the corona. Hence, the assumption of a patchy worm-like structure in solution was based on TEM studies.
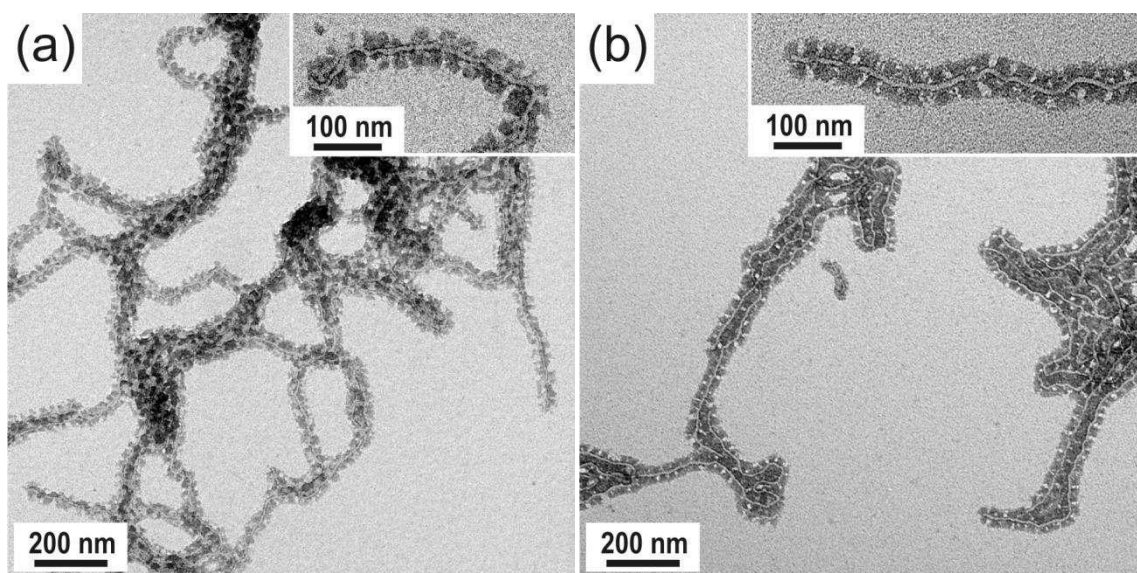
Figure 4.1. TEM micrographs of the self-assembled structure of $S_{47d}E_{24}M_{29}^{86}$ (1 g L^{-1}) in THF (a) and deuterated THF (b). The PS domains are stained with RuO$_4$ and therefore visible as dark grey areas.

Figure 4.1 shows a TEM micrograph of the structures formed by quenching a solution of $S_{47d}E_{24}M_{29}^{86}$ from 65 °C to 20 °C. In order to distinguish the different compartments in the corona in the dried state, the PS domains were stained with RuO$_4$. The TEM micrographs clearly exhibit similar patch-like compartments of the corona both in THF (see Figure 4.1(a)) and in deuterated THF (see Figure 4.1(b)). Hence, a change in the corona structure due to isotope effects of the solvent can be ruled out. In many sections an alternating array of the PS patches along the core of the worm-like crystalline core micelles is observed. THF is a good solvent for both PS and PMMA and the adopted random-coil configuration of the chains results in different dimensions of the hemi-shells. A detailed discussion about TEM

and cryo-TEM studies on worm-like crystalline core micelles formed by SEM terpolymers can be found elsewhere.[35,36]

4.3.2. Solution structures as obtained from SANS

Scattering techniques provide knowledge about the solution structure without perturbing the sample. Moreover, in the case of neutron scattering, contrast variation using deuterated monomers reveals details of the internal structure in a unique way. SANS data taken at highest contrast between solvent and solute are used to explore the shape of the entire species. At intermediate and low contrast local details of the self-assembled structures can be detected. The scattering intensities of such a contrast series can be interpreted by applying models with appropriate geometry and scattering length density distribution.[38-42]

Scattering intensity. SANS determines the scattering intensity $I(\boldsymbol{q})$ as a function of the scattering vector $\boldsymbol{q}$ and the concentration of the dissolved particles. In addition to the coherent scattering intensity $I_{coh}(\boldsymbol{q})$, there is always an incoherent contribution I_{incoh} that is due to the protons present in the particles under consideration. The scattering intensity can be written as

$$I(\boldsymbol{q}) = I_{\text{coh}}(\boldsymbol{q}) + I_{\text{incoh}} \,. \tag{1}$$

Note that in the notation the dependence on the concentration of the dissolved particles is suppressed. The $\boldsymbol{q}$-independent incoherent contribution I_{incoh} of individual particles must be subtracted carefully from experimental data in order to obtain meaningful results on the structure and interaction of the dissolved particles.[41] Due to the mesoscopic scale of the particles, the solvent will be modeled as structureless continuum providing a homogeneous scattering length density b_{solvent}.

In order to take into account particle polydispersity we consider a multicomponent system involving ν species of particles with particle numbers N_O ($1 \leq O \leq \nu$) in the volume V. Each particle of a species O carries n_O scattering units. In the case of the triblock terpolymer micelles under consideration, it proves convenient to assign an index j ($1 \leq j \leq n_O$) to scattering units, and to order them such that units $1 \leq j \leq n_O^{(E)}$ belong to the compound PE, $n_O^{(E)} + 1 \leq j \leq n_O^{(E)} + n_O^{(M)}$ belong to the compound PMMA, and $n_O^{(E)} + n_O^{(M)} + 1 \leq j \leq n_O$

belong to the compound PS. The coherent contribution to the scattering intensity in the ν-component system is given by

$$I_{\mathrm{coh}}(\boldsymbol{q}) = \sum_{\mathrm{O,P}=1}^{\nu} I_{\mathrm{OP}}(\boldsymbol{q}),\qquad(2)$$

with the partial scattering intensities

$$I_{\mathrm{OP}}(\boldsymbol{q}) = \frac{1}{V}\left\langle\left|\sum_{j=1}^{n_{\mathrm{O}}}\sum_{k=1}^{n_{\mathrm{P}}}\sum_{\alpha=1}^{N_{\mathrm{O}}}\sum_{\gamma=1}^{N_{\mathrm{P}}}\Delta\,\tilde{b}_{j\mathrm{O}}^{(\alpha)}\Delta\tilde{b}_{k\mathrm{P}}^{(\gamma)}e^{i\boldsymbol{q}\cdot\left(\boldsymbol{r}_{j\mathrm{O}}^{(\alpha)}-\boldsymbol{r}_{k\mathrm{P}}^{(\gamma)}\right)}\right|\right\rangle.\qquad(3)$$

Here, $\boldsymbol{r}_{j\mathrm{O}}^{(\alpha)}$ is the position vector of the jth scattering unit of the αth particle of species O. The difference in the scattering length of this scattering unit and the average scattering length of the solvent is denoted as $\Delta\tilde{b}_{j\mathrm{O}}^{(\alpha)}$, and $<>$ denotes an ensemble average. It proves convenient to decompose the partial scattering intensities according to

$$I_{\mathrm{OP}}(\boldsymbol{q}) = \rho_{\mathrm{O}}\omega_{\mathrm{O}}(\boldsymbol{q})\delta_{\mathrm{OP}} + \rho_{\mathrm{O}}\rho_{\mathrm{P}}h_{\mathrm{OP}}(\boldsymbol{q}),\qquad(4)$$

where

$$h_{\mathrm{OP}}(\boldsymbol{q}) = \frac{V}{N_{\mathrm{O}}N_{\mathrm{P}}}\left\langle\left|\sum_{j=1}^{n_{\mathrm{O}}}\sum_{k=1}^{n_{\mathrm{P}}}\sum_{\alpha=1}^{N_{\mathrm{O}}}\sum_{\substack{\gamma=1\\\gamma\neq\alpha}}^{N_{\mathrm{P}}}\Delta\,\tilde{b}_{j\mathrm{O}}^{(\alpha)}\Delta\tilde{b}_{k\mathrm{P}}^{(\gamma)}e^{i\boldsymbol{q}\cdot\left(\boldsymbol{r}_{j\mathrm{O}}^{(\alpha)}-\boldsymbol{r}_{k\mathrm{P}}^{(\gamma)}\right)}\right|\right\rangle.\qquad(5)$$

is a particle-averaged total correlation function for pairs of particles of species O and P. The number density of particles of species O is designated as $\rho_{\mathrm{O}} = N_{\mathrm{O}}/V$. The particle-averaged intramolecular correlation function

$$\omega_{\mathrm{O}}(\boldsymbol{q}) = \frac{1}{N_{\mathrm{O}}}\left\langle\left|\sum_{j=1}^{n_{\mathrm{O}}}\sum_{k=1}^{n_{\mathrm{P}}}\sum_{\alpha=1}^{N_{\mathrm{O}}}\Delta\,\tilde{b}_{j\mathrm{O}}^{(\alpha)}\Delta\tilde{b}_{k\mathrm{O}}^{(\alpha)}e^{i\boldsymbol{q}\cdot\left(\boldsymbol{r}_{j\mathrm{O}}^{(\alpha)}-\boldsymbol{r}_{k\mathrm{O}}^{(\alpha)}\right)}\right|\right\rangle\qquad(6)$$

characterizes the scattering length distribution, and hence also the geometric shape of particles of species O. While the particle-averaged intramolecular correlation functions account for the interference of radiation scattered from different parts of individual particles in a scattering experiment, the local order in the fluid is characterized by the total

correlation functions. For flexible particles the intramolecular correlation functions depend on the particle number density and follow from a statistical average over particle configurations. As suggested by the imaging data (see Figure 4.1), the tribock terpolymer micelles may be considered as worm-like core-shell cylinders with phase-separated shells. In the scattering vector regime of a SANS experiment both the contour length and the persistence length cannot be resolved for rather long and stiff cylindrical particles.[41,44] As a prerequisite for the following analysis we have confirmed that the scattering intensity of a homogeneous weakly bendable cylinder with the same configuration as the triblock terpolymer micelle shown in the inset of Figure 4.1(b) is nearly indistinguishable from the scattering intensity of a corresponding homogeneous rigid cylinder in the scattering vector regime accessible by SANS. Hence, only the scattering intensity of rigid cylinders is considered in the analysis of the SANS experiments. In the limit of a continuous distribution of scattering units, the intramolecular correlation function of randomly oriented core-shell cylinders is given by

$$\omega_O(q) = \frac{1}{4\pi} \int\limits_0^{2\pi} \mathrm{d}\phi \int\limits_0^{\pi} \mathrm{d}\theta \, \sin\theta \, F_O(q,\theta,\phi) F_O^{\star}(q,\theta,\phi) \qquad (7)$$

with

$$F_O(q,\theta,\phi) = \int\limits_{-L/2}^{L/2} \mathrm{d}z \int\limits_0^{\infty} \mathrm{d}r\, r \int\limits_0^{2\pi} \mathrm{d}\phi_r \, \Delta b_O(r,\phi_r,z) e^{i\boldsymbol{q}\cdot\boldsymbol{r}} . \qquad (8)$$

Here, $\boldsymbol{q} = q(\sin\theta\cos\phi, \sin\theta\sin\phi, \cos\theta)$ is the scattering vector described by spherical coordinates and $\boldsymbol{r} = (r\cos\phi_r, r\sin\phi_r, z)$ denotes the position vector of a scattering unit of an individual core-shell cylinder described by cylindrical coordinates. The origin of the coordinates is taken to be the center of the cylinder of length L and $\Delta b_O(r,\phi_r,z)$ denotes the scattering length density function, which specifies the internal structure of an individual core-shell cylinder. For the triblock terpolymer micelles the index O in eqn (2), (4), (7), and (8) allows one to take into account polydispersity of the scattering length density function.

Janus type and patchy cylinders. As Figure 4.2 illustrates, the cylinders are characterized by a core-shell structure with a PE core of radius R_E marked in gray and a biphasic PS-PMMA

shell consisting of regions of unlike size and scattering length densities shown in blue and red. Hence the scattering length density function equals Δb_E, Δb_S, and Δb_M in the regions marked in gray, blue, and red, respectively. More specifically, two shell patterns will be distinguished. (i) Figure 4.2(a): A Janus-type architecture, *i.e.* the shell consists of two homogeneous hemi-shells which might have different or similar extensions (R_S and R_M) and unlike scattering length densities. (ii) Figure 4.2(b): The two inhomogeneous hemi-shells consist of alternating regions of scattering length densities. Here, D_S and D_M describe the lengths of the alternating regions of the so-called patchy cylinder.
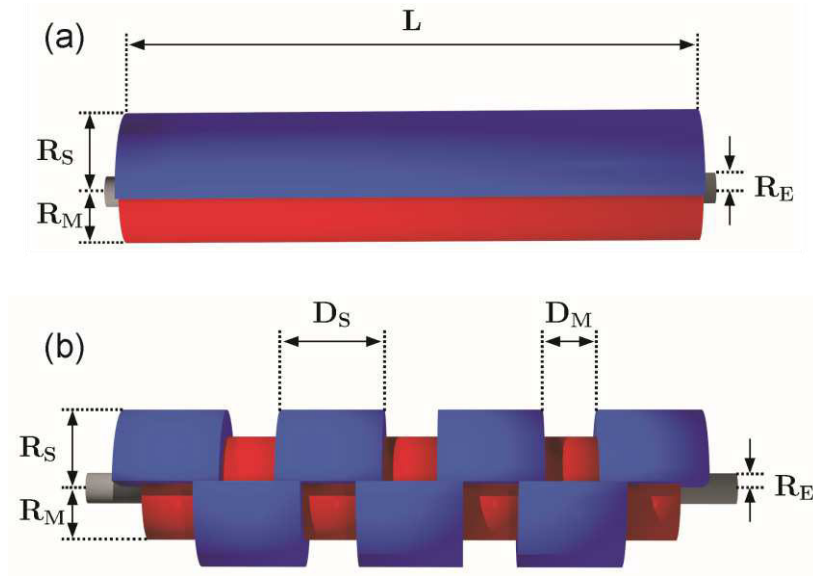
Figure 4.2. Illustrations of two possible architectures of micro phase-separated shells of cylindrical particles. The cylinders are characterized by a core-shell structure with a PE core of radius R_E marked in gray and a biphasic PS-PMMA shell consisting of regions of unlike size and scattering length densities marked in blue and red. In the main text the cylindrical particles are denoted as Janus cylinders (a) and patchy cylinders (b).

Figure 4.3(a) displays the scattering intensity for noninteracting $(h_{OP}(q) = 0)$ and monodisperse $(\nu = 1)$ cylinders of length $L = 425.5$ nm and radii $R_E = 4.3$ nm, $R_M = 15.5$ nm, $R_S = 22.0$ nm as calculated from eqn (1) - (8). The dashed line shows the result for Janus cylinders (see Figure 4.2(a)), while the solid line represents the scattering intensity of patchy cylinders (see Figure 4.2(b)) with $D_M = D_S = 22.4$ nm. All scattering intensities are normalized to the volume fraction $\phi = \rho_O/V_O$, where V_O is the particle volume. Moreover, the ratio of the scattering length density differences of PS and PE is $\Delta b_S/\Delta b_E = -0.751$, where $\Delta b_E = b_{solvent} - b_E$ and $b_E = -0.34 \times 10^{10}$ cm^{-2} are the scattering length densities of the solvent and PE, respectively. For comparison, three values of the ratio of the

scattering length density differences of PS and PMMA $\Delta b_{\mathrm{S}}/\Delta b_{\mathrm{M}}$ are considered, where $\Delta b_{\mathrm{S}}/\Delta b_{\mathrm{M}} = 6.859$ (data set in the middle) corresponds to PS and PMMA in THF$_{\mathrm{H}}$.
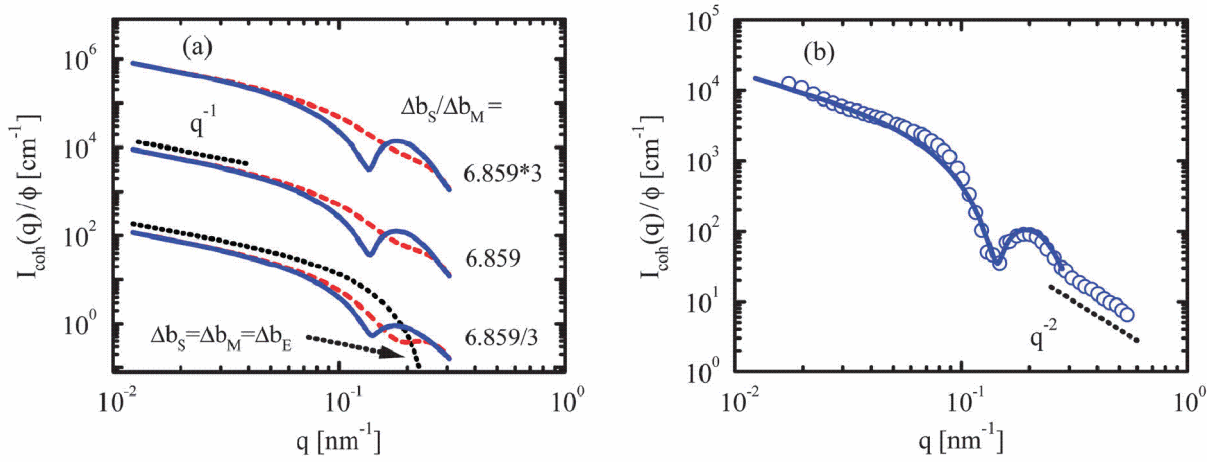
Figure 4.3. (a) Comparison of the scattering intensity $I_{\mathrm{coh}}(q)/\phi$ of Janus cylinders (dashed lines, see Figure 4.2(a)) with the scattering intensity of patchy cylinders (solid lines, see Figure 4.2(b)) with $D_{\mathrm{M}} = D_{\mathrm{S}} = 22.4$ nm. The curves have been calculated according to eqn (1)-(8) with $h_{\mathrm{OP}}(\mathbf{q}) = 0$ and $v = 1$, *i.e.*, for noninteracting and monodisperse cylinders. The remaining model parameters are given by $L = 425.5$ nm, $R_{\mathrm{E}} = 4.3$ nm, $R_{\mathrm{M}} = 15.5$ nm, $R_{\mathrm{S}} = 22.0$ nm, $\Delta b_{\mathrm{S}}/\Delta b_{\mathrm{E}} = -0.751$ and $\Delta b_{\mathrm{E}} = 0.52 \times 10^{10}$ cm^{-2}. Moreover, the ratio of the scattering length density difference of PS and PMMA decreases from top to bottom according to $\Delta b_{\mathrm{S}}/\Delta b_{\mathrm{M}} = 6.859$ x 3, 6.859, 6.859 / 3, where the value 6.859 corresponds to the actual experimental system discussed in panel (b). In addition the lower dotted line depicts the scattering intensity of a homogeneous cylinder with $\Delta b_{\mathrm{S}}/\Delta b_{\mathrm{E}} = \Delta b_{\mathrm{S}}/\Delta b_{\mathrm{M}} = 1$ and $R_{\mathrm{M}} = R_{\mathrm{S}} = 15.5$ nm. For clarity the upper and lower data sets have been shifted up and down, respectively, by a factor of 10^2. (b) Measured scattering intensity of the triblock terpolymer micelles (10 g L^{-1}) in THF$_{\mathrm{H}}$ (symbols) together with the calculated results for noninteracting patchy cylinders (solid line). The model parameters are the same as for the solid middle line in panel (a) except of $D_{\mathrm{M}} = 14.0$ nm and $D_{\mathrm{S}} = 29.0$ nm. The dotted lines in panels (a) and (b) represent two asymptotic scaling laws as discussed in the main text.
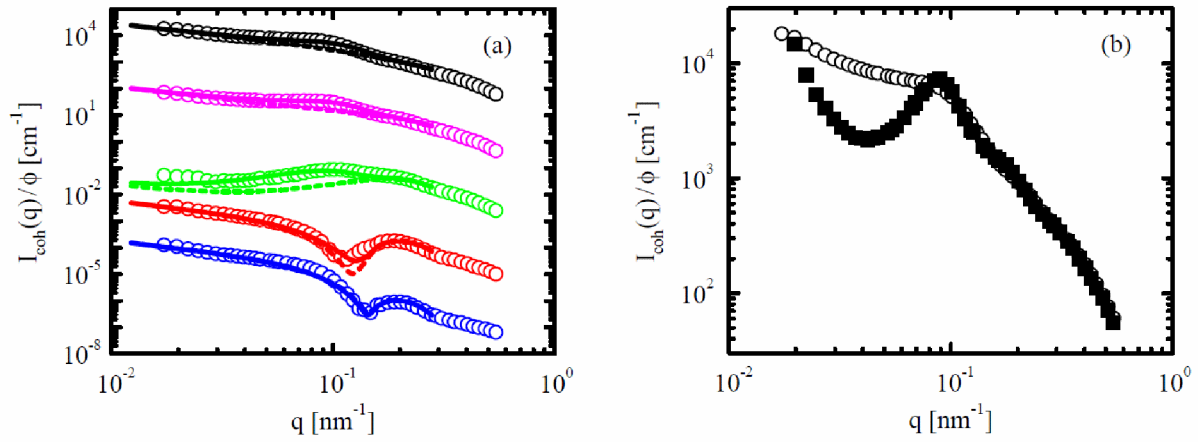
The scattering intensities shown in Figure 4.3(a) have the following features. They exhibit the q^{-1} scaling relation (short dotted line) for small scattering vectors which is characteristic for the linear arrangement of scattering units along the main axis of a cylinder. For the patchy cylinders (solid lines), the scattering intensity exhibits a minimum at $q \approx 0.14$ nm^{-1}, while for the Janus cylinders no minimum is observed, provided $\Delta b_{\mathrm{S}}/\Delta b_{\mathrm{M}} \gtrsim 6.589/3$. From the figure it is apparent that the existence or absence of a minimum of the scattering intensity at intermediate scattering vectors allows one to distinguish Janus cylinders from patchy cylinders, provided the ratio of two scattering length density differences of the biphasic shell is sufficiently large. In addition we note that the scattering intensity of a homogeneous

cylinder of similar size does not exhibit a minimum at $q \approx 0.14$ as is apparent from the lower dotted line in Figure 4.3(a).

In Figure 4.3(b) the experimental scattering intensity of the triblock terpolymer micelles in pure THF$_H$ is compared to the calculated results for noninteracting patchy cylinders. For the morphological study this contrast condition is well suited due to the fact that the scattering pattern mainly is determined by the deuterated PS patch of the shell. The model parameters are the same as for the solid middle line in Figure 4.3(a) except for the lengths of the alternating regions of the shell which are given by $D_M = 14.0$ nm and $D_S = 29.0$ nm. Hence we take into account that the size of the PMMA block (M$_{29}$) characterized by D_M, R_M is smaller than the size of the PS block (S$_{47d}$) characterized by D_S, R_S. The ratio of the size of the three-dimensional patches $D_S(R_S^2 - R_E^2)/(D_M(R_M^2 - R_E^2)) = 4.35$ is similar to the cube of the ratio of the mass fractions of the one-dimensional PS and PMMA chains $(47/29)^3 = 4.26$. From the figure it is apparent that the experimentally determined scattering intensity (symbols) exhibits a pronounced minimum at $q \approx 0.14$ nm^{-1} which is characteristic for a patchy cylinder as discussed above. The deviations between the experimental data and the calculated results (solid line) for intermediate scattering vectors $q \in [0.03, 0.1]$ are due to the fact that the PS and PMMA blocks do not form perfect patchy half-cylinders as is assumed in the model shown in Figure 4.2(b). Nevertheless, the combination of Figure 3(a) and (b) demonstrates that patchy triblock terpolymer micelles are indeed present in THF$_H$. For comparison we emphasize that experimentally determined scattering intensities of Janus cylinders do not exhibit minima at intermediate scattering vectors in agreement with the calculated results shown in Figure 4.3(a).[38]

Although eqn (7) and (8) have been derived for a rigid cylinder of a definite shape illustrated in Figure 4.2, in reality concentration fluctuations of the PS and PMMA polymer chains contribute to the scattering intensity. On the basis of our experience with various polymer nanoparticles[43-46] we expect that the contribution of the polymer concentration fluctuations becomes important for large scattering vectors $q \gtrsim 0.3$ nm^{-1}. Within a Gaussian approximation the scaling relation $I_{coh}(q) \sim q^{-2}$ is valid for large scattering vectors as indicated by the dotted line in Figure 4.3(b). Moreover, we have confirmed that moderate size polydispersity (e.g., $D_S = 29.0 \pm 3.0$ nm) does not lead to pronounced changes of the

calculated scattering intensity. Therefore, one may consider a monodisperse model system as an appropriate approximation.

Figure 4.4. (a) Measured scattering intensity $I_{coh}(q)/\phi$ of the triblock terpolymer micelles at concentration 10 g L^{-1} (symbols). The scattering length densities of the solvent increases from bottom to top ($b_{solvent} = 0.18, 1.36, 3.23, 5.13, 6.32 \times 10^{10}$ cm^{-2}) while the corresponding ratios of the scattering length density differences of the micelles are given by $\Delta b_S/\Delta b_M = 6.859, -19.731, -1.531, -0.337, -0.033$ and $\Delta b_S/\Delta b_E = -0.751, -0.187, -0.057, -0.015, -0.002$, with $\Delta b_E = b_{solvent} - b_E$ and $b_E = -0.34 \times 10^{10}$ cm^{-2}. The four lower scattering intensities are shifted down by a factor of $10^2, 10^4, 10^6, 10^8$, respectively. The dashed lines represent calculated results for noninteracting ($h_{OP}(q) = 0$) patchy cylinders using the same model parameters as in Figure 4.3(b). In the case of the solid lines a contribution of the total correlation function $h_{OP}(q)$ to the scattering intensity is taken into account. For the lowest scattering length density of the solvent the solid line is nearly indistinguishable from the dashed line. (b) Comparison of the normalized measured scattering intensity of the triblock terpolymer micelles at concentration 10 g L^{-1} (open circles) with the corresponding data at 40 g L^{-1} (solid squares) in fully deuterated THF ($b_{solvent} = 6.32 \times 10^{10}$ cm^{-2}). The differences between the open and solid symbols reflect pair correlations between the micelles.

Contrast Variation. Figure 4.4(a) displays SANS intensities of the triblock terpolymer micelles in different THF$_D$: THF$_H$ mixtures corresponding to different scattering length densities of the solvent (symbols). Such a contrast variation allows consistency checks of the theoretical modeling because the contribution of the three polymers PE, PMMA, and PS to the scattering intensity depends sensitively on the scattering length density of the solvent. The figure demonstrates that varying the scattering length contrast leads to marked differences in the scattering intensities. In particular, the minima of the scattering intensities of the lower two data sets disappear upon increasing the scattering length density of the solvent (upper three data sets) due to an increasing contribution of PE to the scattering intensity. The pronounced minima reflect the phase-separated shell of patchy cylinders (see

Figure 4.2(b)) while the homogeneous PE core cylinder does not lead to a minimum in this scattering vector regime.

The dashed lines in Figure 4.4(a) show the calculated results for noninteracting patchy cylinders using the same model parameters as in Figure 4.3(b). Some features of the measured scattering intensities such as the disappearance of the minimum upon increasing the scattering length density of the solvent are captured by the theoretical approach. However, the calculated results for noninteracting patchy cylinders and the experimental data deviate due to interactions between the micelles. The concentration 10 g L^{-1} is ten times higher than the one used for the TEM micrographs shown in Figure 4.1. This rather high polymer concentration was necessary in order to obtain a good signal-to-noise ratio. We emphasize that neither modeling the cores of the elongated micelles as one-dimensionally connected objects such as worm-like or helical-like chains nor taking into account the semicrystallinity of PE[47] leads to a peak of the scattering intensities at $q \approx$ 0.1 nm^{-1} in the cases of dominating contributions of PE to the scattering intensities (upper three data sets in Figure 4.4(a)). In order to justify the argumentation based on our additional calculations of various intramolecular correlation functions, we have performed a scattering experiment for an even higher micelle concentration 40 g L^{-1} in fully deuterated THF (solid squares in Figure 4.4(b)). Indeed the observed peak of the scattering intensity is more pronounced as compared to the one for 10 g L^{-1} (open circles in Figure 4.4(b)) due to increased interparticular correlations. This interpretation is consistent with the observation that the 40 g L^{-1} sample was rather viscous whereas the 10 g L^{-1} sample exhibited fluid-like properties. Moreover, a third sample containing 50 g L^{-1} triblock terpolymer micelles formed a free-standing gel in a simple test tube inversion experiment due to enhanced interparticular correlations.

In order to understand the liquid structure in more detail, the particle-averaged total correlation function $h_{OP}(\mathbf{q})$ defined in eqn (5) has been calculated using the polymer reference interaction site integral equation theory (see ref. 48 and references therein). In contrast to the successful application of this theoretical approach to various polymer nanoparticles,[43,45-47,49] it was not possible to achieve such good agreement between the integral equation theory for the rigid patchy cylinders shown in Figure 4.2(b) and the

experimental data sets across the entire q-range and for all scattering length contrasts given by the symbols in Figure 4.4(a). The differences between the measured and calculated results may be due to a number of possible factors with the most critical being the model assumption that the PS and PMMA polymer chains form a rigid biphasic shell. Due to molecular flexibility, the contribution to the scattering features from intermolecular PS and PMMA correlations is less pronounced than the corresponding one of a rigid biphasic shell.

Having observed that the integral equation theory for the initial rigid patchy cylinders did not lead to a good description of all available scattering data, only contributions to the particle-averaged total correlation function arising from patchy cylinders with an effective radius $R_{\mathrm{eff}} = 11.5$ nm were considered. The calculated scattering intensities from this model (solid lines in Figure 4.4(a)) are comparable to the experimental data. Notably, little overall contribution to the scattering features was observed from the total correlation function in the case of the lowest scattering length density of the solvent (lowest data set in Figure 4.4(a)), due to the presence of both positive and negative contributions of the compartments of the triblock terpolymer micelles. The peak at $q \approx 0.1$ nm^{-1} observed for the three upper data sets in Figure 4.4(a) can be interpreted as a sign of intermediate range order with a characteristic real space distance of $2\pi/q \approx 63$ nm. Future theoretical work may focus on a detailed understanding of local order in fluids consisting of patchy cylinders.

Finally, we note that the experimentally determined scattering intensities shown in Figure 4.4(a) can be split consistently into three parts according to (see ref. 42 and references therein)

$$I_{\mathrm{coh}}(\boldsymbol{q}) = \left(\tilde{b} - b_{\mathrm{solvent}}\right)^2 I_{\mathrm{S}}(q) + 2\left(\tilde{b} - b_{\mathrm{solvent}}\right)I_{\mathrm{SI}}(q) + I_{\mathrm{I}}(q)\,, \qquad (9)$$

Where $\tilde{b} \approx 3.2 \times 10^{10}$ cm^{-2} is the average scattering length density of the triblock terpolymer micelles. The first term $I_{\mathrm{S}}(q)$ is the normalized scattering intensity of chemically homogeneous micelles, while $I_{\mathrm{I}}(q)$ is related to the scattering length inhomogeneity of the triblock terpolymer micelles. The cross term $I_{\mathrm{SI}}(q)$ between the former contributions can take negative values. In general all three terms can be extracted from experimental data if scattering intensities have been measured at least at three different scattering length densities of the solvent. For the triblock terpolymer micelles under consideration the

scattering length density independent term $I_I(q)$ is very similar to the middle data set in Figure 4.4(a). Moreover, $I_S(q)$ can be considered as the normalized scattering intensity measured at infinite contrast, where the last two terms in eqn (9) can be neglected. The functional shape of $I_S(q)$ is similar to the upper data set in Figure 4.4(a) for $q \lesssim 0.1$ nm^{-1}.

4.4. Conclusion

SANS data have been collected for polystyrene-*block*-polyethylene-*block*-poly(methyl methacrylate) triblock terpolymer micelles in organic solvents. The structure of these micelles dissolved in protonated tetrahydrofuran has been elucidated by comparing the experimentally determined scattering intensity to the calculated one for a patchy cylinder (see Figure 4.3(b)). Moreover, the theoretical analysis revealed that SANS allows one to distinguish patchy cylinders from Janus cylinders (see Figure 4.3(a)). The combined experimental and theoretical study shows the presence of alternating polystyrene and poly(methyl methacrylate) regions in the shell of the patchy, cylindrical triblock terpolymer micelles (see Figure 4.2(b)).

It has not been possible to use the polymer reference integral equation theory for rigid patchy cylinders to interrogate the scattering data of the triblock terpolymer micelles at rather high concentration in various mixtures of protonated and deuterated tetrahydrofuran. The principle reason for this may be that the amorphous polystyrene and poly(methyl methacrylate) chains forming the shell of the core-shell micelles require chain flexibility to be taken into account. However, consistent information was obtained by separating the data analysis into two portions, analyzing the scattering data considering noninteracting patchy cylinders (see dashed lines in Figure 4.4(a)) and taking into account interparticular correlations from patchy cylinders with an effective shell radius (see solid lines in Figure 4.4(a)). Upon further increasing the micelle concentration the SANS data show, categorically, the presence of pronounced interparticular correlations (see Figure 4.4(b)).

4.5. References

[1]   S. Förster, *Ber. Bunsenges. Phys. Chem.*, 1997, **101**, 1671.

[2]   F. S. Bates and G. H. Frederickson, *Physics Today*, 1999, **52**, 32.

[3]   I. W. Hamley, S.-M. Mai, A. J. Ryan, J. P. A. Fairclough and C. Booth, *Phys. Chem. Chem. Phys.*, 2001, **3**, 2972.

[4]   T. Hellweg, in *Self Organized Nanostructures of Amphiphilic Block Copolymers II*, ed. O. Borisov and A. H. E. Müller, Springer, Heidelberg, 2012, p. 1.

[5]   A.-V. Ruzette and L. Leibler, *Nat. Mater.*, 2005, **4**, 19.

[6]   J. Rodriguez-Hernandez, F. Checot, Y. Gnanou and S. Lecommandoux, *Prog. Polym. Sci.*, 2005, **30**, 691.

[7]   N. Haberkorn, M. C. Lechmann, B. H. Son, K. Char, J. S. Gutmann and P. Theato, *Macromol. Rapid Comm.*, 2009, **30**, 1146.

[8]   M. Motornov, Y. Roiter, I. Tokarev and S. Minko, *Prog. Polym. Sci.*, 2010, **35**, 174.

[9]   J. K. Kim, S. Y. Yang, Y. Lee and Y. Kim, *Prog. Polym. Sci.*, 2010, **35**, 1325.

[10]   H.-C. Kim, S.-M. Park and W. D. Hinsberg, *Chem. Rev.*, 2010, **110**, 146.

[11]   N. Hadjichristidis, H. Iatrou, M. Pitsikalis, S. Pispas and A. Avgeropoulos, *Progr. Polym. Sci.*, 2005, **30**, 725.

[12]   J. Dupont and G. Liu, *Soft Matter*, 2010, **6**, 3654.

[13]   J. Z. Du and R. K. O'Reilly, *Chem. Soc. Rev.*, 2011, **40**, 2402.

[14]   K. Zhang, M. Jiang, D. Chen, *Prog. Polym. Sci.*, 2012, **37**, 445.

[15]   A. O. Moughton, M. A. Hillmeyer, T. P. Lodge, *Macromolecules*, 2012, **45**, 2.

[16]   A. Walther and A. H. E. Müller, *Soft Matter*, 2008, **4**, 663.

[17]   A. Walther, K. Matussek and A. H. E. Müller, *ACS Nano*, 2008, **2**, 1167.

[18]   I. K. Voets, R. Fokkink, T. Hellweg, S. M. King, P. de Waard, A. de Keizer, M. A. Cohen Stuart, *Soft Matter*, 2009, **5**, 999.

[19]   S. Jiang, Q. Chen, M. Tripathy, E. Luijten, K. S. Schweizer and S. Granick, *Adv. Mater.*, 2010, **22**, 1060.

[20]   I. Kretzschmar and J. H. Song, *Curr. Opinion Coll. Interf. Sci.*, 2011, **16**, 84.

[21]   R. Erhardt, A. Böker, H. Zettl, H. Kaya, W. Pyckhout-Hintzen, G. Krausch, V. Abetz and A. H. E. Müller, *Macromolecules*, 2001, **34**, 1069.

[22]   S. C. Glotzer and M. J. Solomon, *Nat. Mater.*, 2007, **6**, 557.

[23]   A. B. Pawar and I. Kretzschmar, *Macromol. Rapid Commun.*, 2010, **31**, 150.

[24]   Y. Liu, V. Abetz and A. H. E. Müller, *Macromolecules*, 2003, **36**, 7894.

[25]   T. M. Ruhland, A. H. Gröschel, A. Wather and A. H. E. Müller, *Langmuir*, 2011, **11**, 9807

[26]   P. E. Theodorakis, W. Paul and K. Binder, *Macromolecules*, 2010, **43**, 5137.

[27]   I. Erukhimovich, P. E. Theodorakis, W. Paul and K. Binder, *J. Chem. Phys.*, 2011, **134**, 054906.

[28]   P. E. Theodorakis, H.-S. Hsu, W. Paul and K. Binder, *J. Chem. Phys.*, 2011, **135**, 164903.

[29]   M. Lazzari and A. Lopez-Quintela, *Macromol. Rapid Commun.*, 2009, **21**, 1785.

[30]   J. Dupont, G. J. Liu, K. Niihara, R. Kimoto and H. Jinnai, *Angew. Chem., Int. Ed.*, 2009, **48**, 6144.

[31]   X. Wang, G. Guerin, H. Wang, Y. Wang, I. Manners and M. A. Winnik, *Science*, 2007, **317**, 644.

[32]   T. Gädt, N. S. Ieong, G. Cambridge, M. A. Winnik and I. Manners, *Nat. Mater.*, 2009, **8**, 144.

[33]   F. He, T. Gädt, I. Manners and M. A. Winnik, *J. Am. Chem. Soc.*, 2011, **133**, 23.

[34]   J. Qian, M. Zhang, I. Manners and M. A. Winnik, *Trends Biotechnol.*, 2010, **28**, 84.

[35]   H. Schmalz, J. Schmelz, M. Drechsler, J. Yuan, A. Walther, K. Schweimer and A. M. Mihut, *Macromolecules*, 2008, **41**, 3235.

[36]   J. Schmelz, M. Karg, T. Hellweg and H. Schmalz, *ACS Nano*, 2011, **5**, 9523.

[37]   T. Fütterer, A. Nordskog, T. Hellweg, G. H. Findenegg , S. Foerster and C. D. Dewhurst, *Phys. Rev. E: Stat., Nonlinear, Soft Matter Phys.*, 2004, **70**, 041408.

[38]   A. Walther, M. Drechsler, S. Rosenfeldt, L. Harnau, M. Ballauff, V. Abetz and A. H. E. Müller, *J. Am. Chem. Soc.*, 2009, **13**, 4720.

[39]   C. E. Williams in *Neutron, X-Ray and Light Scattering*, ed. P. Lindner and T. Zemb, Elsevier Science Publisher, Oxford, 1991, p. 101.

[40]   N. P. Balsara, D. J. Lohse, W. W. Graessley and R. Krishnamoorti, *J. Chem. Phys.*, 1994, **100**, 3905.

[41]   *Polymers and Neutron Scattering*, ed. J. S. Higgins and H. C. Benoit, Clarendon Press Ithaca, Oxford, 1996.

[42]   S. Rosenfeldt, M. Ballauff, P. Lindner and L. Harnau, *J. Chem. Phys.*, 2009, **130**, 244901.

[43]   Y. Yan, L. Harnau, N. A. M. Besseling, A. de Keizer, M. Ballauff, S. Rosenfeldt and M. A. Cohen-Stuart, *Soft Matter*, 2008, **4**, 2207.

[44]   K. Henzler, S. Rosenfeldt, A. Wittemann, L. Harnau, S. Finet, T. Narayanan and M. Ballauff, *Phys. Rev. Lett.*, 2008, **100**, 158301.

[45]   C. N. Rochette, S. Rosenfeldt, K. Henzler, F. Polzer, M. Ballauff, Q. Tong, S. Mecking, M. Drechsler, T. Narayanan and L. Harnau, *Macromolecules*, 2011, **44**, 4845.

[46]   K. Henzler, B. Haupt, S. Rosenfeldt, L. Harnau, T. Narayanan and M. Ballauff, *Phys. Chem. Chem. Phys.*, 2011, **13**, 17599.

[47]   C. H. M. Weber, A. Chiche, G. Krausch, S. Rosenfeldt, M. Ballauff, L. Harnau, I. Göttker-Schnetmann, Q. Tong and S. Mecking, *Nano Lett.* 2007, **13**, 2024.

[48]   L. Harnau, *Mol. Phys.*, 2008, **106**, 1975.

[49]   S. Bolisetty, S. Rosenfeldt, C. Rochette, L. Harnau, P. Lindner, Y. Xu, A. H. E. Müller and M. Ballauff, *Colloid Polym. Sci.* 2009, **287**, 129.

5. Corona Structure on Demand: Tailor-Made Surface Compartmentalization in Worm-Like Micelles via Random Cocrystallization

Joachim Schmelz, and Holger Schmalz*

Makromolekulare Chemie II, Universität Bayreuth, 95440 Bayreuth, Germany
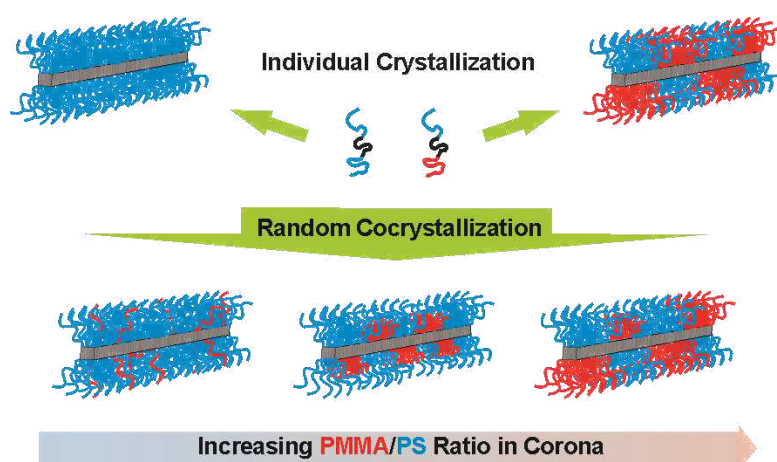
ABSTRACT:

We present a straightforward approach to well-defined 1D patchy particles utilizing crystallization-induced self-assembly. A polystyrene-*block*-polyethylene-*block*-poly(methyl methacrylate) (PS-*b*-PE-*b*-PMMA) triblock terpolymer is cocrystallized in a random fashion with a corresponding polystyrene-*block*-polyethylene-*block*-polystyrene (PS-*b*-PE-*b*-PS) triblock copolymer to yield worm-like crystalline-core micelles (wCCMs). Here, the corona composition (PMMA/PS fraction) can be easily adjusted via the amount of PS-*b*-PE-*b*-PMMA triblock terpolymer in the mixture and opens an easy access to wCCMs with tailor-made corona structures. Depending on the PMMA fraction, wCCMs with a mixed corona, spherical PMMA patches embedded in a continuous PS corona, as well as alternating PS and PMMA patches of almost equal size can be realized. Micelles prepared by cocrystallization show the same corona structure as those prepared from neat triblock terpolymers at identical corona composition. Thus, within a certain regime of desired corona compositions the laborious synthesis of new triblock terpolymers for every composition can be circumvented.

5.1.Introduction

Over the past decades, major effort was laid on the development of bottom-up approaches based on block copolymer self-assembly to efficiently produce structures in the nanometer to micrometer range, where conventional top-down methods reach their limits.[1-6] An intriguing class of self-organized nanostructures with unique morphologies are multicompartment micelles exhibiting compartmentalized cores and/or coronas.[7,8] The combination of different chemical environments in close proximity holds the potential to carry multiple incompatible payloads within one nanoparticle.[9-11] For example, micelles with multiple compartments in the core can be produced by the self-assembly of linear[12-15] or star-shaped[16] triblock terpolymers in selective solvents, as well as from diblock/diblock[17,18] or diblock/triblock[19] copolymer mixtures. While significant progress was achieved in the production of core-compartmentalized nanostructures, corona compartmentalization mainly was investigated in the so-called Janus particles with exactly two opposite compartments (faces) of different chemistry or polarity. Janus particles of various shapes have been produced and shown to exhibit remarkable properties, like outstanding surface activity and the hierarchical ordering into superstructures.[20-23] In contrast, patchy micelles bearing multiple corona compartments are less well examined.[8,24-27] Due to the lack of convenient production strategies for patchy 1D and 2D assemblies, the majority of these particles is spherical in nature. One elegant method to produce patchy 1D nanostructures based on cylindrical micelles utilizes the self-assembly of an ABC triblock terpolymer in selective solvents for the end blocks.[28] Using a similar approach even double and triple helices were formed highlighting the enormous potential of this class of soft patchy particles as building blocks for defined mesoscopic assemblies.[29] A highly intriguing way to manufacture well-defined cylindrical micelles is based on block copolymers bearing crystallizable blocks.[30,31] Harnessing the "livingness" of this crystallization-driven self-assembly allows not only to produce cylindrical micelles with defined lengths and length distributions,[32-34] but also to form more complex micellar architectures like block *co*-micelles with a block-type compartmentalized corona by sequential cocrystallization, as shown for poly(ferrocenyl dimethylsilane) (PFS) containing block copolymers.[34,35] Using this approach multiblock *co*-micelles with up to nine corona compartments have been realized.[36] In addition, a blend of

different PFS containing diblock copolymers was shown to randomly cocrystallize resulting in mixed micelles with crystalline PFS cores.[37]

We have recently combined the concept of surface compartmentalization with crystallization-driven self-assembly to produce worm-like crystalline-core micelles (wCCMs) with a patch-like microphase-separated corona. The self-assembly of polystyrene-*block*-polyethylene-*block*-poly(methyl methacrylate) triblock terpolymers (PS-*b*-PE-*b*-PMMA) in good solvents for the PE middle block in the molten state (e.g. toluene, THF) resulted in wCCMs with a crystalline PE core surrounded by a patch-like compartmentalized corona of PS and PMMA, as proven by a combination of transmission electron microscopy (TEM) and nuclear Overhauser effect spectroscopy (NOESY).[38] Here, only symmetric triblock terpolymers with end blocks of comparable length were studied. Because of the similar space requirements of both corona blocks in THF an almost alternating array of PS and PMMA corona patches was observed.[39] In this paper we show that the corona microphase separation of these one-dimensional nanostructures can be not only adjusted by the composition of the triblock terpolymers, but, even more elegantly, by random cocrystallization of two triblock copolymers. This technique allows to tune the corona composition and structure on demand within a certain regime, circumventing the need to synthesize a new triblock terpolymer for each desired corona structure.

5.2. Results and Discussion

In order to investigate possible influences of the corona block lengths on the resulting morphology, the asymmetric PS-*b*-PE-*b*-PMMA triblock terpolymers **1a** and **1b** were synthesized (sample abbreviations are explained in Table 5.1). For both polymers, the degrees of polymerization of PS and PMMA in the corona differ significantly. We applied the previously developed protocol to produce well-defined wCCMs in THF solution (1 g/L).[39] Consequently, the polymers first were dissolved in THF at temperatures well above the melting temperature of PE in order to erase any thermal history, followed by isothermal crystallization at 20 °C and subsequent annealing slightly below the melting point of PE (details are given in the *Experimental Part*). More information on the molecular and thermal characteristics of the used triblock copolymers (Table 5.2) and micro-differential scanning

calorimetry (μDSC) traces of **1a** and **1b** in 10 g/L toluene solutions (Figure 5.5) can be found in the Supplementary data.

Table 5.1. Corona compositions and average PMMA patch sizes of the prepared wCCMs.

Sample	Polymer[a]	w_M[b] [%]	d_M[c] [nm]
1a	$S_{660}E_{1350}M_{350}$	34	6.3 ± 2.1
1b	$S_{330}E_{1360}M_{760}$	69	∞[e]
1c	$S_{380}E_{880}S_{390}$	0	-
1d	$S_{340}E_{700}M_{360}$	51	12.7 ± 3.3
2a	**1c/1d** = 90/10[d]	5	-
2b	**1c/1d** = 70/30[d]	15	3.0 ± 0.8
2c	**1c/1d** = 50/50[d]	25	3.2 ± 0.9
2d	**1c/1d** = 30/70[d]	35	5.8 ± 1.5
2e	**1c/1d** = 10/90[d]	46	9.2 ± 2.4

a) Subscripts denote the number average degree of polymerization of the respective polymer blocks.

b) Weight fraction of PMMA in the corona of the wCCMs.

c) Average thickness of PMMA patches in the corona as determined by TEM image analysis.

d) Weight ratio of triblock copolymers used for cocrystallization.

e) Continuous PMMA corona.

In **1a**, the PS block is twice as long as the PMMA block. Still, upon crystallization wCCMs with a microphase-separated corona are obtained as revealed by TEM (Figure 5.1a). In order to visualize the corona structure all TEM micrographs in this publication were acquired after selective staining of PS with RuO_4 vapour, that is, PS domains appear dark. It is noted that cryo-TEM cannot be used to study the microphase separation within the corona due to lack of contrast.[38] The significantly lower PMMA content in the corona of the wCCMs produced from **1a** leads to spherical PMMA patches (bright) that are embedded in a continuous PS matrix (dark) and located close to the PE core (bright). In **1b** the block ratio of the outer blocks is reverted. Here, PMMA accounts for about 70% of the corona. Again, wCCMs with a patch-like surface compartmentalization are formed (Figure 5.1b). However, now the PMMA chains build up a continuous corona and PS forms spherical patches near the PE core. The actual dimensions of the PMMA corona cannot be seen, as PMMA is not stained by RuO_4 and

presumably partially degraded by the electron beam.[40] According to scanning force microscopy (Figure 5.6) the overall diameters of wCCMs formed by **1a** and **1b** are equal ($d \approx$ 80 nm). Hence, the corona extensions in TEM should be comparable, too, as indicated by the dashed white lines in Figure 1b.
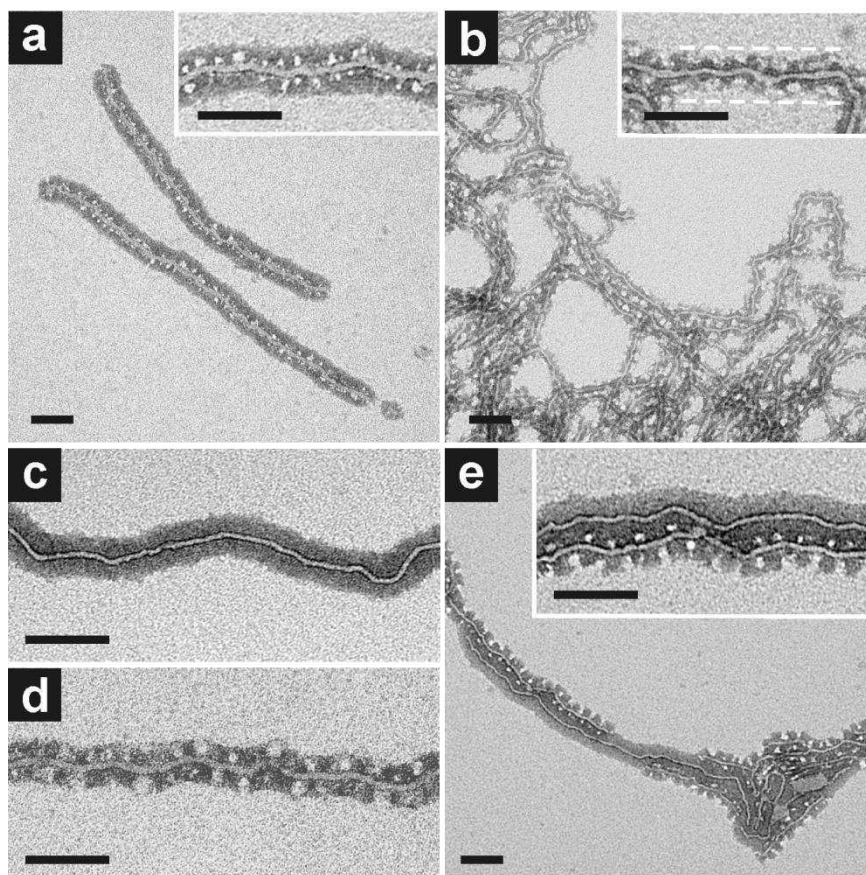

Figure 5.1. TEM micrographs of wCCMs formed by **1a**, **1b**, **1c** and **1d** (a-d). The dashed white line in b) shows the estimated dimensions of the corona. e) Mixture of wCCMs formed by **1c** and **1d** (50/50 w/w). Scale bars: 100 nm.

In order to avoid the time-consuming synthesis of new triblock terpolymers for any desired corona structure, random cocrystallization of mixtures of **1c** and **1d** displays an attractive alternative. When crystallized individually, **1c** and **1d** form wCCMs with a homogeneous corona of PS (Figure 5.1c) or a compartmentalized corona with PS and PMMA patches of comparable size (Figure 5.1d), respectively.[39] Once crystallized, these wCCMs are stable below the melting point of the PE core ($T_m \approx 49$ °C, Table 5.2). After one week, a 50/50 (w/w) mixture of preformed wCCMs of **1c** and **1d** still shows the two separate species (Figure 5.1e). The formed wCCMs in general tend to aggregate upon drying during TEM sample preparation, which can be observed especially in the image of the mixture. However, due to

the good visibility of the light PE core different wCCMs still can clearly be distinguished. Before sample preparation all prepared wCCM solutions exhibited a slightly bluish colour due to the scattering of the long wCCMs (Tyndall effect). The scattering for the **1c/1d** mixture was not increased compared to pure **1c** and **1d** showing that no pronounced aggregation occurs already in solution.

To tune the corona structure on demand we cocrystallized mixtures of **1c** and **1d** at different weight ratios while keeping the overall concentration constant (1 g/L). Sample preparation was conducted as described above for the asymmetric triblock terpolymers.
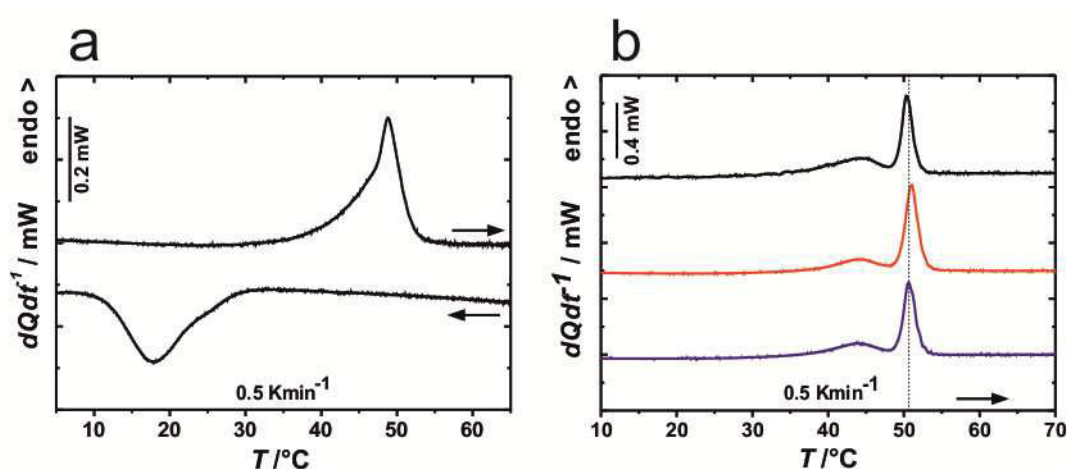
Figure 5.2. a) Micro-differential scanning calorimetry (μDSC) heating and cooling traces of a 50/50 (w/w) mixture of **1c** and **1d** (10 g/L in toluene). b) Comparison of μDSC heating traces of wCCM solutions (10 g/L in toluene) of **1c** (black), **1d** (red) and their 50/50 (w/w) mixture (blue) after annealing at 45 °C for 3 h.

Micro-differential scanning calorimetry (μDSC) measurements on a cocrystallized mixture of **1c** and **1d** (50/50 w/w) show that the peak crystallization (T_c = 17.8 °C) and melting temperature (T_m = 48.8 °C) are comparable to those of the neat triblock co- and terpolymers **1c** and **1d**, respectively, and no significant broadening of the transitions can be traced (Figure 5.2a, Table 5.2).[39] Moreover, identical annealing conditions (45 °C for 3 h) can be applied to the cocrystallized wCCMs (Figure 5.2b). Annealing results in an increased thickness and a more uniform size distribution of the PE crystallites in the wCCM cores, as revealed by the shift of the mean melting endotherm to higher temperatures and the significant narrowing of the endotherm. This supports a random cocrystallization and confirms that the structure formation again is driven by crystallization, that is, in analogy to neat **1c** and **1d**.
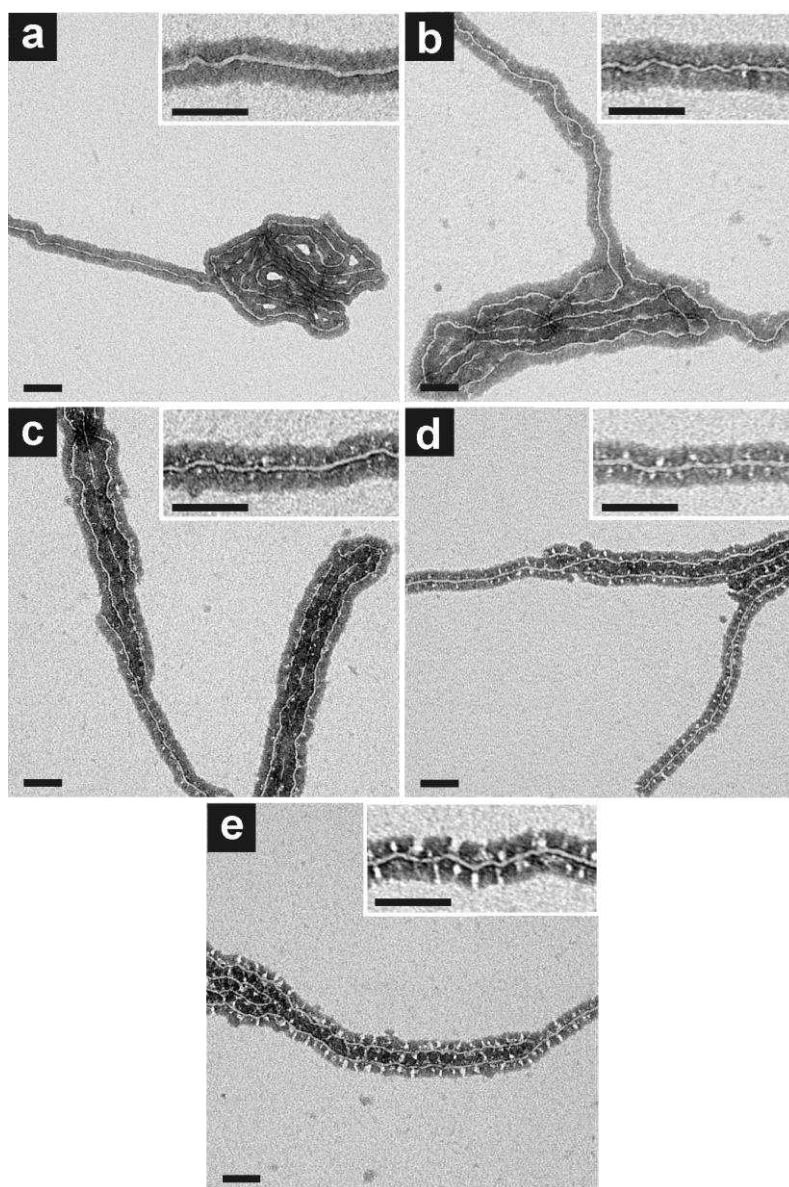
Figure 5.3. TEM micrographs of wCCMs formed via random cocrystallization of **1c** and **1d** in 1 g/L THF solutions at ratios (**1c/1d**) of 90/10 (a), 70/30 (b), 50/50 (c), 30/70 (d), 10/90 (e). Scale bars: 100 nm.

TEM investigation of the different cocrystallized samples (Figure 5.3) shows that the corona structure of the formed wCCMs is highly homogeneous for each sample. Thus, **1c** and **1d** indeed do cocrystallize in a random fashion. It is noted that the thickness of the semicrystalline PE cores for the cocrystallized wCCMs does not change within the limits of accuracy of the measurements ($d_{core} = 6 \pm 1$ nm for wCCMs formed by **1c, 1d** and their mixtures). This is reasonable, as chain folding upon crystallization and thus the crystallite thickness is mainly determined by the amount of ethyl branches in the PE block, which is comparable for **1c** and **1d** (Table 5.2). Furthermore, there seems to be no significant

influence of the corona composition on the curvature of the PE core. This might be attributed to the crystalline nature of the core resulting in a certain stiffness.

Due to the low PMMA content in the corona (w_M = 5%), no patch-like structure can be observed for sample **2a**. Already at w_M = 15% (sample **2b**) few small compartments of PMMA can be located near the PE core (for PMMA patch sizes please see Table 5.1). Upon further increasing w_M, the number and size of these nearly spherical PMMA compartments grow continuously (samples **2c**, **2d**). In sample **2e** (w_M = 46%) many of these patches already reach out from the PE core to the corona surface, as is the case for wCCMs formed by neat **1d** (Figure 5.1d). Comparable results were obtained by extracting the brightness distributions of the corona pixels from the TEM micrographs of the cocrystallized samples (Figure 5.7), which allows to probe the corona composition over an ensemble of wCCMs (for details the reader is referred to the Supplementary data). Here, a shoulder develops at higher brightness values, which correspond to the non-stained PMMA patches, with increasing content of **1d** in the mixture.

The evolution of the corona structure upon changing w_M is in analogy to block copolymer self-assembly in the bulk state, where a decreasing content of one polymer block leads to an increasingly confined situation, too, e.g. lamellae first become cylinders and finally spheres.[41] For marginal contents of one of the polymer blocks, no phase separation occurs for moderate segregation strengths, as observed in sample **2a**. Notably, the corona structure and PMMA patch size of wCCMs formed by sample **2d** closely resemble those of the asymmetric triblock terpolymer **1a** having a comparable PMMA content (Figure 5.1a). This highlights that random cocrystallization of a triblock copolymer mixture and self-assembly of neat PS-*b*-PE-*b*-PMMA triblock terpolymers produce identical structures at a given corona composition.
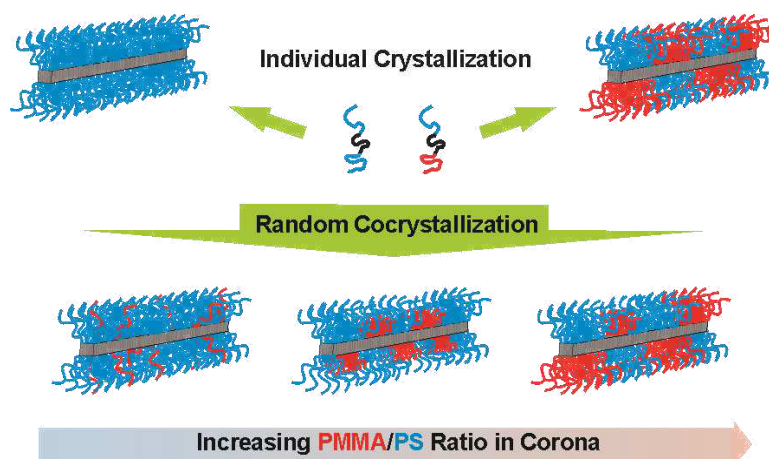
Figure 5.4. Sketch of structures that can be self-assembled from **1c** ($S_{380}E_{880}S_{390}$) and **1d** ($S_{340}E_{700}M_{360}$) in THF (PS: blue, PMMA: red, PE: black/grey).

5.3. Conclusion

In conclusion, we introduce a versatile approach for the production of stable one-dimensional patchy nanostructures with precise control of the corona structure via straightforward cocrystallization of triblock copolymer mixtures. Due to the random fashion of this cocrystallization, the ratio of the corona-forming blocks (PS and PMMA) in the block copolymer mixture determines the resulting corona structures. These can be tuned continuously from a homogeneous PS corona over spherical PMMA patches of different number and size embedded in a continuous PS corona to almost alternating PS and PMMA patches (Figure 5.4). Strikingly, the corona structure of wCCMs in a cocrystallized triblock copolymer mixture is identical to that of a neat triblock terpolymer with the same corona composition. Therefore, this strategy is suited to circumvent the arduous synthesis of tailor-made triblock terpolymers for every desired corona structure within a certain range of corona compositions and, thus, makes a whole library of well-defined patchy nanostructures readily available.

5.4. Experimental

Synthesis. Polystyrene-*block*-poly(1,4-butadiene)-*block*-polystyrene and polystyrene-*block*-poly(1,4-butadiene)-*block*-poly(methyl methacrylate) were synthesized *via* sequential

anionic polymerization in cyclohexane and toluene, respectively. Subsequently, the corresponding polyethylene containing triblock co- and terpolymers, polystyrene-*block*-polyethylene-*block*-polystyrene and polystyrene-*block*-polyethylene-*block*-poly(methyl methacrylate), were obtained by catalytic hydrogenation of the polybutadiene middle block to polyethylene using Wilkinson´s catalyst. Detailed information about used materials, purification methods and the polymerization procedure can be found in previous publications.[39,42]

Sample preparation. For morphological studies using *transmission electron microscopy (TEM)* the solutions were diluted to 0.5 g/L and drop-coated onto carbon-coated copper grids. Selective staining of PS was achieved by exposure of the dried samples to RuO_4 vapour for 20 min. Elastic bright-field TEM was performed on a Zeiss 922 OMEGA EFTEM (Zeiss NTS GmbH, Oberkochen, Germany) operated at 200 kV. Zero-loss filtered images ($\Delta E = 0$) were recorded at an electron dose of about 104 e·nm^{-2}s^{-1} (exposure time: 1 s), registered digitally by a bottom mounted CCD camera system (Ultrascan 1000, Gatan) and processed with a digital imaging processing system (Gatan Digital Micrograph 3.9 for GMS 1.4). Average PMMA patch sizes were evaluated from at least 100 measurements.

Transmission Electron Microscopy (TEM). For morphological studies using TEM the solutions were diluted to 0.5 g/L and drop-coated onto carbon-coated copper grids. Selective staining of PS was achieved by exposure of the dried samples to RuO_4 vapour for 20 min. Elastic bright-field TEM was performed on a Zeiss 922 OMEGA EFTEM (Zeiss NTS GmbH, Oberkochen, Germany) operated at 200 kV. Zero-loss filtered images ($\Delta E = 0$) were recorded at an electron dose of about 104 e·nm^{-2}s^{-1} (exposure time: 1 s), registered digitally by a bottom mounted CCD camera system (Ultrascan 1000, Gatan) and processed with a digital imaging processing system (Gatan Digital Micrograph 3.9 for GMS 1.4). Average PMMA patch sizes were evaluated from at least 100 measurements.

Image Analysis. For the pixel intensity distributions (Figure 5.7, Supplementary data) the intensity values of the corona pixels of the wCCMs were extracted from several TEM images for each sample using ImageJ. The peak maxima of the resulting distributions, which correspond to the mean intensity values of the dark polystyrene domains (selectively stained with RuO_4), were normalized in height to facilitate comparison between the different

cocrystallized wCCMs. The shown pixel intensity distributions consist of at least 300k pixels for each sample. Due to geometric reasons slightly different extents of staining are obtained on different parts of the TEM grids. Furthermore, poly(alkyl (meth)acrylates) are known to undergo partial degradation upon exposure to the electron beam.[40] Hence, this investigation is not intended to provide quantitative results, but to qualitatively support the trend of increasing PMMA patch number and size over an ensemble of wCCMs upon increasing the content of **1d** in the cocrystallized wCCMs.

Scanning Force Microscopy (SFM). SFM images were taken on a Digital Instruments Dimension 3100 NanoScope IV operated in TappingMode. Samples were prepared on polished silicon wafers by dip-coating from a 0.03 g/L solution of the wCCMs in THF, prepared by dilution of the corresponding 1 g/L solution.

Micro-Differential Scanning Calorimetry (μDSC). μDSC was performed on a Setaram μDSC III using closed "batch" cells at a scanning rate of 0.5 K/min. The pure solvent was used as a reference. More detailed information on the measurement procedure, especially for the annealing experiments, can be found elsewhere.[39]

5.5. References

1. Whitesides, G. M.; Grzybowski, B. *Science* **2002**, *295*, 2418-2421.

2. Stupp, S. I.; LeBonheur, V.; Walker, K.; Li, L. S.; Huggins, K. E.; Keser, M.; Amstutz, A. *Science* **1997**, *276*, 384-389.

3. Hayward, R. C.; Pochan, D. J. *Macromolecules* **2010**, *43*, 3577-3584.

4. Förster, S.; Plantenberg, T. *Angew. Chem. Int. Ed.* **2002**, *41*, 688-714.

5. Riess, G. *Prog. Polym. Sci.* **2003**, *28*, 1107-1170.

6.   Fustin, C. A.; Abetz, V.; Gohy, J. F. *Eur. Phys. J. E* **2005**, *16*, 291-302.

7.   Moughton, A. O.; Hillmyer, M. A.; Lodge, T. P. *Macromolecules* **2012**, *45*, 2-19.

8.   Du, J.; O'Reilly, R. K. *Chem. Soc. Rev.* **2011**, *40*, 2402-2416.

9.   Chi, Y.; Scroggins, S. T.; Fréchet, J. M. J. *J. Am. Chem. Soc.* **2008**, *130*, 6322-6323.

10.   Lodge, T. P.; Rasdal, A.; Li, Z.; Hillmyer, M. A. *J. Am. Chem. Soc.* **2005**, *127*, 17608-17609.

11.   Marsat, J.-N.; Heydenreich, M.; Kleinpeter, E.; Berlepsch, H. V.; Böttcher, C.; Laschewsky, A. *Macromolecules* **2011**, *44*, 2092-2105.

12.   Cui, H.; Chen, Z.; Zhong, S.; Wooley, K. L.; Pochan, D. J. *Science* **2007**, *317*, 647-650.

13.   Gröschel, A. H.; Schacher, F. H.; Schmalz, H.; Borisov, O. V.; Zhulina, E. B.; Walther, A.; Müller, A. H. E. *Nat. Commun.* **2012**, *3*, 710.

14.   Kubowicz, S.; Baussard, J.-F.; Lutz, J.-F.; Thünemann, A. F.; von Berlepsch, H.; Laschewsky, A. *Angew. Chem. Int. Ed.* **2005**, *44*, 5262-5265.

15.   Von Berlepsch, H.; Böttcher, C.; Skrabania, K.; Laschewsky, A. *Chem. Commun.* **2009**, 2290-2292.

16.   Li, Z.; Kesselman, E.; Talmon, Y.; Hillmyer, M. A.; Lodge, T. P. *Science* **2004**, *306*, 98-104.

17.   Lutz, J.-F.; Geffroy, S.; von Berlepsch, H.; Böttcher, C.; Garnier, S.; Laschewsky, A. *Soft Matter* **2007**, *3*, 694-698.

18.   Zheng, R.; Liu, G.; Yan, X. *J. Am. Chem. Soc.* **2005**, *127*, 15358-15359.

19.   Schacher, F.; Betthausen, E.; Walther, A.; Schmalz, H.; Pergushov, D. V.; Müller, A. H. E. *ACS Nano* **2009**, *3*, 2095-2102.

20.   Hu, J.; Zhou, S.; Sun, Y.; Fang, X.; Wu, L. *Chem. Soc. Rev.* **2012**, *41*, 4356-4378.

21.   Loget, G.; Kuhn, A. *J. Mater. Chem.* **2012**, *22*, 15457-15474.

22.   Walther, A.; Müller, A. H. E. *Soft Matter* **2008**, *4*, 663-668.

23.   Zhang, K.; Jiang, M.; Chen, D. *Prog. Polym. Sci.* **2012**, *37*, 445-486.

24.   Pawar, A. B.; Kretzschmar, I. *Macromol. Rapid Commun.* **2010**, *31*, 150-168.

25.   Yoon, J.; Lee, K. J.; Lahann, J. *J. Mater. Chem.* **2011**, *21*, 8502-8510.

26.   Glotzer, S. C.; Solomon, M. J. *Nat. Mater.* **2007**, *6*, 557-562

27. Christian, D. A.; Tian, A.; Ellenbroek, W. G.; Levental, I.; Rajagopal, K.; Janmey, P. A.; Liu, A. J.; Baumgart, T.; Discher, D. E. *Nat. Mater.* **2009**, *8*, 843-849.

28. Njikang, G.; Han, D. H.; Wang, J.; Liu, G. J. *Macromolecules* **2008**, *41*, 9727-9735.

29. Dupont, J.; Liu, G. J.; Niihara, K.; Kimoto, R.; Jinnai, H. *Angew. Chem. Int. Ed.* **2009**, *48*, 6144-6147.

30. Qian, J. S.; Zhang, M.; Manners, I.; Winnik, M. A. *Trends Biotechnol.* **2010**, *28*, 84-92.

31. Lazzari, M.; Lopez-Quintela, M. A. *Macromol. Rapid Commun.* **2009**, *30*, 1785-1791.

32. Gilroy, J. B.; Gädt, T.; Whittell, G. R.; Chabanne, L.; Mitchels, J. M.; Richardson, R. M.; Winnik, M. A.; Manners, I. *Nat. Chem.* **2010**, *2*, 566-570.

33. Petzetakis, N.; Dove, A. P.; O'Reilly, R. K. *Chem. Sci.* **2011**, *2*, 955-960.

34. Wang, X.; Guerin, G.; Wang, H.; Wang, Y.; Manners, I.; Winnik, M. A. *Science* **2007**, *317*, 644-647.

35. Gädt, T.; Ieong, N. S.; Cambridge, G.; Winnik, M. A.; Manners, I. *Nat. Mater.* **2009**, *8*, 144-150.

36. He, F.; Gädt, T.; Manners, I.; Winnik, M. A. *J. Am. Chem. Soc.* **2011**, *133*, 9095-9103.

37. Cambridge, G.; Guerin, G.; Manners, I.; Winnik, M. A. *Macromol. Rapid Commun.* **2010**, *31*, 934-938.

38. Schmalz, H.; Schmelz, J.; Drechsler, M.; Yuan, J.; Walther, A.; Schweimer, K.; Mihut, A. M. *Macromolecules* **2008**, *41*, 3235-3242.

39. Schmelz, J.; Karg, M.; Hellweg, T.; Schmalz, H. *ACS Nano* **2011**, *5*, 9523-9534.

40. Goldacker, T.; Abetz, V.; Stadler, R.; Erukhimovic, I.; Leibler, L. *Nature* **1999**, *398*, 137-139.

41. Matsen, M. W.; Bates, F. S. *Macromolecules* **1996**, *29*, 1091-1098.

42. Ruckdäschel, H.; Sandler, J. K. W.; Altstädt, V.; Rettig, C.; Schmalz, H.; Abetz, V.; Müller, A. H. E. *Polymer* **2006**, *47*, 2772-2790.

5.6. Supporting Information

Table 5.2. Molecular characteristics and thermal properties of the used triblock copolymers.

Sample	Polymer[a]	Polymer[b]	PDI[c]	$x_{1,2\text{-}PB}$[d]	Et / 100 C[e]	T_c[f] [°C]	T_m[f] [°C]	T_a[g] [°C]
1a	$S_{660}E_{1350}M_{350}$	$S_{48}E_{27}M_{25}{}^{141}$	1.07	0.13	3.5	21.0	45.0	41.0
1b	$S_{330}E_{1360}M_{760}$	$S_{23}E_{26}M_{51}{}^{148}$	1.03	0.13	3.4	22.0	46.0	41.0
1c	$S_{380}E_{880}S_{390}$	$S_{38}E_{23}S_{39}{}^{105}$	1.04	0.10	2.7	19.0	48.7	45.0
1d	$S_{340}E_{700}M_{360}$	$S_{39}E_{21}M_{40}{}^{91}$	1.04	0.10	2.6	17.5	49.1	45.0

a) Subscripts denote the number average degree of polymerization of the respective polymer blocks.

b) Subscripts give the weight percentage of the polymer blocks and the superscript corresponds to the overall number average molecular weight in kgmol^{-1}.

c) Polydispersity index of the PB-containing precursor polymer (THF-SEC with PS calibration).

d) Molar fraction of 1,2-butadiene repeating units before hydrogenation of PB to PE.

e) Ethyl branches per 100 main chain carbon atoms after hydrogenation.

f) Peak crystallization (T_c) and melting (T_m) temperature, determined via μDSC on 10 gL^{-1} toluene solutions.

g) Applied annealing temperature.
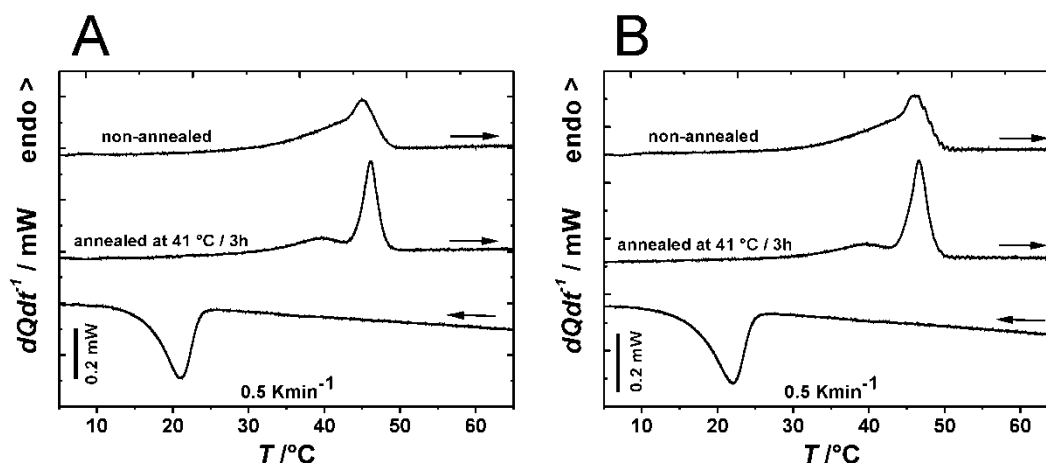
Figure 5.5. Micro-differential scanning calorimetry (μDSC) heating (without and after annealing) and cooling traces of **1a** (A) and **1b** (B) performed on 10 g/L toluene solutions.
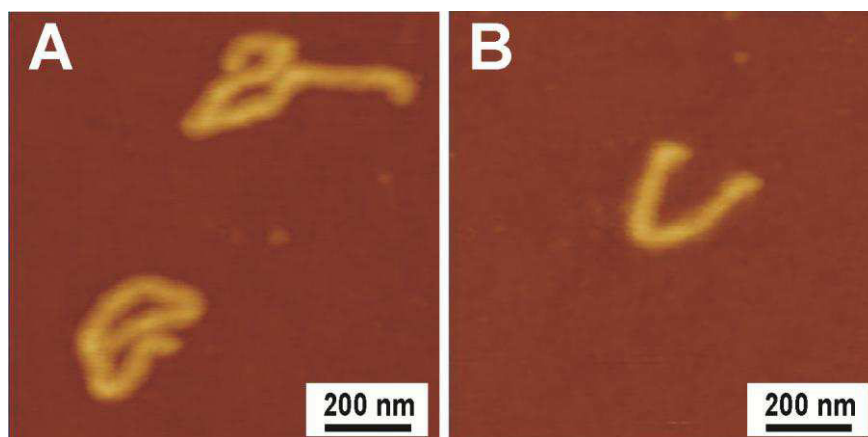
Figure 5.6. SFM topography images of wCCMs formed by **1a** (A) and **1b** (B) in 1 g/L THF solutions (Δz = 30 nm).

In wCCMs formed by **1b** the majority of the corona consists of PMMA (w_M = 69%) and therefore a continuous PMMA corona with embedded small PS patches is formed (Figure 5.1b). However, as PMMA is not stained by RuO_4 and presumably partially degraded by the electron beam, it cannot be distinguished from the neat carbon film using transmission electron microscopy (TEM) and the overall dimensions of the micellar corona are not visible. Thus, scanning force microscopy (SFM) was performed to compare the wCCM diameters, d, of **1a** and **1b** (Figure 5.6). For both samples similar average diameters were obtained (d_{1a} = 76 $\pm$ 5 nm, d_{1b} = 78 $\pm$ 5 nm) as expected because of the similar overall degrees of polymerization of the corona blocks (Table 5.2). As a result, we suppose the total extension

of the coronas from wCCMs formed by **1a** and **1b** to be comparable as illustrated in Figure 5.1b.
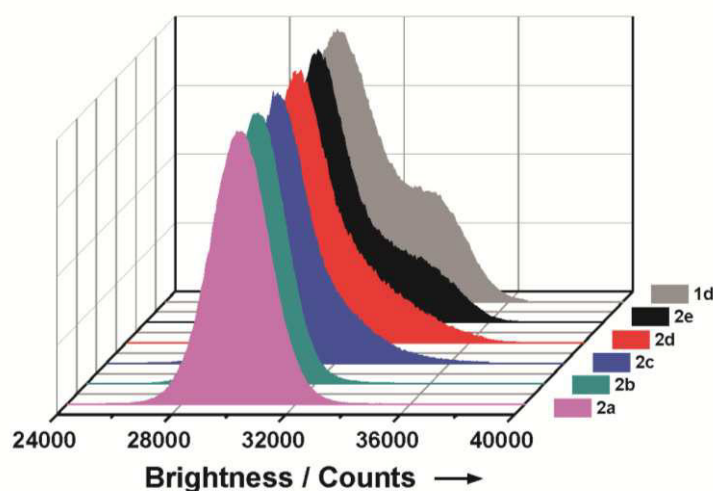
Figure 5.7. Brightness distributions of the pixels within the micellar corona obtained via TEM image analysis of the cocrystallized wCCMs (samples **2a**-**2e**) and pure **1d** for comparison.

From TEM micrographs of the different cocrystallized wCCMs intensity distributions of the corona pixels were extracted (Figure 5.7). This technique allows probing the corona composition over an ensemble of wCCMs rather than single ones by visual TEM micrograph inspection. Here, the main peaks in the brightness distributions correspond to the stained dark appearing PS compartments of the corona, as can be deduced from the brightness distribution of sample **2a** (no PMMA patches visible, cf. Figure 5.3a). For **2b** the amount of PMMA patches still is too low to result in a significant change of the peak shape. However, the pixel intensity distributions of wCCMs formed by **2c**-**2e** clearly exhibit a developing shoulder towards higher brightness. This correlates very well with the increasing PMMA content in the corona and the corresponding increase in PMMA patch number and size observed in the TEM micrographs (Figure 5.3). As expected, this shoulder is most pronounced for the wCCMs formed by the neat triblock terpolymer **1d**. Hence, this method confirms the results obtained by visual inspection of the TEM micrographs, even though, due to the staining procedure and a possibly partial degradation of PMMA caused by the electron beam, only qualitative results can be extracted.
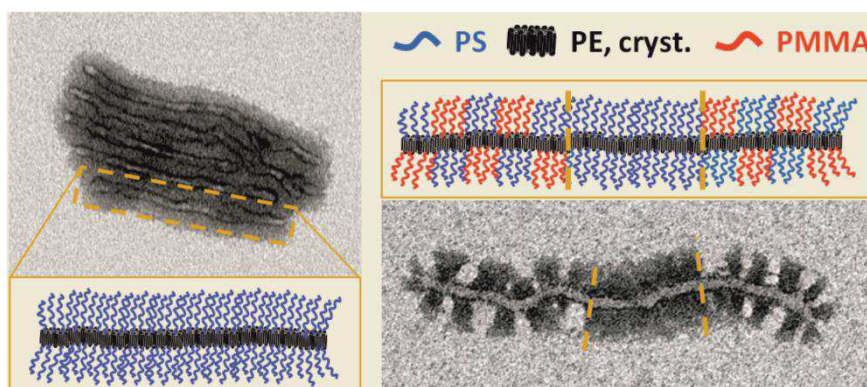
6. Length Control and Block-Type Architectures in Worm-Like Micelles with Polyethylene Cores

Joachim Schmelz,[a] Andreas E. Schedl,[a] Christoph Steinlein,[a] Ian Manners,[b] and Holger Schmalz[a],*

a) Makromolekulare Chemie II, Universität Bayreuth, 95440 Bayreuth, Germany

b) School of Chemistry, University of Bristol, Bristol BS8 1TS, U.K.

ABSTRACT:

We present evidence for "living"-like behavior in the crystallization-driven self-assembly of triblock copolymers with crystallizable polyethylene middle blocks into worm-like crystalline-core micelles (CCMs). A new method of seed production is introduced utilizing the selective self-assembly of the triblock copolymers into spherical CCMs in appropriate solvents. Seeded growth of triblock copolymer unimers from these spherical CCMs results in worm-like CCMs with narrow length distributions and mean lengths that depend linearly on the applied unimer-to-seed ratio. Depending on the applied triblock copolymer, polystyrene-*block*-polyethylene-*block*-polystyrene (SES) or polystyrene-*block*-polyethylene-*block*-poly(methyl methacrylate) (SEM), well-defined worm-like CCMs with a homogeneous or patch-like corona, respectively, can be produced. In a subsequent step, these worm-like CCMs can be used as seeds for the epitaxial growth of a different polyethylene containing triblock copolymer. In this manner, ABA-type triblock *co*-micelles containing blocks with a homogeneous polystyrene corona and those with a patch-like polystyrene/poly(methyl methacrylate) corona were prepared. While the epitaxial growth of SEM unimers to worm-like SES CCMs with a homogeneous corona yields triblock *co*-micelles almost quantitatively, the addition of SES unimers to patchy SEM wCCMs results in a mixture of ABA- and AB-type block *co*-micelles together with residual patchy wCCMs. Following reports on self-assembled block-type architectures from polymers containing core-forming polyferrocenylsilane blocks, these structures represent the first extension of the concept to block *co*-micelles from purely organic block copolymers.

6.1.Introduction

The development of living and/or controlled polymerization techniques revolutionized the field of polymer science.[1] Living anionic polymerization was discovered in 1956[2] and enabled the synthesis of polymers with narrow molecular weight distributions and complex architectures for the first time.[3] Due to the high requirements on purity and the limited range of applicable monomers, efforts to achieve a similar degree of control by the use of different polymerization methods were undertaken and resulted in living cationic polymerization,[4] living ring-opening metathesis polymerization,[5] and controlled radical polymerization methods like atom transfer radical polymerization (ATRP), nitroxide-mediated polymerization (NMP) or reversible addition-fragmentation chain-transfer polymerization(RAFT).[6-11] Especially, the synthesis of well-defined block copolymers[12,13] as well as cylindrical block copolymer brushes[14] has become a cornerstone of modern soft matter research. Over the years, a myriad of different solution structures has been produced using the self-assembly of block copolymers triggered by changes in pH, temperature or solvent environment.[15-24] The ability to manufacture defined nanostructures in bulk as well as in solution opened up a variety of possible applications, such as nanostructured polymer blends or intelligent drug delivery vehicles.[25-29]

Recently, the principle of controlled living living growth was transferred to the next level. Instead of polymerizing angstrom-sized monomers, block copolymers with crystallizable poly(ferrocenyl dimethylsilane) (PFDMS) blocks were shown to crystallize in a living fashion resulting in cylindrical micelles with lengths from the nanometer to the micrometer range and polydispersities down to 1.01.[30,31] In analogy to controlled/living polymerization techniques, a different PFDMS containing block copolymer can be added to the "living" cylindrical micelles producing ABA triblock *co*-micelles.[30] Here, the second block copolymer was added as unimers in a small amount of common solvent and subsequently grows epitaxially from the ends of the precursor cylinders. If the crystal lattice mismatch of another core-forming block is small enough, even heteroepitaxial growth is possible, as shown for a poly(ferrocenyl dimethylgermane) containing block copolymer.[32] Additionally, this technique provides access to even more complex structures like "brush layers" of cylindrical micelles on homopolymer surfaces or scarf-like micelles, that is, cylindrical micelles grown from

platelet-like aggregates, too.[32] Recently, among the block copolymer systems that are known to form one-dimensional structures *via* crystallization-induced self-assembly[33] "living"-like self-assembly was also reported for cylindrical micelles produced from block copolymers containing poly(ferrocenyl diethylsilane),[34] poly(3-hexylthiophene)[35] and enantiopure polylactide.[36] However, the length distributions of the micelles produced by these block copolymers were not as narrow as for PFDMS based cylinders. One-dimensional block *co*-micelles were up to now only reported for diblock copolymers containing PFDMS or poly(ferrocenyl dimethylgermane). With regard to two-dimensional structures, a similar "living" behavior was observed for crystallizable poly(ethylene oxide) (PEO) blocks.[37] Here, the sequential addition of a PEO homopolymer and a PEO-*b*-PS diblock copolymer resulted in platelets with an alternating "channel-wire" array of "wires" with a PS corona and "channels" without a corona.

In general, recent efforts concerning the "living" growth to block-type architectures focused on diblock copolymers that form micellar blocks with homogeneous coronas. By using triblock terpolymers instead, the incorporation of surface-compartmentalized blocks into block *co*-micelles should be possible, too. The solution self-assembly of triblock terpolymers to one-dimensional structures results in a patch-like ("patchy") surface compartmentalization if it is induced by the collapse of the middle block – irrespective of the core state (crystalline or amorphous) – and the two outer blocks are sufficiently incompatible towards each other.[38,39] These structures are candidates for the directed incorporation of functional inorganic nanoparticles and/or dyes in spatially separated corona compartments and have the potential for further self-assembly into supramicellar mesostructures, *e.g.* helices.[40]

Previously, we reported the crystallization-induced self-assembly of triblock co- and terpolymers with semicrystalline PE middle blocks to form worm-like crystalline-core micelles (wCCMs).[39,41] If self-assembled using polystyrene-*block*-polyethylene-*block*-polystyrene (SES) triblock copolymers (equal outer blocks) these micelles bear a homogeneous corona, whereas the use of polystyrene-*block*-polyethylene-*block*-poly(methyl methacrylate) (SEM) triblock terpolymers (different incompatible outer blocks) results in patchy coronas. The average length of the wCCMs decreases with decreasing crystallization

temperature.[41] Here, the increased nucleation density at lower crystallization temperatures results in an increased number of wCCMs and thus in fewer unimers available per growing micelle. However, using this method a precise length control is not possible. As nucleation occurs statistically, the resulting length distributions were rather broad for all crystallization temperatures ($L_w/L_n \approx 1.3$).

In this work, we address the question whether seeded growth techniques can also be applied to polyethylene containing triblock copolymers to produce wCCMs with defined lengths and narrow length distributions. For this purpose preformed spherical crystalline core micelles (sCCMs) based on SES or SEM triblock copolymers are explored as seeds for the controlled growth of the corresponding triblock copolymer unimers into worm-like micelles with a homogeneous or patchy corona, respectively. Furthermore, in the second part the grown wCCMs are used to investigate their propensity to add unimers of a different triblock copolymer to produce ABA type triblock *co*-micelles via epitaxial growth. Similarities and differences with respect to the living self-assembly observed for poly(ferrocenyl dimethylsilane) containing block copolymers by Winnik and Manners et al. will be discussed.

6.2. Results and Discussion

Seeded Growth. The use of seeded growth for the crystallization-driven self-assembly of cylindrical micelles is known to enable the production of micelles with defined lengths and narrow length distributions (low L_w/L_n values).[31,34,35] These seeds are usually produced by ultrasonication of preformed cylindrical micelles under cryogenic conditions resulting in short "stub-like" micelles with $L_w/L_n \approx 1.05$. Alternatively, cylindrical micelles can be heated to a temperature, where due to partial dissolution only small fragments are left over, a technique known as self-seeding.[42]

Here, we use an alternative method for producing well defined seeds which is based on our previous observation that the morphology of crystalline-core micelles (CCMs) formed by triblock terpolymers with polyethylene middle blocks can be easily adjusted by the solvent environment.[41] Self-assembly in bad solvents for the polyethylene block in the molten state (dioxane, dimethylacetamide) results in well-defined spherical crystalline core micelles (sCCMs), whereas in good solvents for the polyethylene block (toluene, THF) worm-like

crystalline-core micelles (wCCMs) are formed. The exclusively one-dimensional growth in good solvents for the PE middle block was observed for different triblock copolymers with varying composition and overall molecular weight and, thus, was attributed to its middle block position in the triblock copolymers. Consequently, sCCMs as seeds were produced from a polystyrene-*block*-polyethylene-*block*-polystyrene ($S_{380}E_{880}S_{390}$, subscripts denote the number average degree of polymerization) triblock terpolymer in a 10 g/L dioxane solution to reduce the amount of dioxane that is present in the final solvent mixture during the subsequent seeded growth process (molecular characteristics and thermal properties of the SES triblock copolymer can be found in Table 6.1). Therefore, the polymer was dissolved above the melting temperature of PE in dioxane (T_m = 74 °C) and subsequently cooled to room temperature. As dioxane is a bad solvent for PE, monodisperse spherical micelles are formed already before crystallization occurs at T_c = 43 °C and subsequent crystallization upon further cooling takes place in each micellar core individually.

Table 6.1. Molecular characteristics and thermal properties of the used triblock copolymers.

Polymer[a]	M_n [kg/mol][b]	PDI[c]	Et / 100C[d]	T_c [°C][e]	T_m [°C][e]	α [%][e]
$S_{380}E_{880}S_{390}$	105	1.04	2.7	21.8	51.8	50
$S_{340}E_{700}M_{360}$	91	1.04	2.6	18.3	52.0	51

a) subscripts denote the average degree of polymerization

b) number-average molecular weight determined by a combination of THF-SEC and ^{1}H-NMR

c) polydispersity index of the respective poly(1,4-butadiene) (PB) containing precursor triblock copolymer (before hydrogenation) as obtained by THF-SEC using a polystyrene calibration

d) average amount of ethyl branches per 100 main chain carbon atoms resulting from 1,2-addition in the polymerization of PB, determined by ^{1}H-NMR of the precursor triblock copolymer

e) peak melting (T_m) and crystallization (T_c) temperatures as well as degree of crystallinity of the PE middle block determined from μDSC measurements of 10 g/L THF solutions at a scanning rate of 0.5 K/min.[41]

For transmission electron microscopy (TEM) investigation all samples prepared in this publication were stained by RuO_4, which is known to selectively stain PS. In the micrograph sCCMs with a light, slightly rectangular PE core and a dark PS corona are observed (Figure 6.1). The number-average core length and the total micelle radius have been determined to

L_n = 11 ± 1 nm with L_w/L_n = 1.01 and R_{total} = 21 ± 2 nm, respectively. This is in good agreement with dynamic light scattering from which a hydrodynamic radius of R_h = 23 nm is obtained (Inset in Figure 6.1). This direct self-assembly approach allows the production of uniform seeds on a large scale and thus represents a versatile alternative to the established methods.
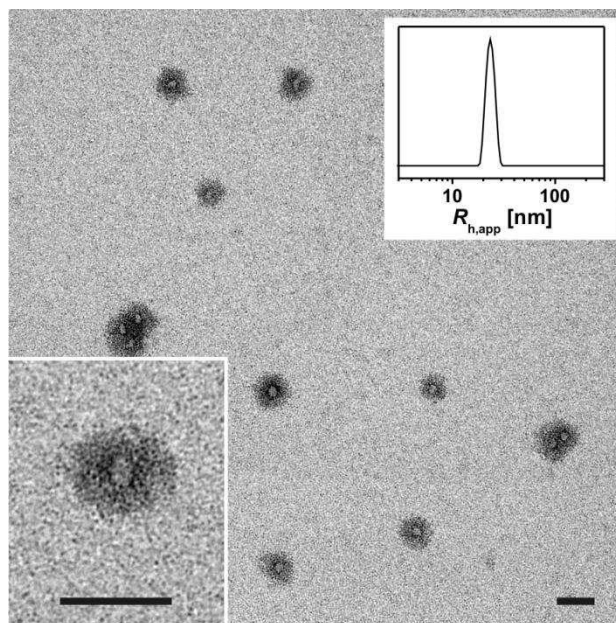

Figure 6.1. TEM micrographs of sCCMs self-assembled from SES in dioxane; scale bars: 50 nm. Inset: DLS CONTIN plot of a 1 g/L solution of SES sCCMs in dioxane (θ = 90°).

Scheme 6.1. Preparation of wCCMs with controlled lengths *via* seeded growth (A) and subsequent epitaxial growth to triblock *co*-micelles (B).
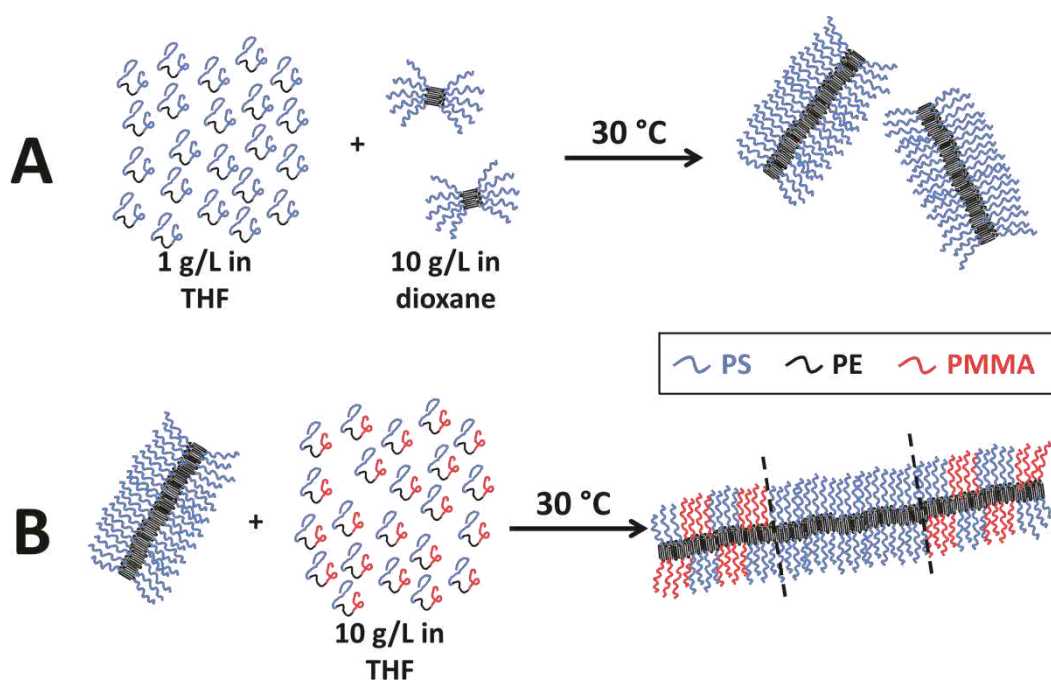
As one-dimensional growth in our system was shown to only occur in good solvents for the PE middle block, that is, solvents that dissolve PE above its melting temperature like THF and toluene, seeded growth was performed in THF. In order to provide unimers that are able to grow to preformed seeds usually the same block copolymer is dissolved in a small amount of common solvent. However, as there is no solvent that dissolves crystalline PE at room temperature, SES unimers had to be produced thermally by heating a THF solution above the melting temperature of the PE block (T_m = 52 °C).[41] Consequently, the subsequent seeded growth should be conducted at a temperature between T_m and the crystallization temperature T_c = 21.8 °C, to ensure that unimers are still able to crystallize onto the provided seeds while on the other hand no significant homogeneous nucleation of the unimers occurs (Scheme 6.1A). Thus, a 1 g/L THF solution of SES was heated to 65 °C for 30 min and subsequently quenched to 30 °C. This procedure was directly followed by the addition of small amounts of the seed solution (10 g/L in dioxane), so that unimer-to-seed weight ratios of U/S = 3, 6, 9, …, 18 were obtained. Noteworthy, even for the highest seed content (U/S = 3) the dioxane content in the resulting solution is only about 3 vol%. These solutions were kept at 30 °C for two weeks. After the solutions were allowed to cool down to room temperature TEM samples were prepared for each U/S ratio. This procedure is denoted as the "one-step growth process" in the following text.
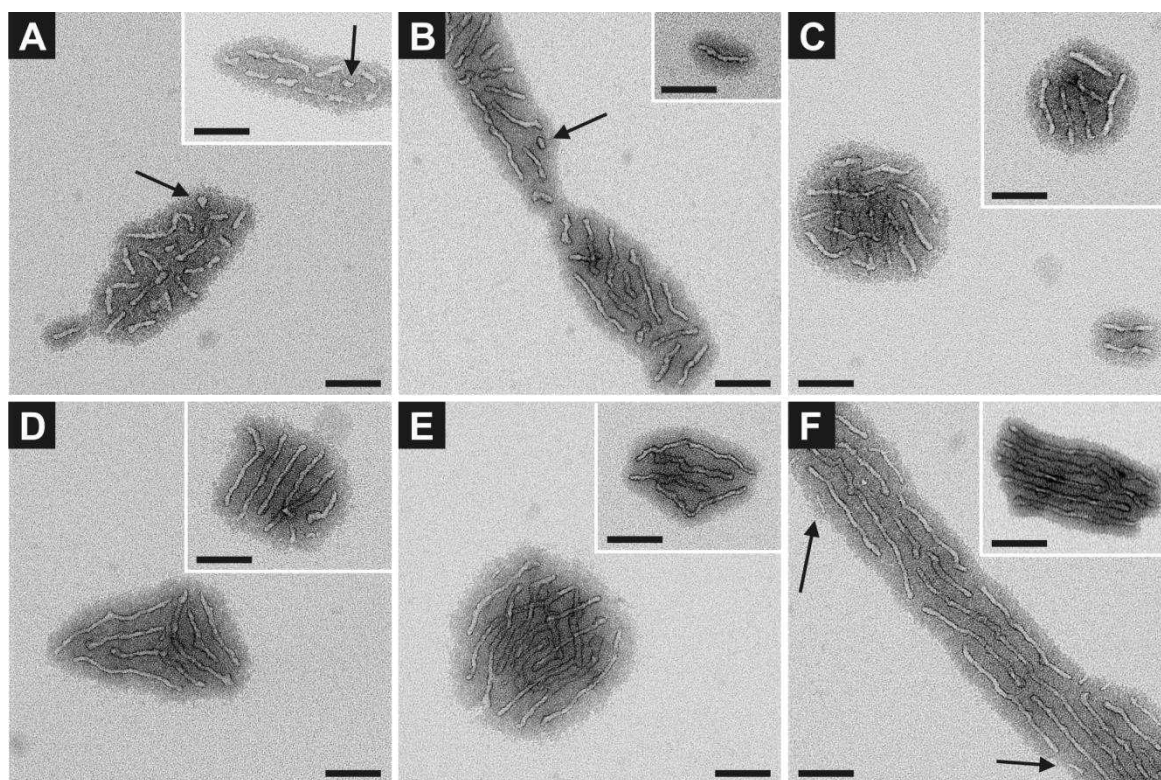
Figure 6.2. TEM micrographs of SES wCCMs formed by seeded growth at 30 °C in 1 g/L THF solutions applying U/S ratios (wt/wt of polymer) of 3 (A), 6 (B), 9 (C), 12 (D), 15 (E) and 18 (F). Arrows depict still remaining sCCMs at low U/S ratios (A, B) and short wCCMs with thinner PE cores at high U/S ratio (F), respectively. Scale bars: 100 nm.

In all micrographs of the formed wCCMs a light PE core is detected together with a stained, dark PS corona can be traced (Figure 6.2). Although these wCCMs tend to aggregate upon drying during TEM sample preparation, their PE cores can be clearly distinguished from the PS corona as the high energy amorphous fold interface between core and corona is also preferentially stained by RuO_4.[39] It is relevant to note that the observed aggregation only arises from TEM sample preparation as in the corresponding apparent hydrodynamic radii distribution obtained from dynamic light scattering larger aggregates are clearly absent (Figure 6.7). A plot of the number-average wCCM core length, L_n, evaluated from the micrographs *vs.* the U/S ratio shows a linear relationship (Figure 6.3, black squares; corresponding length histograms for the wCCMs prepared at different U/S ratios can be found in Figure 6.8). This indicates that the growth of the unimers onto the sCCM seeds proceeds in a "living"-like fashion. The intercept of the linear fit (14 ± 2 nm) is comparable to the core size of the sCCM seeds (11 ± 1 nm), which is also suggestive of selective unimer growth from the seeds.
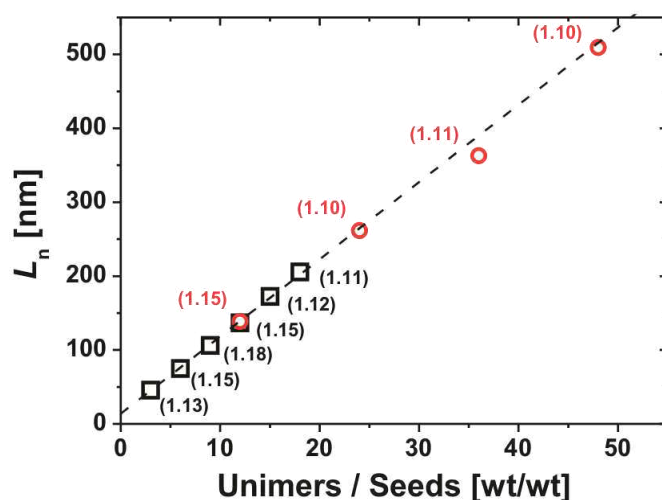
Figure 6.3. L_n *vs.* applied unimer-to-seed ratio for wCCMs prepared in the one-step growth process (black squares) and *via* repetitive unimer addition (red circles). The values given in brackets correspond to the length polydispersities (L_w/L_n) and the dashed line represents a linear fit to the length *vs.* U/S ratio data for the wCCMs produced by one-step growth (black squares).

Notably, the length polydispersities L_w/L_n (Figure 6.3) show an increase up to U/S = 9 and decrease again for higher ratios. A similar increase of L_w/L_n for low U/S ratio with respect to the length polydispersity of the seeds was also observed for the seeded growth of poly(ferrocenyl diethylsilane)-*block*-polydimethylsiloxane (PFDES-*b*-PDMS) diblock copolymers.[34] A possible explanation for this phenomenon might be that in comparison to the addition of unimers to already grown wCCMs unimer addition to sCCMs could be more difficult, that is, "initiation" might be slow with respect to the subsequent growth. Additionally, we are not dealing with perfectly linear PE chains as crystallizable middle blocks. Due to the synthesis of the triblock copolymers *via* sequential anionic polymerization and subsequent hydrogenation of the poly(1,4-butadiene) middle blocks to PE,[39] these blocks contain a small amount of ethyl side branches (Table 6.1) that influence crystallization. As these branches most likely are distributed randomly along the PE blocks and their number may also vary for different triblock copolymer chains, the nucleation efficiency of the pre-assembled sCCMs may vary as well. Consequently, the few observable micelles that still almost look like sCCMs in the micrographs of samples prepared at low U/S ratios (arrows in Figure 2A,B) and, thus, were not able to add unimers in the given time span, might represent sCCMs with PE cores having an above-average amount of ethyl branches.

For higher U/S ratios L_w/L_n decreases again down to 1.11 for U/S = 18. However, for high U/S values a small fraction of significantly shorter wCCMs with thinner cores can be traced (arrows in Figure 6.2F) that most probably have formed during cooling to room temperature after 2 weeks at 30 °C or even later during sample preparation. Consequently, these micelles were not considered for the length evaluation presented in Figure 3. No significant influence of the crystallization temperature on the core diameter was observed in our previous work.[41] Thus, the thinner cores of the wCCMs that form from the remaining unimers in this case might be explained by a fractionation of unimers taking place during the growth to wCCMs. Unimers with a more perfect PE block, *i.e.* fewer ethyl branches, crystallize onto the micelles preferably while those with less perfect PE blocks remain in solution until they form wCCMs at lower temperatures or during sample preparation. Due to the higher amount of chain imperfections, the PE blocks of these unimers are forced to form more folds upon crystallization, resulting in a lower crystallite thickness.[43] Another reason for incomplete unimer consumption might be the low seed concentration at high U/S ratios. As the unimer concentration was kept constant in this experiment, the seed concentration and, hence, the concentration of "living" wCCMs in solution decreases for increasing U/S, presumably resulting in slower unimer consumption. As a result, even after growth for 2 weeks not all unimers are grown to wCCMs and crystallize later at lower temperatures.

It is relevant to note that the unimers forming the small micelles are not available for the seeded growth of regular micelles at 30 °C, which should result in lower values for L_n at high U/S ratios. However, the highest observed fraction of small micelles is about 14% (for U/S = 18). As these micelles exhibit an L_n of about 20 nm, which is by a factor of 10 lower than that of the regularly grown wCCMs at U/S = 18 (L_n = 206 nm), only about 1.4% of the unimers appear to form the smaller micelles. In addition, due to the thinner cores of these micelles, that is, a higher number of folds, even fewer unimers will be needed to obtain a given core length. Consequently, the fraction of unimers that is not available for regular micellar growth is too low to result in a significant deviation from the linear trend in the evaluation of the regularly grown micelles. If the significantly shorter micelles with thinner PE cores are included in the length statistics, L_n is shifted to lower values and the length distribution broadens for U/S = 15 and U/S = 18 (Figure 6.9). However, the formation of these wCCMs

with thinner cores can be avoided by applying a slightly different preparation method, as will now be described.

Even though micelles with controlled lengths of up to 200 nm could be produced, the obviously slower monomer addition at low seed concentrations is an obstacle to the production of even longer wCCMs by the given method. A possible alternative growth method would be to increase the unimer concentration while keeping the seed concentration constant. However, as the crystallization temperature rises with increasing concentration,[41] this leads to a higher probability of homogeneous nucleation and thus might disturb the controlled seeded growth. In order to form longer micelles and still prevent significant dilution of the growing wCCMs, further elongation was conducted *via* repetitive addition of more concentrated unimer solutions (10 g/L in THF) to the wCCMs instead of the one-step growth process described above. Thus, to wCCMs that were grown in a 1g/L THF solution employing a U/S ratio of 6 for 2 days the same amount of unimers was added again as a 10 g/L THF solution and allowed to grow for at least another 2 days. This unimer addition was repeated several times so that total unimer-to-seed ratios of U/S = 12, 24, 36 and 48 were obtained. Here, we assume that in 2 days the vast majority of the unimers is able to grow to the seeds (or to the already grown wCCMs in the later stages) so that upon addition of a further batch the unimer concentration does not exceed 1 g/L significantly. In order to induce growth of eventually remaining unimers onto the wCCMs, two days after the last unimer addition these solutions were cooled down stepwise from 30 °C to 20 °C at a rate of 1 K per 12 h. TEM micrographs of the wCCMs formed in this manner can be found in Figure 6.4. Dynamic light scattering again reveals the absence of aggregates in solution (Figure 6.7).

Length evaluation shows that the repetitive addition of unimers also results in a good length control (Figure 6.3, red circles, length histograms for the different samples can be found in Figure 6.10). The samples prepared for U/S = 12 show comparable values of L_n and L_w/L_n for both preparation methods and also at higher U/S ratios the stepwise growth procedure results in L_n values that still show the linear relationship established for the one-step growth method (Figure 6.3, black squares) and narrow length distributions ($L_w/L_n \approx 1.1$). Noteworthy, no small micelles with thinner cores were traced this time, as was the case for

wCCMs produced by the one-step growth method at high U/S ratio (Figure 6.2F). By this "repetitive growth method", the production of wCCMs with lengths of 500 nm and beyond becomes feasible. Thus, in analogy to the "living" growth of PFDMS-containing block copolymers, in the seeded growth of the SES triblock copolymer the length of the formed wCCMs can be controlled by the U/S ratio, too.
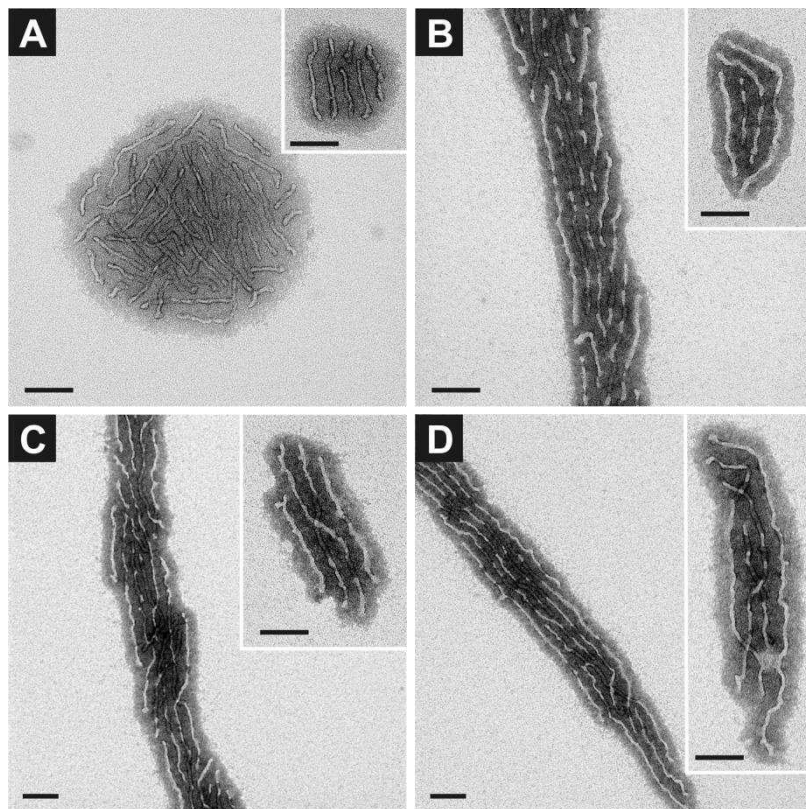

Figure 6.4. TEM micrographs of wCCMs formed from SES at U/S ratios (wt/wt of polymer) of 12 (A), 24 (B), 36 (C) and 48 (D) in THF solutions *via* repetitive unimer addition. Scale bars: 100 nm. It should be noted that the PE cores are partially covered by PS chains and can therefore only be distinguished on careful inspection due to the intensive RuO_4 staining of the amorphous fold interface between core and corona.

A closer inspection of the SES wCCMs formed by the "repetitive growth method" reveals that the PE cores occasionally show some small knobby protrusions (Figure 4). Two possible reasons could account for the formation of these protrusions. Due to the inherent ethyl branches in the PE middle blocks these protrusions might arise from defects in the crystal structure of the PE core. In our previous work, small protrusions could also be traced for not annealed wCCMs formed by a polystyrene-*block*-polyethylene-*block*-poly(methyl methacrylate) triblock terpolymer upon isothermal crystallization.[41] These protrusions almost vanished after annealing, that is, perfection of the PE crystallites in the core, which

resulted in fewer folds and hence an increased crystallite thickness accompanied by a more uniform crystallite thickness distribution. Here, the SES based wCCMs prepared *via* seeded growth were not subsequently annealed which supports this assumption. In addition, in the "repetitive growth method" the wCCMs grow step-wise and for each step nucleation of unimer growth on the pre-formed wCCMs has to take place. This in turn might be a reasonable explanation for the observation that for the "one-step growth process" the formation of protrusions seems to be much less pronounced (Figure 2).

Block *co*-Micelles. Besides the ability to grow polymer chains of controlled length, the production of block copolymers by the sequential addition of different monomers is the key advancement of living and controlled polymerization techniques. Hence, an additional test for the living behavior of the crystallization-driven self-assembly is the epitaxial growth of unimers of a different triblock copolymer onto preformed SES wCCMs (Scheme 6.1B). Thus, wCCM solutions of SES were prepared *via* the one-step seeded growth procedure described earlier in this manuscript applying a unimer-to-seed ratio of 6. After two days a 10 g/L solution of a polystyrene-*block*-polyethylene-*block*-poly(methyl methacrylate) triblock terpolymer ($S_{340}E_{700}M_{360}$, molecular characteristics and thermal properties of the SEM triblock terpolymer can be found in Table 1) in THF was added at 30 °C. This solution also was preheated to 65 °C so that exclusively unimers are present. In order to obtain SEM outer blocks with the same lengths as the SES middle blocks, the double amount of SEM unimers with respect to SES was added. After two more days at 30 °C the solution was cooled down stepwise from 30 °C to 20 °C at a rate of 1 K per 12 h in the same manner as for the production of the SES wCCMs *via* repetitive unimer addition.
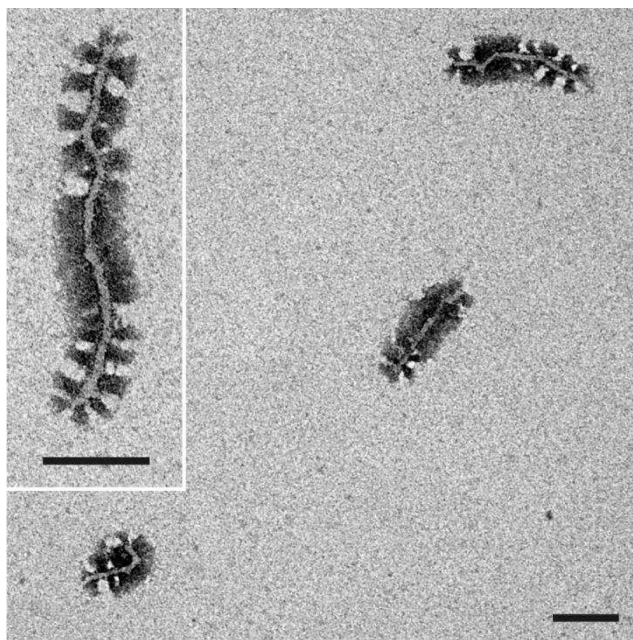
Figure 6.5. TEM micrograph of SEM-b-SES-b-SEM triblock co-micelles prepared via epitaxial growth of SEM unimers onto SES wCCM seeds in a 1g/L THF solution. Scale bars: 100 nm.

TEM investigations of the formed structures show that indeed SEM-*b*-SES-*b*-SEM triblock *co*-micelles are formed (Figure 6.5). Here, middle blocks with a homogeneous PS corona are surrounded by two outer blocks bearing a patch-like corona that consists of alternating PS and PMMA compartments. The PMMA patches are not stained by RuO_4 and therefore appear light, which allows to clearly distinguish them from the intensively stained, dark PS patches. Figure 6.11 shows a collection of different TEM micrographs revealing the homogeneity of the prepared SEM-*b*-SES-*b*-SEM triblock *co*-micelles. The triblock *co*-micelles also show a certain tendency for aggregation upon drying during TEM sample preparation as is the case for SES wCCMs. The homogeneity of the prepared triblock *co*-micelles is further supported by dynamic light scattering showing a monomodal radii distribution and the absence of aggregates in solution (Figure 6.12). SEM-*b*-SES-*b*-SEM triblock *co*-micelles could be obtained with a yield of 97%. The remaining structures consist of about 3% SES-*b*-SEM diblock *co*-micelles and < 1% pure SEM wCCMs as determined from TEM image analysis. As almost no pure SEM wCCMs are formed, the addition of SEM unimers onto the provided SES wCCM seeds is highly favored over homogeneous nucleation highlighting the suitability of the experimental conditions, *i.e.* 30 °C at unimer concentrations around 1 g/L, for controlled epitaxial growth. The number average core length, L_n, of the middle blocks with a homogeneous PS corona is 83 nm, comparable to that of the pure SES wCCMs produced at

U/S = 6 (75 nm, Figure 6.2B), that of the patchy SEM outer blocks 78 nm. While the length distribution of the middle blocks is again rather narrow (L_w/L_n = 1.13), the length polydispersity of the outer blocks is significantly higher (L_w/L_n = 1.27). This together with the fact, that a small fraction of the SES wCCM ends were not able to add SEM unimers, leads to the assumption that not all wCCM ends show exactly the same nucleation efficiency. As already proposed in the first part of this publication for seeded growth of SES unimers onto sCCMs, this might be explained by the statistic distribution of ethyl side branches in the PE main chain of the crystallizable middle blocks. Consequently, the free lateral crystal surfaces at the ends of the wCCMs might exhibit slightly different structures and, thus, different nucleation properties. Here, this phenomenon could be more pronounced as is the case for growth from sCCMs, because during the growth of the SES middle blocks the probability of SES unimers with fewer ethyl side branches, that is, a more ideal PE middle block, to crystallize onto the growing micelles will be higher. This again results in a fractionation as discussed earlier. Hence, unimers with more ethyl branches are more likely situated at the wCCM ends and may cause a slower nucleation of SEM unimers. However, despite the fact that we are dealing with a crystallizable block that bears significant imperfections (ethyl branches), the preparation of SEM-*b*-SES-*b*-SEM triblock *co*-micelles is possible in a controlled way with almost quantitative yield.
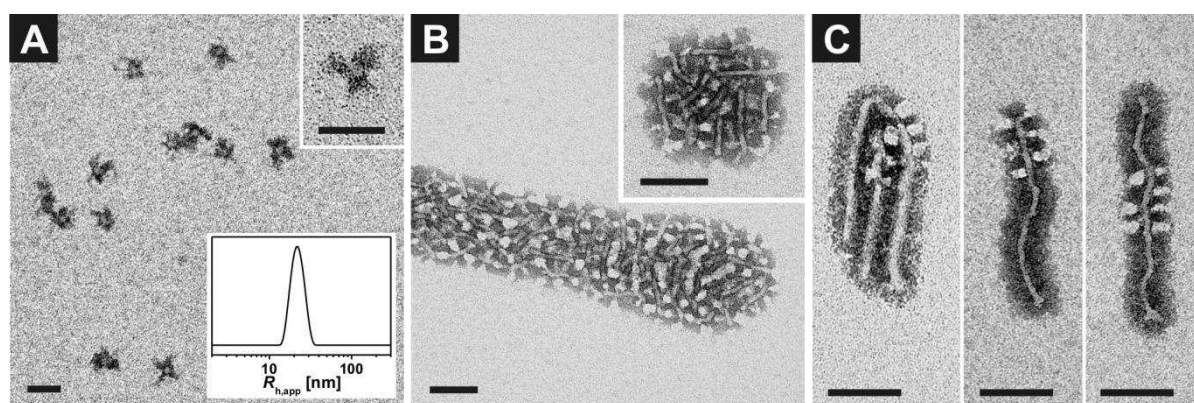

Figure 6.6. TEM micrograph of (A) SEM sCCMs prepared in 10 g/L dioxane solution (Inset: DLS CONTIN plot of a 1 g/L solution of SEM sCCMs in dioxane), and (B) SEM wCCMs prepared by seeded growth at U/S = 6, and (C) selected SES-*b*-SEM-*b*-SES triblock *co*-micelles and SES-*b*-SEM diblock *co*-micelles prepared in 1g/L THF solutions. Scale bars are 50 nm (A) and 100 nm (B, C), respectively.

Applying the same procedure we attempted to produce SES-*b*-SEM-*b*-SES triblock *co*-micelles. For this purpose, sCCMs were prepared from SEM in dioxane followed by the seeded growth of SEM unimers from these seeds at 30 °C in THF (U/S = 6). After two days,

the double amount of SES unimers was added to the preformed SEM wCCMs. The dimensions of the self-assembled SEM sCCMs (Figure 6.6A, L_n = 11 nm with L_w/L_n = 1.01) match those prepared by SES. A precise determination of the total radius of the micelles from TEM micrographs is difficult due to the patch-like surface compartmentalization of the corona, but it can be assumed to be similar to that of the SES sCCMs due to the similar hydrodynamic radius derived from DLS data (Inset in Figure 6.6A, R_h = 22 nm). In addition, the results for the seeded growth yielding SEM wCCMs (L_n = 75 nm, L_w/L_n = 1.07; the corresponding length histogram can be found in Figure 6.13) are comparable to those consisting of SES, clearly showing that this seeded growth approach can be used as well to produce one-dimensional patchy micelles of controlled length and length distribution (Figure 6.6B). However, the epitaxial growth of SES unimers to these SEM micelles did not proceed as successfully as in the reverse case. Here, half of the structures formed are SES-*b*-SEM diblock *co*-micelles (49%) with only 44% of SES-*b*-SEM-*b*-SES triblock *co*-micelles and 5% of remaining pure SEM wCCMs (Figure 6C, additional micrographs can be found in Figure 6.14). The absence of aggregates in solution is again confirmed by DLS (Figure 6.12). In the case where SES outer blocks were able to grow they are longer on average (L_n = 90 nm) than the SEM middle blocks, as now significantly more SES unimers are available per growing chain end. Furthermore, the length polydispersity of the SES outer blocks (L_w/L_n = 1.41) is even higher than that for the SEM outer blocks of the reverse triblock *co*-micelles. Again, no pure SES wCCMs have been observed showing that homogeneous nucleation of unimers is highly improbable under the applied conditions.

Unexpectedly, we observe an asymmetric behavior, that is, unimers of SEM grow significantly better from wCCMs made of SES than the other way round. As the degrees of polymerization of the three blocks as well as the amount of ethyl side branches are comparable for both triblock copolymers (Table 1), these variables presumably are not responsible for this behavior. Thus, the hypothesis arises that the different propensity of epitaxial growth might be influenced by the corona structures in the preformed wCCM seeds. In the "SES-first" approach a triblock terpolymer grows onto wCCMs with a homogeneous corona, whereas in the "SEM-first" approach a triblock copolymer grows onto wCCMs with a patchy corona (Scheme 6.2).

Scheme 6.2. Proposed impact of the corona structure of the applied wCCM seeds on the formation of triblock *co*-micelles.
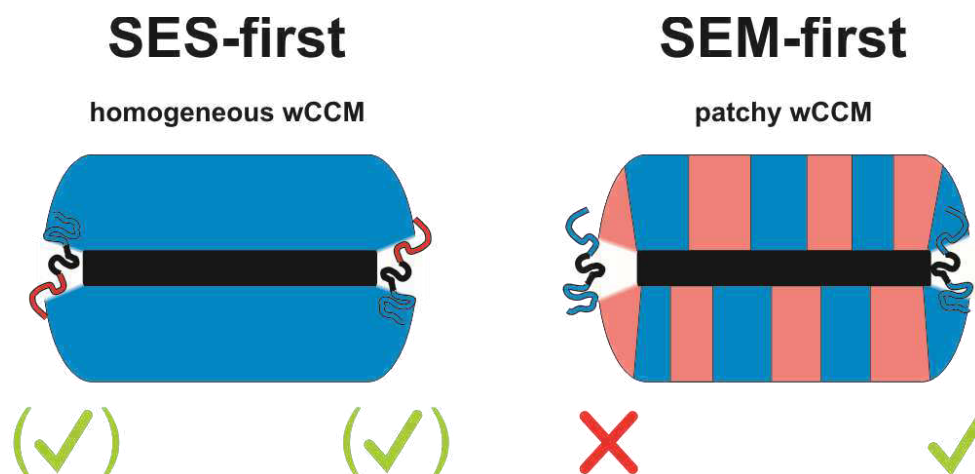
If SEM unimers are added to SES wCCMs ("SES-first") all "living" micellar ends are surrounded by PS chains. Even though PE and PMMA are incompatible with PS, the SEM unimers obviously are able to reach the core allowing the PE block to crystallize onto it. However, as the corona purely consists of PS, each end of a SES wCCM has the same corona structure and, hence, an equal probability to add SEM chains to the crystalline core. For the reverse situation, that is, addition of SES unimers to preformed SEM wCCMs ("SEM-first"), we face a completely different situation. These wCCMs exhibit a patchy corona with alternating compartments of PS and PMMA resulting in potentially different environments of the free lateral crystal surfaces. If a micellar end is encompassed mainly by PS chains, a SES unimer can easily migrate into the corona and deposit onto the PE core of the micelle. A wCCM end that is surrounded by PMMA chains on the other hand is incompatible to all three blocks of the SES unimers. Thus, wCCM ends with a PMMA-rich corona simply might not be able to add SES unimers within the time span in which they grow to those ends that are surrounded mainly by PS. As a result, the inherently different ability of wCCM ends to nucleate the growth of SES unimers vastly increases the fraction of formed SES-*b*-SEM diblock *co*-micelles and remaining SEM wCCMs.

6.3. Conclusion

In the first part of the manuscript, we presented the production of worm-like crystalline-core micelles (wCCMs) with controlled lengths and narrow length distributions down to L_w/L_n = 1.1 using a PS-*b*-PE-*b*-PS triblock terpolymer (SES). Here, self-assembled spherical crystalline-core micelles (sCCMs) were used as nuclei for the growth of triblock copolymer unimers. With this new method of seed formation for "living"-like crystallization-driven self-assembly, the preceding production of sacrificial cylindrical micelles that are commonly applied in the seeded growth of block copolymers containing poly(ferrocenyl dimethylsilane) or poly(3-hexylthiophene) blocks is not necessary. The average length of the produced wCCMs can be tuned by the applied unimer-to-seed ratio up to at least 500 nm. Furthermore, the possibility to extend the controlled crystallization-driven growth to a PS-*b*-PE-*b*-PMMA triblock terpolymer (SEM) for the first time allows the production of one-dimensional patchy micelles with narrow length distributions.

Upon addition of a different triblock copolymer to already grown wCCMs epitaxial growth to block *co*-micelles could be achieved. The addition of SEM unimers to preformed SES wCCMs with homogeneous corona results in ABA-type (SEM-*b*-SES-*b*-SEM) triblock *co*-micelles with a homogeneous inner block and patchy outer blocks in high yields. In the reversed case, however, a mixture of AB-type (SES-*b*-SEM) diblock *co*-micelles and ABA-type (SES-*b*-SEM-*b*-SES) triblock *co*-micelles is formed by the addition of unimers of a SES triblock copolymer to patchy SEM wCCMs. This asymmetric behavior is explained by the different incompatibility of the corona blocks in alternating compartments of patchy wCCMs towards the growing unimers, that is, wCCM ends surrounded predominantly by PS chains are easily accessible for SES unimers, while for those with a PMMA-rich corona epitaxial growth is hindered significantly.

Due to the fact that we do not achieve a complete blocking efficiency in the block *co*-micelles and the length polydispersities are higher compared to the living self-assembly of PFDMS containing block copolymers, we refer to this process as controlled crystallization-driven self-assembly rather than living self-assembly. Nevertheless, after the discovery of block *co*-micelle formation in 2007 for block copolymers containing crystallizable PFDMS

blocks,[30] our results show that this concept can also be extended to PE containing block copolymers. By the use of triblock terpolymers even more complex block *co*-micelles including blocks with a surface-compartmentalized corona are accessible. Due to the inherent structural imperfections (ethyl branches) of the PE blocks in our system that most of the common crystallizable polymers do not share, the concept of living/controlled crystallization-driven self-assembly should be generally applicable to semicrystalline block copolymers if suitable conditions for unimer growth to already existing micelles can be found, *e.g.* a specific solvent environment and/or temperature.

6.4. Methods

Synthesis of Triblock Copolymers. Polystyrene-*block*-poly(1,4-butadiene)-*block*-polystyrene (SBS) and polystyrene-*block*-poly(1,4-butadiene)-*block*-poly(methyl methacrylate) (SBM) were synthesized *via* sequential anionic polymerization in cyclohexane and toluene, respectively, followed by catalytic hydrogenation of the polybutadiene middle block to polyethylene. Detailed information about used materials, purification methods and the polymerization procedure can be found in previous publications.[41,44]

Seed Preparation. A 10 g/L dioxane solution of the respective triblock copolymer was produced by dissolution of the polymer at 90 °C overnight. This solution was quenched in air to room temperature resulting in spherical crystalline-core micelles (sCCMs) that were used as seeds.

Seeded Growth. 6 mL of unimer solutions of the respective triblock copolymers were obtained by dissolution in THF (1 g/L) at 65 °C for at least 30 min. These solutions were quenched to 30 °C before adding different amounts of the seeds (10 g/L in dioxane) at unimer-to-seed ratios (U/S, wt/wt of polymer) from 3 to 18, corresponding to 200 µL down to 33 µL of seed solution. After 2 weeks at 30 °C in a thermostated shaker unit (Ditabis Cooling-Thermomixer MKR13) the solutions were quenched in air before TEM sample preparation ("one-step growth process").

In the second experiment ("repetitive grow method") worm-like crystalline-core micelles (wCCMs) firstly were produced using the technique described above and a U/S ratio of 6. After 2-4 days of shaking at 30 °C the same amount of unimers was added again as a preheated (65 °C for 30 min) 10 g/L THF solution (600 μL) in order to restore a unimer concentration of about 1 g/L and at the same time avoid significant dilution of the wCCM concentration. This procedure was repeated several times so that solutions with final U/S ratios of 12, 24, 36 and 48 were obtained. After the final unimer addition the solutions were kept at 30 °C for at least 2 more days and subsequently cooled to 20 °C stepwise at a rate of 1 K per 12 h, in order to facilitate the controlled growth of unimers with less ideal PE blocks containing above-average amounts of ethyl side branches.

Block *co*-Micelles. For the preparation of SEM-*b*-SES-*b*-SEM triblock *co*-micelles, firstly, the SES wCCMs that afterwards form the middle block of the block *co*-micelles were produced at a U/S ratio of 6 for 2 d at 30 °C as described above. Subsequently, the double amount of SEM unimers was added as a 10 g/L THF solution (1.2 mL) that again was preheated to 65 °C for 30 min. After another 2 days at 30 °C the solution was cooled to 20 °C stepwise at a rate of 1 K per 12 h. The preparation of SES-*b*-SEM-*b*-SES triblock *co*-micelles was conducted in the reverse way under otherwise identical conditions. Hence, SEM wCCMs were produced *via* the seeded growth of unimers to SEM sCCMs followed by addition of the double amount of SES unimers.

Transmission Electron Microscopy (TEM) samples were prepared by placing a drop of the diluted solution (0.5 g/L) on a carbon-coated copper grid. After 20 s, excess solution was removed by blotting with a filter paper. Subsequently, elastic bright-field TEM was performed on a Zeiss 922 OMEGA EFTEM (Zeiss NTS GmbH, Oberkochen, Germany) operated at 200 kV. Zero-loss filtered images ($\Delta E = 0$) were registered digitally by a bottom-mounted CCD camera system (Ultrascan 1000, Gatan) and processed with a digital imaging processing system (Gatan Digital Micrograph 3.9 for GMS 1.4). Staining was performed with RuO_4 vapor for at least 20 min. RuO_4 is known to selectively stain PS, *i.e.*, PS domains appear dark, which enables to distinguish between PS and PMMA domains in the corona of the micelles. Average values of the SES and SEM wCCM lengths were determined from at least 100 measurements using ImageTool (University of Texas Health Science Center, San

Antonio). For the characterization of the triblock *co*-micelles about 200 micelles were evaluated. Due to better visibility, these average lengths were obtained by measuring the PE core length. In case micelles with thinner cores self-assembled during sample preparation or previous cooling (see Figure 6.2F), these were not taken into account, as their formation did not occur at the conditions suitable for controlled growth. The number average and weight average micelle lengths, L_n and L_w, respectively, were calculated from the obtained lengths as follows:

$$L_n = \frac{\sum_{i=1}^{n} N_i L_i}{\sum_{i=1}^{n} N_i} \qquad (1) \qquad\qquad L_w = \frac{\sum_{i=1}^{n} N_i L_i^2}{\sum_{i=1}^{n} N_i L_i} \qquad (2).$$

Dynamic Light Scattering (DLS). DLS measurements were performed on an ALV DLS/SLS-SP 5022F compact goniometer system equipped with an ALV 5000/E operated in cross-correlation mode at a scattering angle of 90° and a He-Ne laser (λ_0 = 632.8 nm) was employed as light source. The decalin bath of the instrument was thermostated to 20 °C using a LAUDA Proline RP 845 thermostat. Data evaluation of the DLS experiments was performed using the CONTIN algorithm,[45] which yields an intensity-weighted distribution of relaxation times (τ) after an inverse Laplace transformation of the intensity auto-correlation function. These relaxation times were transformed into translational diffusion coefficients and further into hydrodynamic radii using the Stokes-Einstein equation.

6.5. References

1. *Controlled and Living Polymerizations: From Mechanisms to Applications*; Müller, A. H. E., Matyjaszewski, K., Eds.; Wiley-VCH: Weinheim, 2009.

2. Szwarc, M. *Nature* **1956**, *178*, 1168-1169.

3.   Hsieh, H. L.; Quirk, R. P. *Anionic Polymerization: Principles and Practical Applications*; Marcel Dekker: New York, 1996.

4.   Goethals, E. J.; Du Prez, F. *Prog. Polym. Sci.* **2007**, *32*, 220-246.

5.   Bielawski, C. W.; Grubbs, R. H. *Prog. Polym. Sci.* **2007**, *32*, 1-29.

6.   Braunecker, W. A.; Matyjaszewski, K. *Prog. Polym. Sci.* **2007**, *32*, 93-146.

7.   Gregory, A.; Stenzel, M. H. *Prog. Polym. Sci.* **2012**, *37*, 38-105.

8.   Matyjaszewski, K.; Tsarevsky, N. V. *Nat. Chem.* **2009**, *1*, 276-288.

9.   Ayres, N. *Polym. Rev.* **2012**, *51*, 138-162.

10.   Hawker, C. J.; Bosman, A. W.; Harth, E. *Chemical Reviews* **2001**, *101*, 3661-3688.

11.   Moad, G.; Rizzardo, E.; Thang, S. H. *Aust. J. Chem.* **2009**, *62*, 1402-1472.

12.   Hadjichristidis, N.; Pispas, S.; Floudas, G. A. *Block Copolymers: Synthetic Strategies, Physical Properties, and Applications*; John Wiley & Sons: Hoboken, New Jersey, 2003.

13.   Hamley, I. W. *Block Copolymers in Solution: Fundamentals and Applications*; Jon Wiley & Sons: Chichester, 2005.

14.   Yuan, J.; Müller, A. H. E.; Matyjaszewski, K.; Sheiko, S. S., In *Polymer Science: A Comprehensive Reference*, Müller, A. H. E.; Wooley, K. L., Eds. Elsevier: Oxford, 2012; Vol. 6, pp 199-264.

15.   Zhang, L.; Eisenberg, A. *Science* **1995**, *268*, 1728-1731.

16.   Lodge, T. P. *Macromol. Chem. Phys.* **2003**, *204*, 265-273.

17.   Lazzari, M.; Lopez-Quintela, M. A. *Adv. Mater.* **2003**, *15*, 1583-1594.

18.   Rodríguez-Hernández, J.; Chécot, F.; Gnanou, Y.; Lecommandoux, S. *Prog. Polym. Sci.* **2005**, *30*, 691-724.

19.   Riess, G. *Prog. Polym. Sci.* **2003**, *28*, 1107-1170.

20.   Hamley, I. W. *Soft Matter* **2005**, *1*, 36-43.

21.   Rabotyagova, O. S.; Cebe, P.; Kaplan, D. L. *Biomacromolecules* **2011**, *12*, 269-289.

22.   Moughton, A. O.; Hillmyer, M. A.; Lodge, T. P. *Macromolecules* **2012**, *45*, 2-19.

23.   Cui, H.; Chen, Z.; Zhong, S.; Wooley, K. L.; Pochan, D. J. *Science* **2007**, *317*, 647-650.

24. Discher, B. M.; Won, Y.-Y.; Ege, D. S.; Lee, J. C.-M.; Bates, F. S.; Discher, D. E.; Hammer, D. A. *Science* **1999**, *284*, 1143-1146.

25. Ruzette, A. V.; Leibler, L. *Nat. Mater.* **2005**, *4*, 19-31.

26. Botiz, I.; Darling, S. B. *Mater. Today* **2010**, *13*, 42-51.

27. Topham, P. D.; Parnell, A. J.; Hiorns, R. C. *J. Polym. Sci., Part B: Polym. Phys.* **2011**, *49*, 1131-1156.

28. Jackson, E. A.; Hillmyer, M. A. *ACS Nano* **2010**, *4*, 3548-3553.

29. Hamidi, M.; Shahbazi, M. A.; Rostamizadeh, K. *Macromol. Biosci.* **2012**, *12*, 144-164.

30. Wang, X.; Guerin, G.; Wang, H.; Wang, Y.; Manners, I.; Winnik, M. A. *Science* **2007**, *317*, 644-647.

31. Gilroy, J. B.; Gädt, T.; Whittell, G. R.; Chabanne, L.; Mitchels, J. M.; Richardson, R. M.; Winnik, M. A.; Manners, I. *Nat. Chem.* **2010**, *2*, 566-570.

32. Gädt, T.; Ieong, N. S.; Cambridge, G.; Winnik, M. A.; Manners, I. *Nat. Mater.* **2009**, *8*, 144-150.

33. Lazzari, M.; Lopez-Quintela, M. A. *Macromol. Rapid Commun.* **2009**, *30*, 1785-1791.

34. Gädt, T.; Schacher, F. H.; McGrath, N.; Winnik, M. A.; Manners, I. *Macromolecules* **2011**, *44*, 3777-3786.

35. Patra, S. K.; Ahmed, R.; Whittell, G. R.; Lunn, D. J.; Dunphy, E. L.; Winnik, M. A.; Manners, I. *J. Am. Chem. Soc.* **2011**, *133*, 8842-8845.

36. Petzetakis, N.; Dove, A. P.; O'Reilly, R. K. *Chem. Sci.* **2011**, *2*, 955-960.

37. Chen, W. Y.; Li, C. Y.; Zheng, J. X.; Huang, P.; Zhu, L.; Ge, Q.; Quirk, R. P.; Lotz, B.; Deng, L.; Wu, C.; Thomas, E. L.; Cheng, S. Z. D. *Macromolecules* **2004**, *37*, 5292-5299.

38. Njikang, G.; Han, D. H.; Wang, J.; Liu, G. J. *Macromolecules* **2008**, *41*, 9727-9735.

39. Schmalz, H.; Schmelz, J.; Drechsler, M.; Yuan, J.; Walther, A.; Schweimer, K.; Mihut, A. M. *Macromolecules* **2008**, *41*, 3235-3242.

40. Dupont, J.; Liu, G. J.; Niihara, K.; Kimoto, R.; Jinnai, H. *Angew. Chem. Int. Ed.* **2009**, *48*, 6144-6147.

41. Schmelz, J.; Karg, M.; Hellweg, T.; Schmalz, H. *ACS Nano* **2011**, *5*, 9523-9534.

42. Qian, J.; Guerin, G.; Lu, Y.; Cambridge, G.; Manners, I.; Winnik, M. A. *Angew. Chem. Int. Ed.* **2011**, *50*, 1622-1625.

43. Guérin, G.; Raez, J.; Manners, I.; Winnik, M. A. *Macromolecules* **2005**, *38*, 7819-7827.

44. Ruckdäschel, H.; Sandler, J. K. W.; Altstädt, V.; Rettig, C.; Schmalz, H.; Abetz, V.; Müller, A. H. E. *Polymer* **2006**, *47*, 2772-2790.

45. Provencher, S. W. *Comput. Phys. Commun.* **1982**, *27*, 213-227.

6.6. Supporting Information
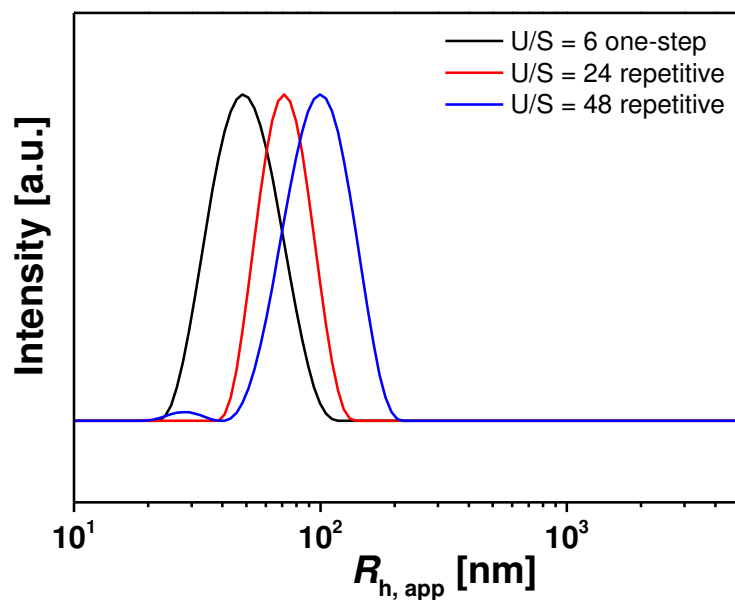
Figure 6.7. Apparent hydrodynamic radii distributions obtained from DLS data of $S_{380}E_{880}S_{390}$ wCCMs (1 g/L, THF, θ = 90°) produced *via* seeded growth at U/S ratios (wt/wt of polymer) of 6 (one-step growth process) as well as 24 and 48 (repetitive monomer addition). The DLS CONTIN plots clearly show the absence of aggregates in solution and the $R_{h,app}$ values increase with increasing U/S ratio in consistency with the L_n data (Figure 6.8, 6.10).
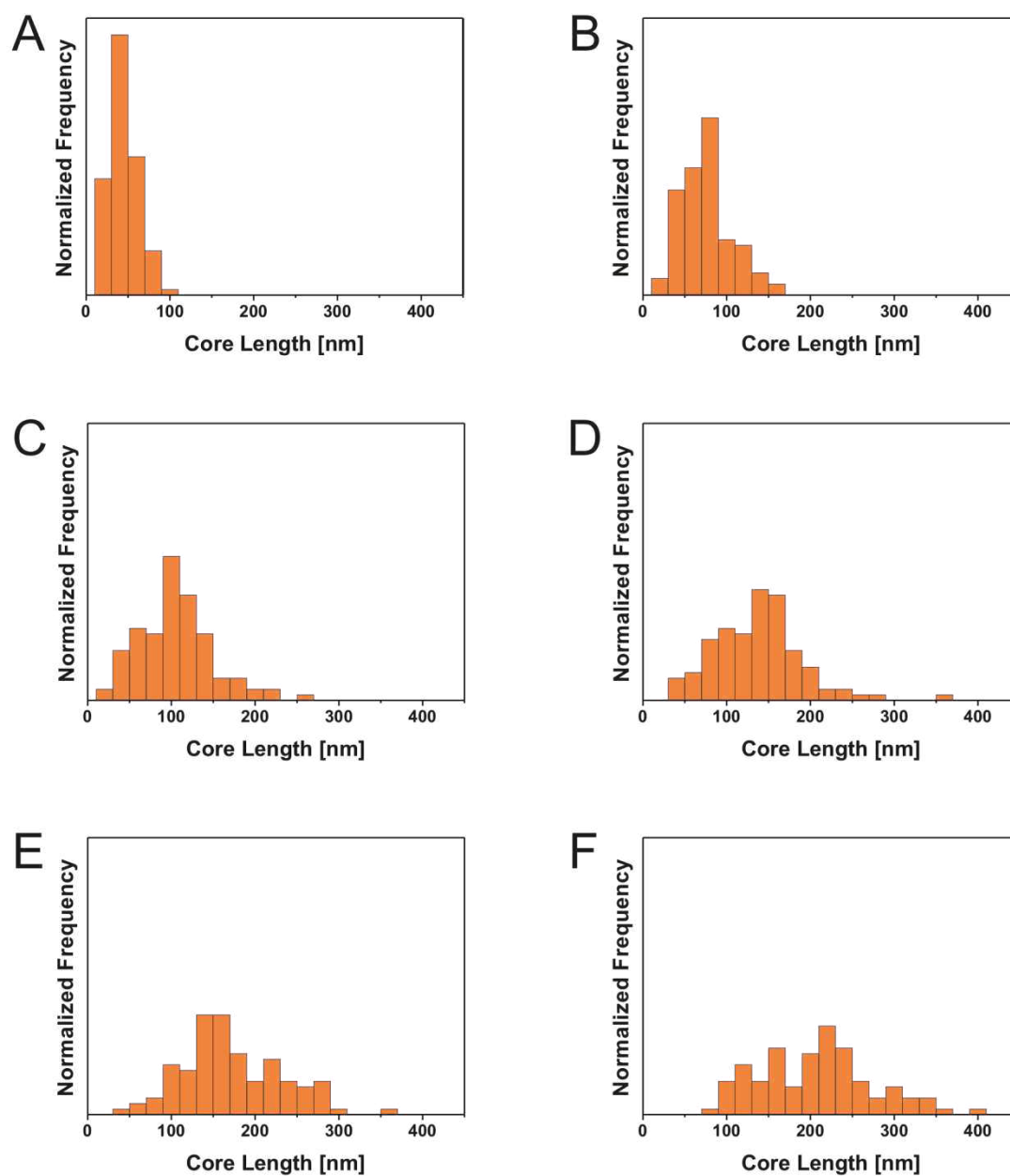
Figure 6.8. Length histograms of SES wCCMs produced *via* seeded growth at U/S = 3 (A), 6 (B), 9 (C), 12 (D), 15 (E) and 18 (F).
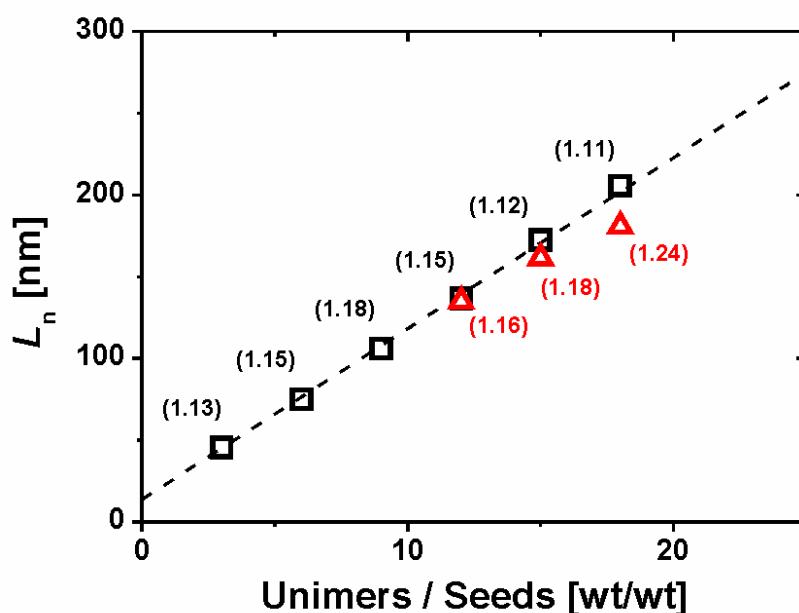
Figure 6.9. L_n *vs.* applied unimer-to-seed ratio (wt/wt of polymer) for wCCMs prepared *via* the one-step growth process. Length statistics were evaluated counting only the wCCMs that grew regularly at 30 °C (black squares) or including those with thinner cores formed upon subsequent cooling (red triangles). The values given in brackets correspond to the length polydispersities (L_w/L_n) and the dashed line represents the linear fit to the length *vs.* U/S ratio data for the regularly grown wCCMs (black squares).

Figure 6.9 shows the number average PE core lengths (L_n) and the length polydispersities for the regularly grown $S_{380}E_{880}S_{390}$ wCCMs prepared by one-step growth at 30 °C (black squares). As mentioned in the main manuscript, a small fraction of significantly shorter micelles with thinner PE cores were traced along with these regularly grown wCCMs (Figure 6.2F). If the short micelles, which were presumably formed upon subsequent cooling, are included in the length statistics, the average PE core length of the micelles significantly deviates from the linear relationship for high unimer-to-seed ratios (U/S ≥ 12, red triangles in Figure 6.9).
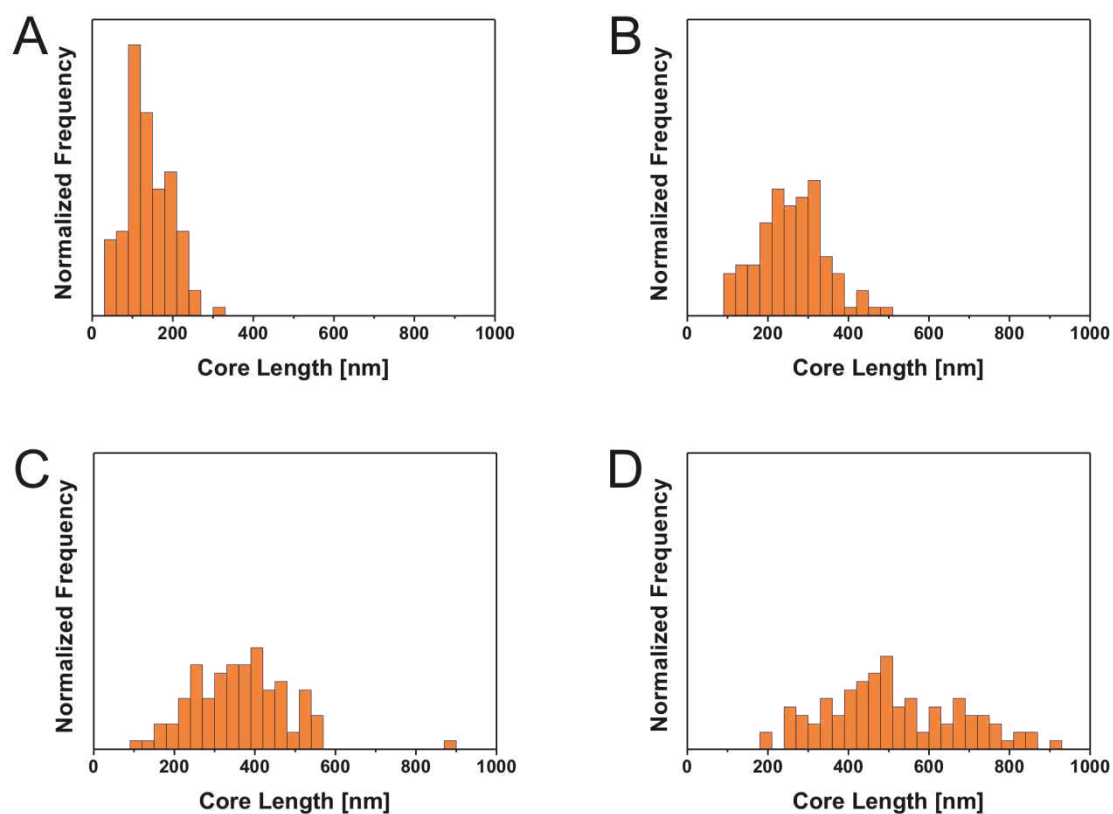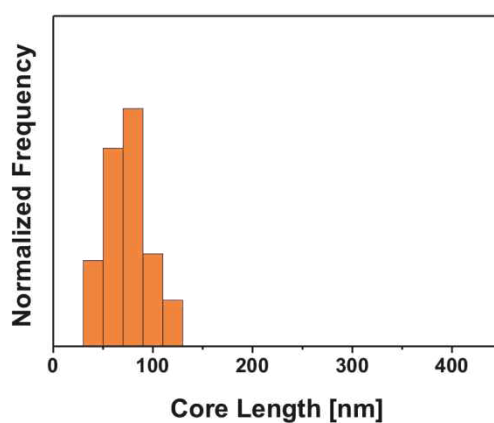
Figure 6.10. Length histograms of SES wCCMs produced *via* repetitive unimer addition. Total U/S ratios are 12 (A), 24 (B), 36 (C) and 48 (D).
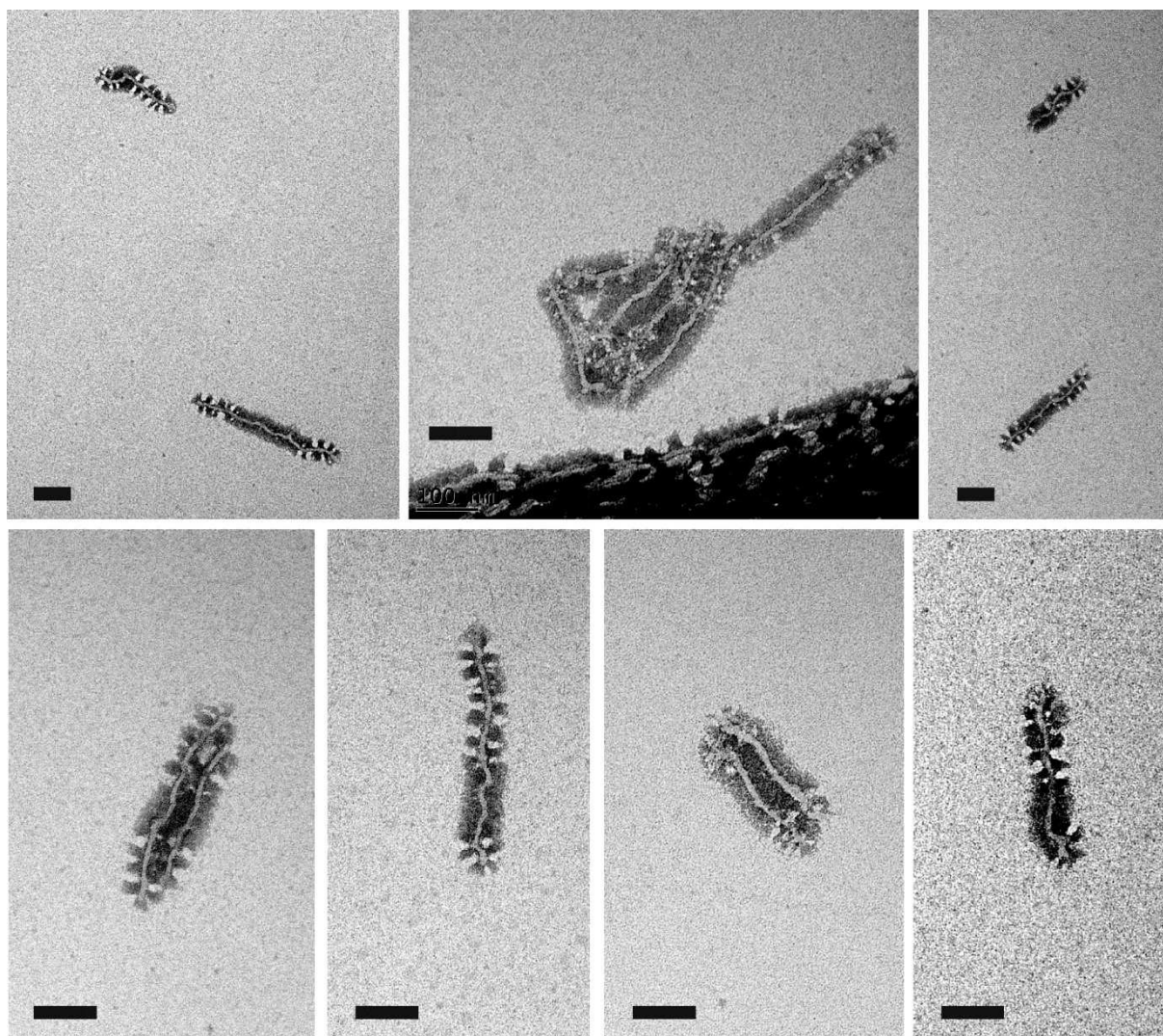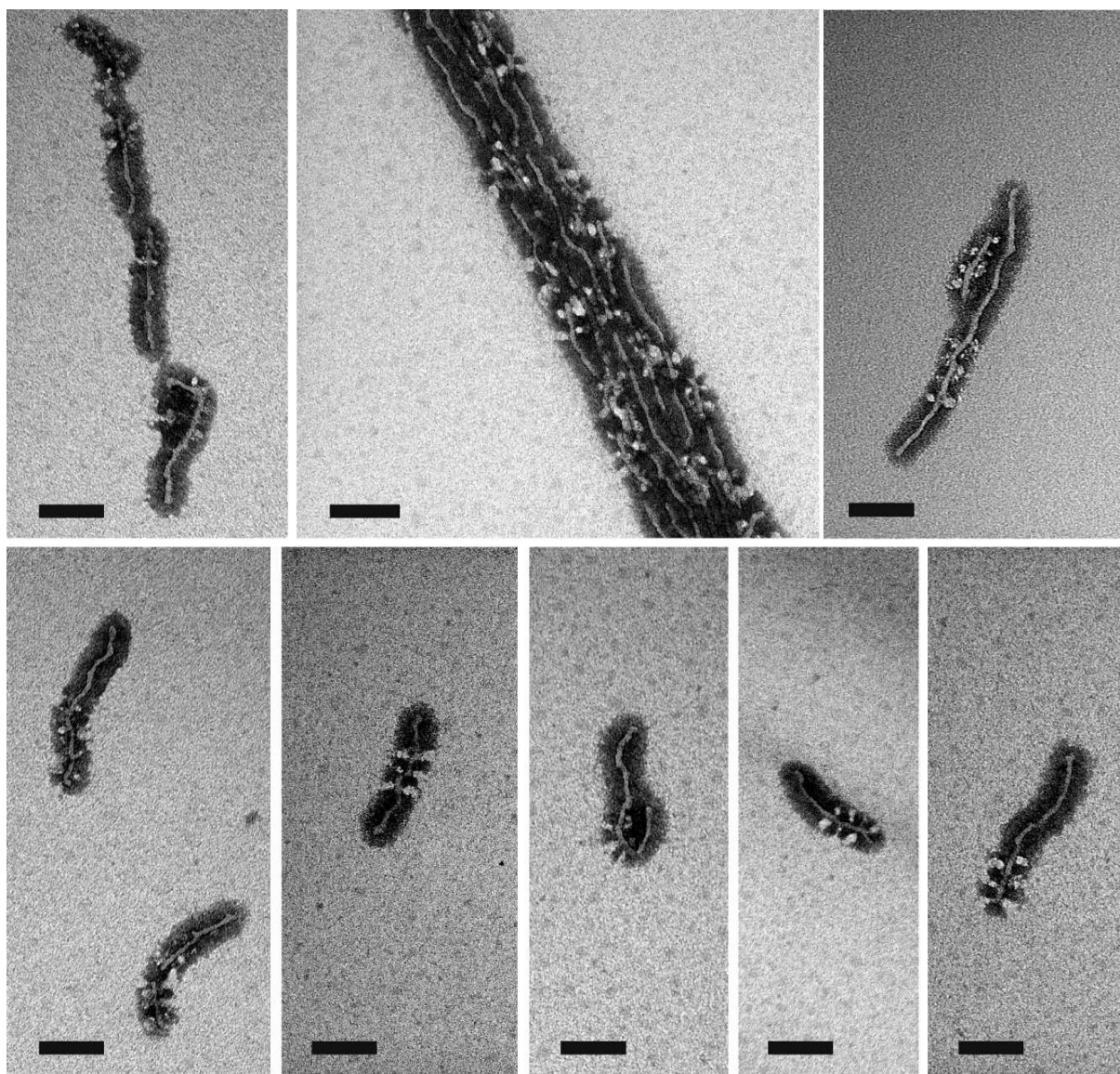
Figure 6.11. TEM micrographs of SEM-*b*-SES-*b*-SEM triblock *co*-micelles prepared *via* epitaxial growth of SEM unimers onto SES wCCM seeds in a 1g/L THF solution. Scale bars: 100 nm. The triblock *co*-micelles also show a certain tendency to aggregate upon drying during TEM sample preparation.
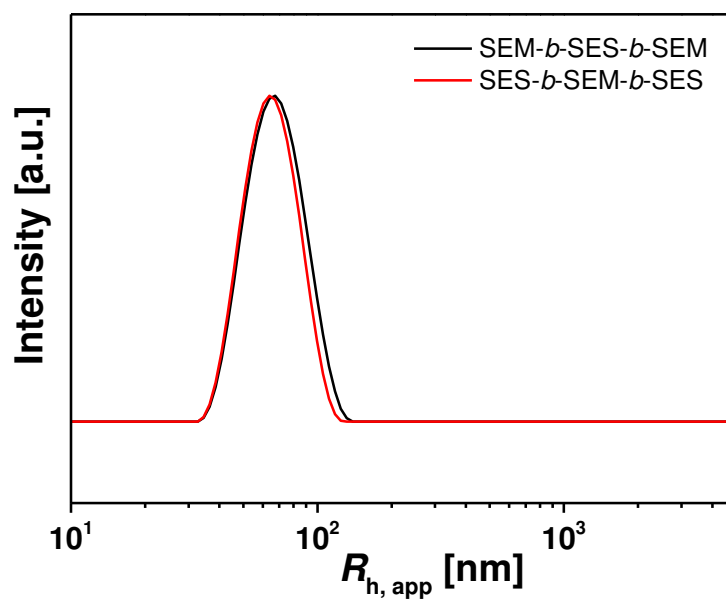
Figure 6.12. Apparent hydrodynamic radii distributions obtained from DLS data of SEM-*b*-SES-*b*-SEM triblock *co*-micelles as well as mixtures of SES-*b*-SEM-*b*-SES triblock and SES-*b*-SEM diblock *co*-micelles obtained *via* epitaxial growth from SES and SEM wCCM seeds, respectively (1 g/L, THF, θ = 90°). The DLS CONTIN plots clearly show the absence of aggregates in solution.

**Figure 6.13.** Length histogram of SEM wCCMs produced *via* seeded growth at U/S = 6.

Figure 6.14. TEM micrographs of SES-*b*-SEM-*b*-SES triblock and SES-*b*-SEM diblock *co*-micelles formed *via* epitaxial growth of SES unimers onto SEM wCCM seeds in a 1g/L THF solution. Scale bars: 100 nm. The observed aggregation of the block *co*-micelles only arises from TEM sample preparation as the corresponding DLS data reveal the absence of aggregates in solution (Figure 6.12).

7. Interfacial Activity of Patchy Worm-Like Micelles

Joachim Schmelz, Daniela Pirner, Marina Krekhova, Thomas M. Ruhland, Holger Schmalz*

Makromolekulare Chemie II, Universität Bayreuth, 95440 Bayreuth, Germany
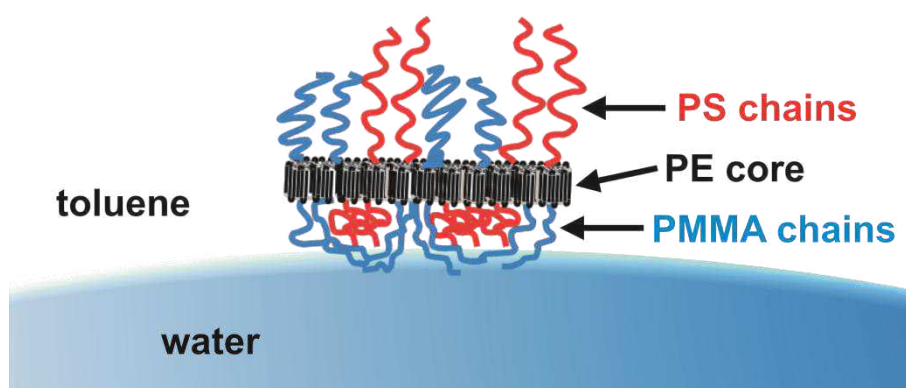
ABSTRACT:

The interfacial activity of self-assembled worm-like crystalline-core micelles (wCCMs) with a patchy polystyrene/poly(methyl methacrylat) (PS/PMMA) corona and a semi-crystalline polyethylene (PE) core is studied at the toluene/water interface. Their interfacial activity is shown to be superior to that of unimolecularly dissolved PS-*b*-PB-*b*-PMMA (PB = polybutadiene) triblock terpolymers with PS/PMMA outer blocks and wCCMs with a homogeneous PS corona. Strikingly, the interfacial activity is comparable to that of Janus cylinders well separated PS/PMMA hemishells and similar length. From these findings an adaptation of the corona chains of the patchy wCCMs to the toluene/water interface is proposed.

7.1.Introduction

Surface compartmentalization in nanoparticles leads to a variety of unique fields of application, e.g. the self-assembly into hierarchical superstructures or the selective incorporation of multiple nanoparticles or dyes in defined spatial confinement.[1,2] Another fascinating attribute of surface-compartmentalized nanostructures is their outstanding surface activity. The combination of the "Pickering" effect[3-5] valid for particles at interfaces with the amphiphilicity of classical surfactants makes them ideal candidates for a new generation of superior surfactants or to produce functional assemblies.[6]

Research on surface-compartmentalized nanostructures up to now mainly focused on Janus particles that, named after the two-faced Roman god Janus, exhibit exactly two opposing hemishells of different chemistry and/or polarity.[7,8] Dense, solid Janus colloids with sizes ranging in the micrometer region and slightly below have been synthesized using various techniques during the last decade, mainly resulting in spherical geometries.[9-12] Stepping down further in size, block terpolymer based spherical, cylindrical, ribbon-like and disc-like Janus micelles with cross-linked cores were prepared via a template-assisted approach.[13-16] Triggered by theoretical works predicting an up to 3-fold increase in the surface activity of spherical Janus structures with respect to homogeneous particles,[17] experimental efforts to explore the potential of Janus particles as surfactants were undertaken. Böker, and Krausch et al. observed a reduction of the oil-water interfacial tension for iron-oxide/gold Janus particles that was significantly higher than that observed for the respective uniform particles.[18] Furthermore, Janus particles of varying geometry (spherical, cylindrical, disc-like) prepared by the template-assisted approach were shown to exhibit superior surface activity compared to the unimolecularly dissolved triblock terpolymer precursors used for their synthesis.[16,19,20] For Janus cylinders a more pronounced reduction of the interfacial tension was observed with increasing cylinder length.[20] Additional studies have suggested that parameters such as size, aspect ratio, form and shape of Janus particles play a significant role for their surface activity, particle orientation and packing geometry.[19,21-23] With a view on industrial application, amphiphilic spherical Janus micelles were successfully used as stabilizers in emulsion polymerization revealing advantageous properties, including the

stabilization of surface areas significantly higher compared to the cross-section of the micelles.[24,25]

Patchy particles – bearing multiple different corona compartments – have only been explored to a much lower extent,[1,26,27] and, in addition, mostly spherical particles were investigated.[28-30] Liu et al. prepared patchy cylinders, vesicles and tubes from a triblock terpolymer via dialysis into different non-solvents for the middle block.[31] Even the formation of double and triple helices via wrapping and fusing of small patchy cylindrical micelles was observed using a similar block terpolymer.[32] Lately, crystallization-driven self-assembly – known to promote the formation of one-dimensional micelles[33-35] – was used to prepare worm-like micelles with a patch-like microphase separation in the corona.[36-38] It is noted that crystallization-induced self-assembly also allows for the production of crystalline-core micelles with a block-type compartmentalized corona.[39-41] Although patchy particles do not share the characteristic geometry of Janus particles, the different hemishells on opposing sides, they should also benefit from their non-homogeneous corona in terms of surface activity. Despite the envisaged application of patchy particles for the stabilization of emulsions,[42] to the best of our knowledge, the surface activity of particles with multiple corona compartments was not yet investigated.

Hence, we hereby present a study on the interfacial activity of worm-like crystalline-core micelles (wCCMs) with a patchy corona consisting of multiple polystyrene and poly(methyl methacrylate) compartments and a semi-crystalline polyethylene (PE) core. These structures significantly decrease the interfacial tension at the toluene-water interface as shown by pendant-drop tensiometry and the effect is similar to that observed for Janus cylinders of similar size. Furthermore, the influence of the corona size and composition of the patchy wCCMs on the interfacial tension is investigated.

7.2. Experimental Section

Synthesis of Triblock Copolymers. The used PE containing triblock co- and terpolymers were synthesized by catalytic hydrogenation of the corresponding PB containing block copolymers produced *via* sequential anionic polymerization in non-polar solvents, as can be found elsewhere.[37,43] The preparation of the Janus cylinders used for comparison can be found in an earlier study.[20]

Preparation of Worm-like Crystalline-Core Micelles (wCCMs). Solutions of wCCMs in toluene or THF were prepared using the following procedure. The triblock copolymers were dissolved at a concentration of 1 g L^{-1} and then heated in a water bath to at least 65 °C, *i.e.* above the melting temperature of PE, resulting in unimeric solutions. Subsequently, these solutions were quenched to the desired crystallization temperature (T_c, Table 7.1) to form the wCCMs and kept at this temperature for 24 h followed by an additional annealing step at the temperature T_a (Table 7.1) for 3 h to obtain a more regular patchy structure of the corona, as published earlier.[37,38] In 1,4-dioxane, wCCM solutions were obtained by dialysis, as direct self-assembly in 1,4-dioxane results in the formation of spherical CCMs. Therefore, the samples were first prepared in THF as described above and then dialyzed against 1,4-dioxane for several days by replacing the solvent twice. Subsequently, the wCCM solutions in 1,4-dioxane were diluted to 1 g L^{-1}. For all preparation steps gentle stirring or shaking was applied.

Pendant-Drop Tensiometry. Samples in toluene or 1,4-dioxane in a concentration range of 0.25 to 2 g L^{-1} were measured using a Dataphysics OCA 20 tensiometer at room temperature. The drop profile was recorded using a CCD camera and the fitting was performed with the Dataphysics software package. The low-concentrated solutions were prepared from 1 g L^{-1} solutions by dilution. The 2 g L^{-1} solution was prepared directly as described above. For all measurements clean and dust-free glass cuvettes were used. The droplet phase (water in case of toluene or PFO in case of 1,4-dioxane) was generated with a manual dosage system using 1 mL syringes with straight blunt tip (diameter 0.8 mm). All measurements were performed at least twice to check the reproducibility. The quasi-equilibrium interfacial

tension was determined by averaging the values of the interfacial tension measured during the last 30 min of the experiment.

7.3. Results and Discussion

Table 7.1. Molecular and thermal characteristics of the used triblock copolymers and average length of self-assembled wCCMs.

Sample	Polymer[a]	DP_{corona} / x_{PS}[b]	T_c[c] [°C]	T_a[c] [°C]	l[d] [nm]	γ[e] [mN m^{-1}]
SEM1	$S_{340}E_{700}M_{360}$	700 / 0.49	20	45	520 (140)	17.6 (0.3)
SEM2	$S_{140}E_{690}M_{160}$	300 / 0.47	30	40	560 (130)	19.4 (0.1)
SEM3	$S_{280}E_{1190}M_{300}$	580 / 0.48	34	48	540 (160)	18.0 (0.1)
SEM4	$S_{330}E_{1360}M_{760}$	1090 / 0.3	20	40	780 (240)	18.1 (0.1)
SEM5	$S_{490}E_{1470}M_{610}$	1100 / 0.45	20	40	850 (250)	17.7 (0.2)
SEM6	$S_{660}E_{1350}M_{350}$	1010 / 0.65	18	40	710 (200)	18.9 (0.1)
SES	$S_{380}E_{880}S_{390}$	770 / 1	20	45	690 (230)	19.4 (0.1)
Janus[20]	$S_{430}B_{290}M_{500}$	930 / 0.46	-	-	800	18.0 (0.1)
SBM[f]	$S_{340}B_{350}M_{360}$	700 / 0.49	-	-	-	19.4 (0.4)

[a] subscripts give the number-average degree of polymerization of the respective block; [b] overall degree of polymerization of the corona blocks PS and PMMA (DP_{corona}) and molar fraction of PS units in the wCCM corona (x_{PS}); [c] applied temperatures of isothermal crystallization (T_c) and annealing (T_a), respectively; [d] average wCCM length derived from TEM image analysis (standard deviation in parenthesis); [e] quasi-equilibrium interfacial tension determined by averaging the values of the interfacial tension measured during the last 30 min of the experiment (standard deviation in parenthesis); [f] precursor of SEM1 prior to hydrogenation, unimolecularly dissolved in toluene.

In this publication we investigate the interfacial activity of patchy worm-like crystalline-core micelles (wCCMs) self-assembled from polystyrene-*block*-polyethylene-*block*-poly(methyl methacrylate) (PS-*b*-PE-*b*-PMMA) triblock terpolymers. After dissolution of the triblock terpolymers in toluene (1 g L^{-1}) above the melting temperature of the PE middle blocks, the solution was kept at the desired temperature of isothermal crystallization (T_c) for one day to trigger crystallization-induced self-assembly into worm-like micelles with a semicrystalline PE core and a patch-like compartmentalized corona of PS and PMMA. An additional annealing step was performed to achieve a perfection of the core structure as well as a more

pronounced microphase separation in the corona.[37,38] The used triblock co- and terpolymers as well as the applied crystallization and annealing temperatures are summarized in Table 7.1. A detailed morphological characterization of the investigated wCCMs can be found in our previous publications.[37,38] Selected TEM micrographs of SEM and SES wCCMs can be found in Figure 7.3.

For this study, the toluene/water interface was chosen for mainly two reasons. Firstly, the wCCMs can directly be self-assembled in toluene and, secondly, toluene and water are immiscible and exhibit a high interfacial tension, criteria that are essential to achieve reproducible results. In these measurements toluene was used as the solution phase and water, due to its higher density, as the droplet phase. The interfacial tension at the pristine toluene/water interface was determined to γ = 33.1 mN m^{-1} (Figure 7.4).

**A**   **B**   **C**
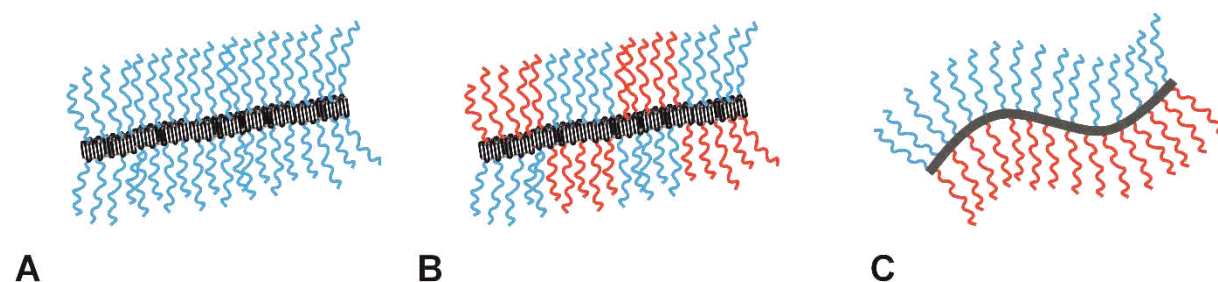
Scheme 7.1. Overview of the investigated micelles: wCCMs with A) homogeneous and B) patchy corona, and C) Janus cylinders (PS = blue, PMMA = red, core = semi-crystalline PE (A, B) or crosslinked PB (C)).

To clarify if the combination of the Pickering effect of the worm-like micelles with the slightly amphiphilic properties due to the patchy PS/PMMA corona results in a synergistic effect, wCCMs formed by a symmetric PS-*b*-PE-*b*-PMMA triblock terpolymer (SEM1, equal length of end blocks) are compared to PS-*b*-PB-*b*-PMMA (SBM, PB = polybutadiene) unimers and wCCMs with a homogeneous PS corona formed by a PS-*b*-PE-*b*-PS (SES) triblock copolymer. A schematic depiction of the investigated one-dimensional micellar structures can be found in Scheme 7.1. The used SBM is the non-hydrogenated PB-containing precursor triblock terpolymer of SEM1 and, thus, the lengths of the PS and PMMA blocks are identical. However, as the PB block is amorphous and well soluble in toluene at ambient temperature, in contrast to the PE block in SEM1, the SBM triblock terpolymer is molecularly dissolved. The worm-like SES micelles with a homogeneous PS corona exhibit a comparable length with respect to that of the SEM1 wCCMs and bear corona blocks with a similar degree of

polymerization (Table 7.1). Thus, the interfacial activities of SBM unimers and SES wCCMs represent suitable benchmarks for SEM1 wCCMs. The corresponding pendant drop tensiometer measurements are displayed in Figure 7.1A. The interfacial tension at the water/toluene interface shows a rapid decrease at early stages of adsorption for all samples. Subsequently, the decrease slows down and finally the interfacial tension approaches a plateau (quasi-equilibrium interfacial tension). In the presence of SEM1 wCCMs the quasi-equilibrium interfacial tension (γ(SEM1) = 17.6 mN m^{-1}) is significantly lower than for SBM unimers (γ(SBM) = 19.4 mN m^{-1}) and SES wCCMs (γ(SES) = 19.4 mN m^{-1}), highlighting the beneficial combination of surface compartmentalization (amphiphilicity) with the Pickering effect of the wCCMs. While for SBM unimers the interfacial tension reaches a constant value at relatively short times, for solutions containing SES and SEM1 wCCMs establishing a quasi-equilibrium state takes about 2 h. On one hand, the diffusion of unimers to the droplet surface might be faster than for the considerably larger micellar structures and, on the other hand, the arrangement of the wCCMs at the interface will take much longer. Moreover, the interfacial tension for SES wCCMs decreases rather slowly, whereas SEM1 reaches values below 20 mN m^{-1} much faster, pointing to a higher affinity of the patchy wCCMs toward the interface attributable to the weak amphiphilic character of the patchy corona. In addition, we studied the concentration dependence of the interfacial tension and found a significant decrease of the quasi-equilibrium interfacial tension upon increasing concentration of SEM1 based wCCMs in the toluene phase (Figure 7.1B). A comparable behavior was observed for SBM Janus cylinders, too, and is attributed to an increasing surface pressure of adsorbing wCCMs with increasing concentration.[20]

The interfacial activity of SEM1 wCCMs at the toluene/water interface was directly compared to that of SBM Janus cylinders used in an earlier work.[20] Strikingly, the quasi-equilibrium interfacial tension in the presence of the Janus cylinders (γ(Janus) = 18.0 mN m^{-1}) is within the accuracy of the technique in the same range as for SEM1(Figure 7.1A). Here, it has to be noted that the length of the PS and PMMA corona blocks and the total length of the Janus micelles (800 nm) are higher than those of the wCCMs formed by SEM1, while the molar fraction of PS units in the corona is comparable for both (Table 7.1). Consequently, a higher reduction of the interfacial tension in case of the Janus cylinders might be expected as an increase in the average length of Janus cylinders was shown to enhance the adsorption

at the interface and, thus, results in lower plateau values.[20] In order to examine whether this unexpected finding occurs only for the system toluene/water, we studied the interfacial activity of SEM1 wCCMs with dioxane as the solution phase and perfluorooctane (PFO) as the droplet phase, too. Here, earlier investigations resulted in an quasi-equilibrium interfacial tension of γ(Janus) = 7.7 mN m^{-1} in the presence of Janus cylinders with a length of 800 nm[20] and again the plateau value of the patchy wCCMs was found to be comparable (γ(SEM1) = 7.3 mN m^{-1}, Figure 7.5).
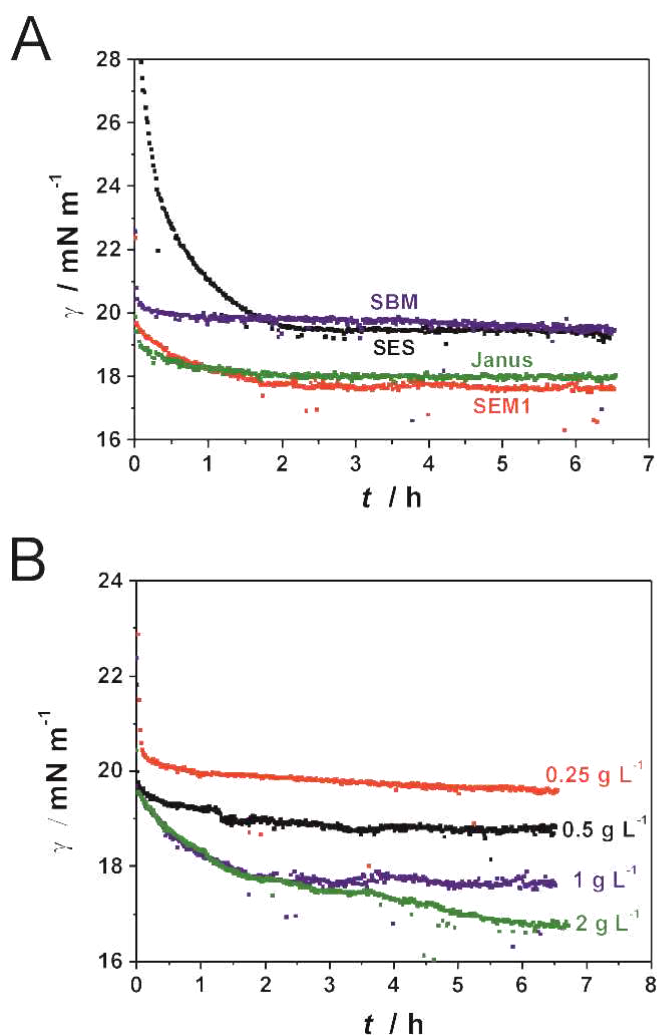
Figure 7.1. A) Interfacial tension isotherms of 1 g L^{-1} solutions containing SBM unimers, SES wCCMs with a homogeneous corona, SEM1 wCCMs with a patchy corona and SBM Janus cylinders. B) Interfacial tension isotherms of differently concentrated solutions of wCCMs formed by SEM1.

In the first place, one would assume that Janus cylinders exhibit a higher interfacial activity compared to cylindrical structures with a patchy corona. The segregation of the PS/PMMA corona into two hemishells should be ideally suited to arrange at the liquid-liquid interface.

However, wCCMs with multiple compartments of PS and PMMA obviously achieve similar results. This leads to the assumption that the corona chains are able to adapt to the interface. Based on a comparison of Hildebrandt solubility parameters of the corona blocks with that of water and toluene (Table 7.2) the following model for a toluene/water interface is proposed (Scheme 7.2). In the toluene phase PS and PMMA are soluble, whereas PS exhibits a slightly better solubility compared to PMMA.[44] Although water is a non-solvent for both corona blocks, the more polar PMMA chains are most likely oriented toward the water phase and probably act as a shielding layer for the even less polar PS blocks and the PE core. Conversely, the PS chains at the same side of the wCCMs facing the water droplet surface collapse close to the PE core or even fold around the core in order to reach into the toluene phase where possible.
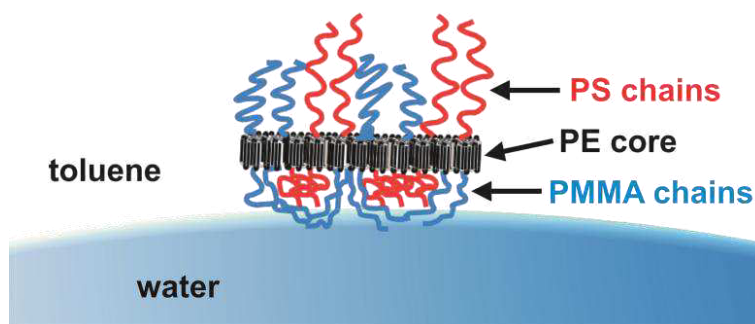

Scheme 7.2. Proposed orientation of patchy wCCMs at the toluene/water interface and adaptation of the corona chains.

Prior studies on Janus cylinders already revealed a strong influence of the cylinder length on the interfacial properties.[20] However, the impact of the corona composition and the corona thickness has not yet been addressed. In order to investigate the influences of the corona structure in more detail, the toluene/water interfacial tension in the presence of two series of SEM based wCCMs was studied. Notably, the average lengths of the formed wCCMs in each series did not vary significantly (Table 7.1) and, thus, is not expected to exert a significant influence on the interfacial activity. In the first series, SEM1-3, the molar fraction of PS units (x_{PS}) in the corona of the wCCMs was kept constant, while the overall degree of polymerization (DP_{corona}) of both corona blocks was varied. The interfacial tension isotherms displayed in Figure 7.2A clearly show an increase in interfacial activity, i.e., decrease in interfacial tension, upon increasing length of the corona blocks. The quasi-equilibrium interfacial tension decreases continuously from γ(SEM2) = 19.4 mN m^{-1} for DP_{corona} = 300

down to γ(SEM1) = 17.6 mN m^{-1} for DP_{corona} = 700. This shows that a more extended corona of the worm-like micelles enhances their ability to stabilize interfaces, which is in agreement with theoretical predictions.[6] In the second series, SEM4-6, wCCMs with comparable overall degree of polymerization of the corona blocks but different molar fraction of PS units in the corona were examined (Figure 7.2B). Here, the interfacial tension isotherms exhibit only a weak dependence on the corona composition, with quasi-equilibrium interfacial tensions for wCCMs with an asymmetric corona composition (γ(SEM4) = 18.1 mN m^{-1}, γ(SEM6) = 18.9 mN m^{-1}) being slightly higher compared to wCCMs with a symmetric corona composition (γ(SEM5) = 17.7 mN m^{-1}). This points to a minor influence of the corona composition on the interfacial properties of patchy wCCMs.
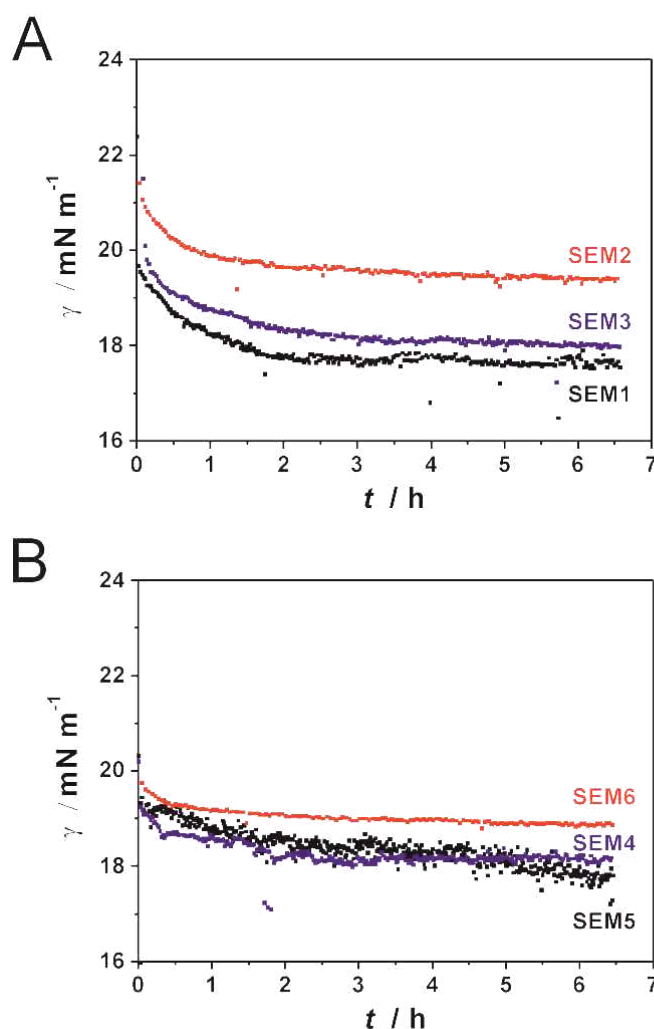
Figure 7.2. Interfacial tension isotherms of 1 g L^{-1} solutions containing wCCMs formed by SEM1-3 (A) and SEM4-6 (B).

7.4.Conclusion

A first study of the interfacial activity of self-assembled worm-like crystalline-core micelles (wCCMs) with polyethylene (PE) cores and a patchy corona of polystyrene (PS) and poly(methyl methacrylate) (PMMA) at the toluene/water interface is presented. The ability of these patch-like surface-compartmentalized nanostructures to reduce the quasi-equilibrium interfacial tension is significantly higher compared to that of single chains of the precursor triblock terpolymer or wCCMs with a homogeneous PS corona. This highlights the beneficial synergy of the particular nature of the investigated wCCMs (Pickering effect) and the amphiphilicity of the patchy PS/PMMA corona. Strikingly, the interfacial activity of the investigated patchy wCCMs is comparable to that of SBM Janus cylinders with similar dimensions and corona composition, even though the Janus structure with two corona hemishells of PS and PMMA might be regarded as more suitable for the stabilization of interfaces than micelles with multiple corona patches on both sides. Screening of a series of wCCMs formed by different PS-*b*-PE-*b*-PMMA triblock terpolymers with varying compositions and molecular weights revealed that the overall degree of polymerization of the corona chains, i.e., the thickness of the corona, is a crucial parameter that influences the interfacial activity of these nanostructures at the toluene/water interphase. Besides, the composition of the corona in terms of molar fraction of PS units seems to play a minor role. From the presented results a rearrangement of the wCCM corona chains at the liquid/liquid interface is proposed rendering patchy wCCMs a new class of adaptive surfactants. Due to the comparably simple preparation of these structures directly in solution by crystallization-induced self-assembly, applications in the stabilization of emulsions and/or polymer blends can be imagined. Future investigations will concentrate on the production of wCCMs with a strong amphiphilic corona by incorporating water-soluble polymer blocks.

7.5. References

1   J. Du and R. K. O'Reilly, *Chem. Soc. Rev.*, 2011, **40**, 2402-2416.

2   K. Zhang, M. Jiang and D. Chen, *Prog. Polym. Sci.*, 2012, **37**, 445-486.

3   S. U. Pickering, *J. Chem. Soc.*, 1907, **91**, 2001-2021.

4   W. Ramsden, *Proc. R. Soc. London*, 1903, **72**, 156-164.

5   P. Pieranski, *Phys. Rev. Lett.*, 1980, **45**, 569-572.

6   A. Böker, J. He, T. Emrick and T. P. Russell, *Soft Matter*, 2007, **3**, 1231-1248.

7   J. Hu, S. Zhou, Y. Sun, X. Fang and L. Wu, *Chem. Soc. Rev.*, 2012, **41**, 4356-4378.

8   A. Walther and A. H. E. Müller, *Chem. Rev.*, 2013, DOI: 10.1021/cr300089t.

9   V. N. Paunov and O. J. Cayre, *Adv. Mater.*, 2004, **16**, 788-791.

10   L. Hong, S. Jiang and S. Granick, *Langmuir*, 2006, **22**, 9495-9499.

11   K.-H. Roh, D. C. Martin and J. Lahann, *Nat. Mater.*, 2005, **4**, 759-763.

12   Z. Nie, W. Li, M. Seo, S. Xu and E. Kumacheva, *J. Am. Chem. Soc.*, 2006, **128**, 9408-9412.

13   R. Erhardt, A. Böker, H. Zettl, H. Kaya, W. Pyckhout-Hintzen, G. Krausch, V. Abetz and A. H. E. Müller, *Macromolecules*, 2001, **34**, 1069-1075.

14   Y. Liu, V. Abetz and A. H. E. Müller, *Macromolecules*, 2003, **36**, 7894-7898.

15   A. Wolf, A. Walther and A. H. E. Müller, *Macromolecules*, 2011, **44**, 9221-9229.

16   A. Walther, X. André, M. Drechsler, V. Abetz and A. H. E. Müller, *J. Am. Chem. Soc.*, 2007, **129**, 6187-6198.

17   B. P. Binks and P. D. I. Fletcher, *Langmuir*, 2001, **17**, 4708-4710.

18   N. Glaser, D. J. Adams, A. Böker and G. Krausch, *Langmuir*, 2006, **22**, 5227-5229.

19   T. M. Ruhland, A. H. Gröschel, N. Ballard, T. S. Skelhon, A. Walther, A. H. E. Müller and S. A. F. Bon, *Langmuir*, 2013, **29**, 1388-1394.

20   T. M. Ruhland, A. H. Gröschel, A. Walther and A. H. E. Müller, *Langmuir*, 2011, **27**, 9807-9814.

21   B. J. Park, T. Brugarolas and D. Lee, *Soft Matter*, 2011, **7**, 6413-6417.

22   B. J. Park and D. Lee, *ACS Nano*, 2011, **6**, 782-790.

23   B. J. Park and D. Lee, *Soft Matter*, 2012, **8**, 7690-7698.

24   A. Walther, M. Hoffmann and A. H. E. Müller, *Angew. Chem., Int. Ed.*, 2008, **47**, 711-714.

25   R. Ayeward, *Soft Matter*, 2012, **8**, 5233-5240.

26   A. B. Pawar and I. Kretzschmar, *Macromol. Rapid Commun.*, 2010, **31**, 150-168.

27   J. Yoon, K. J. Lee and J. Lahann, *J. Mater. Chem.*, 2011, **21**, 8502-8510.

28   D. A. Christian, A. Tian, W. G. Ellenbroek, I. Levental, K. Rajagopal, P. A. Janmey, A. J. Liu, T. Baumgart and D. E. Discher, *Nat. Mater.*, 2009, **8**, 843-849.

29   S. C. Glotzer and M. J. Solomon, *Nat. Mater.*, 2007, **6**, 557-562.

30   M. D. McConnell, M. J. Kraeutler, S. Yang and R. J. Composto, *Nano Lett.*, 2010, **10**, 603-609.

31   G. Njikang, D. H. Han, J. Wang and G. J. Liu, *Macromolecules*, 2008, **41**, 9727-9735.

32   J. Dupont, G. J. Liu, K. Niihara, R. Kimoto and H. Jinnai, *Angew. Chem., Int. Ed.*, 2009, **48**, 6144-6147.

33   M. Lazzari and M. A. Lopez-Quintela, *Macromol. Rapid Commun.*, 2009, **30**, 1785-1791.

34   J. B. Gilroy, T. Gädt, G. R. Whittell, L. Chabanne, J. M. Mitchels, R. M. Richardson, M. A. Winnik and I. Manners, *Nat. Chem.*, 2010, **2**, 566-570.

35   J. Schmelz, F. H. Schacher and H. Schmalz, *Soft Matter*, 2013, **9**, 2101-2107.

36   H. Schmalz, J. Schmelz, M. Drechsler, J. Yuan, A. Walther, K. Schweimer and A. M. Mihut, *Macromolecules*, 2008, **41**, 3235-3242.

37   J. Schmelz, M. Karg, T. Hellweg and H. Schmalz, *ACS Nano*, 2011, **5**, 9523-9534.

38   J. Schmelz and H. Schmalz, *Polymer*, 2012, **53**, 4333–4337.

39   T. Gädt, N. S. Ieong, G. Cambridge, M. A. Winnik and I. Manners, *Nat. Mater.*, 2009, **8**, 144-150.

40   F. He, T. Gädt, I. Manners and M. A. Winnik, *J. Am. Chem. Soc.*, 2011, **133**, 9095-9103.

41   P. A. Rupar, L. Chabanne, M. A. Winnik and I. Manners, *Science*, 2012, **337**, 559-562.

42   S. Granick and L. Hong, *US Pat.,* 0305219 A1, 2010.

43   H. Ruckdäschel, J. K. W. Sandler, V. Altstädt, C. Rettig, H. Schmalz, V. Abetz and A. H. E. Müller, *Polymer*, 2006, **47**, 2772-2790.

44   M. S. Kent, M. Tirrell and T. P. Lodge, *J. Polym. Sci., Part B: Polym. Phys.*, 1994, **32**, 1927-1941.

7.6. Supporting Information
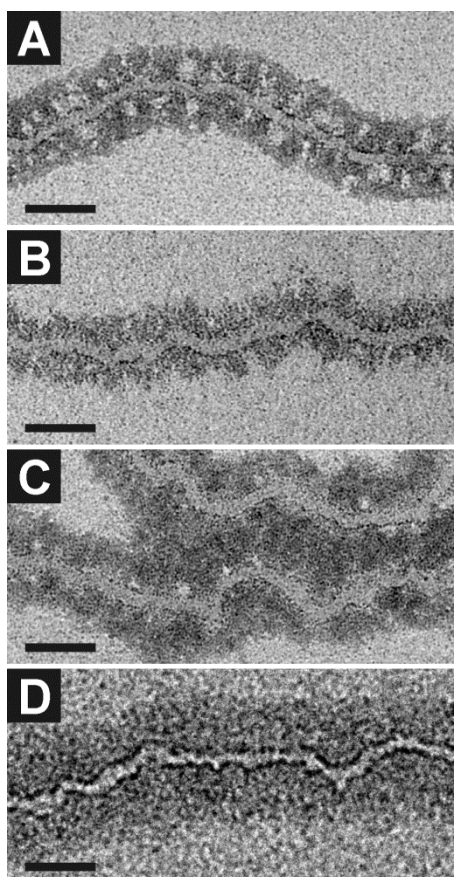
Figure 7.3. Selected TEM micrographs (scale bars = 50 nm) showing the corona structure of A) SEM1, B) SEM4, C) SEM6 and D) SES wCCMs formed in toluene (1g L^{-1}). For all samples PS was selectively stained by RuO$_4$ vapour, resulting in dark PS domains. PMMA domains and the PE core appear bright. A more detailed characterization of the morphology can be found in our previous work.[1,2]
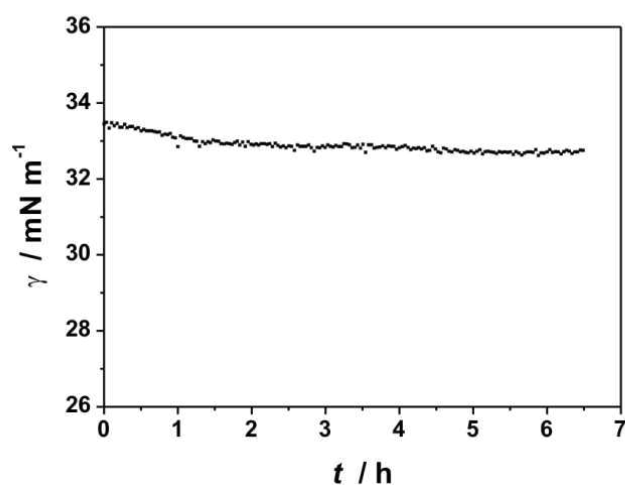
Figure 7.4. Interfacial tension isotherm of the pristine toluene/water interface.
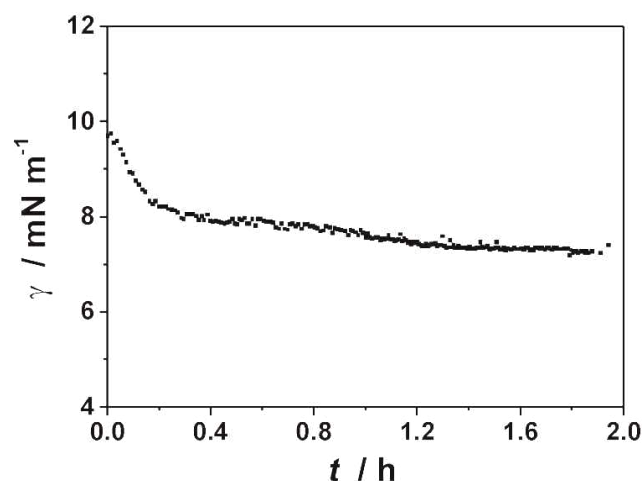
Figure 7.5. Interfacial tension isotherm of a 1 g L^{-1} solution of wCCMs formed by SEM1 at the dioxane/PFO interface (γ_0(dioxane/PFO) = 10.75 mN m^{-1}).

Table 7.2. Hildebrandt solubility parameters δ^3 of the wCCM corona blocks and the solvents used for the interfacial tension measurements.

Polymer/ Solvent	δ [MPa$^{1/2}$]
PS	18.5
PMMA	19.0
toluene	18.2
water	48.0

References

1   J. Schmelz, M. Karg, T. Hellweg and H. Schmalz, *ACS Nano*, 2011, **5**, 9523-9534.

2   J. Schmelz and H. Schmalz, *Polymer*, 2012, **53**, 4333-4337.

3   A.F.M. Barton, *CRC Handbook of Polymer-Liquid Interaction Parameters and Solubility Parameters*, CRC Press: Boston, 1990.

8. Scientific Contributions

8.1. List of Publications

1. **Schmelz, J.**; Schacher, F.H.; Schmalz, H.
   "Cylindrical Crystalline-Core Micelles: Pushing the Limits of Solution Self-Assembly",
   Soft Matter **2013**, *9*, 2101.

2. **Schmelz, J.**; Schedl, A.E.; Steinlein, C.; Manners, I.; Schmalz, H.
   "Length Control and Block-Type Architectures in Worm-like Micelles with
   Polyethylene Cores", *Journal of the American Chemical Society* **2012**, *134*, 14217.

3. Gröschel, A.H.; Walther, A.; Löbling, T.; **Schmelz, J.**; Hanisch, A.; Schmalz, H.; Müller,
   A.H.E.
   "Facile, Solution-Based Synthesis of Soft, Nanoscale Janus Particles with Tunable
   Janus Balance", *Journal of the American Chemical Society* **2012**, *134*, 13850.

4. **Schmelz, J.**; Schmalz, H.
   "Corona Structure on Demand: Tailor-Made Surface Compartmentalization in Worm-
   Like Micelles via Random Cocrystallization", *Small* **2012**, *53*, 4333.

5. Rosenfeldt, S.; Lüdel, F.; Schulreich, C.; Hellweg, T.; Radulescu, A.; **Schmelz, J.**;
   Schmalz, H.; Harnau, L.
   "Patchy Worm-Like Micelles: Solution Structure Studied by Small-Angle Neutron
   Scattering", *Physical Chemistry Chemical Physics* **2012**, *14*, 12750.

6. **Schmelz, J.**; Karg, M.; Hellweg, T.; Schmalz, H.
   "General Pathway toward Crystalline-Core Micelles with Tunable Morphology and
   Corona Segregation", *ACS Nano* **2011**, *5*, 9523.

7. Reinicke, S.; **Schmelz, J.**; Lapp, A.; Karg, M.; Hellweg, T.; Schmalz, H.
   "Smart Hydrogels Based on Double Responsive Triblock Terpolymers", *Soft Matter*
   2009, *5*, 2648.

8. **Schmelz, J.**; Drechsler, M.; Yuan, J.; Walther, A.; Schmalz, H. "Surface-Compartmentalized Nanostructures via Crystallization Induced Self-Assembly of Triblock Terpolymers", *Polymeric Materials: Science and Engineering* **2008**, *99*, 680.

9. Reinicke, S.; **Schmelz, J.**; Schmalz, H. "pH- and Temperature-Sensitive Hydrogels Based on Triblock Terpolymers", *Polymer Preprints (American Chemical Society, Division Polymer Chemistry)* **2008**, *49*(2), 459.

10. Schmalz, H.; **Schmelz, J.**; Drechsler, M.; Yuan, J.; Walther, A.; Schweimer, K.; Mihut, A. "Thermo-Reversible Formation of Wormlike Micelles with a Microphase-Separated Corona from a Semicrystalline Triblock Terpolymer", *Macromolecules* **2008**, *41*, 3235.

8.2. Contributions to National and International Conferences

1. **Makromolekulares Kolloquium**, Freiburg, Germany, February 2008
   Poster Presentation: *Thermo-Reversible Formation of Cylindrical Micelles with a Compartmentalized Corona from a Semicrystalline ABC Triblock Terpolymer*
   Poster Prize

2. **236th ACS National Meeting**, Philadelphia, USA, August 2008
   Poster Presentation: *Surface-Compartmentalized Nanostructures via Crystallization Induced Self-Assembly of Triblock Terpolymers*

3. **23rd Conference of the ECIS**, Belek (Antalya), Turkey, September 2009
   Oral Presentation: *Surface-Compartmentalized Nanostructures via Crystallization-Induced Self-Assembly of Triblock Terpolymers*

4. **Bayreuth Polymer Symposium**, Bayreuth, Germany, September 2009
   Poster Presentation: *Surface-Compartmentalized Nanostructures via Crystallization-Induced Self-Assembly of Triblock Terpolymers*
   Poster Prize

5. **24th Conference of the ECIS**, Prag, Czech Republic, September 2010
   Poster Presentation: *Core-Crystalline Wormlike Micelles (CCWMs): A Toolbox for Complex Surface-Compartmentalized Nanostructures*

6. **Stadler Minerva Student Workshop**, Beer Sheva and Ein Gedi, Israel, March 2011
   Oral Presentation: *Crystalline-Core Micelles (CCMs): A Toolbox for Complex Surface-Compartmentalized Nanostructures*

Glossary

1D	one-dimensional
2D	two-dimensional
b	*block*
b	scattering length density
c	concentration
CCD	charge-coupled device
CCM	crystalline-core micelle
$CDCl_3$	chloroform-d_1
cryo-TEM	cryogenic transmission electron microscopy
D	diameter
D_M, D_S	lengths of PMMA and PS compartments, measured parallel to the core (SANS model)
DCM	dichloromethane
DLS	dynamic light scattering
DMAC	*N,N*-dimethylacetamide
DP	degree of polymerization
*d*SBM, *d*SEM	SBM or SEM with deuterated polystyrene blocks
DSC	differential scanning calorimetry
dQ/dt	heat flow
I, I_S	scattering intensity
l	length

L_n	number average PE core length
L_w	weight average PE core length
M_n	number-average molecular weight
MALDI-ToF	matrix-assisted laser desorption/ionization time-of-flight (mass spectroscopy)
MCM	multicompartment (core) micelle
NMR	nuclear magnetic resonance
NOESY	nuclear Overhauser effect spectroscopy
o	ortho
P2VP	poly(2-vinyl pyridine)
P3HT	poly(3-hexylthiophene)
P4VP	poly(4-vinyl pyridine)
PAA	poly(acrylic acid)
PAN	polyacrylonitrile
PB	polybutadiene
PBMA	poly(*n*-butyl methacrylate)
PBO	poly(butylene oxide)
PCEMA	poly(2-cinnamoyloxyethyl methacrylate)
PCL	poly(ε-caprolactone)
PDI	polydispersity index
PDLA	poly(ᴅ-lactide)
PDMA	poly(*N,N*-dimethyl acrylamide)

Glossary

PDMAEMA	poly(*N,N*-dimethylaminoethyl methacrylate)
PDMS	polydimethylsiloxane
PE	polyethylene
PEO	poly(ethylene oxide)
PEP	poly(ethylene-*alt*-propylene)
PFDES	poly(ferrocenyl diethylsilane)
PFDMG	poly(ferrocenyl dimethyl-germane)
PFDMS	poly(ferrocenyl dimethyl-silane)
PFP	poly(ferrocenyl phenyl-phosphine)
PFMES	poly(ferrocenyl methylethyl-silane)
PFMPS	poly(ferrocenyl methylphenyl-silane)
PFO	perfluorooctane
PFS	polyferrocenylsilane
PGMA	poly(glyceryl monometh-acrylate)
PI	polyisoprene
PLLA	poly(L-lactide)
PMMA	poly(methyl methacrylate)
POEGMA	poly(oligoethylene glycol methacrylate)
PPO	poly(propylene oxide)
PS	polystyrene
P*t*BMA	poly(*tert*-butyl methacrylate)
P*t*BA	poly(*tert*-butyl acrylate)

P*t*BS	poly(*tert*-butoxystyrene)
q	scattering vector
R	radius
R_E, R_M, R_S	radii of PE core, PMMA and PS compartment, measured from the core center (SANS model)
$R_{h,app}$	apparent hydrodynamic radius
SANS	small-angle neutron scattering
SAXS	small-angle X-ray scattering
SBM	polystyrene-*block*-poly(1,4-butadiene)-*block*-poly(methyl methacrylate)
SBS	polystyrene-*block*-poly(1,4-butadiene)-*block*-polystyrene
sCCM	spherical crystalline-core micelle
SCF	self-consistent mean field
SCN	surface-compartmentalized nanostructure
SEC	size exclusion chromatography
sec-BuLi	*sec*-butyllithium
SEM	polystyrene-*block*-polyethyl-ene-*block*-poly(methyl meth-acrylate)
SES	polystyrene-*block*-polyethyl-ene-*block*-polystyrene
SFM	scanning force microscopy
SLS	static light scattering
t	time
T_a	annealing temperature
T_c, T_{cryst}	crystallization temperature

T_m	melting temperature	α_{PE}	degree of crystallization
t_{SF}	time of structure formation	γ	interfacial tension
TEM	transmission electron microscopy	δ	Hildebrandt solubility parameter
THF	tetrahydrofuran	Δz	height range
U/S	unimer-to-seed ratio	λ	wavelength
w	weight	μDSC	micro-differential scanning calorimetry
w	weight content		
wCCM	worm-like crystalline-core micelle	χ	Flory-Huggins interaction parameter
x	molar content		

Acknowledgment

Acknowledgment

At first, I'd like to thank my supervisor Dr. Holger Schmalz for bringing up the interesting topic that I was allowed to work on and for the time we spent on scientific discussion, providing me with new ideas and alternative points of view if my mind got stuck. The detailed proof-reading of the manuscripts helped a lot to improve them as well as my writing. I further appreciate the given possibility to change my weekly schedule by doing home office on Fridays since my daughter was born, which helped a lot.

Thanks to Prof. Axel Müller for welcoming me in his group and for being my doctoral advisor. The constantly good mood in MC2 is largely due to his suggestions for barbecues, hikes and other group activities.

I further thank Prof. Müller and Dr. Schmalz for the possibility to present my research at conferences in Germany and around the world including the US, Turkey and Israel.

Many thanks to MC2 in general, for being what it is because of people being who they are. I will never forget the numerous after-work sessions discussing about scientific and nonscientific, important and nonimportant things that completed or contrasted the work days, whatever was necessary.

Special thanks to our technical assistants without whom a thesis might take a few years longer:

- Marietta Böhm and before her Sabine Wunder for the conservation of our GPC equipment and lots of measurements
- Melanie Förtsch and Annika Pfaffenberger for measuring some TEM samples
- Annette Krökel for help with some experiments (especially on Fridays) and for always knowing where things in MC2 are to be found
- Dane Blasser and Susanne Edinger for their help in the anionic lab

Thanks to our secretary Gaby Rösner-Oliver for help with all the various forms one has to fill in during a PhD thesis and for the organization of our trips to Freiburg, our group seminar, our price reduction for delayed pizzas and more.

Acknowledgment

Erklärung

Die vorliegende Arbeit wurde von mir selbstständig verfasst, und ich habe dabei keine anderen als die angegebenen Hilfsmittel und Quellen benutzt.

Ferner habe ich nicht versucht, anderweitig mit oder ohne Erfolg eine Dissertation einzureichen oder mich der Doktorprüfung zu unterziehen.

Bayreuth, den 07.05.2012

Joachim Schmelz